

Enhancing Heat Transfer and Thermal Management Efficiency in Micro Heat Sinks through Machine Learning Algorithms

Mohammad Abdullah Hossain Harris

Sustainable Engineering and Energy Technologies

School of Physics, Engineering and Computer Science

Supervisory Team:

Professor Hongwei Wu (University of Hertfordshire)

Dr. Anastasia Angelopoulou (University of Westminster)

Dr. Wenbin Zhang (Nottingham Trent University)

Examination Team:

Professor Yuying Yan (University of Nottingham)

Dr. Guogang Ren (University of Hertfordshire)

*Submitted to the University of Hertfordshire in partial fulfilment of
the requirement of the degree of Doctor of Philosophy*

October 2024

Declaration of Originality

I declare that the work in this dissertation was carried out under the requirements of the University's Regulations and Code of Practice for Research Degree Programmes and has not been submitted for any other academic award. Except where indicated by the specific reference in the text, the work is the candidate's work. Any views expressed in the dissertation are those of the author.

The following research output fully/directly contributed and was used in this PhD thesis:

1. **Harris, M.**, Babar, H. and Wu, H., 2025. Assessing Thermohydraulic Performance in Novel Micro Pin-Fin Heat Sinks: A Synergistic Experimental, Agile Manufacturing, and Machine Learning Approach. *International Journal of Heat and Mass Transfer*, 239, p.126581.
2. **Harris, M.**, Angelopoulou, A., Wu, H. and Zhang, W., 2024, July. Comparative Analysis of Micro/Minichannel Flow Boiling Pattern Recognition and Classification using a Combined CNN-Clustering Algorithms Approach. In *2024 14th International Conference on Pattern Recognition Systems (ICPRS) (pp. 1-9)*. IEEE.
3. **Harris, M.**, Wu, H., Angelopoulou, A., Zhang, W., Hu, Z. and Xie, Y., 2024. Heat transfer optimisation using novel biomorphic pin-fin heat sinks: An integrated approach via design for manufacturing, numerical simulation, and machine learning. *Thermal Science and Engineering Progress*, p.102606.
4. **Harris, M.**, Wu, H. and Sun, J., 2024, Investigating Heat Transfer and Flow Characteristics under Different Wall Heating Conditions in Novel Micro Pin-Fin Heat Sinks. in *Proceedings of the 9th World Congress on Momentum, Heat and Mass Transfer (MHMT'24)*. 9th World Congress on Momentum, Heat and Mass Transfer (MHMT 2024), London, United Kingdom, 11/04/24.
5. **Harris, M.** and Wu, H., 2023, Numerical Simulation of Heat Transfer Performance in Novel Biomorphic Pin-Fin Heat Sinks. in *8th International Conference on Experimental and Numerical Flow and Heat Transfer (ENFHT' 23)*.
6. **Harris, M.**, Wu, H., Zhang, W. and Angelopoulou, A., 2022. Overview of recent trends in microchannels for heat transfer and thermal management applications. *Chemical Engineering and Processing-Process Intensification*, 181, p.109155.

Other research output that partially/indirectly contributed to this PhD thesis:

7. **Harris, M.**, Wu, H. and Toet, W., 2024. Reverse Engineering and Performance Enhancement of a NACA Duct for Cockpit Cooling in a GT4 Racing Car. In *4th SPECS Research Conference, University of Hertfordshire, Hatfield, UK* (Accepted/In Press).
8. Data Study Group Team., **Harris, M.**, et al., 2022. In *Data Study Group Final Report* (Alan Turing Institute). Casting the Future: understanding failure in turbine manufacture for Rolls Royce (Embargoed).
9. **Harris, M.**, 2021. An investigation on engine mass airflow sensor production via TQM, TPM, and Six Sigma practices. *Operations Research Forum* (Vol. 2, No. 4, p. 61). Cham: Springer International Publishing.
10. **Harris, M.** Wu, H., Angelopoulou, A. and Zhang, W., Flow Boiling Regime Classification Using SIM-CLR Approach in Novel Hybrid Bioinspired Micro Pins. (Under Submission Process in the *International Communications in Heat and Mass Transfer*)
11. **Harris, M.** Wu, H., Sustainable Manufacturing of Micro Heat Sinks: A Life Cycle and Circular Economy Perspective. (Under Submission Process in *Journal of Cleaner Production*)
12. Wu, Z., Yan, Z., Zhu, Y. Ji, C., Zhou, D., **Harris, M.**, Wu, H. Synthesis and antifouling testing of fluoro silicon-based superhydrophobic coatings for high-salt wastewater treatment by a short two-step method. (Under Submission Process in *Desalination*)

Note: The findings used in this thesis have been published in 4 peer-reviewed journal articles and 3 peer-reviewed conference papers. Chapter 2 contains content from (3) and (6); Chapter 3 partially uses material from (9); Chapter 4 includes findings from (3) and (5). Chapter 5 findings are from (1) and (4); Chapter 6 findings have been published in (2).

Signed: *Mohammad Harris*

Dated: 02/10/2024

Dedicated to my Mum, Aunts, family, grandparents, and everyone rooting for me in life.

(This page has been intentionally left blank)

Abstract

The growing power densities and rapid miniaturisation of modern electronics necessitate advanced thermal management solutions beyond conventional heat sinks, which struggle with limited performance and adaptability. This research is the first of its kind to simultaneously combine machine learning, numerical simulations, and experimental investigations while incorporating manufacturing philosophies, creating a comprehensive methodology that establishes a new benchmark to provide holistic thermal management solutions. The proposed bioinspired designs via hybrid pin-fin structures inspired by mushrooms, scutoids, cruciform flowers, and flying fish represent a departure from conventional configurations. Due to strategic modifications, these unique geometries exhibited a **30-70%** increase in heat transfer potential, coupled with reduced thermal resistance and enhanced flow manipulation. The research is also the first to systematically incorporate such complex nature-inspired structures into micro heat sinks, showing the potential for high thermal efficiency whilst addressing manufacturability. Additionally, the integration of machine learning significantly advanced the design process by enabling rapid, high-accuracy predictions of thermal characteristics and flow behaviours. Using ensemble learning and combined techniques the developed models achieved over **90%** accuracy in predicting heat transfer coefficients and classifying complex flow regimes. This novel application of smart data-driven methods transformed the traditionally laborious optimisation process, reducing computational time by **60-70%** and allowing real-time performance monitoring. The introduction of such predictive capabilities for HTC, new correlations, sustainability analyses, and a custom data pipeline for flow regime identification represents a leap forward in artificial intelligence use in heat transfer research. Furthermore, to enhance scalability, a hybrid production strategy integrating Lean, Agile, and Design for Manufacturing resulted in a **43%** reduction in production cost, a **29%** savings in energy consumption, and a **19%** cut in carbon emissions. Therefore, the research findings align with UK Net Zero and the EU Green Deal and Digital Agenda goals to present a practical model for developing high-performance thermal management solutions with minimal detrimental environmental impact. Thus, this research bridges the gap between theoretical innovation and practical implementation, offering a transformative framework for next-generation thermal management by adding new dimensions and strategies in air-cooled, liquid-cooled, and flow-boiling systems. Its contributions have a wide range of applications in high-performance electronics, automotive and aerospace thermal systems, and renewable energy technologies, setting a new benchmark for adaptable, efficient, and sustainable global cooling solutions.

Acknowledgements

Personal Life

Well, here we are at the acknowledgements section — the part of the thesis where I get to pause, take a deep breath, and express my heartfelt gratitude to all the incredible people who've supported, encouraged, and cheered me on throughout this journey. It's been a long road, full of highs, lows, rock bottoms, and everything in between, and none of it would have been possible without the wonderful people in my life. So, buckle up for a slightly emotional (and maybe even a bit funny) tribute to all those who've helped me get to this point.

First and foremost, my eternal gratitude goes to Allah SWT. Without His constant guidance and unwavering blessings, nothing would be possible. Next, Mum (Afsari Begum) — putting your name here because this PhD is just as much as yours as mine. Honestly, words can't fully capture how much your love and support have meant to me throughout this process. You've been my rock, my sounding board, and my biggest fan — often all at once. Whether it was patiently listening to me rant about thesis woes or helping me stay grounded when I thought the academic world was crumbling, you've been there through it all. I know this thesis may have felt like a never-ending saga (and trust me, I've felt the same at times!), but your unwavering belief in me has been the driving force that kept me going. Thank you for always being there, with just the right words, and helping me navigate this crazy journey.

To my aunts, I owe so much of my sanity to you. Your wisdom, humour, and incredible knack for knowing when I needed a distraction (or an honest pep talk) have been invaluable. Whether you were offering sage advice, spoiling me with unexpected treats, or simply reminding me that life exists outside of the thesis bubble, you've provided comfort and support in countless ways. You've been more than just family — you've been my source of laughter, perspective, and strength. Thank you for lifting me when I needed it most.

To my Dad, brothers, little nephew, sister, and the rest of my family, thank you for being the best support system a person could ask for. Whether you understood the intricacies of my research or not (and let's be honest, there were plenty of moments where even I wasn't entirely sure what I was doing!), your encouragement and belief in me never wavered. You've been my foundation throughout this process and knowing I had you all behind me made everything just a little bit easier. I know there were moments when I may have seemed like I was on another planet, buried in my laptop, but you never stopped cheering me on. Special thanks to my wonderful grandparents, whose constant love, guidance, and belief in the importance of education inspired me to keep going, even when the finish line seemed far away.

To my friends around the world, spanning 6 continents, I can't thank you enough for sticking with me through this academic adventure. Whether we were worlds apart or just down the road, your support has been a lifeline. From the late-night texts checking in on me (and making sure I hadn't completely lost my mind) to the spontaneous calls that always seemed to come at exactly the right time, you've all played a massive role in keeping me sane. You've reminded me that there's life outside of academia — something I sometimes forget when I'm being a workaholic — and you've kept me laughing with reels and memes even when the stress levels

were high. Special thanks to the friends who had no idea what my thesis was about but listened anyway and sent memes — your patience deserves a medal.

I also want to take a moment to thank the people who are no longer here with us but whose influence and love have shaped me and my journey. To those family members and friends who I've lost along the way, your memory has been a constant source of strength. You've left a lasting imprint on my life, and I've carried your spirit with me through the ups and downs of this process. You may not be here to see this thesis completed, but I hope I've made you proud.

Professional Life

Now, on to the academic side of things. To my principal supervisor, Professor Hongwei Wu, I truly don't know where to begin with my thanks. Your guidance, wisdom, and patience have been the backbone of this thesis. From the very first meeting to the final draft, you've been a constant source of support. You challenged me when I needed it, gave me space to explore my ideas, and always replied to me with just the right advice regardless of whether it was morning or midnight. Your feedback was invaluable, and your belief in my work helped me push through the moments of doubt and uncertainty. I'm deeply grateful for the time and energy you've invested in this project and for always encouraging me to aim higher. I've learned so much from you, not just about research, but about resilience, work ethic, focus, and the importance of perseverance. The trip to Turkey with you was a big highlight of my PhD.

To my secondary supervisors, Dr. Anastasia Angelopoulou and Dr. Wenbin Zhang, thank you for your insightful comments and thoughtful feedback throughout this process. Your expertise helped me see my research from different perspectives, and your advice was critical in shaping this work into what it is today. I'm incredibly grateful for the time you took to guide me, offer constructive criticism, and provide the encouragement I needed at each stage. Your support has been an essential part of this thesis, and I couldn't have done it without your input. It was also nice meeting Wenbin at the start of my PhD, whilst I got to meet Anastasia at the end of my PhD journey.

And, of course, to my colleagues – where would I be without you? You've made this journey far less lonely, and almost all the time, fun and interesting. From the shared frustrations over (we all know what we are talking about) to the little victories we celebrated (even if it was just successfully formatting a document), you've been the best kind of academic family. You've all played a role in making this journey bearable, whether through brilliant discussions or just commiserating over how many cups of coffee it took to get through a particularly rough day. I won't name names, because frankly, you're all equally important to me, and picking favourites would be impossible. Just know that I'm endlessly grateful for each one of you — for the advice, the laughs, the much-needed reality checks, and the encouragement. This experience wouldn't have been the same without you. However, would just like to give a special mention to (soon to be Dr.) Hamza Babar for being an excellent colleague and friend during my PhD.

To everyone who's been a part of this journey, whether mentioned here or not, thank you from the bottom of my heart. This thesis is as much a testament to your support as it is to my work. We've made it to the finish line, and I couldn't have done it without you.

Nomenclature

Latin Symbols

A	Area, m ²
C_p	Specific heat capacity, J/kg · K
D	Diameter, m
D_h	Hydraulic diameter, m
HTC/h	Heat transfer coefficient, W/ m ² K
H	Height, m
K/k	Thermal conductivity, W/m · K
L	Length, m
\dot{m}	Mass flow rate, kg/s
N	Number of points
Nu	Nusselt number, -
Pr	Prandtl Number, -
Pu	Pumping power use, W
\dot{Q}/Q	Heat transfer rate, W/m ²
R	Thermal resistance, K/W
Re	Reynolds number, -
R_{th}	Thermal resistance, K/W
SA	Surface area, m ²
T	Temperature, °C/K
U,V,W	Dimensionless parameter
u,v,w	Directional velocity, m/s
V	Volume, m ³
W	Width, m
x,y,z	Directional vectors
X,Y,Z	Dimensionless parameter
Z	Random variable

z	Z-score
----------	---------

Greek Symbols

Σ	Covariance
η	Efficiency, dimensionless
ε	Epsilon
μ	Fluid viscosity, kg/m · s
μ_i	Mean vector
ρ	Fluid density, kg/m ³
φ	Phi
δ	Rate of change
σ	Standard deviation

Subscripts/Superscripts

a	air
b	base
bc	base case
f	fluid
F	fin
i	i-th value
in	inlet
nc	new case
o	outlet
s	surface
th	thermal
ts	test section

Abbreviations and Full Form

AL	Aluminium	DT	Diamond/tetrahedral Top
AM/3D	Additive Manufacturing	DV	Dependent Variable
ANN	Artificial Neural Network	DW	Deionized Water
AR	Aspect Ratios	EFE	Exocoetidae -inspired with Filleted Edges
BCS	Bare Copper Surface	EGaIn	Eutectic Gallium-Indium
BS	Biphilic Surface	EN	Elastic Net
CFAS	Cruciform Flower with Astroid Splitters	ESE	Exocoetidae -inspired with Sharp Edges
CFD	Computational Fluid Dynamics	ETC	Etching
CFSM	Cruciform Flower with Secondary Mini/Microchannels	FE	Fin Efficiency
CHF	Critical Heat Flux	FEEDS	FEEDS
CM	Commercially/Pre-made	FRIN	Further Research Is Needed
CML	Combined Model	FSC	Fan-Shaped Cavity Microchannel
CMOS	Complementary Metal Oxide Semiconductor	GBR	Gradient Boosting Regression
CNN	Convolutional Neural Network	GMM	Gaussian Mixture Model
CNT	Carbon Nanotube	HCPV	High Concentrated Photovoltaic
COP	Coefficient of Performance	HF	Heat Flux
CPV	Concentrated Photovoltaic	HTC	Heat Transfer Coefficient
CT	Conical Top	HTF	Heat Transfer Fluid
CSFT	Conical Stem Flat Top	HTP	Heat Transfer Performance
CU	Copper	HY	Hybrid Nanofluid/microfluids
DCHE	Desiccant-coated Heat Exchanger	IV	Independent Variable
DH	Hydraulic Diameter	KM	K-means Clustering
DMAIC	Define, Measure, Analyse, Improve, Control	KNN	K-nearest Neighbours
		LI	Lithography
		LOHC	Liquid Organic Hydrogen Carriers
		LR	Linear Regression

MAE	Mean Average Error	PDF	Probability Density Function
MAPE	Mean Absolute Percentage Error	PDMS	Polydimethylsiloxane
MC	Microchannels	PHT	Plain Hexagon Top
MCH	Micro Heat Sinks	PIF	Performance Improvement Factor
MCHE	Microchannel Heat Exchanger	PLR	Polynomial Regression
MCHS	Microchannel Heat Sink	PMMA	Polymethyl Methacrylate
MEDS	Materials, Experimental, Design, Sustainability	PSDT	Pentagonal Stem Diamond Top
MF	Mass Flux	PW	Porous Wall
MHS	Micro Heat Sink	RF	Random Forest
MLM	Multi-layered Microchannel	RMSE	Root Mean Squared Error
MLP	Multilayer Perceptron	RQ	Research Question
MLR	Multiple Linear Regression	RR	Ridge Regression
MM	Micromachining	SEM	Scanning Electron Microscope
MMC	Manifold Microchannel	SF	Scutoid Fin
MPF	Micro Pin-Fin	SPF	Square Pin Fin
MPFHS	Micro Pin-Fin Heat Sinks	SVR	Support Vector Regression
MSE	Mean Squared Error	SWOT	Strength, Weakness, Opportunity, and Threat
MT	Mushroom/hexaprism Top	TED	Turbulent Eddy Dissipation
MTC	Moisture Transfer Coefficient	TEG	Thermo-electric Power Generator
NM	Numerical Method	TFA	Time-Frequency Analysis
NN	Neural Networks	TKE	Turbulent Kinetic Energy
NWH	No Wall Heating	TS	Test Surfaces
OAM	Other Analysis Methods	UA	Uncertainty Analysis
OB	Objectives	WF	Working Fluid
OFM	Other Fabrication Method	WH	Wall Heating
OMT	Other Materials	XGB	XGBoosting
OWF	Other Working Fluids		
PCM	Phase Change Materials		

Table of Contents

Declaration of Originality	i
Abstract	iv
Acknowledgements	v
Nomenclature	vii
Table of Contents	x
List of Figures	xv
List of Tables	xvii
Chapter 1: Introduction	1
1.1 Research Background and Motivation	2
1.1.1 Role of Micro Heat Sinks	3
1.2 Problem Statement	5
1.3 Research Aim, Questions and Objectives	8
1.4 Thesis Outline	9
1.5 Research Significance and Limitations	11
Chapter 2: Literature Review	14
2.1 Background to the Chapter	15
2.2 Fundamental Heat Transfer Mechanisms	16
2.3 Boiling Heat Transfer Mechanisms	17
2.3.1 Nucleate Boiling	18
2.3.2 Film Boiling	19
2.3.3 Transition Boiling	19
2.3.4 Flow Boiling	20
2.3.5 Variations of Primary Boiling Modes	20
2.4 Thermal Management Techniques	22
2.5 Micro Heat Transfer: Recent Trends and Perspectives Overview	23
2.5.1 Material Perspective	25
2.5.2 Enhanced Flow Control Perspective	31

2.5.3	Design Perspective	37
2.5.4	Sustainability Perspective	45
2.6	Overview of Identified Research Scope and Trends.....	47
2.6.1	Trends in Micro Heat Transfer	52
2.6.2	Key research themes and sub-themes	53
2.7	Focus on Pin-fin Heat Sinks	57
2.7.1	Micro pin-fin strategies.....	59
2.8	Intersection of Machine Learning and Micro Heat Sinks.....	65
2.8.1	Design Optimisation of Heat Sinks.....	66
2.8.2	Advanced Cooling Technologies.....	67
2.8.3	Machine Learning and Predictive Models for Thermal Systems.....	67
2.8.4	Boiling Regime Classification	68
2.8.5	Flow Regime Identification and Prediction	69
2.8.6	Bubble Dynamics and Heat Transfer Modelling	69
2.8.7	Research Gaps.....	70
2.9	Integration of Manufacturing Philosophies	72
2.10	Summary of Literature Review.....	75
Chapter 3: Methodology		78
3.1	Background to the Chapter	79
3.1.1	Research Strategy.....	80
3.2	CFD Simulation Setup	81
3.2.1	Geometry Creation and Meshing	81
3.2.2	Boundary Conditions and Solver Settings	82
3.2.3	CFD Results and Post-processing.....	83
3.2.4	Model Validation and Limitations	83
3.3	Heat Sink Fabrication Setup	84
3.4	Hybrid Manufacturing Benefits and Sustainability Analysis	88
3.4.1	Main Parameters Driving Costs.....	89

3.4.2	Impact Assessment and Calculations.....	90
3.4.3	Verification of the Hybrid Strategy through Machine Learning	91
3.5	Experimental Setup.....	92
3.5.1	Heat Sink Material and Working Fluid.....	94
3.5.2	Wall Temperature Variations.....	95
3.5.3	Experimental Validation	99
3.6	Machine Learning Setup	102
3.6.1	Role of Machine Learning and Artificial Intelligence.....	102
3.6.2	Data Collection and Processing	102
3.6.3	Feature Selection.....	103
3.6.4	Model Training and Algorithms	104
3.6.5	Hyperparameter Tuning and Validation	104
3.6.6	Evaluation Metrics	104
3.6.7	Sample Process Flow	105
3.7	Summary of Methodology Chapter	106
Chapter 4: Evaluation of Biomorphic Extended Top Pin-Fin Heat Sinks.....		107
4.1	Background to the Chapter	107
4.2	Initial Design Investigation.....	107
4.2.1	Discussion of Findings.....	109
4.3	Finalised Prototype Heat Sink Design	111
4.3.1	Biomorphic Design for Manufacturing (DfM) Philosophy	112
4.3.2	Numerical Simulation Setup and Validation	116
4.3.3	Results.....	122
4.3.4	Discussion of Findings.....	137
4.3.5	Summary of Chapter	144
Chapter 5: Thermohydraulic Assessment of Bio-inspired Hybrid Micro Pin-Fins		146
5.1	Background to the Chapter	146
5.2	Initial Design Investigation.....	146

5.3	Discussion of Results	148
5.4	Finalised Prototype Micro Pin-Fin Heat Sink.....	150
5.4.1	New Heat Sink Designs, Rationale, and Manufacturing	151
5.4.2	Data Reduction.....	156
5.4.3	Results.....	158
5.4.4	Building empirical correlation models.....	168
5.4.5	Machine learning-driven analysis	171
5.4.6	Summary of Chapter	177
Chapter 6: Flow Boiling Regime Classification in Microchannel Heat Sinks		178
6.1	Background to the Chapter	178
6.2	Research Scope	178
6.3	Overview of available technologies.....	179
6.4	Clustering Algorithms for Flow Boiling.....	181
6.5	Strategic Process Plan.....	182
6.5.1	Dataset Description.....	184
6.5.2	Data Pipeline.....	185
6.6	Results and Discussion	187
6.6.1	CNN Classification	187
6.6.2	Clustering Results	189
6.6.3	Comparative Analysis.....	190
6.7	Research Impact and Limitations.....	193
6.8	Summary of Chapter	195
Chapter 7: Conclusion.....		196
7.1	Advancing the Next Generation of Thermal Management Strategies	197
7.2	Summary of Key Findings.....	197
7.2.1	RQ1: What are the key recent advancements and limitations in micro heat sink technologies for heat transfer and thermal management?	197

7.2.2	RQ2: What insights can experimental and numerical investigations provide into the performance of bioinspired heat sinks, and how can these findings contribute to improved thermal efficiency?	198
7.2.3	RQ3: How can machine learning approaches be applied to optimise heat sink design and enhance thermal management in light of current limitations in traditional methods?	199
7.2.4	RQ4: How can sustainable design principles and manufacturing philosophies be integrated into developing next-generation heat sinks, ensuring performance optimisation and environmental responsibility?	200
7.3	Cross-case Synthesis	201
7.4	Research Limitations and Future Recommendations	203
7.5	Concluding Remarks and Research Impact	204
7.5.1	Innovation in Bioinspired Geometries	204
7.5.2	Application of Machine Learning for Design and Development:	205
7.5.3	Sustainability Integration in High-Performance Cooling Solutions:	205
7.5.4	Framework for Next-Generation Thermal Management Systems.....	205
7.5.5	Overall Impact	205
	References	207
	Appendices.....	237
	Appendix A: Overview of Recent Trends Table.....	237
	Appendix B: CNC Machine Specification	243
	Appendix C: Python Codes and Raw Data	244
	C1: Python Script for Sustainability and Cost Analysis.....	244
	C2: Python Script for Sample Bagging and Stacking Regression.....	248
	C3: Python Script for Sample Principal Data Analysis (PCA)	249
	C4: Python Script for Base CNN Architecture.....	252
	Appendix D: Published Research.....	255
	Afterwords	262

List of Figures

Fig. 1.1 Micro heat sink trends and applications	4
Fig. 1.2 Evolution of electrical components [4]	5
Fig. 1.3 Research SWOT analysis	13
Fig. 2.1 Typical boiling curve [46]	18
Fig. 2.2 Overview of thermal management techniques	23
Fig. 2.3 Summary of MEDS framework.....	46
Fig. 2.4 Research distribution map	48
Fig. 2.5 Different microchannel designs and manufacturing trends: (a) Design shapes; (b) Fabrication strategies; (c) Hydraulic diameter; (d) Aspect ratio	49
Fig. 2.6 Material trends: (a) Material choice (b) Working fluids	50
Fig. 2.7 Further research needs: (a) FRIN trend (b) Analysis trends.....	51
Fig. 2.8 Research trend of micro pin-fin heat sinks	65
Fig. 2.9 Manufacturing philosophy integration into the research.....	74
Fig. 3.1 Research Onion describing the overall research methodology	81
Fig. 3.2 Sample setup and boundary conditions	83
Fig. 3.3 Manufacturing equipment and process.....	84
Fig. 3.4 Finished machined parts	86
Fig. 3.5 Design quality assurance	88
Fig. 3.6 Main cost factor parameters	90
Fig. 3.7 Savings for different categories.....	91
Fig. 3.8 Actual vs Predicted cost comparison.....	92
Fig. 3.9 Experimental setup and instruments.....	94
Fig. 3.10 Housing modification and dimensions for a detachable heat sink setup.....	96
Fig. 3.11 Wall temperature variations for heating blocks and heat sinks	98
Fig. 3.12 Experimental validation.....	100
Fig. 3.13 Guideline for machine learning optimisation	106
Fig. 4.1 Bio-inspired/biomorphic heat sink designs	108
Fig. 4.2 Temperature distribution from the top view and outlets	110
Fig. 4.3 Pressure distribution in the heat sinks	110
Fig. 4.4 Heat transfer comparison.....	111
Fig. 4.5 Base design and 3D-printed new prototype design	113

Fig. 4.6 All biomorphic scutoid pin-fin designs: a) Plain Hexagon Top (PHT), b) Conical Top (CT), c) Diamond Top (DT), d) Mushroom Top (MT)	116
Fig. 4.7 Grid independence test results	120
Fig. 4.8 Numerical validation of the simulation	120
Fig. 4.9 3D Mesh visualisation of fluid and solid domains for the pin-fins	122
Fig. 4.10 Heat transfer coefficient comparison with different Re	123
Fig. 4.11 Nusselt Number comparison with different Re	124
Fig. 4.12 Thermal resistance comparison with different Re	125
Fig. 4.13 Fin efficiency comparison with different Re	126
Fig. 4.14 Pressure drop comparisons	127
Fig. 4.15 Comparison of machine learning model performance	129
Fig. 4.16 (a)-(d). Temperature contours of all scutoid pin-fins (planar views).	131
Fig. 4.17 (a)-(d). Velocity contours of all scutoid pin-fins (side view).	133
Fig. 4.18 (a)-(d). Turbulent kinetic energy contours of all pin-fins (top view)	135
Fig. 4.19 (a)-(d) Velocity streamlines with TKE outlet contours (isometric view)	136
Fig. 4.20 Mass, volume, and heat transfer performance comparison at $Re = 13500$	138
Fig. 4.21 Colourmap and summary of heat transfer performance of all design	140
Fig. 5.1 Initial micro pin-fin heat sink designs	147
Fig. 5.2 Temperature distribution from the top view	149
Fig. 5.3 Pressure distribution in the heat sinks	149
Fig. 5.4 Pin-fin surface dimensions and drawing	154
Fig. 5.5 New heat sink designs and inspirations	155
Fig. 5.6 (a)-(d) Nusselt Number comparison	159
Fig. 5.7 Thermal resistance performance	162
Fig. 5.8 (a)-(d) Pressure drop and pumping power comparison	164
Fig. 5.9 Correlation matrix for parameters	170
Fig. 5.10 Model comparison for original and augmented synthetic data	175
Fig. 6.1 Different flow regimes	183
Fig. 6.2 Sample data augmentations	185
Fig. 6.3 Architecture for data pipeline and model implementations	187
Fig. 6.4 CNN classification accuracy	188
Fig. 6.5 (a)-(i) comparative analysis for algorithms	189

Fig. 6.6 Data split performance comparison	192
Fig. 6.7 Complex boiling patterns.....	195
Fig. 7.1 Summary of knowledge contributions arising from this research.....	206

List of Tables

Table 1: Summary of trends, gaps, and research direction for the thesis	76
Table 2: Experimental equipment range and accuracy	93
Table 3: Measuring apparatus range and accuracy	101
Table 4: Grid independence test results	108
Table 5: Details of geometrical data for all designs	114
Table 6: Sample grid independence test accuracy results.....	119
Table 7: Data for machine learning model performance	129
Table 8: Numerical validation and grid independence test results	148
Table 9: Summary of key design feature details.....	154
Table 10: Empirical correlation equations.....	171
Table 11: Different regression algorithm performance	172
Table 12: Model metrics	190
Table 13: Key highlights and differences	191

Chapter 1: Introduction

Chapter Precursor: Bangla

“As the act, so the result”

This Bengali proverb from my homeland, Bangladesh, embodies the principle that intentional actions lead to meaningful outcomes. Starting my PhD during the COVID-19 pandemic lockdowns, I ventured into micro heat sink technologies—an area new to me—which required resilience and purposeful effort. The Introduction chapter sets the foundation of the thesis, emphasising how deliberate choices—such as adopting sustainable design principles and advanced methodologies—directly shape the research's impact. By connecting my cultural background to my academic journey, the chapter illustrates that thoughtful research actions lead to significant advancements in thermal management and sustainability, reflecting the essence of the proverb.

1.1 Research Background and Motivation

Consumer, industrial, and digital electronic devices are omnipresent today. The advent of Industry 4.0 and rising computational power have led to the integration of electronic devices into almost every application. As of 2024 reports, the global consumer electronics market is expected to bring over \$1 trillion, despite the COVID-19 pandemic-related slowdowns [1]. Additionally, the demand for more compact devices has surged, though this comes with the challenge of managing higher operating power and increased heat dissipation [2,3]. While these devices have become more powerful and portable, advancements in thermal management technologies have not kept pace, necessitating continuous improvements and innovation.

Effective thermal management has evolved beyond technical necessity to become a binding factor for success and sustainability across industries. In electronic devices, efficient cooling is critical to prevent overheating, ensuring the reliability and longevity of smartphones, microprocessors, and high-performance computing systems [4]. In aerospace, precise thermal control is essential for maintaining optimal performance and safety, while in the automotive sector, advanced thermal management systems improve engine efficiency and extend the lifespan of electric vehicle batteries [5]. Similarly, in industrial settings, enhanced heat transfer capabilities can significantly boost machinery efficiency and reduce energy consumption, aligning with global sustainability goals.

In response to these trends, microtechnology such as micro heat sinks, particularly those based on microchannels (MC), have emerged as innovative solutions to modern thermal management challenges. Microchannels offer a promising pathway towards both improved performance and environmental responsibility. The development of microchannel heat sink (MCHS) technology can be credited to Tuckerman and Pease [6]. Faced with heat dissipation challenges in high-performance computer chips, their work in the 1980s led to a breakthrough by miniaturising heat sinks, significantly improving heat removal capabilities. Since then, MCHS technologies have evolved across multiple sectors, particularly in reducing energy consumption while maintaining high efficiency.

Microtechnology generally refers to technologies with features on the micrometre scale. One key parameter in microchannel design is the characteristic length or hydraulic diameter (DH), particularly in non-circular tubes and channels. Many researchers define microchannels as those with a DH of one millimetre or less, calculated by dividing the cross-sectional flow area by the wetted perimeter [7]. By leveraging high surface area-to-volume ratios of

microchannels, these systems greatly enhance convective heat transfer, making them ideal for cooling applications in several industries. Recent innovations, such as pin-fins, microstructures, nanofluids, and flow boiling, are among the most promising techniques for optimising heat transfer in micro-heat sinks (MHS) [8]. Originally developed for computing and electronics, microchannel or micro heat sinks are now widely used in pharmaceuticals, biochemistry, automotive, aerospace, and energy production industries [9–11]. Their key advantages include compactness, high heat exchange efficiency, and cost-effectiveness. Additionally, microchannel technology aligns with the growing demand for sustainable solutions by reducing the energy footprint — aligned with the European Union (EU) 2050 sustainability goals [12,13].

With ongoing advancements in technology, experimental techniques, and manufacturing processes, there is significant potential to further enhance micro heat sink (MHS) performance, especially in addressing the challenges brought about by the rapid miniaturisation of electronic devices. This research is motivated by the need to improve both the efficiency and sustainability of next-generation MHS designs, leveraging cutting-edge technologies and integrating various methods. A comprehensive review of current trends, experimental approaches, and analyses of microchannels is crucial for identifying existing research gaps and driving future innovations in performance optimisation and sustainable design.

1.1.1 Role of Micro Heat Sinks

Micro heat sinks, including microchannels and micro pin-fins, offer exceptional thermal management in compact applications [4]. Although the exact definition of microchannels can vary and is up for debate, in this research, micro heat sinks are considered to have channels or paths with dimensions of 1mm or less [11]. Microchannels feature small channels that enhance heat transfer efficiency through a large surface area and optimised fluid dynamics, making them ideal for high-performance computing and microelectronics. Micro pin-fins, with their array of small pins, increase surface area and improve convection, providing excellent heat dissipation in high-density electronics [14]. These designs are particularly advantageous in space-constrained environments, delivering superior thermal performance than traditional heat sinks. However, they are expensive to manufacture, and the trade-off between thermohydraulic performance, energy consumption, and design complexity requires careful consideration. Nonetheless, they are one of the most promising currently available technologies; therefore, this research will deep-dive into heat sink technologies, specifically microchannel-based heat sinks with pin-fins. Fig. 1.1 gives the bibliometric output and maps the research landscape of

micro heat sinks using a SCOPUS search, highlighting interconnected themes such as heat transfer, design, and application. Prominent keywords like "thermal management", "design", and "application" indicate areas of intense research activity. This overview underscores the diverse focus within the field and points to opportunities for further exploration and innovation.

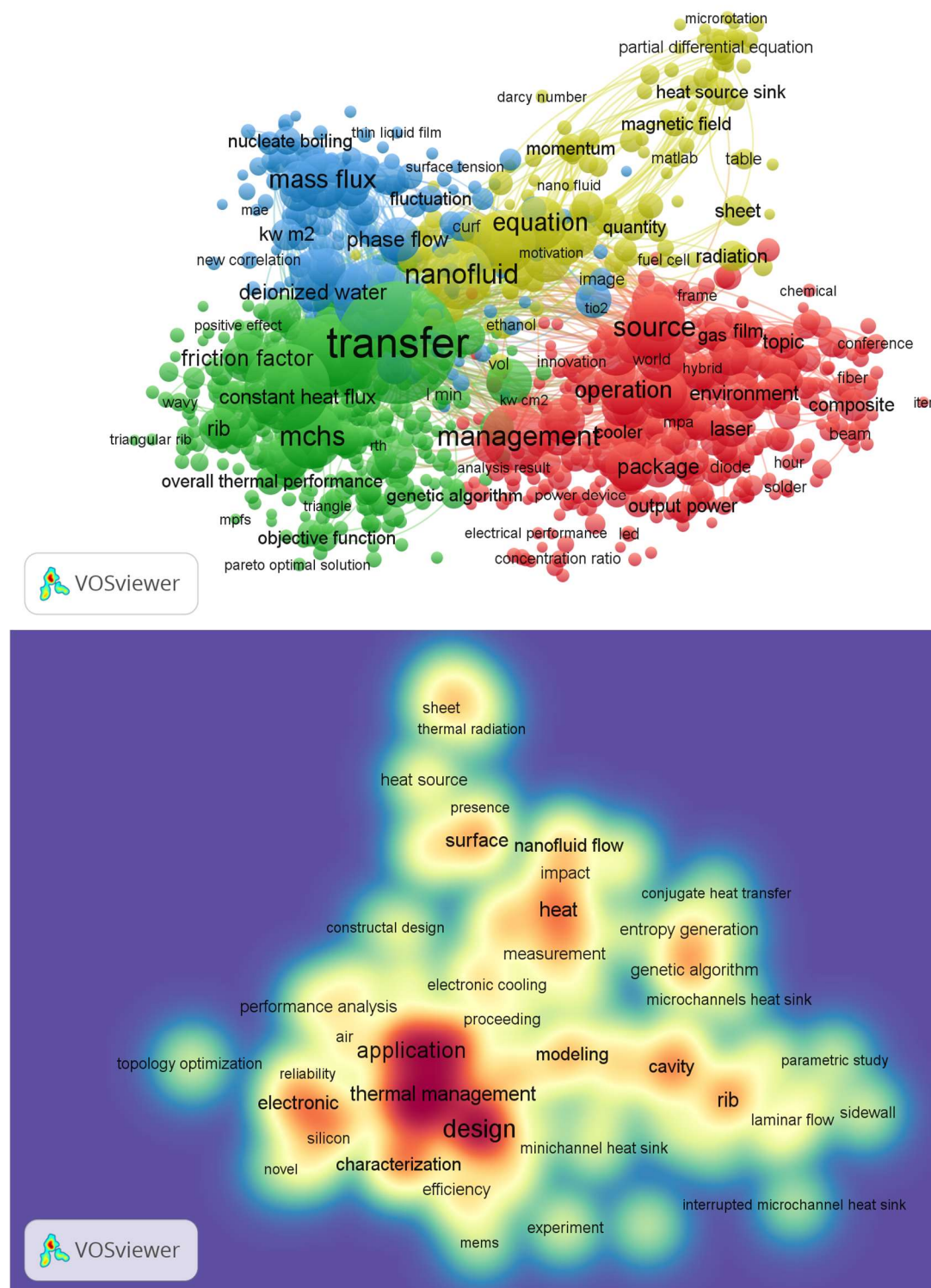


Fig. 1.1 Micro heat sink trends and applications

1.2 Problem Statement

Electric component miniaturisation is creating more powerful and portable devices every year, following the concepts of Moore's Law — the number of packed transistors in integrated circuits doubles each year with minimal cost increase [15]. However, this progress comes with significant challenges, particularly regarding the increased heat generated inside these densely packed components. The heat accumulation or flux buildup within electronic devices can lead to performance degradation, a shorter device lifespan, and in extreme cases, permanent damage to internal components [16]. Addressing this heat build-up/heat flux has thus become a critical concern, particularly as poor thermal management systems not only reduce the efficiency and reliability of electronic devices but also result in increased energy consumption and negative environmental impacts [17,18]. Fig. 1.2 shows the growth of electronic chip components over the years taken from the works of He, et al. [4].

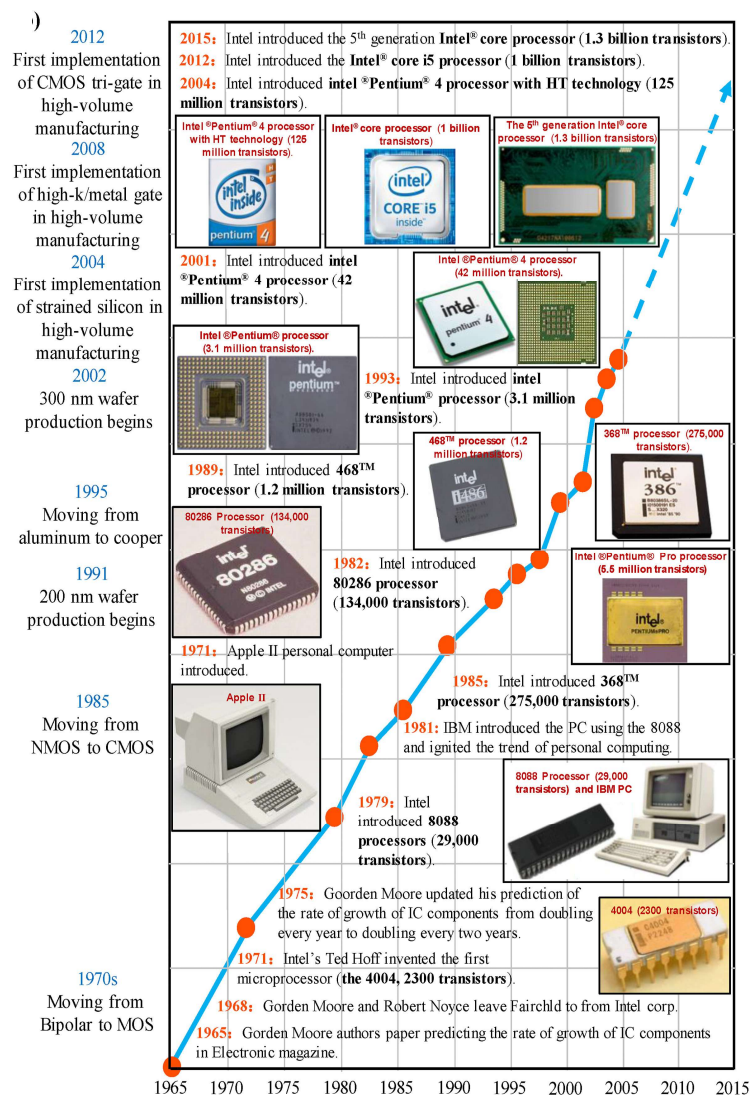


Fig. 1.2 Evolution of electrical components [4]

In response to these challenges, various cooling technologies and thermal management strategies have been developed. These range from conventional methods, such as heat sinks [19], film cooling, and flow boiling [10,20], to more advanced approaches like nanomaterial-based cooling systems [21], phase-change materials, microchannel heat exchangers, and synthetic jet cooling [22]. More recently, machine learning and artificial intelligence (AI) integration have offered innovative potential in optimising thermal management solutions. Among these technologies, pin-fin-based heat sinks have garnered attention due to their ability to enhance the surface area for heat transfer and generate turbulence, which improves thermal performance [14].

Nevertheless, as electronic devices continue to shrink and power densities increase, traditional geometries face limitations in their effectiveness. Relying solely on conventional designs is inadequate for addressing the rising thermal demands of miniaturised electronics [23]. The key challenge lies in developing advanced micro-scale heat transfer systems that can efficiently dissipate heat while maintaining the compact form factor required by modern electronic devices. Hybrid, bio-inspired, and micro pin-fins (MPFs) present a promising solution. By increasing the available surface area for heat transfer through conduction, convection, and radiation, MPF heat sinks provide passive cooling mechanisms that significantly improve device thermal management and extend product lifespans [24–26].

A major concern, however, is that the design and optimisation of heat sinks must align with the growing demand for sustainability in manufacturing and product development. The electronics industry is under increasing pressure to reduce energy consumption and carbon emissions, especially as governments and industries set stricter environmental standards. Poorly managed thermal systems not only waste energy but also contribute to larger ecological footprints. Therefore, thermal management solutions must not only focus on performance but also address environmental challenges through sustainable design, materials, and manufacturing processes [27]. Developing heat sinks that meet both performance and sustainability criteria requires an agile approach to product development. Companies must be able to rapidly prototype and refine heat sink designs to ensure they meet evolving environmental regulations while maintaining thermal efficiency.

Moreover, from a design and optimisation perspective, the effectiveness of pin-fin-based heat sinks is determined by several factors, including their geometrical configurations (such as the shape, spacing, and height of the fins), the working fluid used, and the thermal conductivity

of the materials. The performance of a heat sink is also influenced by its thermal load or heat flux, as well as the environmental conditions in which it operates [10,28]. Also, the fluid flow around the heat sink plays an important role in determining its cooling performance. While increasing the flow rate can improve heat transfer through enhanced convection, it can also lead to undesirable effects such as higher noise levels, increased pressure drops, and the need for larger fans or more powerful pumps. Consequently, achieving an optimal balance between cooling efficiency, device size, and energy consumption is essential [4].

Furthermore, from an experimental perspective, two-phase flow systems, particularly flow boiling mechanisms within micro heat sinks, add another layer of complexity to thermal management [29]. The interaction between liquid and vapour phases within these systems gives rise to varied flow patterns and heat transfer dynamics, which can be difficult to predict and control accurately. Classifying flow boiling regimes, therefore, becomes a critical task in optimising microchannel heat sink designs for specific operational conditions. Accurate classification helps engineers to tailor microchannel designs, maximising heat dissipation while minimising thermal resistance, pressure drops, and energy consumption [30]. However, the classification of these flow regimes presents challenges related to subjectivity, interpretability, and generalisability, which require innovative solutions to overcome [31].

From a fabrication perspective, material selection and manufacturing processes are equally important in determining the effectiveness, cost, and scalability of pin-fin-based heat sinks. The materials used in these heat sinks must strike a balance between thermal conductivity, weight, and financial feasibility, depending on the application [32]. Additionally, the manufacturing of micro pin-fins presents its own set of challenges. The high aspect ratios and microscale dimensions of the fins make fabrication complex, and any defects during the process can significantly impact heat transfer performance. Furthermore, the relatively large surface area required for pin-fin heat sinks to be effective can limit their integration into devices with minimal available space [33]. As a result, the design, material, and manufacturing methods all contribute to the complexity of optimising micro pin-fin heat sinks for modern applications.

As a result, all these challenges tie into sustainability concerns. Traditional manufacturing processes may not always prioritise environmental efficiency, leading to increased material waste and energy consumption. Agile product development, which allows for iterative design improvements and quick adaptation to new sustainability standards, is critical in this context. The adoption of sustainable materials and manufacturing techniques, alongside advanced

digital tools like machine learning, can contribute to greener, more efficient heat sinks, further supporting global efforts to reduce the environmental footprint of the electronics industry [34].

Recent advances in computational techniques, such as machine learning (ML) and artificial intelligence (AI), have opened up new opportunities for optimising thermal management systems. While most traditional research in this field has focused on experimental and numerical validation-based design optimisation, machine learning offers the potential to provide novel insights that may not be achievable through conventional methods [35]. In addition, machine learning has shown potential in addressing challenges by improving the accuracy and objectivity of flow pattern classification. Thus, by integrating machine learning techniques with simulations and experiments, researchers can expand the research space and efficiently enhance the predictive accuracy of heat sink performance models [36,37]. However, the application of machine learning in thermal management is still in its early stages, and further research is needed to fully explore its potential to provide holistic solutions [38].

To summarise, while the miniaturisation of electronic devices has driven the need for more efficient and compact thermal management systems, developing next-generation micro heat sinks presents several technical, material, design, and sustainability challenges. Advancements in machine learning, fabrication techniques, and two-phase flow understanding offer promising avenues for addressing these challenges. However, further research is needed to optimise heat sink designs that balance thermal performance with sustainability, size, cost, energy, and process efficiency. Agile product development, underpinned by sustainable engineering practices, is essential to the future of thermal management solutions.

1.3 Research Aim, Questions and Objectives

Heeding to the literature findings and assessing the current industrial needs, in this thesis, novel bio-inspired pin-fin heat sinks are proposed — whilst integrating manufacturing considerations and machine learning for enhanced process efficiency. Therefore, the main aim of this research is to develop novel hybrid bio-inspired pin-fin heat sinks, implement machine learning algorithms to optimise the design process, improve heat transfer efficiency, and overall thermal management while addressing challenges related to data availability, sustainability, and product development. To achieve the research aim, the following research questions (RQs) and objectives (OBs) were formulated. The method to build RQs and OBs was inspired and adapted from the works of Farrell, et al. [39]:

- RQ1:** What are the key recent advancements and limitations in micro heat sink technologies for heat transfer and thermal management?
- OB1:** To comprehensively review recent advancements and limitations in micro heat sink technologies, identifying current gaps and opportunities in heat transfer and thermal management.
- RQ2:** What insights can experimental and numerical investigations provide into the performance of bioinspired heat sinks, and how can these findings contribute to improved thermal efficiency?
- OB2:** To carry out investigations on bioinspired heat sinks, analysing their performance under various thermal conditions and extracting insights that contribute to improved design and heat transfer efficiency.
- RQ3:** How can machine learning approaches be applied to optimise heat sink design and enhance thermal management in light of current limitations in traditional methods?
- OB3:** To develop and apply machine learning algorithms for optimising the design and thermal management process of micro heat sinks, addressing the limitations of traditional design methods and improving overall efficiency.
- RQ4:** How can sustainable design principles and manufacturing philosophies be integrated into developing next-generation heat sinks, ensuring performance optimisation and environmental responsibility?
- OB4:** To critically appraise and integrate sustainable design principles and manufacturing approaches into developing next-generation heat sinks, ensuring a balance between performance optimisation, cost, and environmental responsibility.

1.4 Thesis Outline

This thesis is structured into several chapters, revolving around the main research aim, and each chapter focuses on a critical aspect of the research question and objectives, thermal management, and machine learning optimisation. The following give the chapter summaries.

Chapter 1: Introduction

The opening chapter establishes the foundational context and motivation for the research, addressing the escalating demand for effective thermal management in modern electronic

devices due to rising power densities. It introduces micro heat sinks as a promising solution, emphasising their significance across various sectors. This chapter also articulates the problem statement, research aim, questions, and objectives. Moreover, it underlines the importance of the study and its limitations.

Chapter 2: Literature Review

This chapter undertakes a thorough review of existing literature on the principles of heat transfer, as well as boiling heat transfer mechanisms. It examines contemporary thermal management techniques and emerging trends in micro-scale heat transfer, effectively addressing RQ1. Furthermore, the chapter considers material, design, and sustainability aspects in the development of micro heat sinks, contributing to RQ4. Additionally, the review highlights the synergy between machine learning and micro heat sinks, exploring optimisation, predictive modelling, and advanced cooling technologies. Finally, research gaps are identified, and key findings from the literature are summarised, aiding in answering the RQ2 to RQ4.

Chapter 3: Materials and Methods

Here, the materials and methodologies employed in the experimental and computational studies of bio-inspired pin-fin heat sinks are outlined. The chapter details the experimental setup, simulation tools, and machine learning algorithms used for design optimisation and thermal performance evaluation. It also provides a comprehensive explanation of the fabrication processes, data collection techniques, analytical methods, and validation procedures.

Chapter 4-6: Results and Discussion

The chapters lay the groundwork for decisions underpinning the final heat sink designs. It initially investigates, explores, and presents key findings concentrating on the numerical simulation results regarding the heat transfer performance of bio-inspired/biomorphic pin-fin heat sinks. Comparative analyses of different pin-fin geometries are presented, evaluating the potential for enhancing heat transfer efficiency through innovative design strategies, while machine learning is employed to improve Heat Transfer Coefficient (HTC) predictions.

Building on the findings and design rationale from the air-cooled heat sink, the following chapters examine the hydrodynamic performance of the finalised, manufactured micro pin-fin designs, extending the scope to hybrid pin-fin configurations used in numerical simulations. Experimental data are integrated with machine learning regression models to optimise

predictions, enhancing the accuracy related to heat transfer and fluid flow metrics. New correlation models have also been built for the best-performing design.

Lastly, these chapters explore the intersection of machine learning and boiling regime classification, particularly within flow boiling systems in microchannels and micro heat sinks. It demonstrates how ML models, when integrated, can outperform traditional methods in understanding, classifying/predicting flow patterns, thereby improving thermal performance.

Chapter 7: Conclusion, Limitations, and Future Work

This chapter summarises the principal findings and contributions of the research. It reflects on the achievement of the research objectives and addresses the research questions posed at the outset. The conclusion underscores the value of integrating bio-inspired design, machine learning, and sustainable engineering to push the boundaries of micro heat sink technology. Suggestions for future research directions are also proposed.

References, Appendices, and Afterwords

These sections consolidate the comprehensive list of sources cited throughout the thesis. The appendices provide supplementary materials that support the core content of the thesis. Finally, in the afterwords, the author reflects on the research journey, discussing the challenges encountered, personal insights gained, and the broader implications of the research, particularly its potential impact on industry and sustainability.

1.5 Research Significance and Limitations

This research brings several noteworthy contributions to the field of thermal management, with its innovative approach to developing bio-inspired pin-fin micro heat sinks. One of the most significant contributions is the integration of machine learning techniques to optimise the design and development process of heat sinks. By leveraging machine learning, this research offers a data-driven method for identifying optimal design parameters for heat transfer predictions, providing alternative analysis methods, and reducing computational and experimental time. This not only enhances the accuracy of design processes but also enables the prediction of complex thermal behaviours that traditional methods might miss.

Another research strength is the multidisciplinary nature of the study. To the best of the author's knowledge, it is perhaps the only research that successfully combines experimental work, numerical simulations, and artificial intelligence, whilst considering manufacturing philosophies, allowing for a comprehensive evaluation of the heat sinks' performance under

various conditions such as air-cooled, liquid-cooled, and multiphase systems. This holistic approach provides a deeper understanding of the heat transfer mechanisms and offers a robust foundation for future research and industrial applications.

Additionally, the holistic focus on sustainability adds a critical dimension to the research. By incorporating sustainable design and manufacturing principles, this study addresses current performance needs and future environmental responsibilities. It aligns with global sustainability goals by proposing solutions that not only enhance thermal efficiency but also minimise environmental impact through the use of sustainable materials and agile product development. This focus ensures that the designs are relevant and feasible in a market increasingly driven by ecological considerations.

Moreover, the study provides practical insights for industry applications. The proposed bio-inspired pin-fin heat sinks, with their optimised geometries, offer a solution for modern high-performance electronics, where compactness, efficiency, and reliability are paramount. The study's findings have the potential to influence a wide range of industries, from consumer electronics to automotive and aerospace, offering adaptable solutions that meet the growing demands for both thermal performance and sustainability.

While the research offers a comprehensive examination of bio-inspired pin-fin micro heat sinks, several limitations must be acknowledged. Optimisation through machine learning models is dependent on the quality and availability of training data. Given the specialised and relatively novel nature of micro heat sinks, limited data availability could impact the accuracy of the models. Additionally, the reliance on representativeness and the relevance of selected features further underscores the importance of data quality in achieving reliable results. Although the study integrates both experimental data and numerical simulations, replicating real-world operating conditions—particularly in two-phase flow boiling systems—presents challenges. Experimental constraints, including equipment limitations, measurement precision, and result reproducibility, introduce further uncertainties into the findings.

Beyond data limitations, practical constraints arise in terms of material efficiency, cost, and environmental impact, all critical to the sustainability focus of the research. The assumed uniformity of material properties, as well as simplifications in geometry within computational fluid dynamics (CFD) simulations, could overlook some real-world complexities. Boundary conditions such as fixed temperature or heat flux, and the assumption of steady, incompressible flow in CFD models, may also not fully capture the variability of operational conditions.

Additionally, achieving the balance between cost-effective and scalable manufacturing processes for micro-scale structures remains a key challenge, particularly as the study aims to balance economic feasibility with environmental responsibility. By clearly outlining these constraints and assumptions, a clearer context for the inherent limitations within the methodology is provided, guiding the interpretation of results and their application in future.

In summary, this study is an important work that successfully integrates cutting-edge technologies and sustainable design principles, significantly enhancing heat sink performance optimisation. Its potential to influence both research and industrial practice makes it an important contribution to the evolving landscape of heat transfer solutions. Nevertheless, the author acknowledges any limitations or criticism arising from this work. Addressing these limitations in future studies will enhance the robustness and broader applicability of the proposed designs, refining their potential within the field of thermal management. Fig. 1.3 shows the sample Strength, Weakness, Opportunities, and Threats (SWOT) analysis performed that summarises the research strengths and limitations, serving as a guideline for the overall research process.

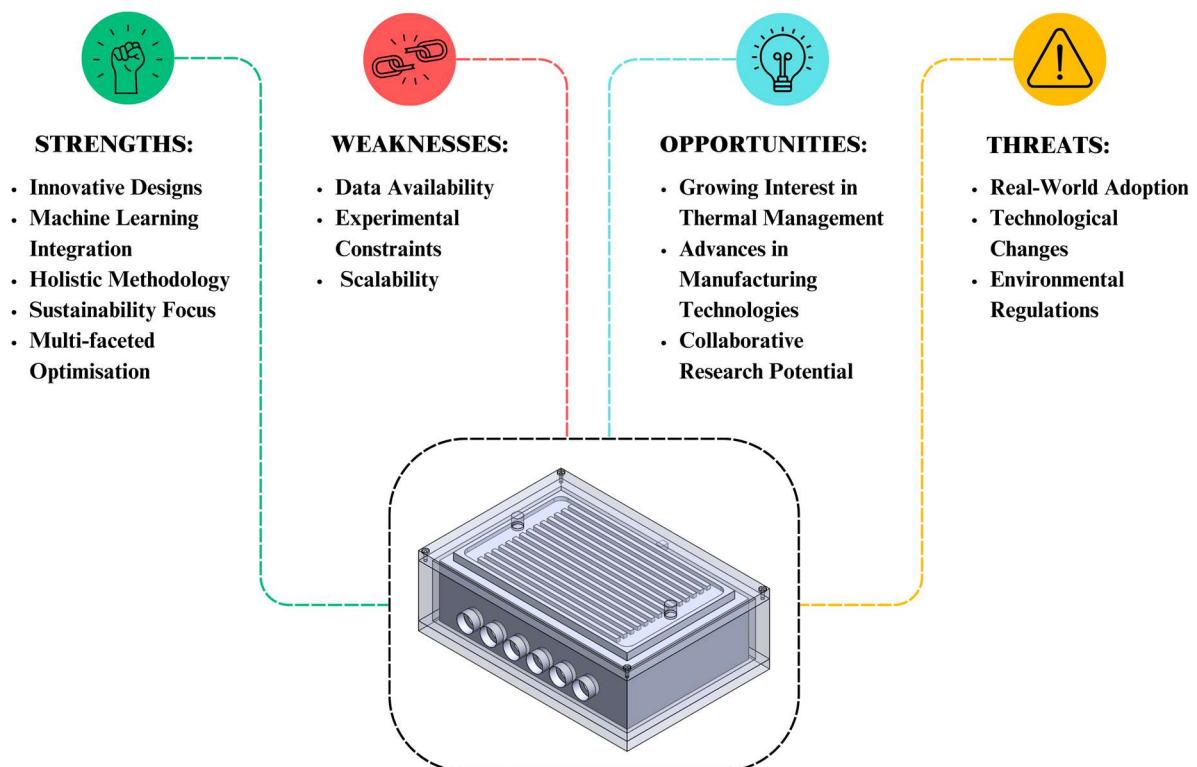


Fig. 1.3 Research SWOT analysis

Chapter 2: Literature Review

Chapter Precursor: English

“All that is gold does not glitter,

Not all those who wander are lost;

The old that is strong does not wither,

Deep roots are not reached by the frost.”

— JRR Tolkien

This quote mirrors my 10-year academic journey in the UK and sets the tone for the Literature Review. Just as the true value isn't always immediately visible and exploration isn't aimless, my deep dive into micro heat sink technologies has been a meaningful journey of discovery. The chapter explores foundational studies—the deep roots of the field—that, while not always in the spotlight, provide essential support for innovation. By highlighting these enduring contributions, the Literature Review parallels my growth, emphasising that perseverance and profound understanding lead to significant advancements in research

2.1 Background to the Chapter

As we are pushing the boundaries of what our everyday gadgets can do, they are generating more and more heat, creating a pressing challenge for engineers and designers. For instance, imagine trying to keep your smartphone cool during long gaming/social media sessions or ensuring your laptop does not overheat during an intense work project. These everyday situations underscore the critical role of effective thermal management. Even a few decades ago, cooling electronic devices was relatively straightforward, often relying on passive methods such as natural airflow. However, devices are now packed with high-performance components in increasingly confined spaces, pushing the limits of traditional cooling methods. This shift has driven the development of more advanced solutions, turning heat management into a sophisticated engineering and global sustainability challenge.

Thermal management techniques are generally categorised into passive and active systems. Passive techniques utilise natural processes to dissipate heat. This might involve spreading heat through the three fundamental heat transfer methods, namely, conduction, convection, and radiation. These methods are often simpler and do not require additional power, making them cost-effective for many applications. On the other hand, active thermal management involves using external energy or pumping power to enhance cooling. This category includes fans, liquid cooling systems, and thermoelectric coolers. All these solutions introduce diverse mechanisms to actively move heat away from sensitive components, allowing for better temperature control.

This literature review section dives into the various electronic cooling techniques available currently, with a particular emphasis on heat sink technology. Heat sinks are critical components that help dissipate heat away from high heat flux electronic components, and their design and mechanisms have evolved significantly over the years. Therefore, the section will explore different types of heat sinks, including traditional and advanced designs, but mainly focus on micro heat sink-based technologies such as microchannels and pin-fin heat sinks; this is because these micro heat sinks are becoming increasingly important as electronic devices move towards the "micro" scale and become compact and powerful.

Overall, this literature review chapter endeavours to provide a detailed understanding of the current advancements in relevant technologies. Here, we will discuss recent research, highlight major innovations, and examine the practical applications of these technologies. By the end of this review, readers will have a clearer picture of the state-of-the-art strategies, techniques in thermal management, and the trends shaping the future of electronic cooling systems.

2.2 Fundamental Heat Transfer Mechanisms

Heat transfer is an integral and critical phenomenon for most modern-day industries, most significantly for electronic devices, power plants, sustainable energy, and thermal management systems. Whether it is for digital applications, engineering systems or even biological processes, all involve different types of heat transfer or exchange on the macro or the micro scale. Heat transfer, in the simplest form, broadly refers to the thermal energy transfer from high-temperature to low-temperature regions; it primarily occurs due to complex physical interplay triggered by the temperature gradients between two points or objects [40]. Currently, designing efficient heat transfer systems is essential for regulatory, safety, performance, economic, and sustainability reasons. Conventionally, there are three primary methods of heat transfer: conduction, convection, and radiation — each working via its unique mechanism. The temperature and thermal energy distribution of a system are dictated by these three heat transfer mechanisms working in unison; however, depending on the type of the system, one heat transfer mechanism may exert a more dominating effect than the others.

Conduction occurs mainly within solid materials due to interactions between atoms or molecules. When heated, the particles gain kinetic energy and vibrate, transferring thermal energy to neighbouring particles. Fourier's law gives the rate of conductive heat transfer:

$$Q = -k \cdot A \cdot \frac{\delta T}{\delta x} \quad (1)$$

Where: Q is the heat transfer rate (W/m^2); k is material's thermal conductivity (W/mK); A is the cross-sectional area (m^2); $\frac{\delta T}{\delta x}$ is the temperature gradient across the material [41].

The equation shows that the heat transfer rate is directly proportional to the temperature gradient and thermal conductivity. High thermal conductivity materials, like metals, are more efficient in transferring heat than insulators like ceramics or plastics. In the context of this research, conduction is not a primary focus due to the lower conductive heat transfer in fluids.

Convection involves heat transfer through the bulk motion of a fluid (liquid or gas). Convection can significantly enhance heat transfer rates compared to conduction alone [42]. It can be classified into natural and forced convection. Natural convection occurs due to buoyancy effects, while forced convection uses external means, such as pumps, to enhance fluid movement and heat transfer [43]. Newton's law of cooling describes convective heat transfer rate as:

$$Q = h \cdot A \cdot (T_s - T_f) \quad (2)$$

Where: Q is the heat transfer rate; h is the convective heat transfer coefficient (HTC, W/m^2K); A is the surface area; T_s is the surface temperature (K); T_f is the fluid temperature.

The Nusselt number (Nu) can also measure convective heat transfer [44], defined as:

$$Nu = \frac{hL}{k} \quad (3)$$

Where: h is the convective heat transfer coefficient; L is a characteristic length; k is the thermal conductivity.

Different flow regimes (laminar, transitional, and turbulent) affect convective heat transfer. In this research, the focus is on forced convection to achieve enhanced heat transfer rates. To analyse flow behaviour and boundary layers, the **Reynolds number (Re)** is calculated by:

$$Re = \frac{\rho \cdot u \cdot L}{\mu} \quad (4)$$

Where: ρ is the fluid density (kg/m^3); u is the velocity (m/s); L is a characteristic length (sometimes referred to as the hydraulic diameter, m); μ is the dynamic viscosity (Ns/m^2) [45].

Radiation is the transfer of heat via electromagnetic waves. Radiation has a minimal impact in this study and is not a primary consideration in the experiments and simulations. However, the Stefan-Boltzmann law quantifies the total radiated power:

$$P = \epsilon \sigma T^4 \quad (5)$$

Where: ϵ is the emissivity of the surface (no unit), σ is the Stefan-Boltzmann constant (W/m^2K^4), and T denotes the temperature. In the context of this research, radiative heat transfer has a minimal impact and will mostly be ignored during experiments, simulations, or any other analysis.

2.3 Boiling Heat Transfer Mechanisms

Boiling heat transfer is a dynamic process in which a liquid undergoes a phase change from a liquid to a vapour while transferring heat from a solid surface. The boiling process can occur in various modes — with distinct characteristics and applications. Therefore, boiling can be classified or characterised by a boiling curve, originally introduced by Nukiyama in the 1930s [46]. When heating a surface in a liquid pool, the heat flux is commonly plotted against the excess temperature ΔT_{excess} , defined as the difference between the surface and liquid saturation

temperatures. Fig. 2.1 illustrates a classical boiling curve governed by surface superheat, which includes natural convection, nucleate boiling, transition boiling, and film boiling; additionally, flow boiling is a type of forced convection boiling. The various modes of boiling heat transfer—nucleate boiling, flow boiling, transition boiling, and film boiling—play important roles in a wide range of applications across multiple industries. Each mode offers distinct advantages and is significant for specific scenarios [47]. The following sections provide a breakdown of different boiling heat transfer modes.

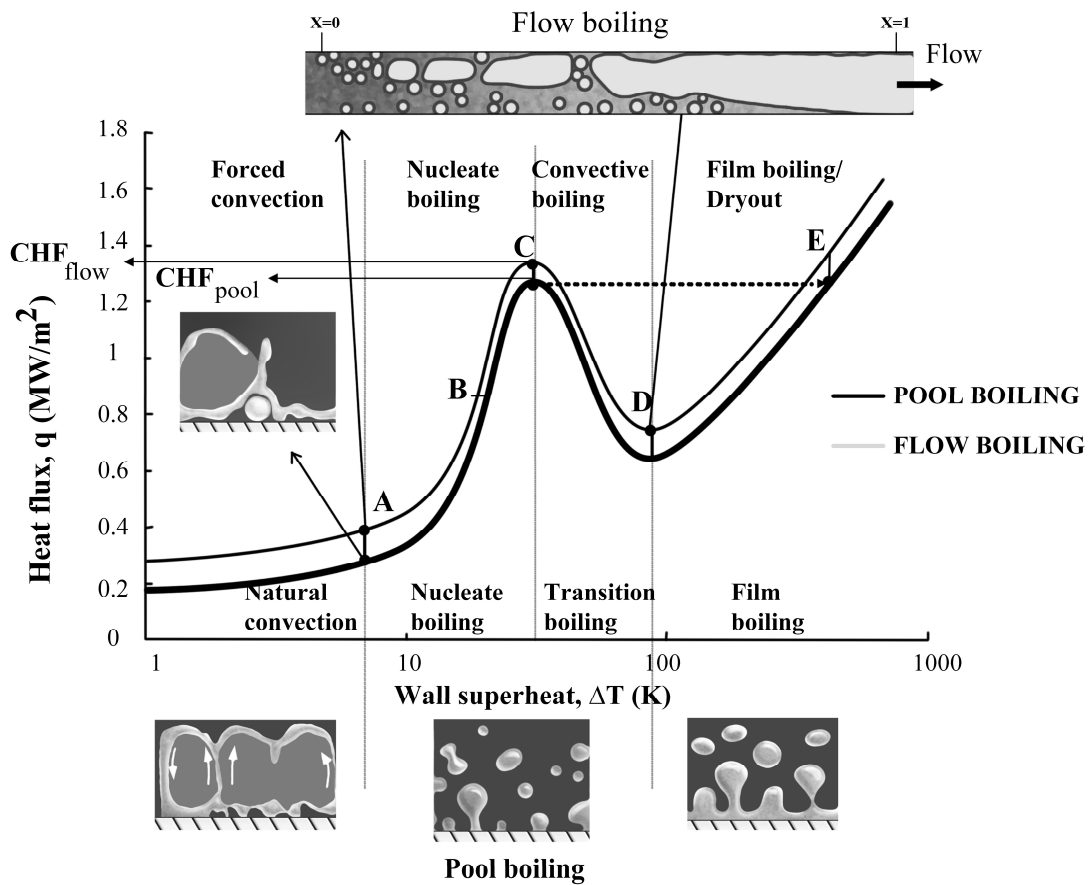


Fig. 2.1 Typical boiling curve [46]

2.3.1 Nucleate Boiling

Nucleate boiling can be characterised by small vapour bubble formations at discrete nucleation sites on a heated surface. The vapour bubbles detach and rise through the liquid, allowing continuous heat transfer. Nucleate boiling is highly efficient at transferring heat, offers high heat transfer coefficients, and is typically the dominant mode of boiling at low heat flux applications. Nucleate boiling is a common observation in conventional applications such as cooking, boiling water, and heating domestic water. In industrial settings, nucleate boiling is employed in electronic cooling components, ensuring they operate within safe temperature

limits. Nucleate boiling is vital in heat exchangers/heat sinks, which require thermal energy transfer between a hot fluid/surface and a colder fluid. The rapid heat transfer rates associated with nucleate boiling make it a preferred choice for achieving efficient heat exchange. Moreover, nucleate boiling can also be found in chemical processing for tasks like solvent recovery, distillation, and chemical synthesis; the efficiency of nucleate boiling in heat transfer aids in maintaining precise temperature control during chemical reactions. Nevertheless, despite its advantages, nucleate boiling can lead to surface fouling due to the accumulation of impurities at nucleation sites. Additionally, at high heat fluxes, nucleate boiling can transition to film boiling, which can reduce heat transfer efficiency [48].

2.3.2 Film Boiling

In film boiling, a thin vapour film forms between the heated surface and the liquid preventing direct contact between the liquid and the surface. This results in a significant reduction in heat transfer efficiency. Film boiling occurs at very high heat fluxes and surface temperatures, and it is characterised by low heat transfer coefficients, leading to equipment overheating if not managed properly. Therefore, film boiling is typically undesirable in most applications due to its reduced heat transfer efficiency [47]. However, in specific applications, film boiling can be important. For instance, in quenching processes, film boiling is intentionally used for rapid cooling of hot metals to harden them and achieve controlled cooling rates to obtain desired material properties. Moreover, understanding film boiling is vital for nuclear reactor safety in predicting/mitigating film boiling, preventing overheating and maintaining reactor integrity.

2.3.3 Transition Boiling

Transition boiling occurs between nucleate boiling and film boiling and is characterised by intermittent contact between the liquid and the heated surface, with vapour and liquid regions coexisting simultaneously. Transition boiling is typically associated with moderate heat fluxes and surface temperatures. Heat transfer rates in transition boiling are higher than in film boiling but lower than in nucleate boiling. Thus, due to its semi-effective heat transfer capabilities, it exists in various applications, including industrial boilers, steam generators, and refrigeration systems. Much like in the case of film boiling, transition boiling helps control the heat transfer process and prevent overheating, contributing to reactor safety. Additionally, transition boiling can occur in heat exchangers and heat sinks under certain conditions. Thus, understanding and managing this mode is essential for maintaining heat transfer and preventing overheating [49].

2.3.4 Flow Boiling

Flow boiling, also known as forced convection boiling, occurs during liquid flows over heated surfaces or through a channel or pipe while undergoing a liquid-to-vapour phase change. The flow boiling process combines the complexities of fluid dynamics and phase change heat transfer and can be generally observed in applications where efficient cooling or heating is required. Flow boiling can be characterised via various two-phase flow patterns, including but not limited to jet flow, annular flow, slug flow, churn flow, stratified flow, and mist flow, among others. The flow boiling patterns depend on many factors such as flow rates, channel geometry, heat flux, surface modifications, etc. — each pattern/flow type has distinct heat transfer characteristics and flow behaviours. Flow boiling involves nucleation sites, similar to nucleate boiling, on the heated surface where small vapour bubbles form. However, in flow boiling, these bubbles are continuously carried away and replaced by the flowing liquid, allowing for more efficient heat transfer [50].

Flow boiling is known for its high heat transfer coefficients, making it a good candidate for applications where efficient heat dissipation or heating is critical. The phase change from liquid to vapour enables substantial heat absorption and finds applications in various industries, including refrigeration, electronics cooling (heat sinks), chemical processing, and power generation. Flow boiling is particularly well-suited for cooling electronic components due to its efficient heat transfer capabilities. Nonetheless, flow boiling can also bring its own set of challenges, such as flow instabilities, pressure drop fluctuations, and the need to predict and manage critical heat flux (CHF) to prevent equipment from overheating [50].

2.3.5 Variations of Primary Boiling Modes

The four primary modes of boiling heat transfer discussed in more initial chapters encompass the most common and significant scenarios in which boiling heat transfer occurs. However, variations and complexities exist depending on various conditions, such as pressure, temperature, and fluid properties. Here are a few sub-categories and variations:

1. **Pool Boiling:** occurs when a liquid boils in a stagnant pool on a heated surface, typically in open vessels or containers. It exhibits similar phase-change modes described above (nucleate, transition, and film boiling) but within a pool of liquid. Pool boiling is essential in both household and industrial settings, contributing to efficient heat generation and transfer for various applications. Its importance lies in its versatility and reliability in heating and cooling processes [51]. Pool boiling is routinely observed

in typical domestic applications, such as cooking on stovetops and heating water in kettles. It fulfils a fundamental role in preparing food and providing household hot water. In industrial settings, pool boiling is used for heating massive volumes of liquids in tanks and vessels. It is also employed in industries ranging from food processing to chemical manufacturing for applications such as refrigeration, heat exchangers and industrial boilers for power generation and heating.

2. **Onset Nucleate Boiling (ONB):** a critical point in the boiling process where the first vapour bubbles begin to form on a submerged heated surface. It triggers the transition from a purely liquid-phase heat transfer to the initiation of nucleate boiling.
3. **Subcooled Nucleate Boiling:** occurs when the bulk liquid temperature (T_m) is below its saturation temperature (T_{sat} , subcooled) and shows nucleation sites on a heated surface — leading to vapour bubble formations. Subcooled nucleate boiling combines characteristics of nucleate boiling and convective heat transfer.
4. **Partial Nucleate Boiling:** in some scenarios, nucleation sites may be active only partially on a distinct portion of a heated surface, leading to partial nucleate boiling and non-boiling regions on the same surface coexisting simultaneously.
5. **Critical Heat Flux (CHF):** CHF represents the maximum heat flux the liquid can sustain without a catastrophic temperature rise. Beyond this point, the heat transfer process becomes unstable, leading to phenomena like vapour explosions, dry-out or burnout [52]. Therefore, accurately predicting and managing CHF is critical in various applications, particularly electronic chips, nuclear reactors, or other high-power electronic applications [53].
6. **Leidenfrost Effect:** happens when a liquid droplet comes into contact with a significantly hotter surface than its boiling point. As a result, instead of instantaneous boiling, the droplet can levitate on a vapour cushion created by rapid vaporisation [54]. It is commonly observed when water droplets skitter across a hot pan or a stovetop.

While these variations and phenomena occur within the primary boiling modes, they are typically considered special cases or transitional behaviours and not separate modes of boiling heat transfer. The primary boiling modes, including nucleate, flow, transition, and film boiling, remain part of the fundamental categories in most practical heat transfer scenarios.

2.4 Thermal Management Techniques

Thermal management mainly falls into active and passive techniques [55]. Passive thermal management relies on natural heat dissipation mechanisms without requiring external power. Among these methods, one of the most effective techniques is through heat sinks, which transfer heat away from electronic components to a larger surface area, allowing it to dissipate into the surrounding environment. Heat sinks are typically manufactured from aluminium or copper due to their high thermal conductivity. Similarly, thermal spreaders are another passive option that helps distribute heat from a hot spot to a larger area. Again, materials like copper, aluminium, or embedded elements such as graphite are often used as thermal spreaders [56]. Moreover, Phase Change Materials (PCMs) are widely used in passive thermal management systems. PCMs, such as paraffin wax, absorb and release stored thermal energy during phase transitions, providing thermal shielding by absorbing large amounts of heat without significant temperature increases [57]. Lastly, heat pipes offer another efficient passive strategy. These sealed tubes contain a liquid that evaporates at the hot end and condenses at the cooled end [58].

Active thermal management uses external power sources to enhance heat transfer. Forced convection, for example, uses fans or blowers to increase airflow over heated sources [59], with axial fans commonly found in desktop computers and blowers in compact spaces. Liquid cooling circulates a coolant through channels to absorb and transport heat away from components, cooling it via a microchannel, radiator or heat exchanger [60]. This method is popular in high-performance computing, gaming systems, and industrial processes, with closed-loop systems requiring minimal maintenance and open-loop systems offering customisation. Thermoelectric Coolers (TECs) utilise the Peltier effect to transfer heat, making them ideal for precision cooling in applications like laser cooling and portable coolers. Peltier modules are used in small-scale cooling, while thermoelectric heat pumps provide temperature control in sensitive devices [61]. Furthermore, techniques like Electrohydrodynamic (EHD) pumps and ultrasonic-assisted cooling use external energy sources within heat sinks [62].

Hybrid thermal management combines passive and active techniques to optimise thermal performance. Examples include heat sinks with fans, which enhance heat dissipation by pairing passive heat sinks with active airflow, and liquid-cooled heat sinks, which integrate liquid cooling with traditional heat sink designs for improved thermal efficiency. Looking at current trends, heat sinks remain the most popular method for cooling electronics [63]. Fig. 2.2

summarises the prevalent thermal management techniques; however, note that this list is not exhaustive and only highlights some major active and passive methods and their application.

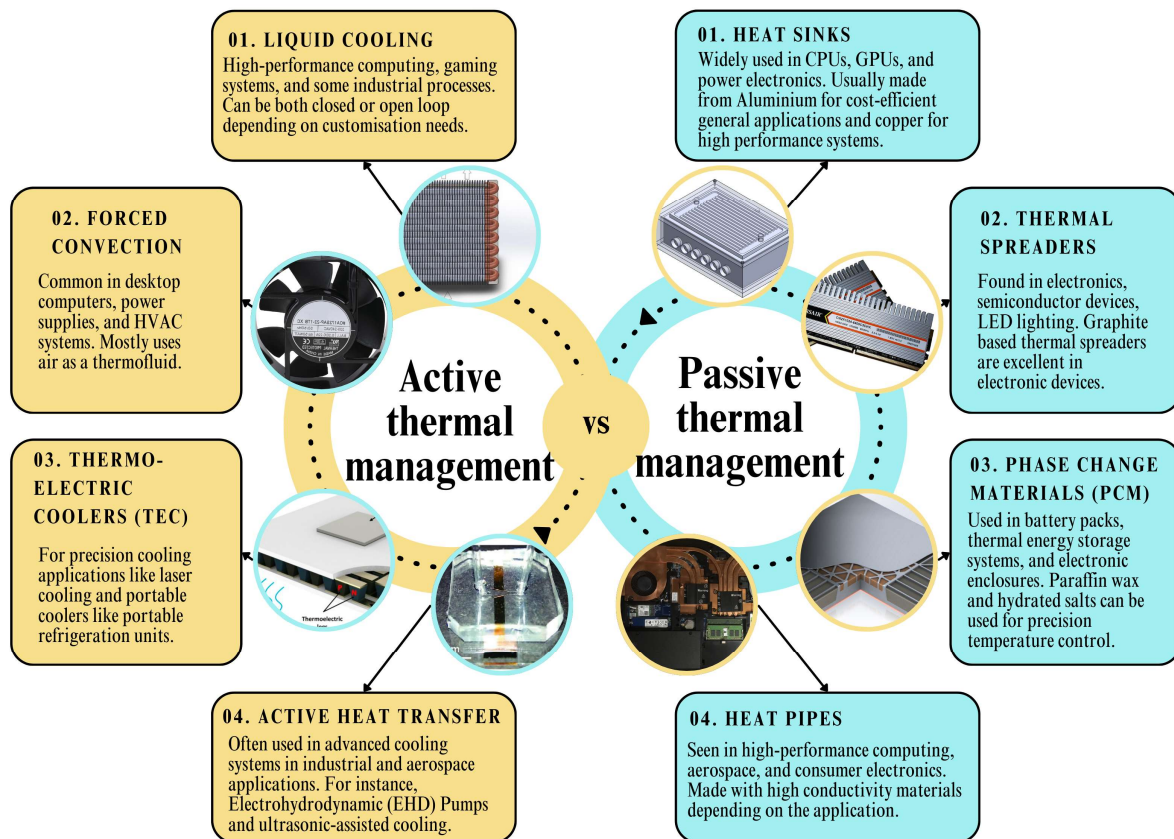


Fig. 2.2 Overview of thermal management techniques

2.5 Micro Heat Transfer: Recent Trends and Perspectives Overview

Due to their effective heat transfer enhancement potential, micro heat sinks (MHS) primarily rely on microchannel-based heat sink (MCHS) technologies. Microchannels are an active area of research; for example, a Google Scholar search with the keyword "microchannel heat transfer" returns 335,000 results (427,000 when including patents). Therefore, understanding current research trends and gaining a holistic overview of recent strategies and methodologies in the literature is essential. Initially, data for this review was collected through descriptive and exploratory analysis, qualitative data, and findings from existing literature. This data was then converted into quantitative results and graphs to analyse and identify potential research gaps and trends in recent microchannel experimental investigations. Reviewing the existing literature helped establish the initial baseline for this thesis. Consequently, a variety of databases were explored, including Google Scholar, OpenAthens, Shibboleth, and journals such as Elsevier, Emerald, IEEE, SAGE, and Springer. Also, the methodology to conduct a

review was inspired and adapted from the work of [2,35,64,65]. The extant research has reviewed MC technologies focusing on electronic cooling [2], configurations and patents [64], heat sink applications [65], and modelling strategies [35].

Therefore, this review adapted from previous work and combined various aspects to produce a more diverse and holistic overview of current research levels, status, and trends in MCHS heat transfer and thermal management applications. The search methodology followed a funnelling process using broad keyword variations to maximise the chance of identifying relevant research articles. The author was mindful of previous studies suggesting methods based on relevance, publishers, year, industries, etc. Acknowledging these suggestions, the inclusion criteria for this literature review were peer-reviewed journal papers, titles or abstracts containing any variations of the used keywords related to MC experiments and investigations. Also, the initial search mainly focused on research papers dating from 2017 to 2023; recently, a five-year timeline has been followed by [35] for their review. Therefore, being mindful of the ever-decreasing product development times [66,67]. The seven-year range was deemed appropriate and selected to be more up-to-date with modern industrial and technological practices and to develop research questions aligned with current scopes.

All microchannel (MC) applications were initially considered the whole population data to determine an optimal sample size. The focus was then narrowed to heat transfer topics, such as cooling, mixing, flow boiling, and related research areas. Ultimately, 100 research papers were selected and appraised for their experimental methods, areas of interest and impact, and recommendations for future investigations. The qualitative findings were categorised into a newly developed Materials, Enhanced Flow Control, Design, and Sustainability (MEDS) framework, which consists of four primary perspectives: material usage, experimental methods, design, and sustainability elements. The MEDS framework systematically helped identify potential research gaps. If articles covered multiple perspectives, qualitative emphasis was placed on experimental methods and research recommendations to categorise literature.

The sample of 100 papers was considered ideal for appraising the current state-of-the-art literature. However, not all research papers were suitable for selection, as some lacked the necessary depth or did not align with the analysis needs of this paper. Initially, searches on Google Scholar based on the keyword and inclusion criteria yielded approximately 17,500 potential research articles. Considering this as the target population, a sample size of 96 was deemed sufficient to make statistical inferences at a 95% confidence level with a 10% margin

of error. The sample size was determined using a combination of suggestions from Farrell, et al. [39] and the SurveyMonkey calculator [68]. Furthermore, it is widely debated that no universal rule exists for determining the appropriate size in convenience sampling. Fellows and Liu [69] have indicated that a sample size of 30 can be acceptable for making statistical analyses and inferences. Therefore, based on these calculations and previous studies, a sample size of 100 was arguably sufficient to assess current literature trends. The following equation was used to calculate the sample size for statistical analysis:

$$\text{Sample size} = \frac{\frac{z^2 \times p(1-p)}{e^2}}{1 + \left(\frac{z^2 \times p(1-p)}{e^2 N}\right)}$$

Where: N = population size (17500); p = population proportion (assumed 50% in this case); z = z-score (1.96); e = margin of error (10% or 0.1).

2.5.1 Material Perspective

2.5.1.1 Working fluids

The use of different working fluids (WF) for MC during multiphase flow has been explored using hydrophobic sunflower oil and water as WF. To illustrate, Chiriac et al. [70] monitored multiphase flows in MC using two immiscible WFs. The flow visualisation and μ PIV (micro micro-particle image velocimetry) measurements validated numerical results qualitatively and quantitatively. Their research advised quantitative exploration of the influence of material properties' ratios and applying similar methods with non-Newtonian fluids with high viscosity.

Hoang et al. [71] experimentally investigated a two-phase cooling heat sink using a hydrophobic dielectric (Novec/HFE-7000) WF. The heat transfer coefficient (HTC) increased with the flow rate in the single-phase and convective boiling region; in the nucleate boiling region, HTC increased notably with heat flux (HF). This increasing trend of HTC with HF was attributed to the refrigerant properties. Compared to water, the WF had lower surface tension and contact angle that generated bubbles with smaller departure diameters; thus, the refrigerant WF experienced nucleate boiling over a greater MC length and produced a positive trend of HTC with HF [72]. Also, HTC improved with reduced subcooling in the heat sink at the cost of increased pressure drop. Thus, the coefficient of performance (COP) was primarily dependent on subcooling in two phases. Fin height reduction produced better thermal performance until the optimum point due to a higher fluid penetrating factor. The experimental

findings can be related to Novec-type WF and utilised for different features: HFs, subcooling, Reynolds numbers, and DH.

Dalkılıç et al. [73] analysed HTC and critical HFs of R134a (generally hydrophobic) in two-phase flows. The results showed that raised vapour quality at constant inlet saturation temperature decreases Critical Heat Flux (CHF) and HTC. At the constant inlet vapour quality, the CHF lowered, and HTC increased with inlet saturation temperature. Nevertheless, a relatively higher temperature difference is required to reach the CHF at reduced temperatures than high inlet saturation temperatures.

Guo et al. [74] researched pressurised filling processes of two working fluids in a porous closed-loop MC; the theoretical presumptions agreed with the experimental results. Their investigation successfully generated acoustic waves via hydrophobic eutectic gallium-indium (EGaIn) compound usage in MC. The recommendation for future work suggested assessing the feasibility of self-aligned comb-shaped single-electrode interdigital transducer (IDT) adoption in the industry.

Alternatively, Abdulbari et al. [75] employed a hydrophilic Xanthan gum as a drag-reduction (DR) agent for flow assessment in MC. The solution exhibited non-Newtonian behaviour due to increased viscosity from increasing concentration. The %DR increased by raising additive concentration, length of MC, and decreasing the width. Future research could involve advanced flow visualisation techniques with polymer molecular weight effect on DR.

Chiriac, et al [76] investigated the interface evolution between two immiscible liquids in a three-branch symmetric microchannel, both numerically and experimentally. The aim was to compare numerical data with experimental results and evaluate the VOF method in Fluent for tracking the interface. Focus is placed on the oil-water interface near the bifurcation in a 400 μm wide, 50 μm high microchannel. Micro-PIV measurements are performed in water, with results confirming the 3D simulations. The flow case is proposed as a benchmark for studying interfaces in branching microchannel geometries.

2.5.1.2 Nanofluids/nanoparticles

Experimental investigations with nanofluid/nanoparticle utilisation are another promising research area. Nanofluids are insoluble particle suspensions using solid materials (within the average size of 0–100 nm) [77]. Compared to pure liquids or water, high nanofluid concentrations show better thermal stability [78]; they can also provide improved cooling solutions and HTC [79]. Martinez et al. [80] developed an experimental methodology for

studying Titanium dioxide (TiO₂)-H₂O-based nanofluids as coolants in MCHS. Nanoparticle dispersion increased the base fluid thermal conductivity (k) within the examined temperature. Furthermore, incorporating nanoparticles into water improved heat dissipation in MCHS for the studied concentration range. The optimum thermal energy gain was shown by the nanofluid having a concentration of 1wt% and $Re = 200$. As a result, a more suitable MCHS nanofluid arrangement can be studied for subsequent research.

Also, Ding et al. [81] appraised the effect of TiO₂-H₂O nanofluids in thermal energy storage (TES) MC to enhance the thermal conductivity (K) of phase change materials (PCM). TiO₂-H₂O nanofluids having 0.5, 0.7, and 1.0 wt% can increase Nusselt number in the melting and solidification process. TiO₂-H₂O nanofluids addition results in increased pressure drop (<9%). Therefore, more TiO₂-H₂O applications with improved pressure drops can be investigated.

Sarafraz and Arjomandi [82] explored the potential usage of liquid metal for HF transfer for next-generation solar thermal energy receivers. Liquid Gallium (Ga) showed superior thermal diffusion, conductivity, improved HTC, and heat transfer rate compared to water. Similarly, nanoparticles augmented HTC due to the internal thermal conductivity of Al₂O₃ and the Brownian motion of Ga nanoparticles. The pressure drop penalties were significantly higher for Ga nano-suspensions and pure Ga compared to water. Thus, Ga suspension applications for high HF applications with reduced pressure drops need assessment.

In a separate study, Sarafraz and Arjomandi [77] investigated low HF conditions using an MCHS for thermal and pressure drop performances; the nanofluid used was copper oxide/indium (CuO/In). Higher HTC was observed for increased HF, peristaltic mass flow, and mass concentrations of over 8%. A high-pressure drop penalty was present for the liquid Indium nanofluid at a mass concentration above 8%. Thus, CuO/In nanofluids application with reduced pressure drop penalties needs analysis.

In another investigation, Sarafraz et al. [83] assessed the thermal performance of MCHS in laminar flow. Silver (Ag) nanofluids improved HTC but at the cost of increased pressure drop, thermal resistance, and friction factor. Hence, the feasibility of Ag/water nanofluids with reduced friction factors and pressure drops in the micro-electric cooling application needs further exploration. Sarafraz et al. [84] also studied thermal performance and fouling inside a MCHS using a carbon-nanotube (CNT)-water nanofluid. The nanofluid produced a higher HTC and reduced temperature profile compared to water. The results also indicated that nanofluid flow rate and mass highly increase HTC. Also, increasing mass concentration

reduced the operating time to reach uniform fouling thermal resistance, but overall thermal resistance decreased with increasing nanofluid concentration. As a result, CNT usage requires further investigation related to friction factors and pressure drop penalty.

On a different take, Simsek et al. [85] experimented with complementary metal oxide semiconductor (CMOS)-compatible monolithic MCHS convection heat transfer and pressure drop using Ag-nanowire suspension. Silver nanofluids showed the highest HTC amongst the examined working fluids, but all had similar hydrodynamic performance. A 56% increased HTC is possible without added pumping power. Thus, the adoption of Ag-nanowire suspension shows promise for heat transfer improvements.

Wang et al. [86] investigated hierarchical microchannels and nanofluids for electronic cooling. It compares rectangular and circular microchannels with varying diameters and nanoparticle concentrations, assessing pressure drop, cooling uniformity, thermal resistance, and heat transfer coefficient. Rectangular microchannel-b has the highest heat transfer coefficient, while microchannel-a shows the lowest cooling uniformity. Circular microchannels generally offer better performance (PEC 1.26 vs. 1.08) but the rectangular microchannels have slightly lower thermal resistance.

2.5.1.3 Surface treatment/manipulation

The extant literature also indicates possibilities through surface manipulation using various materials to reach desired effects. Ahmadi et al. [87] conducted flow boiling experiments on wholly hydrophobic and three mixed wettability surfaces for a high aspect ratio (AR) MC. The biphilic surfaces (BS) performed better than the fully hydrophobic surface. Additionally, BS provided vapour breakup, enhanced flow boiling heat transfer, and reduced the time of bubbly flow regime; however, they extended the slug flow regime. Hence, BS for high heat flux cooling can be examined.

Zhang et al. [88] investigated surface wettability by studying boiling heat transfer features on 3D heterogeneous surfaces with diverse wettability. The highest HTC was found in test surface three (TS3), over six times compared to a bare 2D surface (BCS). The BCS consisted of a copper surface polished with 5000-grit sandpaper having a water droplet contact angle of 88.6° ; the TS3 was a fluoridized copper oxide surface with a contact angle of 156.1° — meaning a hydrophobic/superhydrophobic surface having no affinity to water [89]. However, the highest CHF was in TS2, over 60% more than BCS. The TS2, on the other hand, was made via thermally oxidising the BCS at 400°C to produce an oxidised copper layer with a contact

angle of 8.6° — meaning a hydrophilic surface [89]. Consequently, the synergistic wettability effects and microstructures were linked to producing oblate and conical bubble growth patterns. This research provided a guideline for further MC developments with different wettability exhibiting hydrophobic and hydrophilic characteristics.

Yin et al. [90] examined the chemical absorption effects on the formation of dynamic characteristics and preliminary length of Taylor bubbles. The results highlighted that the absorption process causes gas dynamic pressure drop reduction and increased expansion stage time in the total bubble formation process. Therefore, chemical absorption on bubble formation in MCHS can help lead to novel designs. On the other hand, Venegas et al. [91] evaluated a membrane-based micro-desorber design, working via low heating temperatures. The hot water temperature had a direct relationship with the desorption rate, solution temperature and partial pressure to improve the desorption process. Also, increasing the flow rate resulted in a minor reduction of the effective desorption surface; thus, an extended length may be used to reach initial desorption temperatures.

Jayaramu et al. [92] comparatively assessed surface characteristics on flow boiling heat transfer and pressure in an MCHS using three cases: Case-1, freshly machined surface; Case-2, aged Case-1 channel surface after multiple experimentations; Case-3, aged surface but cleaned using 0.1 M hydrochloric acid. Case-2 performed the worst due to increased wettability and thermal oxidation of the heating surface resulting from the repeated experiments; Case-3 performed the best due to increased nucleation site density, but pressure drop changes are minimal. Accordingly, other material surfaces for flow boiling in MCHS are a good topic for further research.

Surfactant usage is also an exciting area of research. Roumpea et al. [93] investigated droplet formation in an organic continuous phase within MC having surfactants. Surfactant additions reduced the squeezing and dripping regime areas but increased the jetting and threading regime areas. In comparison, surfactant-free solutions produced bigger and lower tip-curvature drops. Mean velocities showed that surfactant improved the local velocity difference between two-phase flows. Therefore, studying the dynamics and effects of droplet formation with various surfactants is worthwhile.

Moreover, Liang et al. [94], under condensation conditions, investigated the heat and moisture transfer characteristics of desiccant-coated heat exchangers (DCHE) and MCHE. The experiments revealed that the temperature of hot water correlates positively with

dehumidification but negatively with heat recovery. High inlet air velocity improved heat transfer while desiccant coating hampers it. Furthermore, the pressure drops increase with airspeed; an increase in cooling water temperature shows a minor reduction in the pressure drop, but the hot water temperature exerts minimal effects.

Jiang et al. [95] enhanced a counterflow diverging microchannel heat sink with microscale cavities and nanoscale coatings, significantly boosting boiling heat transfer. It achieves a 4.8 kW heat dissipation rate without reaching critical heat flux and a coefficient of performance over 150,000, far exceeding previous designs. In a separate study, Jiang et al. improved temperature uniformity and achieved a heat flux of $2677 \text{ kW}\cdot\text{m}^2$, with a 45.1% increase in heat transfer coefficient, a 73.8% reduction in pressure drop, and 123.1% higher performance compared to traditional co-current designs.

Kumar and Singh [96] studied single-phase flow in microchannels of various sizes, with and without micro inserts, analysing thermal-fluid properties such as fluid flow and heat transfer. Testing with distilled water across Reynolds numbers from 125 to 9985 shows that micro inserts significantly enhance heat transfer performance, though they also increase fluid flow resistance. The addition of micro inserts and smaller channel sizes leads to improved overall performance, as assessed by thermal performance factors.

Wang et al. [97] experimented with microchannels with hydrophilic surfaces and hydrophobic dots, focusing on how dot pitch ($122 \text{ }\mu\text{m}$ to $172 \text{ }\mu\text{m}$) affects flow boiling heat transfer and pressure drop. Experiments with deionised water show that smaller pitch distances improve bubble coalescence and flow patterns. Heat transfer coefficient (HTC), critical heat flux (CHF), and pressure drop are strongly influenced by dot pitch and mass flux. A force-balance model helps predict bubble diameters, providing insights for optimising microchannel designs for boiling.

2.5.1.4 Manufacturing techniques

The availability of different manufacturing possibilities presents new development opportunities. Zhang et al. [98] experimented with 3D-printed manifold MCHS with Inconel 718 for high-heat aerospace purposes. The new design exhibited 25% improved heat transfer density at a coefficient of performance (COP) 62. The authors associated the heat transfer density improvement with size optimisation whilst minimising the mass of the plate-fin heat exchangers. The plate-fin heat exchanger sizing was gained by fixing the mass flow rate and COP to match the core design of a manifold MCHE. Furthermore, the researchers reported that

the additively manufactured design improved HTC due to two key factors — high area-to-volume ratio and manifold-MCHE-inspired strategy that showed heat transfer enhancement in earlier studies. However, in terms of pressure drop, it displayed an expected trend where pressure drops increased with increasing Reynolds number. Moreover, additive manufacturing could produce a fin thickness as low as 0.18 mm. Therefore, further 3D-printed manifold investigations could be a worthwhile area for future investigations.

Yameen et al. [99] studied heat transfer properties of an additively manufactured metal MCHE with complex interior designs — the smallest length produced was 0.48 mm. Thus, more 3D design manifolds can be further examined having non-conventional geometry.

Moreover, Bae et al. [100] presented results of a two-phase, embedded cooling system for high HF electronics. Lower pressure drops and improved HTC were expected for higher ARs in SiC MC fabrication. Future research could cater to the following topics: thinner test chips (200 μm) with deeper SiC trenches for overall thermal resistance reduction and improved fin performance, detailed clogging assessment to prevent MC clogging, thermoelectric cooler into the thin-Film Evaporation and Enhanced fluid Delivery System (FEEDS) Manifold-Microchannel (MMC) system for 5 kW/cm² hotspot cooling.

Mohammed et al. [101] explored scaling up Fischer-Tropsch (F-T) synthesis using 3D-printed stainless steel microreactors with Co-Ru-KIT-6 catalysts. Performance was tested in three configurations (stand-alone, two, and four reactors) at both atmospheric pressure and 20 bar, with syngas at a 2:1 H₂ ratio. All configurations showed comparable CO conversion (85.6–88.4%), methane selectivity (~14%), and selectivity for lower hydrocarbons (6.23–9.4%). Higher hydrocarbon (C₅+) selectivity reached 75–82% at 20 bars, demonstrating the potential of microreactors for scalable F-T synthesis.

2.5.2 Enhanced Flow Control Perspective

2.5.2.1 Flow boiling

Flow boiling optimisation is arguably one of the most sought-after research areas for MC-based applications [102]. Flow boiling is a phenomenon caused when fluids move across a heated surface via external means or the naturally occurring buoyancy effect [103]. It is one type of flow where a phase change can occur and is characterised by a continuous two-phase flow of liquid and vapour [104]. However, due to the multiple dependencies and complex mechanisms behind flow boiling, researchers may sometimes focus on the general heat transfer behaviour during flow boiling rather than the bubble dynamics or phase change regimes [70]

Wang et al. [105] monitored the effects of refrigerant properties, mass flux (MF) and saturation temperature on the flow boiling friction pressure drop. The results show that increasing mass flux and reducing saturation temperature positively impact the two-phase friction pressure drop. Increasing mass flux leads to an increased two-phase friction pressure drop mainly due to the increasing liquid-vapour shear forces and partially from the liquid-solid shear forces. Additionally, two-phase friction pressure drops increase from a reduction in the saturation temperature because decreasing the saturation temperature causes enlarged liquid-vapour velocity differences and increased liquid viscosity. Compared to single-side heating, heating from both sides leads to better two-phase friction pressure drops in MC arrays. Subsequent studies can focus on new empirical methods designed using experimental data that predicts data with high accuracy and a lower margin for error.

Panda et al. [106] experimented with two-phase refrigerant maldistribution in the inlet headers of microchannel heat exchangers (MCHE). The loop header exhibited superior distribution performance. They also provided a comprehensive simulation approach for the MCHS header maldistribution problem. Future investigations can cater to developing a full-scale heat exchanger simulation model with air-side calculations, condensate drainage, flow boiling in MCHS, flow expansion in the expander valve, and dynamics of oil and refrigerant.

Xia et al. [107] researched the technique to reduce continuous flow boiling instability with intermittently moving gas-liquid interface that may potentially trigger pressure drop and wall temperature oscillations — leading to flow control issues and security risks. They proposed straight and triangular ridged MCs using multiple sensor setups. A prediction model highlighted that raising inlet flow restriction, reducing inlet temperature and HTC can reduce flow boiling instability significantly, along with unstable boundary slopes.

On a different take, Jia et al. [108] compared flow boiling between novel and traditional rectangular designs with increasing HF from single-phase to CHF. The porous wall (PW) MC improved onset nucleate boiling, CHF, enhanced heat transfer, pressure drop reduction, and two-phase flow instabilities. Additionally, The PW design contained nucleation sites, and pin-fins provided wicking effects.

Lin et al. [109] numerically investigated single bubble growth by developing a custom solver using the VOF method and Hardt's phase-change model. The results showed flow reversal suppression with increased MF but at the cost of reduced flow boiling enhancement. Finned microchannels provided around 40% less thermal resistance and minimal flow reversal

than a micro gap-microchannel setup. Therefore, further experiments to enhance flow boiling in similar configurations need appraisal.

Oudebrouckx et al. [110] presented an innovative prototype system to measure thermal conductivity (K) under flow conditions via the Transient Thermal Offset (TTO) method. Based on their findings, flow rates can be calculated if K and the specific linear calibration curve for a liquid with this value are known. Moreover, if flow rate and the exponential calibration curves can determine absolute K values under continuous flow. Therefore, combined single systems for flow rate measurement and monitoring during flow boiling applications need exploration.

Li et al. [111] presented bidirectional counter-flow microchannels (CFMC) with regulated mass flux, showing significant improvements over traditional parallel-flow designs. Experiments with deionized water reveal a 42.9% to 53.8% increase in critical heat flux (CHF) and up to 170% enhancement in heat transfer coefficients. Uneven mass flux further improves CHF but may reduce the heat transfer coefficient. CFMC also cuts two-phase pressure drop by 53.4% to 66.7% and offers precise control over temperature and pressure, making it a promising approach for optimising microchannel performance.

Tang et al.'s [112] study enhanced flow boiling heat transfer in microchannels by adding expansion areas. Experiments show that microchannels with three expansion areas increase the heat transfer coefficient by up to 43.3% while keeping pressure drop variation within 3 kPa. The expansion areas also reduced inlet temperature fluctuations, indicating better control of boiling instability. Improved heat transfer is attributed to enhanced bubble nucleation and a nonuniform liquid layer near the expansion corners.

2.5.2.2 Phase change flow patterns

Phase change phenomena is another vital element related to MC-based technologies. The term phase change is a broader term that can refer to the transition of one state or phase of matter to another: for instance, solid to liquid, liquid to gas, gas to liquid, or even gas to plasma. Phase changes usually have technical terms such as melting, freezing, condensation, and boiling, amongst many other forms [113]. While the previous section deals mainly with general heat transfer and flow control aspects of flow boiling and two-phase flow, this section caters for the flow regime, patterns, and bubble dynamics. The phase change during flow boiling/condensation changes the fluid volume, crystalline structure, and frictional resistance. Therefore, as the literature indicates, these phase changes impact the HTC, shear forces, and velocity in the liquid-vapour flow regimes — which in turn, affect the overall heat transfer.

Matin and Moghaddam [114] studied elongated bubbles and wavy-annular regime transitions during flow boiling in rectangular MC with varying aspect ratios. The wavy-annular flow transitions link to the thickening of the liquid film and a drastic increase in the vapour velocity; this drastic change makes the interface go into unstable (wavy) transitions. Low vapour velocities resulted in a transition to annular flow with increased channel height (reduced aspect ratio). Therefore, critical shear stress at the vapour-liquid interface was suggested.

Furthermore, Lei et al. [115] investigated the effects of dispersed phase viscosities, continuous phase viscosities, and two-phase flow parameters on droplet length. The dominating factors for flows in annular, slug, droplet, and jet regimes were inertia, interfacial tension, shear, and shear and drag forces, respectively. Viscosity fluctuations in the dispersed phase affected flow pattern transition processes of annular flow to slug flow and slug flow to droplet flow; however, it had minimal effect on slug properties and droplet length. Prediction scaling laws were proposed for the slug and droplet lengths formed by different flow patterns.

Another important investigation was presented by Ronshin and Chinnov [116], who determined a novel method for appraising the two-phase flow patterns and regime boundaries. Transitions from one regime to another can occur as follows: jet to bubble – increasing bubble formation frequency and liquid's superficial speed; jet to a stratified – massive increase in the film region's lower walls and raising superficial gas speed; stratified to annular – significantly increasing the film area's upper wall via an increase in the superficial liquid's speed; bubble to the churn – destroying horizontal liquid bridges and, thus, reducing the frequency of bubble formation via increasing the gas velocity. Slug generation and control during phase change improved thermal management and heat transfer.

Qian et al. [117] investigated dynamic dispersed phase injection flow rate effects on slug generation. The experiments to observe dynamic disperse flow rate showed rectangular waves most affected the slug size. Also, the triangle wave affected the separation distance and the slug generation time comparatively more.

Zhang et al. [118] appraised hydrophobic MC with flow condensation of varying ethanol-water mixtures. The flow condensation was highly dependent on the hydrophobic surface; the ethanol concentration increase resulted in slug/bubble flow and no droplet condensation. Similarly, Kovalev et al. [119] studied a liquid-liquid setup having a very low viscosity ratio. The research findings contradicted extant experiments for low plug velocity. Thus, the proposed usage of experimental values for classifying different plug patterns needs analysis.

Pontes et al. [120] optimised microchannel heat sinks for cooling PV panels. Experiments and simulations explore flow boiling effects, revealing stable bubble flow in narrow channels and bubbly flow in wider ones. Numerical simulations using OpenFOAM capture transient flow dynamics and heat transfer, providing insights into channel design and performance.

Wang et al. [121] examined gas-liquid Taylor flow in a 1×1 mm microchannel. Reducing junction width shortens slugs, enhancing heat transfer, particularly at $\beta = 0.5$. At $\beta = 0.67$, performance drops due to higher pressure loss. For $\beta = 0.33$, slug length changes have minimal effect. Increased mixing velocity improves performance, but at low void fractions, the pressure drop may outweigh heat transfer gains. A new correlation for Nusselt number prediction has an average error of 11.77%.

2.5.2.3 Flow resistance

Flow resistance manipulation has been one of the key strategies for heat transfer at microscales. Microscale is a scale for items at the micrometre level, generally used to describe microscopic items ranging from 1 to 1000 μm [7]. Kravtsova et al. [122] investigated three flow regimes and the resistance effects of external periodic perturbation on flow regime distribution. The average downstream flow velocity changed from a parabolic curve to a three-peak curve — and then — showed a uniform zone after passing the Dean vortex. For the asymmetric flow regime, 33% mixing efficiency growth was obtained.

Garg and Agrawal [123] presented two different investigations related to inflow frictional resistance. Inflow frictional resistance is generally one of the biggest contributors to total flow resistance and depends on the wetted surface and surface roughness [124]. Initially, they measured pressure and temperature in a three-dimensional MC, consisting of planned roughness of varying lengths for gaseous slip flow regimes. Limited penetration for streamlines inside micro-ridges produced reduced contact of slipping gas molecules with the wall surface but increased Re . Therefore, experiments at higher Knudsen numbers could be done to observe gas rarefaction effects on the choking point of the micro-ridges. Also, different orientations and shapes of ridges can be investigated as per the application.

In their second experiment, Garg and Agrawal [125] investigated the effect of adiabatic subsonic choking on frictional resistance for three-dimensional MC in a rarefied gas regime. The choked state of the 3D-MC was noted to be more adiabatic than isothermal. The findings also highlight conditions for AR, Reynolds number, and Knudsen number where significant expansion loss might occur in an MC slip flow. Future research can study the effects of high

Re on highly rarefied choked gas flows at high Knudsen numbers. The Knudsen number (Kn) is a dimensionless parameter characterising the flow's boundary conditions. Kn can be defined by the ratio of the average free path to the average pore diameter [113].

Wang et al. [126] investigated liquid pumping in MC via surface acoustic wave and heat expansion forces. The results showed that a thinner MC (250 μm compared to 500 μm) design with a hydrophobic CYTOP (fluoropolymer) surface boosted pumping velocity by over 130% for experiments with constant liquid volume with identical applied input power. Therefore, there is potential for this technique in small-scale liquid control and deliveries. Moreover, a similar setup for two-phase flow and pressure drop appraisal can be explored.

Ji et al. [127] examined an oil-water mixture emulsification process for flow pattern characterisation having a wide range of Re. High turbulent flow leads to finer and increased monodispersed droplets in the emulsion. In mid-range Re numbers, a high oil volume ratio exhibits laminar flow; this is more noticeable in the 600-300 setup. Analysing droplet means diameter and polydispersity index, unequal configuration produced swirl flow and greater performance than equal size setup for high Re. The 600-300 impingement setup could have potential industrial applications for emulsions at high flow rates. Therefore, future studies should focus on drop deformations/breakup details in MC.

Jin et al. [128] developed a lumped model for a microchannel heat exchanger-based cooling system with feedforward and feedback control strategies. The model shows prediction errors for temperature and pressure within 1%. Feedforward control offers a faster response than feedback, which has longer settling times. Combined feedforward and feedback control ensures quick and stable performance. A scheduled setpoint control optimises pump frequency for varying heat loads, with inaccuracies under 2%, effectively managing system deviations.

2.5.2.4 Thermal resistance

The reduction of thermal resistance is another intriguing research category. Al Siyabi et al. [129] examined the application of a multilayered-microchannel (MLM) heat sink in the highly concentrated photovoltaic (HCPV). The results showed that using MCHS with three layers increased electrical power; temperature reduction was detected in the solar cell when the number of layers increased from one to three for the identical flow rate. Also, the module performed with a better electrical performance outdoors than indoors.

On a different take, Al Siyabi et al. [130] employed multi-layered MCHS for concentrating photovoltaic cooling. The number of layers was inversely proportional to heat sink thermal

resistance and heat source maximum temperature. Thermal efficiency significantly improved due to the heat transfer fluid (HTF) outlet temperature when the number of layers increased from one to three. Moreover, the heat sink could adapt to a range of power ratings with minimal changes in the thermal resistance. Nevertheless, further research is needed to employ MLM heat sinks in a single solar cell CPV module, combining the electrical and thermal performance appraisal using the indoor and outdoor classifications.

Zhai et al. [131] designed and verified a theoretical model to predict flow and heat transfer in MCHS. Convective thermal resistance was found to be an important factor and should be reduced. Furthermore, to minimise entrance effects, the length of the entry channel needs to increase to gain uniform flow distribution. Therefore, similar theoretical frameworks can further aid in improving future MCHS designs.

Tian et al. [132] used direct liquid cooling in microchannels, focusing on heat flux, inlet temperature, flow rate, and hydraulic diameter effects. Direct cooling has a coefficient of performance five times higher than indirect methods. New empirical correlations for the Nusselt number and Darcy friction factor were developed, with errors of 11.6% and 22.2%, respectively. These results aid in designing microchannel condensers.

2.5.3 Design Perspective

2.5.3.1 Aspect ratios

Aspect ratio (AR) is the ratio of two-dimension sizes, usually using the largest against the smallest dimensions [133]; in the case of rectangular ducts/channels, AR is given by dividing the width by height. Numerous authors have indicated the need for further research on the exact effects of aspect ratios. Ozdemir et al. [134] appraised the results of the flow boiling of water in a single rectangular MC with identical hydraulic diameters (DH). Bubbly flows did not exist for the smallest AR (0.5) at the outlet, and the HTC showed a negative relationship with the channel AR until HF values reached around 480–500 kW/m². Channel ARs had a negligible effect on the HTC for higher HF. The researchers recommended further research regarding the impact of AR variation for clarity. Nonetheless, they gave a possible explanation for their findings; for their design, at lower ARs (deep channels), the heat transfer was better due to higher buoyancy effects and a thicker bottom-wetted surface. Alternatively, at higher HFs, the nucleate boiling regions were perhaps replaced with film evaporation regions, making the effect of ARs negligible.

Luo et al. [135] studied hydrodynamics and heat transfer performance (HTP) of annular flow boiling in a high width-to-depth ratio MC. The experiments showed that increased wall HF or inlet quality decreases the thickness of liquid thin film between the interface and the heating wall; thinner liquid films lead to larger local HTC, lower wall temperature, and improved HTP. Nevertheless, the downside of increasing the inlet mass flux is that it decreases the wall's HTC.

Li et al. [136] produced investigations related to aspect ratios in MC. They studied subcooled flow boiling in a high-aspect-ratio, single-side heated MC for varied alignments on hydrophilic and super-hydrophilic surfaces. The findings indicated that, in low mass fluxes, vertical downflow exhibits the highest pressure drop; maximum pressure drop was gained for high mass fluxes during bottom-heated horizontal flow. Also, dominating inertial forces weaken the effect of orientation; the impact of surface wettability is more prevalent for horizontal configuration at a given HF. Consequently, optimised flow orientation and surface wettability for MCHS at different aspect ratios can be further studied.

On a separate occasion, Li et al. [137] experimentally evaluated saturated flow boiling in a single-side-heated vertical narrow MC. All experimental conditions show annular flow patterns and convective evaporation dominated the heat transfer system; thinner liquid film provided increased HTC. Furthermore, the local dry-out phenomenon occurred on the untreated hydrophilic surface, but the super-hydrophilic part kept the liquid film uniform and prevented the phenomenon. The authors suggested a modified correlation formula to calculate the HTC of saturated flow boiling in a vertical narrow AR single-sided heating MC.

Duryodhan et al. [138] assessed mixing in spiral MC designs having different ARs. They visualised homogeneous mixing at a low (0.36) and high (1.2) AR at various angles but having the same Re. Their qualitative analysis of the flow mixing revealed that the spiral MC with higher AR provided comparatively better homogeneous mixing efficiency, but optimum Re and AR balance need consideration. Therefore, ensuing investigations could cater to developing optimised designs for spiral MC designs with superior efficacy. Again, a similar technique utilising high AR was performed by Yin et al. [139], where they analysed water flow boiling using a large AR MC. Their study revealed that nucleate boiling is prevalent in large AR, and HTC correlates to MF. Moreover, HTC for sweeping and churn flow are larger comparatively. The strengthening bubble confinement effect was not observed in large AR MC. Hence, the feasibility elements of large AR MCs can lead to further research.

Cheng et al. [140] studied the impact of groove-wall microchannel parameters (aspect ratio, spacing ratio, and groove depth) on flow boiling heat transfer. Channels with various aspect ratios (1, 2.5, 4) and groove depths (15–45 μm) are tested using deionized water. Results show that aspect ratio significantly affects heat transfer, with the best performance at 2.5. High aspect ratios reduce pressure drops, and critical heat flux occurs more easily at ratio 4. The findings provide insights for optimising groove-wall microchannel design for better heat transfer.

Cui and Liu [141] experimented with an ultrahigh-aspect-ratio copper microchannel heat sink ($\text{AR} = 25$) shows significant improvements in heat transfer compared to lower aspect ratios ($\text{AR} = 1, 5, 15$). It achieves up to 40.95% better critical heat flux and 40.28% lower thermal resistance, despite having ten times lower mass flux. The improved performance is due to effective heat transfer from nucleate bubbles and enhanced evaporative heat transfer at HFs.

Marseglia et al. [142] evaluated nine microchannel heat sinks (MCHs) with different aspect ratios (1.33, 2, 4) and wall thicknesses (0.25–0.75 mm), testing single and two-phase flows using HFE-7100. Three inlet temperatures were used: ambient (18–25°C), intermediate (38–42°C), and near saturation (55–58°C). Results showed that narrower channels provide better thermal performance but higher pressure losses, while wider wall thicknesses improve heat transfer coefficients and reduce pressure losses.

2.5.3.2 Geometry/shape manipulation

Achieving the desired performance through changing geometries is probably the most followed technique to reach the desired HTP in MC. For instance, Abdo et al. [143] determined the optimum configuration for integrated MCHS in a CPV (hybrid concentrator photovoltaic)-TEG (thermoelectric power generator) combined system; this caused a minimal effect on the system performance. However, the new design achieved reduced mean solar cell temperatures and higher performance than the previous design. They suggested design improvements via a TEG with greater conversion efficiency and a more effective heat sink to minimise heat release.

Ringkai et al. [144] studied the characteristics of water-in-oil droplets at the interfacial surface in an offset T-junction MC — with different radii. They noted that minor increases in the channel size produce a significant increase in the overall liquid flow. Likewise, increasing the radius of the offset MC increases the cross-sectional area but decreases the distilled water phase's velocity. Lastly, droplet sizes increased with radius and were approximately equal to the width of the MC.

Vinoth and Sachuthanathan [145] compared heat transfer and flow characteristics of an oblique finned MCHS having pentagonal and triangular cross-sections. The pentagonal MCHS shows better characteristics in heat transfer, thermal resistance, flow characteristics, and pressure drop than the triangular design. In addition, the mixing of nanoparticles ($\text{Al}_2\text{O}_3 + \text{CuO}$) into the working fluid revealed a greater heat transfer rate than a single nanofluid.

Hou and Chen [146] designed and simulated MCHE with three re-entrant cavity shapes (circular, trapezoidal, and rectangular). The findings pointed out that increased flow rate leads to higher pressure drops in the MCHEs; the rectangular shape had the most pressure drop and Darcy friction coefficients. Similarly, an increased flow rate leads to a gradual increase in hot water temperature in MCHE; circular shapes have the lowest hot water temperature, followed by trapezoidal and rectangular shapes. Moreover, circular re-entrant cavities-based MCHE had the highest combined performance at the examined Reynolds number. Accordingly, subsequent investigations could assess other re-entrant cavity shapes to achieve the optimised design.

Ye et al. [147] evaluated cross-junction MC having gas cavities (MGC) to overcome mass transfer issues in Taylor flow. The results showed MGC bubble shapes being more sensitive to the capillary number due to thicker liquid film and a sharper bubble shape for given conditions; this produces a larger surface area. Also, velocity slip and radial fluctuations at the gas cavity interface notably enhanced liquid transport. Thus, mass transfer in MGC needs further appraisal via manipulating liquid film surfaces.

Nadaraja et al. [148] studied multilayer MC arrangement and its effect on the thermal-hydraulic performance of MC arrays. They found that thermal-hydraulic performance obtained in the two-layer MCHS is lesser compared to single-layer MCHS, going against extant literature findings. The abnormal deviation could be due to manufacturing limitations and heat losses in two-layer MCHS. As a result, further investigation could be done on solving heat loss problems, improving manufacturing precision, and the effects of additional layers on the thermal-hydraulic performance of MCHS.

Li et al. [149] designed and examined MCHS with triangular cavities at sidewalls. The new design performed better than the traditional designs, enlarged the heat transfer area, developed liquid film formation, nucleation intensity and bubble departures, HTC, and lowered pressure drops. Thus, the new design was promising for efficient microelectronic cooling.

Vinoth and Senthil [150] evaluated the influence of channel geometries of three oblique finned MCHS to study heat transfer and hydrodynamic features. Out of the three shapes —

semi-circular, square, and trapezoidal — the trapezoidal cross-section provided better heat transfer for electronic cooling systems. Therefore, more cross-section geometries can be investigated for future research. Walunj and Satyabhama [151] examined three designs for low HF applications. Results showed transitioning from rectangular to parabolic and stepped geometries improved heat transfer, HTC, and reduced incipient temperature.

Ge et al. [152] designed a microchannel with serial converging-diverging geometries, inspired by rock porous structures to enhance mass transfer in two-phase flow with a phase injection ratio of up to 200:1. Experiments showed a fourfold increase in mass transfer compared to classic designs. This was due to dispersed fluid retention before the converging geometry, reducing mass transfer distance, and increased interfacial area at the diverging geometry. The design is ideal for high-phase ratio extraction applications.

Li et al. [153] evaluated counter-flow stepped microchannels (CSMC) to improve boiling two-phase flow. CSMCs with step depths of 100 μm , 200 μm , and 300 μm significantly outperform traditional microchannels, increasing CHF by 50.0%-105.6%, heat transfer coefficient by 35.8%-90.3%, and reducing pressure drop by 61.7%-77.7%. They also better control boiling instability, with reduced pressure oscillations and lower inlet temperature rises. CSMCs, especially with deeper steps, enhance microchannel performance effectively.

Han et al. [154] investigated flow boiling in copper microchannels with a saw-tooth design and an L/D_h ratio of up to 75. By enhancing two-phase mixing and disrupting thermal boundary layers, the heat transfer coefficient (HTC) and critical heat flux (CHF) are significantly improved. At a mass flux of 300 $\text{kg/m}^2\text{s}$, HTC reaches 141.8 $\text{kW/m}^2\text{K}$ and CHF is 280 W/cm^2 , showing improvements of about 87% and 110.7% over plain microchannels. A correlation for predicting CHF is also developed.

Liu et al. [155] analysed an open diverging microchannel heat sink (ODMHS) to improve heat dissipation for future fusion reactors, handling up to 15.6 MW/m^2 at 3 L/min. Compared to straight channels, the ODMHS reduces pressure drop and maintains performance by enhancing channel height. The design offers a practical solution for high HFs in fusion reactors.

Saffar et al. [156] examined how curved microchannels influence droplet trajectory and shape. By varying Reynolds number ($3.5 \leq \text{Re} \leq 7$), surface tension, and droplet size, it was found that surface tension directly affects droplet deformation and trajectory, while, Re , has

little impact. Droplets with sizes ranging from 95 μm to 610 μm in channels with 180° and 270° curvatures were analysed, revealing significant effects of droplet size on deformability.

Wang et al. [157] boosted heat dissipation in electronics by exploring hierarchical microchannel heat sinks (MCHS) with curved and straight corners and adding semi-circular and trapezoidal secondary flow structures. Deionised water proved the most effective. Hierarchical structures enhance heat transfer, with Nusselt numbers rising to 67.32%. The trapezoidal secondary flow structure reduces pressure drop by up to 2.46% and improves heat transfer by 9.70%, achieving the highest performance index of 1.10.

2.5.3.3 Barriers/restrictions

Previous research has shown positive implications when implementing barriers/restrictors to enhance flow boiling, heat transfer, and mixing. Haghighinia et al. [158] experimentally and numerically explored two designs having symmetric and asymmetric circular barriers. The results show that repetitive ‘split and recombine’ produced irregular motions and improved mixing. At bends, folding is the key factor to increase the inter-material area. Additionally, increasing the Reynolds number led to an increase in mixing efficiency in separate parts.

Alternatively, Oudah et al. [159] investigated the effects of different inlet restrictors (IRs) configurations on the thermal-hydraulic performance of flow boiling in an MCHS. All IRs enhanced the CHF performance of the MCHS flow boiling. However, the 5IR setup worked best at low mass flux, whereas the 1IR case worked best at high mass flux. It was also noted that IRs decrease the HTC at low mass flux, increase the HTC at high mass flux and HF, and exhibit higher pressure drop penalties in all cases. Consequently, optimum MC dimensions with IRs should be explored depending on the operational parameters (MF/HF) of the MCHS.

Also, Kumar [160] analysed rectangular and semi-circular type MC grooves using the finite volume method (FVM). It was noted that trapezoidal channels provide 12% more heat transfers; the semi-circular grooves show 16% more heat transfer over rectangular grooves in the trapezoidal MC. For trapezoidal MC, groove width impacts more than channel height.

Moreover, Ma et al. [161] explored optimised MCHS with offset zigzag cavities for enhanced flow boiling. The nucleate boiling area near the inlet showed severe instability and flow reversal strength improved with low HF. However, increasing flux generated steam that reduced fluctuations. Moreover, zigzag MC raised heat transfer characteristics having lower wall temperature at onset nuclear boiling, HTC, CHF, and enhanced flow boiling stability by

restricting flow reversal and pressure drops. Accordingly, similar MCHS configurations for flow boiling studies could be further examined.

Pan et al. [162] showed a novel prospect by developing a fan-shaped cavity (FSC) MC for comparison with traditional rectangular MCHS. FSC showed superior performance than conventional designs and comparatively small pressure drop penalties. Nevertheless, the degree of coincidence, deviation, and distribution of FSCs have notable effects on HTPs; hence, methods for optimising FSC designs could lead to future research.

Furthermore, Wang et al. [163] examined flow characteristics, mechanism, and underlying heat transfer improvements of bi-directional ribs (BR) MCHS. BR MCHS showed significantly better Nusselt number and heat transfer at identical mass flow rates. Additionally, BR-MCHS produced the highest friction factor and blocking effect.

Memon et al. [164] investigated the impact of secondary flow passages on longitudinally wavy microchannel heat sinks. Two types of flow bifurcations—abrupt (60°) and smooth (30°)—were tested with various inlet-outlet configurations. Results showed that the 30° bifurcation design achieved the highest Nusselt number below a flow rate of $1.8 \times 10^{-6} \text{ m}^3/\text{s}$, while the conventional wavy heat sink performed better above this flow rate. The study provides insights into optimising heat sinks for modern chips, like the Intel® Core™ processor.

Sulaiman and Wang [165] evaluated the effect of adding a contraction before straight fin microchannels using refrigerant R-134a. Two setups were tested: one with a contraction (CBM) and one without (NCBM). The CBM achieved a 3-30% higher heat transfer coefficient and lower pressure drop at low mass fluxes for fully liquid inlets, though this advantage decreased at high mass fluxes. Flow visualisation showed that the CBM prevents flow reversal and stabilises temperature and pressure, unlike the NCBM, which exhibits flow reversal and sluggish bubble behaviour.

2.5.3.4 Pin-fins

Research related to pin-fin designs could be significant, as per the literature. To illustrate, Liao et al. [166] appraised flow boiling heat transfer. The conclusions were: mass velocity was directly proportional to the subcooled temperature variations, augmenting the surface HF generated various flow patterns, phase change on boiling induced almost three times pressure drop, and raising WF saturation temperature increased pressure drop. Therefore, there is scope to study the effects of fin inlet alignments and arrays on the boiling convection heat transfer.

Additionally, Tiwari et al. [167] investigated the role of precise flow patterns in MCHS via a 3D-printed manifold for single-phase flow under low to medium HF conditions. The total HTC for the MCHE reached higher than most available shell and tube heat exchangers. Also, utilising mass-manufactured fin tubes made the overall experimental setup fabrication economically viable. Thus, research is needed for optimised geometry to be used in large-scale heat exchangers. Moreover, the flow pattern in a multitube bundle needs an appraisal for developing shell-ad-tube type MCHE.

Wang et al. [168] studied single-phase flow heat transfer downstream having one pin-fin. The findings noted vortex shedding and large-scale flow mixing caused higher HTC along the pin fin centreline. The numerical model from this experiment also helped trace the heat transfer map of the heater to the fluid and its surroundings.

Vinoth et al. [169] examined a curved finned microchannel heat sink (MCHS) using deionised water, Al_2O_3 /water nanofluid, and $\text{Al}_2\text{O}_3+\text{CuO}$ /water hybrid nanofluid. The MCHS, with a cross-sectional area of $80 \times 53 \text{ mm}^2$, improves heat transfer by 11.98%, performance enhancement coefficient (PEC) by 16.5%, and reduces pressure drop by 30.1% compared to straight channels. Hybrid nanofluid enhances heat transfer by an additional 3.5% and 2.1% over water and nanofluid. The curved finned design's secondary flow significantly boosts performance, making it a promising cooling solution for power converters in electric vehicles.

Zhang et al. [170] addressed heat transfer in microchannel heat sinks by adding fins to create secondary channels. CFD analysis, validated by experiments, shows that optimised fins reduce maximum and average temperatures by 6.67% and 6.75%, improve temperature uniformity by 8.47%, and cut pressure drop by 13.33%. The performance evaluation value is 1.285. The study advises selecting an appropriate mass flow rate to balance cooling efficiency and pump power.

Fu et al. [171] explored flow boiling in a copper foam fin microchannel (FFMC) heat sink with channels $487 \text{ }\mu\text{m}$ wide and $1061 \text{ }\mu\text{m}$ high. The FFMC improves heat transfer by up to 80% and enhances critical heat flux by 25% compared to a solid fin microchannel (SFMC), though pressure drop increases 1.2 to 2 times. It also reduces flow instability, including temperature and pressure drop fluctuations. Nucleate boiling and thin film evaporation dominate at different Bo numbers, with heat transfer increasing at high mass fluxes and varying at low fluxes.

2.5.4 Sustainability Perspective

The initial literature review indicates a lack of research papers that explicitly focus on, cater to or blend sustainability and MC. Nonetheless, some research could be categorised based on the sustainable aspects noted in their investigations or future scopes. For such cases, deductions and inferences were made to link the studies to different sustainable development elements; these papers are discussed in the following paragraphs. Furthermore, the sustainability aspects were also linked to complement the three MEDS perspectives mentioned in the earlier chapters.

Wang et al. [95] studied HTC and moisture transfer coefficient (MTC) variation in an MC under varying sizes and desiccant thicknesses. The experiments showed that heat and MTC increase with airflow velocity. Also, smaller fin and flat tube pitches exhibited larger HTC and MTC. The desiccant thickness negatively affected the HTC but positively impacted the MTC. Furthermore, the Taguchi method analysis concluded that airflow velocity significantly impacts dehumidification. This paper provided a baseline for future design and manufacture of adsorption chillers, heat pumps, energy storage equipment, and atmospheric water collectors based on DCHE application — effectively promoting environmentally sustainable approaches.

Lin et al. [172] investigated flow boiling in a rectangular vertical MC with heterogeneous wetting and silicon surfaces. The combined hydrophobic and hydrophilic surfaces manipulated the bubble dynamics and HTP in flow boiling. Moreover, coating a Teflon solution on different positions of the silicon substrate significantly improved the HTP. Future investigations of more heterogeneous wetting surface usage in engineering applications could positively impact cost and ease of manufacture, which will positively impact profits and economic sustainability.

Li et al. [173] investigated reactant flow rate and pin–fin design effects in MC reactors via time-frequency analysis for two-phase flow pattern transition. The pin–fin outlet reactors suppress the upstream compressible slug fluctuation to produce a conversion of 59.0% for 5 ml/h, the highest value for H₂O₂ decomposition in MC reactors ever noted. Therefore, there is potential to utilise and mitigate two-phase flow instabilities in MC catalytic reactors and dehydrogenation of liquid organic hydrogen carriers (LOHCs). LOHCs lead to relatively safer, cheaper storage materials and cleaner energy systems. Similarly, Ali et al. compared hydrogen production from perhydro-dibenzyl-toluene in stirred tanks and continuous-flow microchannel reactors. The microchannel reactor achieved up to 88% hydrogen yield, outperforming the stirred tank. A kinetic model showed favourable conditions for dehydrogenation, making the

microchannel reactor a promising option. Thus, MC-based dehydrogenation and LOHC would aid economic and environmental sustainability in the overall production and supply chain.

Lastly, social sustainability is perhaps the most complex sustainability aspect. Nevertheless, the work of Bhattacharjee et al. [174] does indicate the potential of producing socially sustainable developments via MC technologies. Bhattacharjee et al. [174] developed an MC-based strain sensor that showed three times increased resistance value for 10% strain — better than most existing strain sensors. Also, the sensor was responsive to different bending and twisting due to effective strain. Therefore, the implications of employing feedback control with the strain sensor help to control a robotic finger motion using human interactions.

On a different note, Kumar and Kumaraguruparan [175] proposed a personal cooling system (PCS) for firefighters using vapour compression refrigeration to reduce heat stress. Tested with two condensers (MC-1 and MC-2) and capillary tubes (0.84 mm and 1.18 mm) in high temperatures, the 1.18 mm tube with MC-2 performed best. The system weighs 4.335 kg, with a battery. By improving firefighter performance and safety, this research enhances social sustainability through better working conditions in extreme environments. Consequently, similar future technological advancements will further promote diversity and inclusivity in the industrial workforce, especially for people with disabilities — directly impacting and enhancing social sustainability. Fig. 2.3 summarises the key themes based on the MEDS Framework. While the framework is not exhaustive or comprehensive due to the diverse factors, methods, and available information, it offers a valuable generalisable holistic overview.

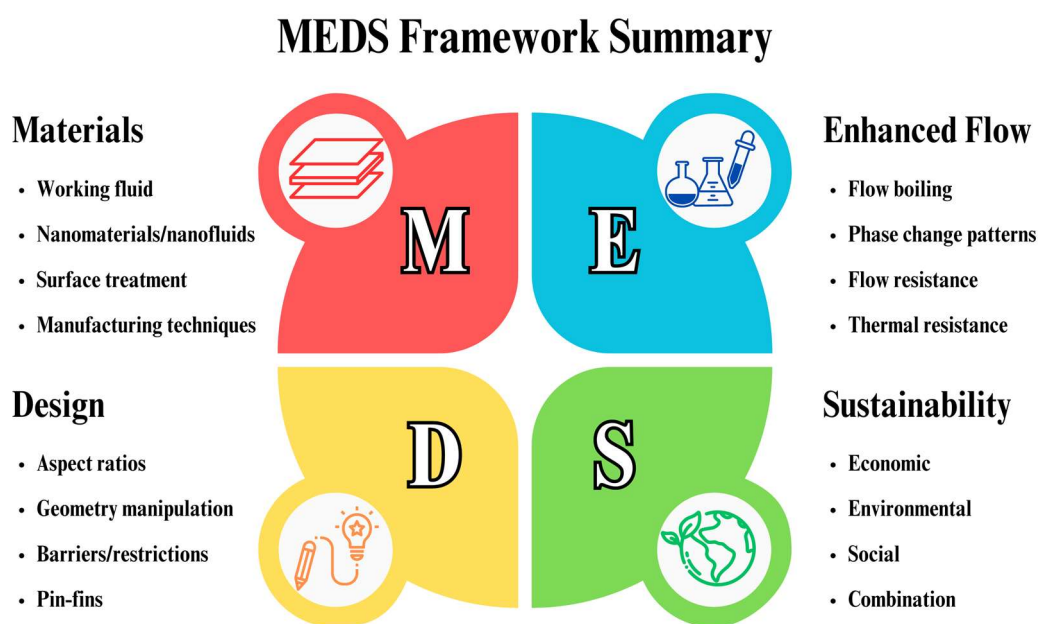


Fig. 2.3 Summary of MEDS framework

2.6 Overview of Identified Research Scope and Trends

After scanning the available literature, it was noted that there was a scarcity of recent papers providing detailed assessments of experimental methods and trends in MC. However, some authors have categorised partial data/research related to MC shapes or working fluids for their experiments or other purposes. Therefore, it can be said that due to the diverse factors and means available for MC-based experimentation, finding a generalised trend is challenging. Therefore, this research overview will arguably be the first to identify and appraise general trends and elements needed for MC experimentation. Additionally, the chosen strategy is aligned with the four perspectives in the MEDS framework and the ethos of tackling smaller issues to lead to wider technological advancements. All the common critical elements (along with their data) were extracted from the sample of 100 papers used for qualitative analysis. Appendix A highlights all the data and summarises the findings from earlier chapters for visualisation and analysis purposes; the table has been categorised in reverse chronological order and grouped using the MEDS elements.

As sustainability is one of the research themes, the initial focus was on regional research contributions to gain a broad understanding of current trends. Fig. 2.4 presents the research distribution by geographical region (note: papers with first authors from Turkey are included in Europe as they are eligible for EU funding, and Russia is also grouped with Europe as its capital lies on the European side). Some countries, like China, are listed as separate categories. It is clear that MC-based experiments are predominantly conducted in China (44%) and the Rest of Asia (ROA) (23%), accounting for two-thirds of all contributions. As MCs are integral to sustainable engineering technologies, MC-related research has a positive impact on sustainability. In comparison, Europe's contribution (18%) is relatively modest, given the alignment of MC technologies with the EU's 2050 climate goals [12]. Moreover, MC research is less frequent in other regions, potentially due to the developing nature of Africa and South America, or differing research priorities in regions like the USA and Australia.

Research Contribution Map

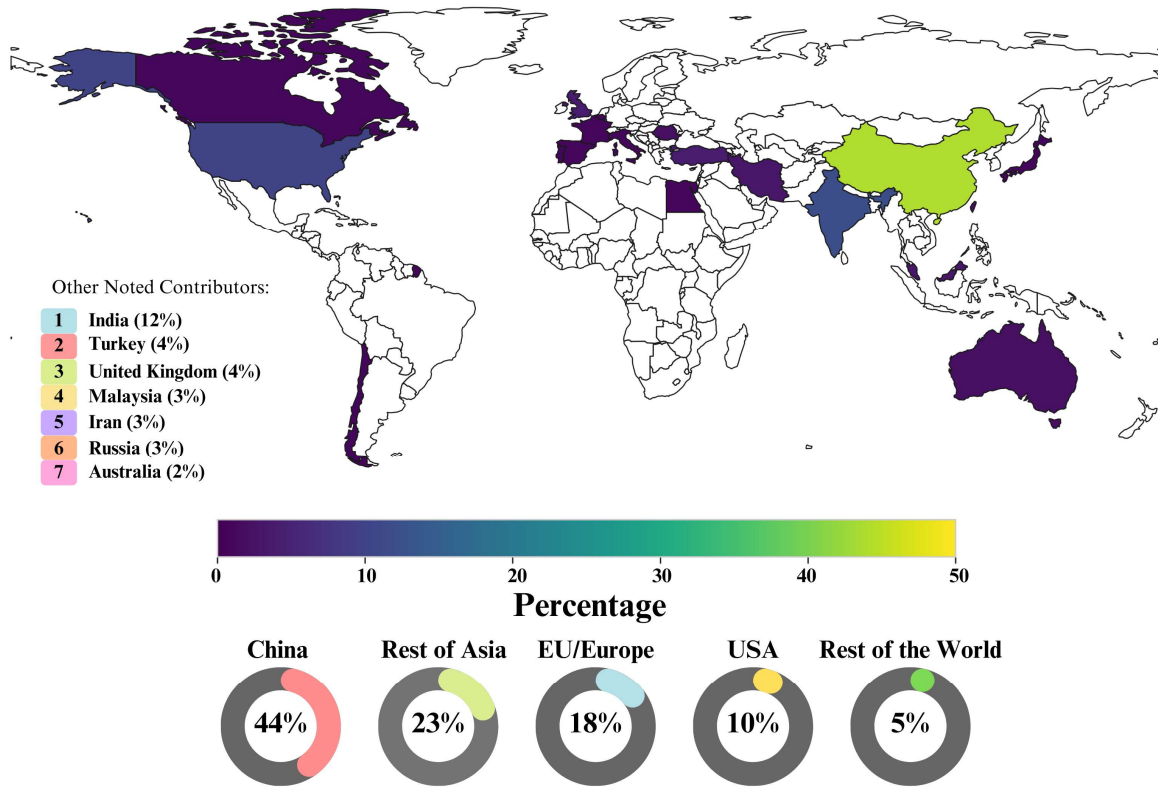


Fig. 2.4 Research distribution map

Before experimenting with or assessing microchannel or micro-heat sink technologies, it is important to evaluate the design, manufacturing processes, and shapes covered in existing research. This approach not only aids in identifying research gaps but also provides a better understanding of the reasoning and challenges behind producing unfeasible or complex structures. Fig. 2.5 (a)-(d) presents a breakdown of various trends related to microchannel shapes, fabrication strategies, hydraulic diameters, and aspect ratios, respectively.

MC Design/Configuration (Design Perspective) – Fig. 2.5 (a) illustrates the design trends for MC shapes and configurations. Some researchers experimented with more than one shape or design during their investigations, resulting in over 100 data samples for MC configurations and shapes, instead of 100. Over the last seven years, the traditional rectangular MC configuration has remained prevalent. However, square and circular shapes, along with Hierarchical (HCL) or T-shaped junctions, have also been employed. Other case-specific structures (12%), such as spiral or curved MCs, are less common. Novel-shaped designs are being experimented with, but rectangular-shaped geometries still dominate.

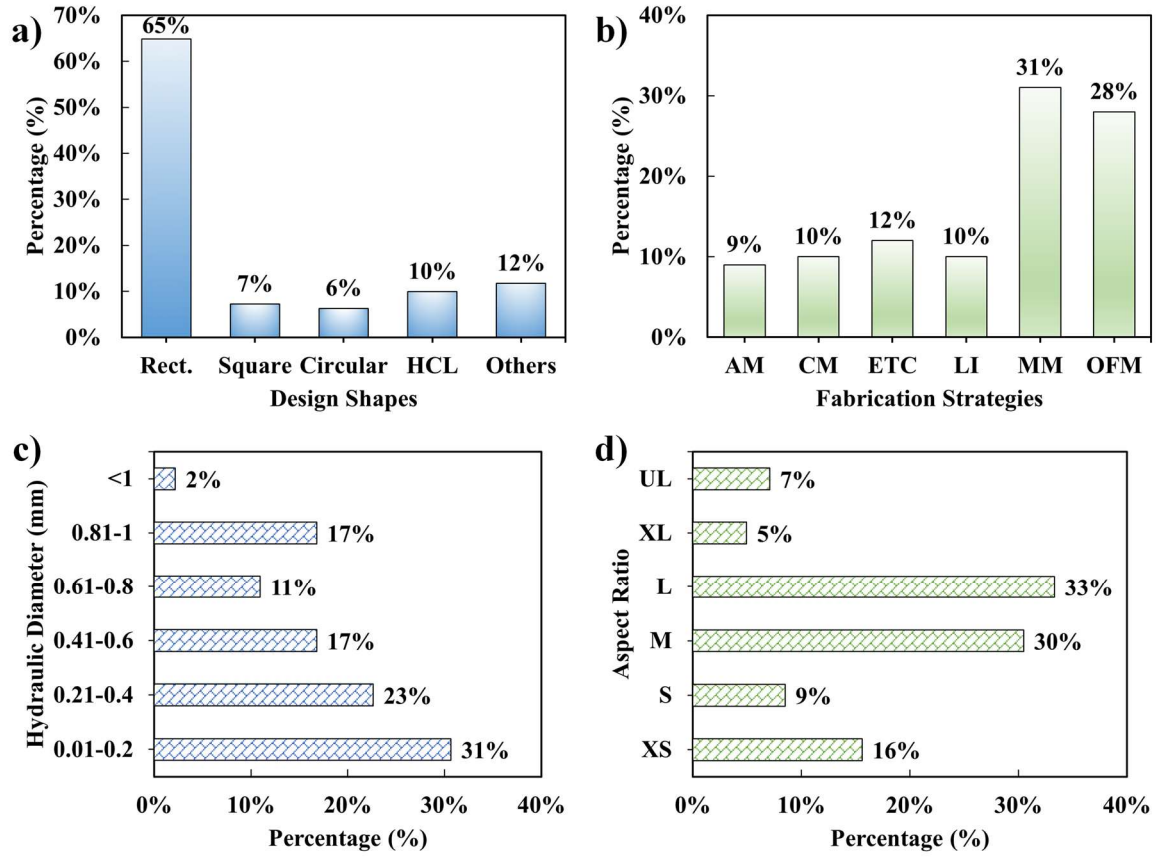


Fig. 2.5 Different microchannel designs and manufacturing trends: (a) Design shapes; (b) Fabrication strategies; (c) Hydraulic diameter; (d) Aspect ratio

MC Fabrication (Design/Sustainability Perspective) – Fig. 2.5 (b) presents the trend of MC fabrication. MC fabrication relies on various methods, including micromachining (MM), etching (ETC), and lithography (LI). On average, MM remains the most consistently used technique (31%). Additionally, LI has seen an overall upward trend, while ETC has generally declined over the years. More recently, there has been a growing, albeit limited, use of 3D-printed (3D) MC-based technologies. In several experiments, researchers opted for commercial or pre-made (CM) MCs. Lastly, around one-quarter chose distinct fabrication methods (OFM) or did not provide sufficient details about their MC fabrication processes. These two categories are combined as OFM, which shows current trends in MC fabrication methods. It is important to know the details of the fabrication process to make the overall life cycle of the microchannel from production to experiment and to usage more sustainable.

Hydraulic Diameter and Aspect Ratios (Design Perspective) – Fig. 2.5 (c) and (d) depict the MC hydraulic diameters (DH) and aspect ratios (AR), respectively. To better evaluate the trend of commonly used DHs in experiments, the data was segmented into intervals of 0.2. Fig.

2.5 (c) visualises the DH trends, showing that approximately 50% of the experiments employed a DH within the 0.01–0.4 range (note: some studies used multiple designs and configurations, leading to a higher data count for DH and AR). Aspect ratios, calculated using the width and height, were presented alongside DH. Given the broad range of AR values, the data was categorised qualitatively into the following: extra-small (XS), small (S), medium (M), large (L), extra-large (XL), and ultra-large (UL). These correspond to the following AR ranges: XS (0.01 – 0.50); S (0.51 – 0.99); M (AR=1); L (1.01 – 5); XL (5.01 – 15); and UL (15+), as shown in Fig. 2.5 (d). About 90% of the experiments used an AR of less than 15, which is logical, as achieving higher ARs with smaller hydraulic diameters significantly affects cost, fabrication time, and product development. This can lead to unsustainable impacts, even if heat transfer is marginally improved by such designs.

Alongside fabrication and design choices, another key factor in developing new types of micro heat sinks is the ease of manufacturability and experimentation, which facilitates faster and more agile product development. Consequently, the choice of material or working fluid becomes critical, as it influences both cost, efficiency and the integrated carbon emissions throughout the product's life cycle. Fig. 2.6 (a)–(b) illustrates the material and working fluid selections over the past seven years.

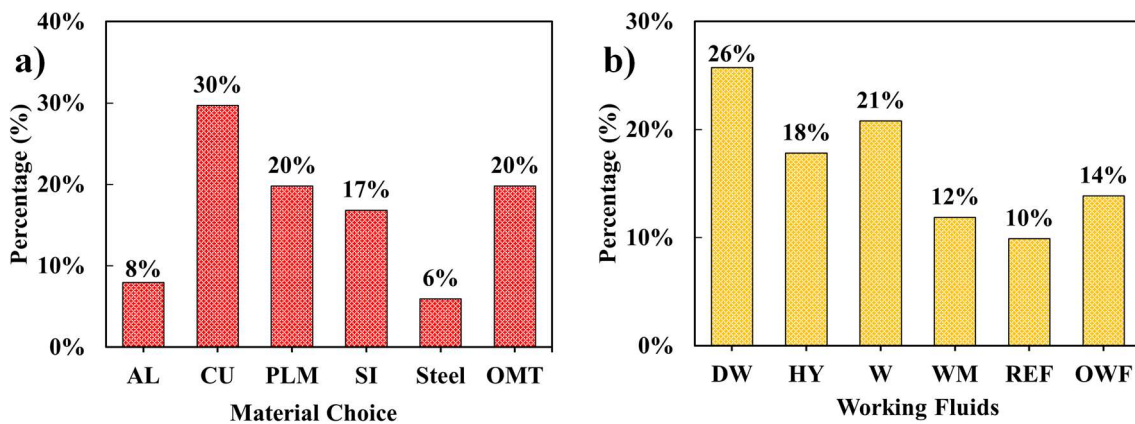


Fig. 2.6 Material trends: (a) Material choice (b) Working fluids

Materials Used (Material/Sustainability Perspective) – A range of materials have been used in MC fabrication. The most commonly used materials include Polymers (PLM), such as Polydimethylsiloxane (PDMS) and Poly-methyl-methacrylate (PMMA), Copper (Cu), Silicon (Si), Aluminium (Al), and Steel. Other materials (OMT) combine less frequently used materials, such as glass, SU-8, and tantalum, gold, amongst others. Fig. 2.6(a) shows the most

frequently used materials for MC experimentation, with the x-axis representing the materials used and the y-axis showing the percentage of experiments or papers that used those materials.

Working Fluids (Material/Sustainability Perspective) – Fig. 2.6(b) depicts the most commonly used working fluids in MC experiments. Water (W) and water-mixture solutions (WM) have been frequently used in recent years, though de-ionised water (DW) remains the top choice. Hybrid nanofluids/micro-fluids (HY), containing elements like aluminium, copper, and silver, have also seen increased use. Other working fluids (OWF) and refrigerants (REF), such as Novec, R134a, and HFE-7100, have generally trended upward in usage. Additionally, nitrogen (N₂) or Argon (Ar) gas has occasionally been used as a working fluid, though its application has been irregular and specific to certain investigations.

Based on the potential research directions and suggestions made by authors in the existing literature, the MEDS framework categorised the literature into areas where Further Research Is Needed (FRIN). The current analysis strategies are also visualised in Fig. 2.7 (a). While the FRIN areas have relatively similar scores, the authors acknowledge possible criticism regarding the methods used to prioritise these areas. Nonetheless, the data on FRIN status and trends provide valuable insights to guide future research.

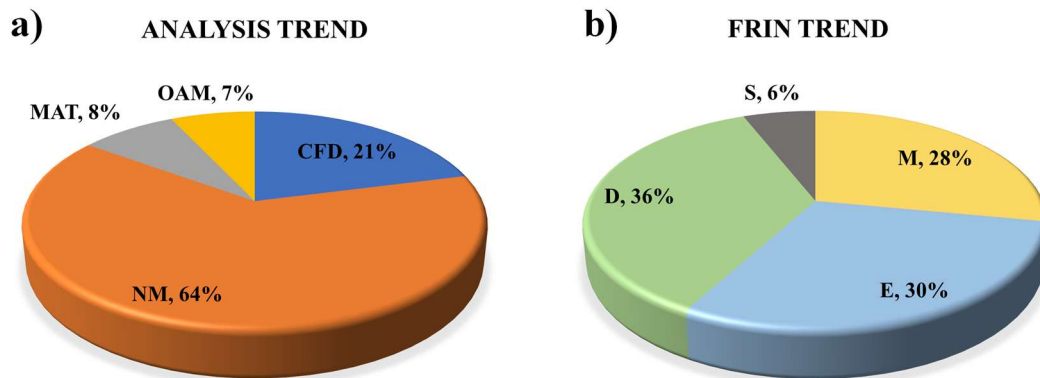


Fig. 2.7 Further research needs: (a) FRIN trend (b) Analysis trends

Analysis Methods (Enhance Flow Control Perspective) – Fig. 2.7 (a) summarises the analysis methods used in MC-based studies. This paper focuses on heat transfer and thermal management applications, with almost all experiments incorporating general flow visualisation analyses. Most researchers employ experimental and numerical methods (NM) to analyse and solve flow equations, with Computational Fluid Dynamics (CFD) being the second most common approach. MATLAB-based simulations have also received some attention, while

other methods (OAM), such as machine learning, uncertainty analysis, and correlation-based investigations, are emerging fields. Nonetheless, experimental and numerical methods remain the dominant approaches for MC studies.

Further Research Requirement (Sustainability Perspective) – Fig. 2.7 (b) exhibits the FRIN trend, showing an upward trend in research needs from a design perspective and a slight decline in the materials area. The design area offers the greatest scope for research (36%), while enhanced flow control (30%) slightly exceeds the material perspective (28%). Additionally, the limited number of papers connecting sustainability (6%) with MC highlights a clear need for further investigations and frameworks addressing this area.

2.6.1 Trends in Micro Heat Transfer

In terms of MCHS designs and shapes, combining traditional rectangular (65%) and square (7%) channels accounts for around three-quarters of all MC structures, while distinct, non-conventional designs combined a total of 22%. This highlights the potential of further exploring alternative MC structures, as conventional geometries have already been widely investigated. One promising direction is the study of pin-fin-based heat sinks, which could offer new avenues for enhancing heat transfer, given that traditional rectangular straight channels have been explored extensively. Additionally, the positive implications of multi-layer and pin-fin-based heat sinks could be a promising direction for future exploration, as they offer an alternative to the extensively studied rectangular straight channels, potentially providing superior heat transfer characteristics, and emerging design approaches such as generative design, low-data driven machine learning, additive manufacturing, and high-precision micro-machining open up novel possibilities. Bio-inspired structures and fractal or mixed designs are becoming viable due to these advancements, though the balance between design complexity, pressure drops, and heat transfer improvements needs careful assessment [176,177].

Regarding material usage in MCs, there is a more distributed trend. PLM (20%), copper (30%), and silicon (17%) are the most common materials. Material choice for mass production must consider factors such as heat transfer performance (HTP), ease of manufacture, cost, and sourcing challenges. This offers another valuable research area, particularly concerning sustainable materials and their lifecycle impacts. MC fabrication methods exhibit a variety of approaches. While some authors detailed their strategies, others did not provide sufficient information (28%, OFM). The data indicates that micro-machining (31%) is the most frequently employed, followed by etching (12%) and lithography (10%). Additive

manufacturing (AM), despite its potential, has only been used in 9% of cases, likely due to cost and complexity considerations. Commercially made MCs (10%) also feature in the data, though these are usually tailored for specific experimental purposes rather than innovation.

Even though 3D-printed MCs show promising potential, the relatively low usage of AM may stem from difficulties in achieving high precision at the microscale or economic feasibility issues. Nevertheless, AM offers sustainability benefits and the ability to create complex shapes from a range of materials including polymers, metals, and ceramics, though standardisation remains a challenge [178]. The rough surface finishes often produced by AM can be advantageous, as they have been shown to enhance heat transfer coefficients (HTC) by reducing pressure drops [92]. Still, further research is needed to evaluate the feasibility of AM usage for microscale experimentation and to assess its overall viability for MC setups.

In terms of working fluids, MC-based experiments typically rely on water-based solutions, which are generally safe and sustainable. However, more work is required to assess the performance and environmental impact of newer refrigerants and mixed metal-based nanofluids, particularly about stability, disposal, and lifecycle emissions. The trends also suggest that larger aspect ratios (AR) warrant further investigation, supporting arguments made in previous studies [139]. Machine learning (ML) and AI techniques could assist in modelling the behaviour of various AR and DH combinations, improving predictions of fluid dynamics and heat transfer performance. Integrating MC systems into cloud computing and digital twins would enable continuous improvement in design and testing. However, challenges such as data availability, overfitting, and the "black box" nature of ML/AI models must be addressed.

Overall, while MC research continues to rely heavily on traditional methods, technological developments are slowly being adopted. Additive manufacturing, machine learning, cloud computing, and digital twins have already begun to influence MC-based technologies. Nonetheless, further investigation, re-evaluation of existing experiments, and combining different strategies are warranted to drive new performance and design innovations. The complexity of this field means that only certain themes and trends were explored, but the insights align well with the RQs and help address the foundational challenges for this thesis.

2.6.2 Key research themes and sub-themes

The key research themes (MEDS) and their sub-themes were determined and were categorised as follows: Materials (working fluids, nanofluids/nanoparticles, and surface treatment/manipulation); Experimental (flow boiling, phase change, flow resistance, thermal

resistance, and manufacturing techniques); Design (aspect ratios, geometry/shape manipulation, barriers, and pin-fins); Sustainability perspective (no general theme, environmental, economic, and social).

Firstly, focusing on the material:

- As per the findings from the literature, utilising hydrophobic refrigerants as a working fluid positively impacts the two-phase flow HTC and extends nucleate flow boiling length, provided the inlet temperature and HFs are increased progressively. Additionally, using two working fluids has generally shown to be reliable compounds during monitoring and verification heat transfer-based experimentation. However, relatively higher temperatures are required for working fluids to be effective, and there is scope for further research due to uncertainty on the effect of hydrophilic/hydrophobicity of working fluids on heat transfer, pressure drop penalties, and especially for non-Newtonian fluid experiments;
- Metal-based nanofluids mixture, especially one containing silver, can significantly improve HTC; nanofluids improve the thermal conductivity of the base fluids. However, increased pressure drops, and friction factors are the leading drawbacks of nanofluid usage. There is also a lack of consensus regarding how nanofluids affect thermal resistance and two-phase flows. Previous studies have indicated long-term stability issues and increased pumping power requirements in nanofluid usage [179]. However, the study of Simsek et al. [85] indicated that nanofluids can increase HTC without adding pumping power. Therefore, the viability of silver nanofluids for reduced pressure drop, friction factors, and two-phase flow needs further research;
- The literature suggested that the trend for common surface treatments was employing different wettability surfaces, surfactant additions, chemical treatment, and desorption. However, high thermal conductivity materials, such as diamond, for surface hydrophilization present alternate options for heat transfer enhancement [180]; albeit, they may not be the most cost-effective solutions. The coating surface appears to produce a significant impact. To illustrate, surface wettability variations in flow boiling investigations improved HTC, and biphilic surfaces (BS) and 3D heterogeneous surfaces provide enhanced flow boiling heat transfer and improved nucleation density. These heat transfer enhancements primarily occur because the thermal boundary layers during two-phase heat transfer rely on cavity size, surface roughness, surface wettability, and surface morphology [88]. For instance, gases trapped in the pores and

cavities can trigger bubble nucleation [181], whilst a hydrophobic surface enjoys a lower interfacial energy barrier than its hydrophilic counterpart [182]. Nevertheless, it is unclear how surface manipulations affect pressure drops and thermal resistance;

- Overall, the studies of Ahmadi et al. [87] and Jayarmu et al. [92] indicated that whilst surface wettability has been studied in pool boiling, there is a lack of research on the effect of surface wettability in flow boiling. Consequently, this gives rise to future research areas. Elevated surface wettability tends to show higher HTC but with higher pressure drops and reduced CHF values. On the other hand, low surface wettability produces comparatively higher CHF values and reduced pressure drops. Furthermore, care must be taken whilst increasing surface wettability as it can lead to the thermal oxidation of materials. A biphilic surface or mixed wettability surface for flow boiling-based applications is perhaps one of the most promising areas, as they contain both types of wettability surfaces to yield the desired results. Therefore, subsequent research can focus on employing different biphilic surfaces for flow boiling pressure drop and thermal boundary layer formation assessment.

Secondly, considering the experimental elements:

- Researchers emphasised flow boiling instability and friction resistance. However, it should be noted that there are some disagreements and a lack of clarity on how flow boiling enhancement can be achieved due to the complex mechanism and number of factors related to flow boiling transition and two-phase flows [104]. Nonetheless, research has shown that frictional pressure drop penalties could be reduced by increasing inlet saturation temperature and adding inlet restrictors;
- Phase change phenomena via slug generation and control lead to improved heat transfer, but critical shear stress and interfacial tension need considerations to gain optimal results;
- MLM heat sink thermal resistance can be reduced by using a multi-layered MCHS, but thermo-electrical performance needs further appraisal;
- Convective thermal resistance and the length of entry channels represent critical factors for enhanced heat transfer. If mixing and turbulent flows are warranted, asymmetrical flow regimes/setup improve general performance;
- Additive manufactured MCHS are also becoming viable candidates and can produce pin-fin with a thickness of 0.18mm. Additively manufactured MCHS have shown improved HTP, but further assessment is required for its feasibility.

Thirdly, appraising the design parameters:

- Appraising the papers, there was no general trend regarding the effect of AR on heat transfer, flow boiling, and pressure drops. However, it was noted that in specific cases, AR could impact the flow mixing, boiling heat transfer, instability, and pressure drops; this is more noticeable at low heat flux conditions. However, there was a lack of clarity regarding how AR (high or low) affects the flow boiling due to the complex mechanism. The findings of this research align with previous studies that claimed that the results of AR effects were contradictory and developing a general conclusion regarding AR effects on flow boiling/two-phase flow is challenging [183,184]. However, depending on the heat flux and mass flux, it can be said that using high AR provide larger nucleate boiling regions, comparatively lesser flow instability, and higher HTC but also causes higher pressure drops. Also, HTC at higher HF is unaffected by small AR; alternatively, HF under 480 kW/m² and mass flux can adversely affect the HTC. For high AR, increasing wall HF reduces the thickness of the liquid film and, in turn, improves the local HTC considerably; nevertheless, researchers need to be mindful of the wall HTC if inlet HF is increased; Large AR have also shown prevalent nucleate boiling region along with improved HTC for churn flow, but these require further verification.
- Improved heat transfer performance and mixing via geometry manipulations can be gained by adding triangular/zigzag cavities at sidewalls, circular/semi-circular re-entry shapes with barriers, and trapezoidal/pentagonal designs. However, flow velocity needs monitoring as increased flow leads to higher pressure drops;
- Barriers can improve flow boiling stability depending on the configuration and operating conditions. At low Heat Flux (HF), multiple-barrier setup delivers better performance; on the other hand, at high HF, fewer/single-barrier had better results. Similarly, grooves, wavy, or zigzag configurations appear to suit more in high heat flux conditions to provide better stability. However, barriers can also disrupt the flow, and provide high friction factors, and flow mixing; thus, care must be taken when implementing barriers to ensure the desired effects. As a result, more studies are required to establish the previous conclusions;
- Overall, adding barriers and flow restrictions, in general, have shown positive performance improvements in microchannels. For single-phase flows, the addition of pin fins provided higher flow mixing and HTC. The general theme also shows that pin-fins are typically employed to increase the surface area for heat transfer enhancement,

but barriers or restrictors show more diverse utilisation. As previous studies indicated, it is arguably complex to claim the best setup for either barrier or pin-fin configurations as flow boiling instability and pressure depend on several factors and further research is needed regarding many dependencies. The same pin-fin may generate significantly different results with surface roughness, heat flux, mass flux, aspect ratios, and nanofluids. However, the findings from this research and recent studies have shown that pin-fin setups can improve flow boiling with reduced pressure drops and instability compared to conventional geometries [185,186].

Lastly, for sustainability, numerous authors suggested that adopting modern technologies to provide better energy-efficient methods will lead to sustainable development and improve overall sustainability. Therefore, it can be debated that all MC-based research indirectly contributes towards sustainable development. However, sustainability remains a complex concept, possessing multiple factors; therefore, finding general research themes is challenging. Nevertheless, different experiments could perhaps be categorised into economic, environmental, and socially sustainable elements. Consequently, presenting diverse research areas to conduct more focused investigations can lead to better long-term sustainable solutions — rather than treating sustainability as an after-effect of MC-based studies.

2.7 Focus on Pin-fin Heat Sinks

The current challenge in electronic thermal management is to develop miniature heat transfer systems capable of dissipating heat quickly and effectively while maintaining the device's size and weight. To address these challenges, one promising solution that has gained significant interest is pin-fin-based heat sinks [24,25]. Pin-fin heat sinks consist of small pins that increase the available surface area for heat transfer. By facilitating more efficient heat transfer, pin-fin heat sinks can cool electronic gadgets and extend their lifespan [26].

The recent extant literature trends highlight diverse experimental and numerical investigations to identify potential solutions to enhance fluid flow and heat transfer performance via pin-fin-based heat sinks; these methods include design modifications [26,187], surface modification [10], nanofluids [188,189], phase change materials [190], two-phase flows [191], inducing flow instabilities [192], amongst many other strategies [193]. Nonetheless, the literature indicates that design or geometrical adjustments mainly remain the focus. To illustrate, İzci et al. [194] numerically explored various single-arrangement pin-fins with shapes such as circular, square, diamond, triangular, cone, and rectangular fins. The results

hinted that rectangular fin had the highest Nusselt Number (Nu) and friction factor, but the cone-shaped fins retained the highest thermal performance index. Also, inline-arrangement pin-fins having splitter plates with circular and square shapes have been numerically investigated by Razavi et al. [195] and Sajedi et al. [196]. They found that utilising splitters behind pin-fins reduces pressure drops and thermal resistance; this was more effective in circular shapes than square pin-fins. Similarly, the numerical assessment of inline circular pin-fins has been done many times [197–199]. It was observed that thermal performance has a positive relationship with the fin height but negative with the fin pitch; traditional setup of opposite positions of inlet and outlet have higher Nu and lower bottom temperature; the gap between the pin-fins and the sidewalls can manipulate heat transfer performance significantly.

Other investigations have analysed triangular [200,201], square [202], rectangular, diamond, oblong, elliptic [203], cones [204,205], hemispherical [206], alternative dimples [207], multi-bulges [208], micropillars [209], textured [210], curved/inclined [211], splitter inserts [212], and grooves [213–215]; it was noted that the porosity and the angle of the fins have a great impact on the thermal performance; diamond-shaped fins had higher Nu, rectangular-shaped had higher pressure drops, and adding splitters, deep grooves, domes, and increasing the circular diameter — whilst reducing the spacing between the fins — improves heat transfer. Additionally, experimental investigations on pin-fin heat sinks have been carried out; however, these are less common than numerical studies, primarily due to the costs and difficulties involved in producing microscale pin-fins and heat sinks. Experimental studies having pin-fins exist in conventional shapes such as circle [216–218], semi-circle [219], conical [220], square [221], diamond, triangle, pentagon, and hexagon [222].

For experimental studies, staggered layouts represent a typical strategy [220,223]. Staggered arrangement pin-fins show that shape affects the vortex resistance, with a circular shape having the maximum resistance and the oval fins maintaining the minimum; the highest heat transfer was present in the hexagonal cross-section; circular fins showed the lowest pressure drops; also, the porosity and fin diameter affects the heat transfer rate. Due to the comparatively lower availability and complexities associated with experimental investigation, many numerical studies are cross-validated using other similar experimental/numerical data [224]. For instance, Xie et al. [225] appraised thermal and hydraulic performances of microchannel pin-fin heat sinks using data from external investigations [226,227]. The results of Xie et al. highlighted that in-lined pin-fins at a 30° inclined angle increase secondary flow at the cost of increased friction, but a steeper inclined angle doesn't necessarily improve heat transfer; 0° inclined angle

performs similarly to other conditions and switching from in-lined to staggered pin-fin arrangement had minimal impact on thermo-hydraulic performance; thus, the exact effects of staggered and inline pin-fin arrangements still needs a better understanding. Nonetheless, the staggered setup is generally more preferred [228,229].

Nonetheless, from a design and optimisation perspective, the effectiveness of pin-fin-based heat sinks depends on several factors, including the heat sink design, working fluid, and the thermal conductivity of the materials. Additionally, pins-fin geometrical configurations, such as shape, spacing, and height, can affect the heat transfer rate or coefficient [224]. Thus, the optimal design of a heat sink needs consideration of the device's thermal load or heat flux, size, shape, and operating environmental conditions [10]. In addition, the fluid flow around heat sinks significantly impacts their cooling performance. Increasing the flow rate can enhance heat transfer by promoting convective cooling. However, high airflow rates can also increase noise levels, induce higher pressure drops, require large fans or pumping power, and ultimately affect the device's size and weight. As a result, achieving the optimum balance between cooling performance and other design considerations is critical [16].

Further appraising more designs, in addition to the conventional geometries, researchers have attempted to utilise non-conventional shapes [230] and experimented with wings [231], hydrofoil [232], non-linear fins [233], NACA aerofoil pin-fins [229,234–236], irregular polygon [237], branched and interrupted [238], U-turn hybrid fins [239], and twisted fins [240]. With the recent rise of additive manufacturing-based heat sinks, more complex shapes are being explored [241,242]. Most recently, Bhandari et al. produced a review of the effects of different common and some unconventional pin-fin shapes [14]. Interestingly, bio-inspired structures and surface morphologies are also increasingly becoming popular in heat sinks; however, the availability of bio-inspired and biomorphic pin-fin heat sink research tends to be scarce; the term ‘biomorphic’ refers to designs that use naturally occurring shapes and patterns. Recent research suggests some implementation of piranha [243], mushroom-shaped [244], tree-shaped [245], petaloid and shark skin-inspired pin-fins [246]. The results related to bio-inspired pin-fins show superior performance over traditional shapes or geometries.

2.7.1 Micro pin-fin strategies

As covered in the earlier section, recent works have highlighted a significant amount of research on pin-fin-based heat sinks, relying on traditional geometries [4,8,34]. However, the prevalence of micro pin-fins (MPFs) and non-conventional or combined and hybrid pin-fins is

an area that requires much more attention to gain a comprehensive understanding of their effectiveness for optimal performance [14]. Peles et al. [247] were among the first to examine micro-pin fins; they investigated heat transfer and pressure drop phenomena in a micro pin-fin bank. A simplified expression for total thermal resistance had been derived, discussed, and experimentally validated. The study examined the impact of geometrical and thermo-hydraulic parameters on total thermal resistance, finding that pin-fin heat sinks can achieve very low thermal resistances comparable to those in microchannel convective flows. An increase in flow temperature significantly reduced thermal resistance. Also, another initial research by Siu-ho et al. [248] tested a copper micro pin-fin heat sink (MPFHS), finding that existing low Reynolds number correlations were inaccurate, highlighting the need for further research into MPF thermal and fluid dynamics — this is arguably still the case in recent years.

Shemelash et al. [249] addressed microprocessor cooling challenges by designing Fibonacci phyllotaxis circular MPFHSs. They used multi-objective optimisation and factorial experiments to determine optimal parameters: 300 μm height, 122.6 μm diameter, and 130 μm phyllotaxis coefficient, with a coolant velocity of 2.263 m/s. This design achieved a maximum temperature of 51.6°C and a pumping power of 0.191 W, showcasing superior heat dissipation. Xu et al. [246] followed a similar bio-inspired MPF strategy. They investigated petaloid and placoid MPFs, inspired by *Clematis Montana* and *Squalus Acanthias*; they analysed thermal-hydraulic characteristics under different conditions and found petaloid fins provided better heat transfer but higher flow resistance, while placoid fins had lower resistance but less heat transfer. Moreover, a new correlation for the Nusselt number and friction factor showed deviations below 2.0% and 4.5%, respectively.

Roosbehi et al. [250] optimised the MPF geometry for improved performance. They varied the vertex angle and relative length and found that a vertex angle of 60° and a relative length of 1 provided the best results. This design improved fluid flow, reducing recirculation and thermal boundary layer effects, and increased the average Nusselt number by 24.46% and thermal performance factor by 23.89% at a Reynolds number of 1,000. Qidwai et al. [251] combined microjets and MPF in a cooling system, optimising geometric parameters such as jet diameter to pin fin diameter ratio, jet diameter to standoff distance, and pin fin pitch. They found that vortex generation significantly influenced heat transfer, achieving optimal performance at specific geometric ratios. The jet Reynolds number had minimal impacts.

Gupta et al. [252] used numerical simulations and NSGA-II to optimise perforated MPFs with square shapes and circular perforations. They focused on maximising the Nusselt number and minimising the friction factor while varying design variables. The study found perforations did not affect stiffness and provided insights into thermohydraulic features, enhancing the understanding of complex cooling systems. Harris et al. [253] also numerically compared square MPFs with a novel biomorphic scutoid pin-fin design under different wall-heating conditions. The results showed that the scutoid design outperforms traditional pin-fins, achieving a higher heat transfer coefficient with lower pressure drop and operating base temperatures. Wall heating improved heat distribution but reduced overall heat dissipation; pressure drop was more influenced by pin-fin geometry than wall heating conditions. Also, Xie et al. [254] studied staggered diamond MPFs in microchannels, analysing pressure drop and heat transfer characteristics. They found stable vortex-wake flow at low Reynolds numbers, but instability at higher Reynolds numbers affected heat transfer, highlighting the importance of vorticity and turbulent kinetic energy in heat transfer.

Micro pin-fins have also been used in combination with refrigerants. Xu et al. [255] developed a petaloid micro pin-fin heat sink (MPFHS) to improve microelectronic cooling. They compared the performance of green refrigerants R1234ze(E) and R1234yf with R134a. R1234ze(E) showed the highest heat transfer coefficient and lowest frictional pressure drop. New correlations were created for the petaloid design, achieving mean deviations of 12.6% for heat transfer and 9.9% for pressure drop. Likewise, David et al. [256] investigated a micro pin-fin microchannel heat sink using R134a refrigerant. They found the heat sink maintained nearly uniform temperatures and showed a peak heat transfer coefficient at an exit vapour quality of 0.55. Their study introduced a cost-effective technique for enhanced cooling performance.

Additionally, some researchers have investigated micro-pin fins with nanofluids. For instance, Ambreen et al. [257] investigated how pin-fin shapes and nanofluids affect heat transfer in heat sinks. Nanofluids improved performance for all pin-fin shapes, with circular fins performing best. At maximum pressure drop, nanofluids led to significant enhancements in heat transfer, with circular, square, and triangular fins achieving Nusselt number improvements of 23.1%, 16.5%, and 8%, respectively. On a separate occasion, Ambreen et al. [258] used a two-phase Eulerian-Lagrangian model to evaluate a MPFHS with water and nanofluids. They found nanofluids improved thermal performance, with the highest average heat transfer coefficient enhancement of 16% at higher particle concentrations and optimal pressure drop. Also, Keshavarz et al. [259] explored the effects of nanofluids and fin

distribution on heat sink performance. Drop-shaped fins increased outlet temperature slightly, but reduced pumping work compared to circular fins. Nanofluids like Al_2O_3 –water improved performance, and staggered fin arrangements provided higher temperatures but required more pumping work than in-line configurations.

Microfluidics cooling is another area where MPF are utilised. Rajan et al. [260] demonstrated microfluidic cooling for 2.5-D system-in-packages using integrated MPFHSs and 3-D printed manifolds. This approach effectively cooled an FPGA, maintaining core temperatures around 30°C while dissipating 107 W of power, with a thermal resistance of 0.074°C/W , showing promise for high-power applications. Sarvey et al. [261] examined microfluidic cooling with a MPFHS integrated into an FPGA. Using deionized water, they achieved an average junction-to-inlet thermal resistance of 0.07°C/W , effectively cooling the FPGA and demonstrating the feasibility of this method for high-density electronic applications. Zhang et al. [262] designed a TSV-compatible MPFHS for high-power 3-D IC stacks, maintaining chip temperatures below 50°C at power densities over 100 W/cm^2 . Their design achieved a 33% reduction in junction temperature compared to air cooling, demonstrating effective cooling for advanced ICs. Renfer et al. [263] utilised vortex-enhanced heat transfer in 3D chip stacks using TSVs and MPFs. They achieved up to 230% increase in local Nusselt numbers and reduced temperature non-uniformity significantly, improving overall thermal performance by up to 190%.

Other investigations to assess the MPFHS performance were by Shi et al. [237] who explored different nozzle shapes for a composite heat sink to manage high heat fluxes in chip technology. They found that diamond nozzles achieved the highest local heat transfer coefficient but had poor performance on the MPF surface. Square nozzles offered the best overall performance with lower thermal resistance and pressure drop, demonstrating effective cooling for high-heat flux chips. Han et al. [264] studied subcooled flow boiling in MPF arrays under varying conditions. They observed that the heat transfer coefficient decreased with increasing heat flux and identified triangular wakes post-bubble nucleation. Their findings emphasised the role of vorticity and flow oscillations in heat transfer. Zhang et al. [265] tested silicon MPF with different pin sizes, achieving a maximum heat transfer coefficient of $60\text{ kW/m}^2\text{K}$. They found that pin density significantly affects performance and used an empirical model to explore trade-offs between electrical and thermal performance. Sarvey et al. [266] explored nonuniform MPF heat sinks for cooling integrated circuits with varying power

densities. Clustering pin-fins over hotspots and spanning the channel width effectively reduced thermal resistance with a modest increase in pressure drop.

Furthermore, machine learning and artificial intelligence-related research is rapidly advancing in pin-finned heat sinks and thermal management for thermal and fluid flow predictions [267], performance enhancement [36], external validation [268], evaluation [269], design optimisation [270], temperature predictions [271], physics-informed neural networks (PINNs) [272], and Bayesian optimisation [273], amongst other applications [274–276]. However, the research focusing on micro pin-fins is limited. The flow characteristics from a macro to micro scale vary greatly depending on many external and physical factors. Nevertheless, some research in MPFHS and machine learning exists. For instance, Markal et al. [277] used machine learning to predict flow boiling behaviour in expanding type micro-pin-fin heat sinks (ETMPFHS). A new database with varying operational conditions was analysed using ML models, including Artificial Neural Networks (ANN), Support Vector Machine (SVM), Regression Trees (RT), and Linear Regression (LR). Results show that ANN is the most accurate for predicting heat transfer, temperature, and pressure, followed by SVM, while RT and LR were less effective.

Lee et al. [278] employed a Multimodal machine-learning approach, combining boiling pattern images with geometric and operational data, to predict heat transfer in micro-pin fin heat sinks. Among the four ML algorithms tested, the Multimodal model excelled, achieving high accuracy with a MAPE of 1.81% for maximum temperature and 0.84% for average temperature. Zhu et al. [279] found that the conventional machine learning model achieved good prediction accuracy with a 4.11% deviation but was limited to the same data domain as its training data. By incorporating transfer learning, the model extended its applicability to new domains, achieving a similar accuracy with a 4.28% deviation when using 70% of new domain data. This demonstrates that transfer learning can effectively broaden the application range of machine learning models for predicting heat transfer in mini channels with micro pin fins.

Kim et al. [280] developed universal machine learning models to predict the thermal performance of micro-pin fin heat sinks with various geometries and operating conditions, surpassing the limitations of existing correlations. Using a database of 906 data points from 15 studies, the machine-learning models were compared with traditional regression models. The machine learning models achieved mean absolute errors (MAEs) of 7.5–10.9%, significantly improving prediction accuracy by approximately fivefold compared to existing correlations.

These models also demonstrated superior accuracy for rare geometric shapes and operating conditions, such as triangular pin shapes or using R134A as a working fluid, highlighting their effectiveness in predicting thermal performance across diverse scenarios.

As part of our literature scanning, we searched in the Scopus document database to evaluate the existing research concerning heat sinks. The search aimed to identify key trends and gaps in the literature over the past 25 years. Our initial broad search used the term "heat sinks" within abstracts, titles, and keywords, resulting in 29184 publications; this search provided a general overview of the development of heat sinks and a research focus on them over the years. It was observed that the research in heat sinks has increased exponentially over the years, especially in the last three years, as heat sinks are an integral component in achieving thermal management and reaching sustainable development goals.

Moreover, to gain deeper insights, we targeted searches combining "heat sink" with specific technologies and methods, such as "micro pin fin" and "machine learning." The search combining "heat sink" and "micro pin fin" yielded 458 publications, accounting for 1.6% of the total. Nonetheless, it should be noted that not all keywords fully capture the relevance of the investigation related to micro pin-fins due to the type of investigation or applications; therefore, this relatively small number suggests limited exploration in integrating micro pin-fin technology with heat sinks despite its potential for enhancing thermal performance. Similarly, combining "heat sink" and "machine learning" returned 124 publications, representing 0.4% of the total. The application of machine learning in optimising heat sink design and performance appears to be emerging, with significant opportunities for innovation and development. Notably, searching for "micro pin fin and machine learning" resulted in only 7 publications. Combining micro pin fin with artificial intelligence resulted in 0 publications, indicating a significant gap in this area.

Although some nature-inspired pin-fin designs exist in different types of heat sinks [8,246,255,281], combining hybrid MFS with biomorphic or bio-inspired designs can significantly impact the design and efficiency of heat sinks; thus, it is an area that needs further investigation. The lack of substantial literature in these niche areas emphasises the need for focused and interdisciplinary research. Integrating technologies like MPF and machine learning into heat sink design could improve cooling efficiency for electronic devices and systems. Therefore, the potential findings of a combined strategy could strongly suggest a promising avenue for current and future investigations, impacting industries reliant on effective

thermal management solutions. Fig. 2.8 shows the trend of research over the years regarding heat sinks and micro pin-fins.

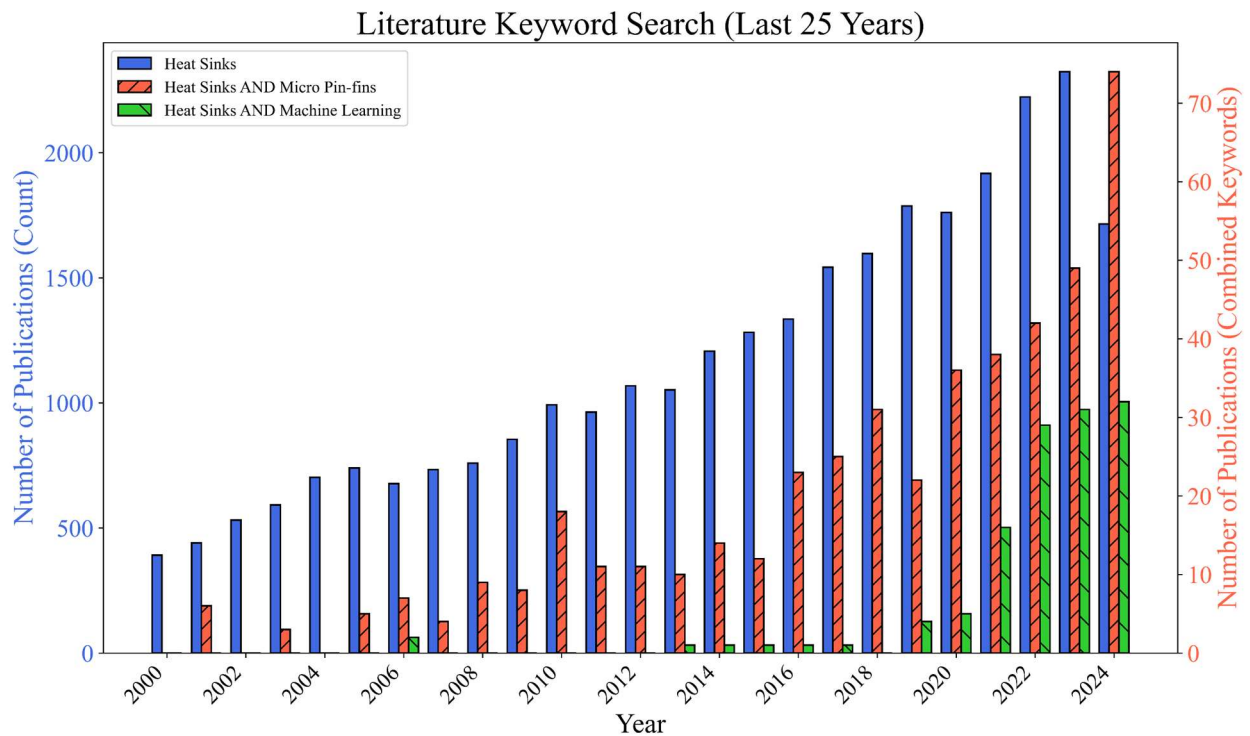


Fig. 2.8 Research trend of micro pin-fin heat sinks

2.8 Intersection of Machine Learning and Micro Heat Sinks

The literature on heat sink optimisation and cooling technologies highlights notable progress in machine learning (ML) and optimisation algorithms to improve thermal management systems. These advancements are vital for enhancing both performance and energy efficiency in electronic devices, particularly in applications that demand highly efficient cooling solutions. Nevertheless, despite these developments, further investigation is required to fully comprehend the underlying mechanisms and to determine how machine learning and artificial intelligence (AI) can provide more comprehensive solutions to complex thermal challenges.

While the integration of ML and AI in micro heat transfer is a rapidly growing field, it remains under-researched. A simple search on Scopus for heat sinks whilst using keywords such as 'pin-fins' and 'machine learning' yields just 15 relevant papers. Similarly, searching for 'flow boiling' combined with 'machine learning' returns only six results. These figures clearly illustrate a significant research gap, particularly when compared to more conventional areas of heat transfer optimisation. This gap becomes even more apparent when 'machine learning' is replaced with 'artificial intelligence,' which further reduces the number of relevant studies. This suggests that although these emerging trends are promising, there remains considerable

potential for developing AI-driven methods to enhance heat transfer performance, particularly in complex systems involving phase change, such as flow boiling.

The existing literature can be broadly divided into three primary areas of focus: design optimisation, cooling technologies, and machine learning applications. Design optimisation typically centres on improving heat sink geometries—such as pin-fin configurations and microchannels—to maximise heat dissipation while minimising pressure drop. Cooling technologies, on the other hand, explore innovations in nanomaterials, surface modifications, and hybrid cooling systems that offer avenues for more efficient thermal management. However, the role of machine learning in these fields is still in its early stages.

There has, however, been growing interest in machine learning applications, particularly in the classification of boiling regimes and identification of flow patterns. Studies in this area investigate how ML models can improve the prediction, classification, and real-time monitoring of boiling processes and flow behaviour. This capability is particularly important for the reliability and performance of cooling systems in applications where phase change plays a significant role. These studies can be grouped into three main categories: boiling regime classification, flow regime identification and prediction, and bubble dynamics modelling. Each of these areas presents distinct challenges and opportunities, particularly when considering the integration of machine learning algorithms that can adapt and improve with real-time data. However, it is important to note that current ML and AI models are data-intensive, prone to overfitting, and may lack the agility needed for product development cycles. Thus, low-data-driven solutions are required to foster more agile and adaptable design frameworks.

The following sections will provide a detailed thematic review, examining recent contributions within these areas, critiquing the innovative methodologies employed, and highlighting where further research could yield the most significant impact.

2.8.1 Design Optimisation of Heat Sinks

Abdollahi et al. [282] explored the impact of square perforations in parallel finned heat sinks, demonstrating that peak performance occurs at high Reynolds numbers (39,900). Their combinatorial algorithm outperforms neural networks in this case, suggesting that traditional optimisation methods still hold value for specific applications. Zohora et al. [283] introduced novel pin-fin designs in microchannel heat sinks, including circular perforated fish fins and elliptical fins, with the latter reducing pressure loss by 67%. These innovative shapes underline the potential of unconventional geometries in thermal optimisation. Yang et al. [284] combined

deep learning and genetic algorithms to optimise pin-fin structures, employing pix2pix networks to predict temperature and pressure distributions. Their approach suggests promising opportunities for square pin-fins and integrating advanced neural networks with simulations to drive further optimisation. Shaeri et al. [285] utilised artificial neural networks (ANN) and greedy search algorithms to optimise air-cooled plate-finned heat sinks, focusing on reducing weight while maintaining heat transfer efficiency. Their effective analysis of performance versus structural integrity shows the importance of ensuring thin fins remain structurally sound. Suzuki et al. [286] applied random forests and neural networks to predict heat transfer and pressure loss in lattice-structured heat sinks, simplifying the design optimisation process by identifying four parameters, thus reducing computational power without sacrificing accuracy.

2.8.2 Advanced Cooling Technologies

Aldaghi et al. [287] explored hybrid cooling technologies combining multi-walled carbon nanotube (MWCNT) nanofluids with forced air convection and phase change materials (NPCM). The study identifies the RL-GMDH deep learning model as particularly effective for predicting PCB temperatures, showing the potential for hybrid cooling in preventing chipset overheating. Salari et al. [288] examined energy storage material (ESM) configurations in heat sinks, discovering that separating the material (HS-ESM-II) significantly enhances cooling performance. Their use of Random Forest and the Harris Hawks Optimiser to fine-tune these configurations underscores how machine learning can optimise complex systems for maximum efficiency. Farahani et al. [289] explored microchannel heat sinks utilising wavy structures, non-Newtonian fluids, and porous media, achieving an 80% improvement when combined with phase change materials. This research highlights the potential of hybrid systems combining different materials and geometries to elevate thermal performance.

2.8.3 Machine Learning and Predictive Models for Thermal Systems

Aksoy et al. [290] optimised heat sinks produced via Direct Metal Laser Sintering (DMLS), achieving a 99.8% accuracy rate with an ensemble-ANN algorithm. Their integration of an interface program for comparing experimental and model results demonstrates the potential for real-time applications in thermal management. Bard et al. [291] utilised support vector machines (SVM) to predict heat transfer coefficients during flow boiling in mini/microchannels. Despite a mean absolute percentage error (MAPE) of 11.3%, the study highlights the challenge of managing outlier data, especially in water-based systems. Herring et al. [292] leverage polynomial regression, random forest, and neural networks to optimise

air-cooled heat sinks, significantly reducing design lead times using large CFD datasets. This approach is particularly beneficial for industries like electronics, where rapid design iteration is critical. Shanmugam and Maganti [293] compared the performance of multiple machine learning models (ANN, XGBoost, LightGBM, and KNN) in predicting thermal resistance in microchannel heat sinks, with XGBoost performing exceptionally well ($R^2 = 0.98$). Their study underscores the importance of feature selection in enhancing model precision. Mengesha et al. [294] contrasted support vector regression (SVR) with kernel ridge regression (KRR) for predicting heat transfer coefficients, achieving an accuracy within $\pm 1.9\%$ of simulated values. Their findings suggest that these models can serve as computationally efficient alternatives to traditional methods. Ghosh et al. [295] employed multi-fidelity Bayesian optimisation, combining low and high-fidelity simulations for gas turbine cooling. This hybrid technique significantly reduces computational costs while boosting heat transfer efficiency, showcasing the value of integrating diverse data sources in thermal management.

2.8.4 Boiling Regime Classification

Barathula et al. [296] leveraged machine learning to classify boiling regimes using acoustic data from pool boiling experiments. Their decision tree ensemble model surpassed binary decision trees and naive Bayes, providing high accuracy and rapid inference. This method significantly improves real-time safety monitoring, which is essential in systems where boiling regimes can unpredictably shift, such as cooling systems. Hobold and Silva [297] utilised machine learning to classify natural convection, nucleate boiling, and film boiling, based on low-resolution images from pool boiling experiments. The use of support vector machines (SVM) and neural networks achieved an accuracy of over 93%, highlighting the power of visual data for regime classification, even when direct physical measurements are absent. Loyala-Fuentes et al. [298] developed machine learning models such as K-nearest neighbours (KNN), random forests, and multilayer perceptrons to classify flow regimes in pulsating heat pipes. Drawing on data from two fluids, their best models produced a flow pattern map that enhanced predictions of regime transitions, reducing uncertainty significantly. Ooi et al. [299] applied machine learning to classify boiling flow regimes in a vertical annulus channel, using support vector machines and KNN. A self-organising map (SOM) identified global regimes from conductivity probe signals, with classification accuracy exceeding 90%, demonstrating ML's ability to categorise flow regimes even with limited sensor data. Manikonda et al. [300] focused on vertical gas-liquid flow regime classification in the oil and gas sector. Their study found KNN to be the most effective model, achieving 98% accuracy in distinguishing between

flow types like bubbly, slug, and churn. The KNN model outperformed multi-class SVMs and clustering methods, proving its effectiveness in real-world applications like flow control.

2.8.5 Flow Regime Identification and Prediction

Seal et al. [301] classified two-phase flow patterns of R-134a in inclined tubes using artificial neural networks (ANNs), achieving over 98% accuracy. Their use of Principal Component Analysis (PCA) for dimensionality reduction, followed by convolutional neural networks (CNNs) for enhanced image classification, resulted in real-time performance, making the method particularly valuable for industrial heat transfer systems. Zhu et al. [302] enhanced flow regime identification by mapping bubble distributions to machine learning features, attaining 86% accuracy in identifying three global flow regimes (e.g., bubbly, slug). This study introduced a new criterion for transitioning between bubbly and slug flow, offering insights into flow dynamics under boiling conditions. The use of unsupervised learning methods such as K-means and K-medoids underscores the importance of clustering techniques in flow regime identification. Schepperle et al. [303] developed a binary image segmentation method combined with a U-Net-based CNN to identify flow regimes and void fractions in microchannel flow boiling. Achieving a Dice score of 99.1% for image segmentation and 91% accuracy in flow regime classification, this method demonstrates the power of CNNs in analysing intricate flow patterns, particularly in applications requiring detailed visualisation.

2.8.6 Bubble Dynamics and Heat Transfer Modelling

He et al. [304] applied machine learning to predict bubble departure frequency in subcooled flow boiling, testing nine regression models on data from four fluids. The XGBoost model outperformed traditional methods, providing reliable predictions and surpassing conventional empirical correlations. This study makes a strong case for the replacement of traditional predictive models with machine learning techniques in boiling heat transfer applications. Hobold and Silva [305] showed how neural networks could estimate heat transfer in boiling processes using only visual data, with models achieving errors as low as 7%. This approach offers a real-time, non-invasive method for monitoring heat flux, with potential for low-cost, compact applications, such as those involving Raspberry Pi systems. Seong et al. [306] used a U-Net-based CNN to segment and track wall-attached bubbles in high-speed video images of boiling, achieving over 90% accuracy in bubble detection. Validated against infrared thermometry, the model estimated boiling parameters with a $\pm 20\%$ accuracy. This combination of visual data and machine learning highlights the potential for improving bubble dynamics

modelling without intrusive sensors. Suh et al. [307] applied CNNs and object detection algorithms to predict boiling curves based on bubble dynamics, achieving a mean error of just 6%. This method provides an automated alternative to traditional heat transfer measurements, offering valuable insights for both research and industrial applications.

2.8.7 Research Gaps

In recent years, a substantial body of research has focused on optimising heat sink designs to enhance heat transfer while minimising pressure drop. These efforts, often leveraging computational models and machine learning techniques, underscore the importance of balancing thermal efficiency with other critical factors such as structural integrity and mechanical stresses. Despite the promising results obtained through machine learning, many studies remain constrained by their reliance on idealised simulations. Consequently, one of the key research gaps involves the need for integrated approaches that account for real-world constraints, including material limitations and mechanical durability. Moreover, the heavy dependence on simulation data highlights the pressing requirement for experimental validation to ensure practical applicability.

Another prominent area of innovation is the exploration of advanced cooling materials, such as nanofluids and phase-change materials, which have demonstrated substantial potential in improving heat transfer. However, the literature reveals several unresolved challenges, including fluid stability, material compatibility, and long-term cost implications. For instance, the degradation of nanofluids and the repeated cycling of phase-change materials raise concerns regarding the durability and commercial viability of these systems. Addressing these factors through long-term studies and real-world testing is essential for advancing the field.

Appraising the current literature, machine learning has proven invaluable for predicting heat transfer, optimising thermal management designs, and reducing computational costs. Nevertheless, the reliance on large datasets introduces new challenges, particularly in cases where experimental data is scarce or difficult to obtain. Additionally, while machine learning models demonstrate impressive accuracy in controlled environments, their robustness under varying operational conditions remains an open question. This signals a significant gap: future research should focus on adapting these models to more complex, real-world datasets.

The convergence of machine learning techniques with innovative materials has led to considerable advancements in thermal management. Despite these technological strides, practical implementation encounters several hurdles, notably scalability, cost, and the need for

extensive real-world validation. Future investigations should prioritise the integration of experimental validation with computational models, exploring the long-term reliability of hybrid cooling systems. Additionally, refining machine learning algorithms to manage the complexity and variability of real-world scenarios remains a crucial research gap.

Machine learning, particularly, deep learning techniques such as convolutional neural networks (CNNs) and decision trees, has demonstrated significant efficacy in classifying boiling and flow regimes. Techniques such as decision trees, support vector machines (SVM), and k-nearest neighbours (KNN) have outperformed traditional approaches, offering the potential for real-time, non-intrusive monitoring of thermal systems. However, these models depend heavily on large experimental datasets, which often do not capture the full range of complexities within industrial conditions. Therefore, extending the reach of these models to encompass more diverse datasets from different sectors or operational settings is critical for ensuring their broader applicability.

One of the more exciting developments in the field has been the application of CNNs for identifying and predicting complex flow regimes, where real-time accuracy and precision have consistently been reported. This synergy between advanced image processing and machine learning holds promises, yet it also exposes another research gap. While these models perform well in controlled settings, they need validation on industrial-scale systems to confirm their robustness across diverse fluid flow conditions. Future research should thus focus on integrating machine learning techniques with broader datasets to ensure these models remain effective across varying operational environments.

In sum, machine learning techniques such as CNNs, XGBoost, and KNN are reshaping the field of thermal management through enhanced real-time monitoring and more precise predictions of flow and heat transfer. Despite these successes, the research community faces several critical gaps. The key gap among them is the need to validate these methods on more complex, real-world datasets to ensure their utility across various industrial applications. Moreover, low-cost, real-time monitoring systems remain a priority to facilitate the broader adoption of these advanced machine learning techniques in thermal management systems.

Key Research Gaps:

1. **Integration of Real-World Constraints:** More comprehensive models must incorporate material limitations, mechanical, and long-term operational considerations.

2. **Experimental Validation:** A significant gap persists in validating machine learning-based optimisation models with experimental data to ensure real-world applicability.
3. **Scalability and Cost:** Future research should address the challenges of scaling advanced cooling systems and reducing their cost to facilitate commercial adoption.
4. **Dataset Limitations:** Extending machine learning models to more diverse datasets from industrial applications are crucial for improving robustness.
5. **Low-Cost Monitoring Systems:** The development of affordable, real-time monitoring solutions using machine learning should be prioritised to encourage broader use.

2.9 Integration of Manufacturing Philosophies

The literature review and past works have shown the diverse ways manufacturing strategies for micro heat sinks [308,309]. However, there is a notable gap in the literature that integrates design and manufacturing philosophies within the processes. In designing a novel pin-fin-based micro-heat sink, integrating various manufacturing philosophies, sustainable practices, and design thinking will be critical for optimising performance, sustainability, cost-effectiveness, and efficiency. Each philosophy offers a unique contribution to the development and production of innovative designs. The following paragraphs highlight the importance of different manufacturing philosophies in developing new micro heat sinks.

Lean manufacturing can be key in reducing material waste during the design and fabrication of the micro pin-fin structure. By streamlining the production process and eliminating inefficiencies, we can ensure that resources such as metals and advanced composites are used effectively, lowering material costs and energy consumption [310]. In practice, we can apply lean principles by conducting process audits to identify wastage, adjusting workflows, and using simulation tools, such as CFD, to optimise design materials.

Six Sigma concepts can be applied to maintain precision and accuracy during the micro-manufacturing process. Given the intricate design of micro pin-fins, controlling variation, in dimensions is crucial for ensuring uniform thermal performance across the entire heat sink. Six Sigma methodologies will be implemented with advanced quality control measures to monitor production variations, and trade-offs, and ensure consistent pin-fin dimensions [311].

Agile manufacturing allows flexibility throughout the design and development phases of the micro pin-fin heat sinks. Rapid prototyping and testing of different pin-fin configurations will be critical in determining the optimal design for heat dissipation. Agile methods will be applied by maintaining an iterative development cycle, where we will continuously test new

pin-fin geometries and combinations, making rapid adjustments to both design and analysis processes based on real-time performance data [312].

Green manufacturing ideas ensure that the production of the micro pin-fin heat sink aligns with sustainability goals. By selecting environmentally friendly materials and processes, we can reduce energy consumption and emissions during production [313]. Additionally, implementing green manufacturing by prioritising materials like recycled metals or composites, and adopting energy-efficient fabrication techniques, such as low-energy micro-machining processes, will minimise the carbon footprint of each heat sink.

Design for Manufacturing and Assembly (DFMA) enables feasible designs, and cost-effective and allows easy assembly for experimentation. By simplifying the design, reducing the number of components, and using materials that are both sustainable and efficient, we can create a heat sink that is easier to manufacture at scale while maintaining or even improving its thermal performance. DFMA will be applied by optimising pin-fin geometry for easy integration into existing manufacturing lines, minimising assembly steps, and using modular components to reduce costs and complexity [314].

Total Quality Management (TQM) embeds quality throughout the development and production of the micro pin-fin heat sinks. By fostering a culture of continuous improvement (Kaizen), TQM will ensure that each design and production stage—from material selection to final assembly—adheres to stringent quality controls. We can apply TQM by implementing regular cross-functional reviews and quality checks at every stage of the product lifecycle, ensuring that feedback is acted on swiftly and integrated into design improvements [315].

Just-In-Time (JIT) philosophies can further reduce waste and increase process efficiency. By aligning production schedules closely with demand, we can reduce inventory costs. JIT will be applied by coordinating closely with suppliers and the in-house manufacturing team to ensure that materials such as metals, experimental consumables, and composites are delivered exactly when needed, minimising storage costs and reducing waste [316].

Sustainable engineering will guide the entire design process by ensuring that each material, process, and design decision prioritises minimal environmental impact. This includes selecting materials that are abundant, readily available in-house, recyclable and have lower carbon footprints, such as advanced composites or bio-based materials [317]. We can apply sustainable engineering by conducting explorative life cycle assessments (LCAs) for materials and processes used, ensuring that the micro pin-fin heat sink is designed to minimise its impact.

Design thinking can foster innovation and user-centric design. By empathising with the needs of industries that require high-performance cooling solutions, the design will evolve to meet specific operational and thermal management challenges [318]. Design thinking will be applied by conducting literature research to understand diverse cooling challenges (this can be air-cooled, single-phase water-cooled, and two-phase cooling) on prototypes, and testing different pin-fins to ensure the final product is high-performing and tailored to industry needs.

By carefully considering and implementing these manufacturing philosophies, the development of novel designs will benefit from optimised processes, high-quality production, and a strong emphasis on sustainability. This holistic approach will allow delivering a product that excels in thermal management, is cost-effective to produce, and meets the growing demand for environmentally responsible solutions. Fig. 2.9 shows how the integration of manufacturing can work in each stage of the design and manufacturing process.

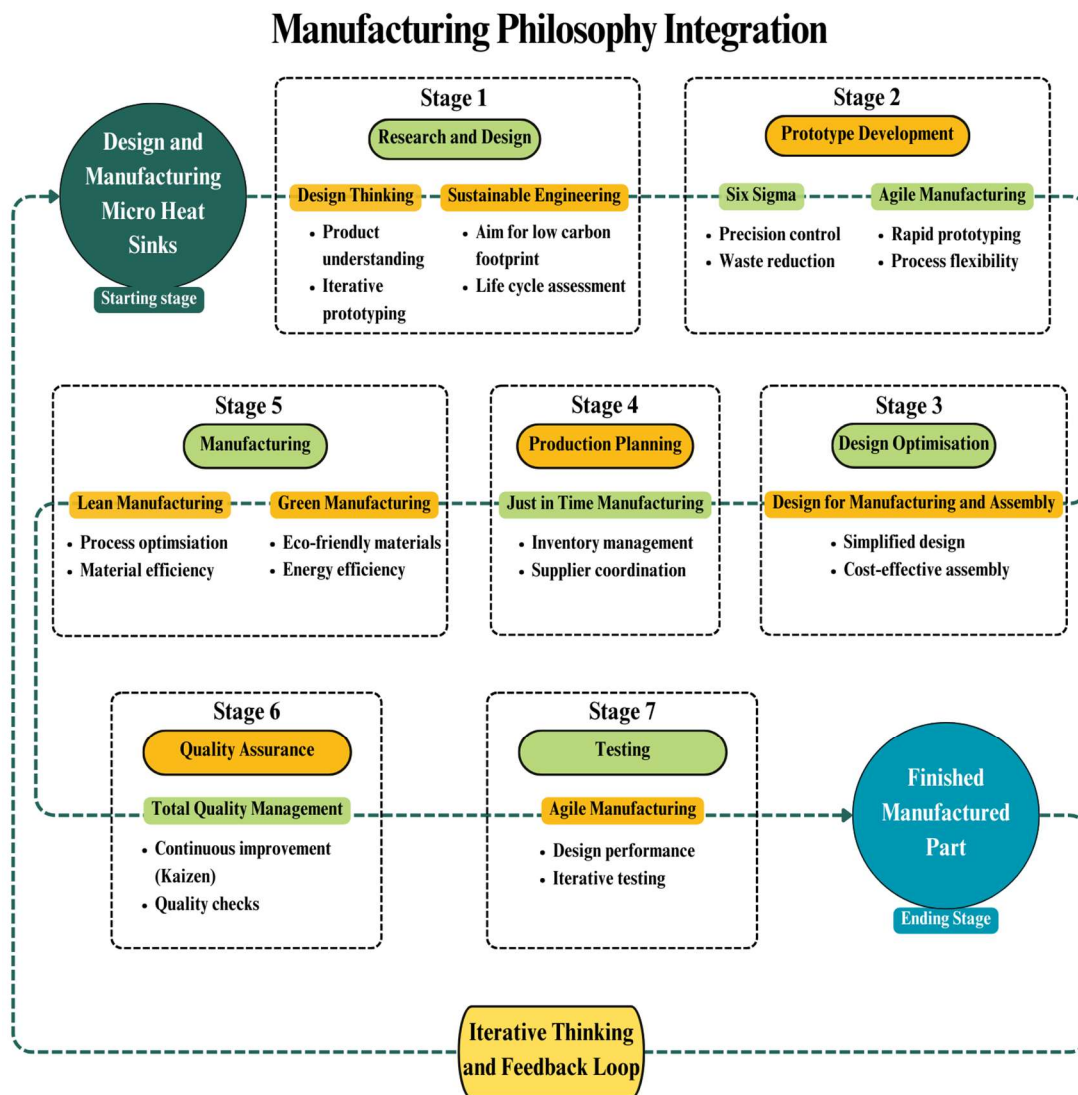


Fig. 2.9 Manufacturing philosophy integration into the research

2.10 Summary of Literature Review

The literature review comprehensively showcased the current research trends and fundamentally shaped the methodology and analysis required to address the research questions and objectives. Section 2.2's exploration of heat transfer fundamentals provided the theoretical foundation for designing this research's experiments and numerical simulations. By grounding the assessment of heat sink performance in established principles, the methods developed allow for a precise evaluation of innovations in micro heat sink technologies, as per RQ1 and OB1.

Sections 2.3 and 2.4, focusing on boiling heat transfer mechanisms and thermal management techniques, highlighted the specific parameters and conditions essential for experimental investigations. These sections are critical for shaping the methodology, especially in the context of bioinspired heat sinks, aligning closely with RQ2 and OB2. Furthermore, by identifying the flow patterns in boiling systems, these sections also inform the analysis techniques—particularly the application of machine learning for flow classification and predictive modelling, corresponding to RQ2 and RQ3.

The review of recent trends in micro heat transfer in Section 2.5, coupled with the findings from existing literature in Section 2.6, set the stage for a comparative analysis that informs both experimental and simulation phases. These sections clarify which performance metrics—thermal resistance, pressure drop, etc.—should be prioritised, while also exposing the limitations of traditional methods, which this research aims to address with machine learning algorithms, linked to RQ2 and RQ3. The analysis of pin-fin geometries in Section 2.7 directly impacted the design of experimental models and simulations, ensuring that the methodologies test novel bioinspired geometries for thermal efficiency, central to RQ2. Similarly, Section 2.8's discussion of machine learning drives the development of optimisation algorithms, ensuring that the design process is informed by data, improving both heat transfer and performance predictions.

Finally, Section 2.9's exploration of sustainable design principles and manufacturing approaches ensured that sustainability was integrated into the methodology. It shaped how performance, cost, and environmental impact are evaluated, aligning with RQ4 and OB4, where balancing high performance with environmental considerations is crucial. Ultimately, the literature review not only identifies gaps but also informs the structure of the methodologies and analytical techniques needed to address them fully.

In this literature review, we explored the diverse methodologies employed in recent research on micro heat sinks, highlighting their contributions and limitations. By examining a range of experimental setups, computational simulations, and machine learning techniques, we identify prevailing trends and best practices within the field. The research plans to leverage CFD for initial simulations, allowing design assessment, viability, and cost feasibility before making necessary adjustments for final manufacturing. Furthermore, we aim to implement data-driven machine learning approaches having less reliance on data-intensive models, effectively accounting for data availability while promoting smart data usage throughout the optimisation process. This strategy ensures that we consider multiple facets of design, performance, and sustainability rather than focusing on a single aspect, thereby promoting a holistic solution that addresses the complexities of micro heat sink technologies. As gaps remain in the literature, particularly in integrating innovative manufacturing philosophies and sustainable design principles, by framing this research within this context, we demonstrate how our methodological choices build upon and address the identified gaps, paving the way for future advancements in heat transfer efficiency. Table 1 summarises the key considerations, trends, gaps, and the resulting directions and proposed methods followed as a result.

Table 1: Summary of trends, gaps, and research direction for the thesis

Category	Existing Trends	Identified Gaps	Proposed Methods
Materials	Copper-based materials, traditional fluids like water and nanofluids	Lack of sustainable material choices; underutilisation of hybrid materials; refrigerant use	Use Aluminium alloys for cost efficiency and air/water as sustainable thermofluids
Heat Sink Design	Rectangular, straight microchannels, and square pin-fin geometries	Limited exploration of non-traditional geometries like bioinspired, or hybrid designs	Develop novel hybrid bio-inspired pin-fin heat sinks (e.g., scutoid, cruciform designs)
Heat Transfer Enhancement	Use of microchannels and pin-fins, surface modifications for heat transfer improvement	Over-reliance on basic geometries; inefficient exploration of turbulence-inducing features	Combine strategies to induce turbulence, vortices, and promote efficient flow mixing

Simulation and Modelling	Focus on CFD simulations for performance evaluation	Gaps in predictive modelling accuracy and lack of integrated ML approaches	Combine CFD simulations with ML models for HTC predictions.
Experimental Methods	Use of standard experimental techniques with single-phase systems	Lack of consensus or standardisation	Investigate both single-phase and two-phase systems, employing advanced test rigs and experimental data validation
Sustainability	Limited consideration of sustainability in heat sink design and manufacturing	Lack of focus on sustainable manufacturing, energy consumption, and carbon emissions	Apply sustainable manufacturing to optimise material use, and reduce energy consumption and carbon emissions
Manufacturing	Use of conventional micromachining techniques for fabrication	Under-explored use of advanced and agile manufacturing methods, lack of cost and time efficiency focus	Integrate additive manufacturing, surface treatments, and JIT principles for more efficient and sustainable fabrication processes
Machine Learning	Non-generalisable, data-intense machine learning models used for performance prediction	Still a growing area of research. Insufficient application of combined ML techniques for design process optimisation and real-time monitoring	Implement combined ML models (ensemble PCA, Neural Networks) for improved prediction accuracy, design process optimisation, and monitoring

Chapter 3: Methodology

Chapter Precursor: Chinese

“The journey of a thousand miles begins with one step.”

(千里之行，始于足下)

— *Lao Tzu*

This proverb by Chinese philosopher Lao Tzu mirrors the essence of the Methodology chapter and my research journey. Starting my PhD amid challenges, each initial step—learning new concepts, designing innovative heat sinks, and overcoming resource limitations—initiated a significant voyage. The PhD thesis methodology was deeply influenced by Chinese collaboration, from my principal supervisor to my heat sinks getting manufactured in China, and now getting assessed from Chinese expert examiners. This reflects how purposeful steps and cross-cultural cooperation have been essential in progressing toward significant achievements in thermal management technologies.

3.1 Background to the Chapter

The research project was methodically divided into four distinct phases, each targeting a specific objective. The initial phase involved an exhaustive review of existing literature and contemporary developments in thermal management systems, aimed at pinpointing key research gaps and directing the course of the investigation. This stage was the foundation for selecting appropriate methodologies and defining the scope of subsequent experimental and simulation-based work. During this phase, the 5 Whys technique was employed to systematically uncover root causes behind identified research gaps, ensuring a focused and thorough exploration of the underlying issues.

In the second phase, iterative numerical simulations were performed, predominantly employing computational fluid dynamics (CFD) in ANSYS Fluent. These simulations established a baseline for the design and optimisation of heat sinks, wherein various design parameters were explored, including geometric configurations and material properties. The feasibility and cost assessments conducted at this stage were pivotal in refining the designs, narrowing down options to those that demonstrated the greatest potential for high-performance heat sinks. To structure this optimisation process, the DMAIC (Define, Measure, Analyse, Improve, Control) framework was utilised, guiding the progression from problem identification to refined solutions.

The third phase focused on setting up the experimental test rig, calibration, and extensive experimental testing of the newly developed hybrid bio-inspired pin-fin heat sinks, assessed for their thermohydraulic performance, specifically, examining the heat transfer coefficient (HTC) and pressure drop characteristics. These experimental tests were essential in backing the practical viability of the bio-inspired design under real-world conditions.

Machine learning (ML) techniques were systematically integrated throughout the project as part of an adaptive approach to augment design exploration and optimisation. Drawing on data from CFD simulations, experiments, external and synthetic data, ML models were developed to predict heat transfer metrics across a wide array of design configurations. This significantly accelerated the design exploration process by reducing dependence on laborious CFD simulations. By training the models on CFD-generated data, when necessary, ML algorithms were able to rapidly estimate HTC values for new design variations, thereby expediting the optimisation process and enabling a more comprehensive exploration of design possibilities. Furthermore, in the latter stages, machine learning played an instrumental role in uncovering

patterns and insights not readily discernible through traditional simulation methods. This facilitated the identification of critical factors most influential on thermal performance, guiding subsequent refinements to heat sink designs.

The final phase was dedicated to a rigorous critical analysis of the results, concentrating on refining methodologies and affirming the robustness of the conclusions. This involved cross-referencing findings from the literature review, numerical simulations, experimental tests, and machine learning predictions. The continuous feedback loop between these methodologies ensured that the conclusions were substantiated and that the machine learning models were optimally trained to enhance accuracy and process efficiency. Both the 5 Whys and DMAIC methodologies were instrumental in this stage, ensuring that all root causes and inefficiencies were addressed, resulting in a more streamlined and effective end outcome.

3.1.1 Research Strategy

While a comprehensive review of the research methodologies is beyond the scope of this thesis, the chosen approach is summarised here. The author's research philosophy was rooted in pragmatism, employing a mixed-method design. Pragmatism allows for the flexible application of insights to practical problems [319], which proved advantageous in this context, where experimental observations and strategic thinking drove data analysis, simulations, and process improvements. Although pragmatism is sometimes critiqued for lacking systematic rigour [320], this study employed a structured approach that mitigated such criticisms.

The mixed-method design, combining both qualitative and quantitative approaches, is argued to offer more robust solutions [321], despite ongoing debates surrounding its methodology [322]. In this research, qualitative insights drawn from existing literature were integrated with quantitative data from experiments and numerical simulations. This integration was essential for formulating objectives and identifying solutions to manufacturing and thermal management challenges. Both approaches were used throughout the investigation, alongside various quality management techniques, to address the research problems effectively. Descriptive analysis and logical deductions were applied where necessary, establishing connections between key concepts, research questions, and data collection strategies.

To ensure the accuracy and validity of the findings, regular feedback from colleagues, technical experts, and supervisors was sought, minimising potential errors in interpretation. Reflexivity was an integral part of the quality assurance process, using checklists adapted from the works of Tracy [323] and Pimple [324]. Although single-case studies are often critiqued

for their lack of generalisability, they are well-suited for detailed, focused investigations [325]. Gustafsson [326] posits that while multi-case studies can yield more robust findings, single-case studies remain appropriate for in-depth exploration, particularly in manufacturing research [327–330]. Accordingly, various single-case and multi-case study designs were explored to aid the investigation. The findings from these single-case investigations were cross-synthesised to develop a comprehensive strategy for the final designs and overall research outcomes.

Despite any critiques and limitations, the chosen research methodology was justified due to its potential for delivering valuable insights, its focus on a relatively unexplored area, and the broad benefits it offers at a macro level. The knowledge gained from this investigation can be adapted to different contexts. Fig. 3.1, adapted from Saunders et al. [319], visually summarises the methodology employed in this study.

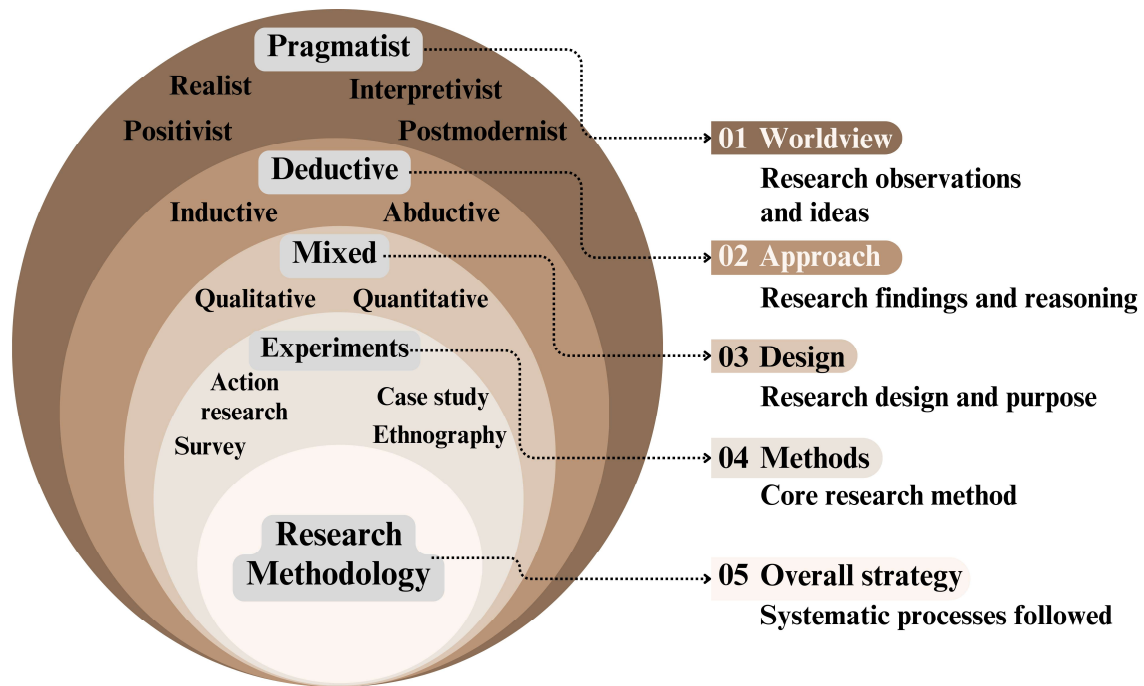


Fig. 3.1 Research Onion describing the overall research methodology

3.2 CFD Simulation Setup

3.2.1 Geometry Creation and Meshing

The geometries for the heat sinks, encompassing both traditional and biomorphic pin-fin structures, were modelled in SolidWorks based on experimental dimensions. Key components, such as the pin fins (solid domain) and (air/water) fluid domain, were incorporated to ensure seamless transfer to ANSYS Fluent for meshing and simulation. The CAD model accurately replicated the experimental setup's physical parameters. The meshing process aimed to

precisely capture the fluid flow and heat transfer dynamics. Element sizing and mesh refinement were focused on areas with high-temperature gradients and critical regions, such as the heat sink walls and pin fins; hybrid and multizone meshing were applied when necessary. A mesh independence study was conducted to determine the optimal mesh density, ensuring further refinement did not significantly alter results. Three mesh types were tested, with deviations of less than 2-3% and orthogonal quality values between 0.75 and 1, confirming mesh reliability. The refinement ratios of Mesh (II)/(I) and (III)/(II) were above 1.3, providing additional validation for grid independence.

3.2.2 Boundary Conditions and Solver Settings

The simulation was conducted using a pressure-based solver under steady-state conditions with gravity effects disabled due to their negligible influence on fluid flow. The energy equation was activated to account for thermal phenomena, and the k- ϵ turbulence model was employed with standard wall functions and near-wall treatment for consistency and computational efficiency. Aluminium, akin to the manufactured heat sinks, was used as the solid material, while water in its liquid phase served as the air/working fluid. Boundary conditions were designed to replicate experimental flow rates, utilising inlet velocity and heat flux as primary parameters, with inlet temperatures ranging between 20°C and 25°C to simulate room temperature conditions. Outlet pressure was fixed at zero. The SIMPLE algorithm facilitated pressure-velocity coupling, with second-order upwind spatial discretisation applied for parameters such as pressure, momentum, and turbulence quantities. Mesh interfaces incorporated coupled contact regions, and hybrid initialisation was employed. Convergence was ensured by reducing a criterion of 10^{-5} for continuity, momentum, energy, and turbulence equations. The chosen settings provided balanced computational accuracy and efficiency, aligning with typical applications of micro heat sink simulations in prior research. Fig 3.2 shows a sample setup and the boundary conditions followed during the CFD simulations.

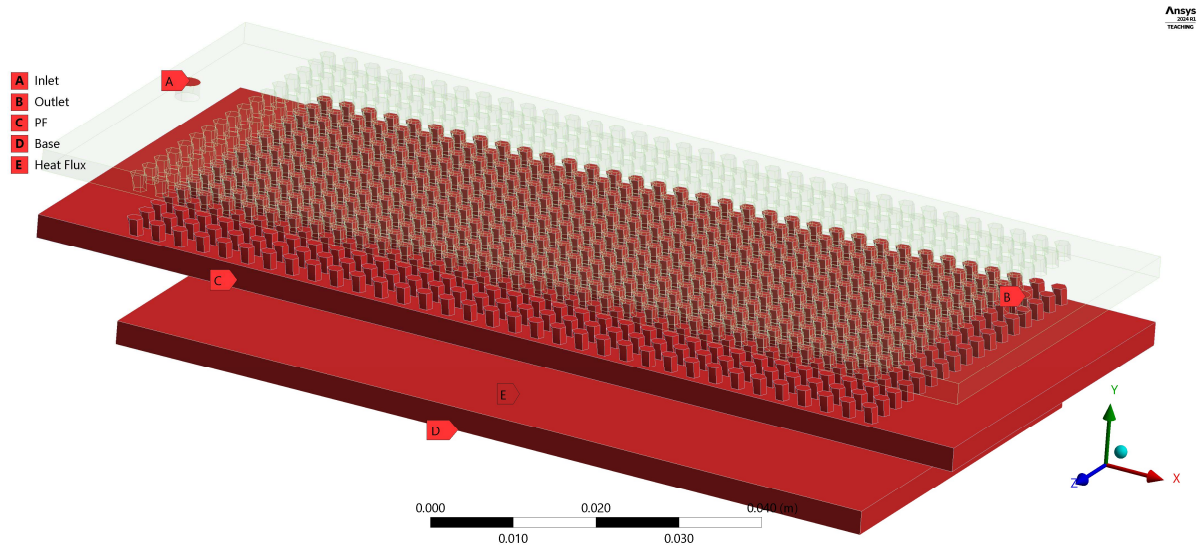


Fig. 3.2 Sample setup and boundary conditions

3.2.3 CFD Results and Post-processing

The CFD simulations provided insights into the fluid flow and thermal behaviour within the heat sinks. Velocity profiles highlighted flow distribution around the pin fins, identifying regions of recirculation and stagnation. Temperature contours revealed hotspots and areas with enhanced heat transfer near pin-fin surfaces. Local heat transfer coefficients were calculated from velocity and temperature data, providing a direct measure of thermal performance. Dimensionless parameters such as the Nusselt number and Reynolds number characterised convective heat transfer and flow regimes, facilitating benchmarking against experimental results. The simulations solved the governing equations for mass, momentum, and energy conservation in fluid flow and heat transfer. Navier-Stokes equations were pivotal in modelling these phenomena. Several pin-fin geometries, including biomorphic/bioinspired and conventional designs, were simulated, allowing for detailed comparisons of thermal and flow performance in the initial stages.

3.2.4 Model Validation and Limitations

Validation of the CFD model was carried out by comparing simulation results with experimental data. Heat transfer coefficients and Nusselt Number values from simulations were compared to experimentally derived values, ensuring that the model captured real-world thermal behaviour. Quantitative error analysis showed a margin of $\pm 10\text{-}15\%$, considered acceptable, although errors were minimised further at higher flow rates through mesh and turbulence model refinements. Despite successful validation, several limitations were acknowledged. Steady-state simulations do not account for transient thermal behaviours such

as fluctuating heat loads or fluid oscillations. Although the mesh independence study achieved a balance between accuracy and computational cost, further refinement in specific areas, particularly around small-scale pin-fin structures, could improve result precision. Additionally, while the $k-\epsilon$ turbulence model was effective, it may not fully capture complex flow patterns, which could be better addressed using advanced techniques like large eddy simulations (LES).

3.3 Heat Sink Fabrication Setup

The manufacturing of the biomorphic micro pin-fin heat sinks was influenced by practical and cost constraints. The heat sinks were produced using a 3-axis milling with CNC machining. One of the primary considerations was tolerance control during machining. While the chosen milling machine easily allowed a tolerance of 0.05mm, achieving a tighter tolerance of 0.01mm presented significant challenges. Thus, the relationship between cost and tolerance could be approximated by an exponential function—stricter tolerance requirements lead to a rapid cost escalation. Therefore, instead of pursuing the tightest possible tolerances, the design prioritised aspects like fin spacing and hole dimensions that directly impact heat sink manufacturability and performance. The manufacturing setup details can be found in Appendix B and Fig. 3.3 shows the manufacturing machine and snapshot of the machining process.



Fig. 3.3 Manufacturing equipment and process

Fin spacing and height considerations: Fin spacing and height were critical design factors. With a 1 mm spacing and 1 mm in height, the milling process divides the height into 20 layers, each milled at a depth of 0.05 mm. Reducing fin spacing to 0.5 mm requires the milling tool to make twice as many passes per layer, effectively doubling processing time and cost. The narrower spacing necessitates more frequent, controlled passes because the tool must remove material in smaller increments to prevent damage to the adjacent fin walls. This process adds

layers or steps, ensuring accuracy and maintaining the structural integrity of each fin. A further reduction to 0.1 mm spacing can exceed equipment capabilities, making machining unfeasible due to increased time and expense — also going against the agile philosophy.

Hole processing constraints: Hole processing constraints also influenced the design. The length-diameter ratio (hole length divided by diameter) is critical for machining ease. Holes with a ratio less than 8 are relatively easy to machine, but as this ratio increases, processing difficulty and cost rise exponentially. For very small holes (e.g., 0.5 mm diameter), the acceptable ratio becomes even more restrictive. These considerations ensured holes remained within manageable ranges for cost-effective manufacturability.

Inline vs staggered configuration: To further optimise manufacturing efficiency and reduce costs, the micro pin-fins were arranged inline rather than staggered. For non-conventional pin-fins, inline configurations can yield better results [229]. Inline arrangements simplify milling paths, reducing tool movement complexity, machining time, and required passes. In contrast, staggered configurations demand more complex paths and additional passes, increasing time and cost. Inline setups also streamline machine alignment, making the process more efficient. Overall, inline designs reduce processing time, complexity, and costs and keep production within budget.

Integration with agile manufacturing concepts: Machining constraints were integral to the design strategy, aligning with agile manufacturing principles that emphasise flexibility, rapid prototyping, and iterative design [312]. Understanding the exponential cost implications of tight tolerances, reduced fin spacing, inline configurations, and challenging hole dimensions allowed the design to optimise key parameters for performance without excessive cost and time. Choosing a 3-axis milling process enabled rapid prototyping and testing of different iterations, quickly identifying feasible designs and balancing performance and manufacturability. In summary, agile manufacturing concepts shaped the final heat sink designs by iterative refining within practical constraints, achieving a balance between innovative geometry, thermal efficiency, and manufacturability. This approach optimised production, ensuring the final products could be produced timely, cost-effectively, and meet performance requirements.

Surface Morphology: The scanning electron microscope (SEM) images and 3D depth map reveal channel and height variations up to 646.78 μm , featuring consistent grooves typical of micro heat sink fabrication due to micro-machining limitations and cost-efficiency needs; the

surface had roughness of 0.8 to 1.6 μm . While the SEM image shows surface textures and grooves, the 3D depth map provides a broader view, highlighting the overall height variations across the surface. The average surface channel depth of around 300-400 μm indicates a fairly consistent topography. This structured roughness can enhance heat transfer by promoting micro-turbulence, while the high surface homogeneity ensures minimal variation in flow and thermal performance. Importantly, the texture affects surface interactions without impacting the material's thermal conductivity, preserving overall heat sink efficiency [331]. Therefore, aiming for an improved surface finish is neither a necessary nor cost-effective strategy, as the existing texture effectively supports the design's thermal performance requirements.

The selection of a 3-axis milling process, while limiting in some respects, allowed for rapid prototyping and testing of different design iterations. This approach enabled the quick identification of feasible designs that balanced performance with manufacturability. In summary, agile manufacturing philosophy and concepts were instrumental in shaping the final heat sink designs. By iteratively refining the designs within the practical constraints, the process achieved a balance between innovative geometry, thermal efficiency, and manufacturability. This approach optimised the production process and ensured that the final products could be produced timely and cost-effectively while meeting the performance requirements. Fig. 3.4 shows the finalised machined part.

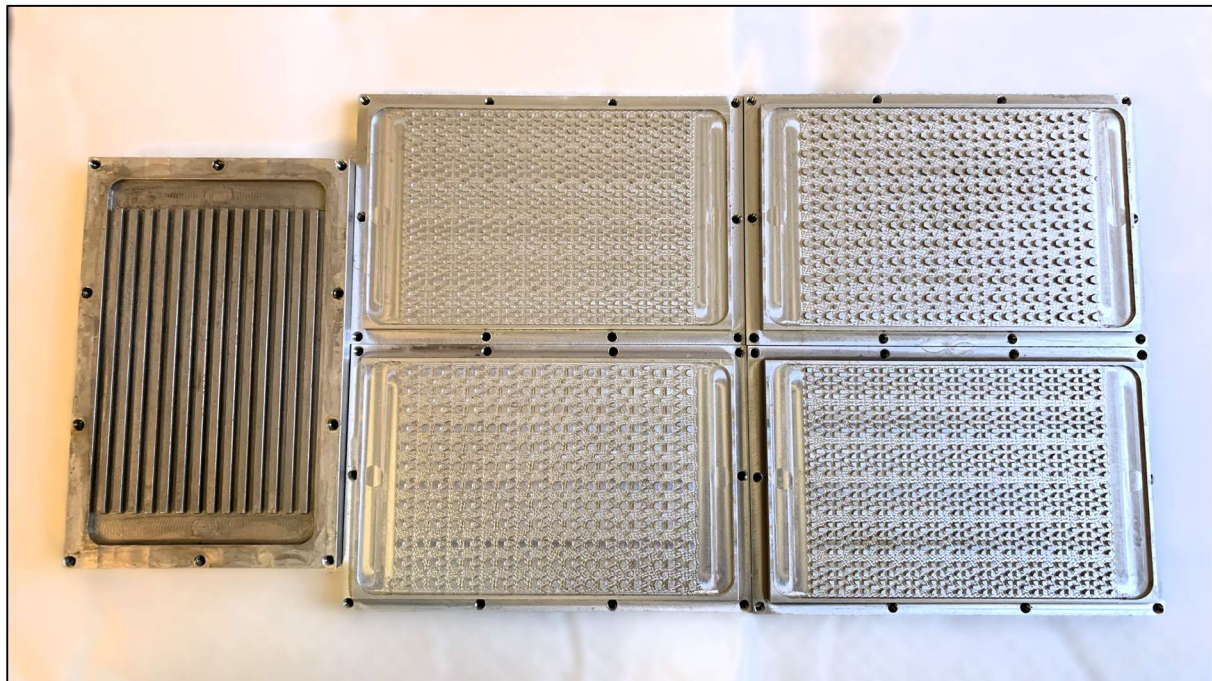


Fig. 3.4 Finished machined parts

For experimental validation and instrument calibration, a micro/minichannel was fabricated in-house, as depicted on the far left of Fig. 3.3. The in-house fabrication of the microchannel allowed for a reduction in costs and ensured a swift turnaround. This approach—emphasising the internal production of simpler components while outsourcing manufacturing more complex parts—reflects efficient manufacturing philosophies aimed at minimising time and cost. Nevertheless, the hybrid pin-fins were outsourced and fabricated in China. Utilising the advanced CNC machine shown earlier, the process was expedited by directly importing SolidWorks or CAD files into the system, thereby reducing the time required for technical drawing preparation. Comparable efficiencies were observed when using additive manufacturing techniques and will be discussed in the latter chapters.

As part of the quality assurance process, the surface characteristics of the outsourced pin-fins were further scrutinised under a digital microscope (KEYENCE Digital VHX-7000 series, UK) with scanning electron microscopy (SEM) images and 3D surface graphs employed to verify surface consistency. The microscale surfaces were largely even, having been treated with alcohol to eliminate impurities and ensure cleanliness, thereby preventing thermal fouling. The surface treatment was meticulously controlled to yield a polished finish without compromising the intricate pin-fins. Fig. 3.5 outlines the design process, from the initial CAD geometry to the machined parts, incorporating SEM imagery and 3D surface profile characteristics of a sample pin-fin section.

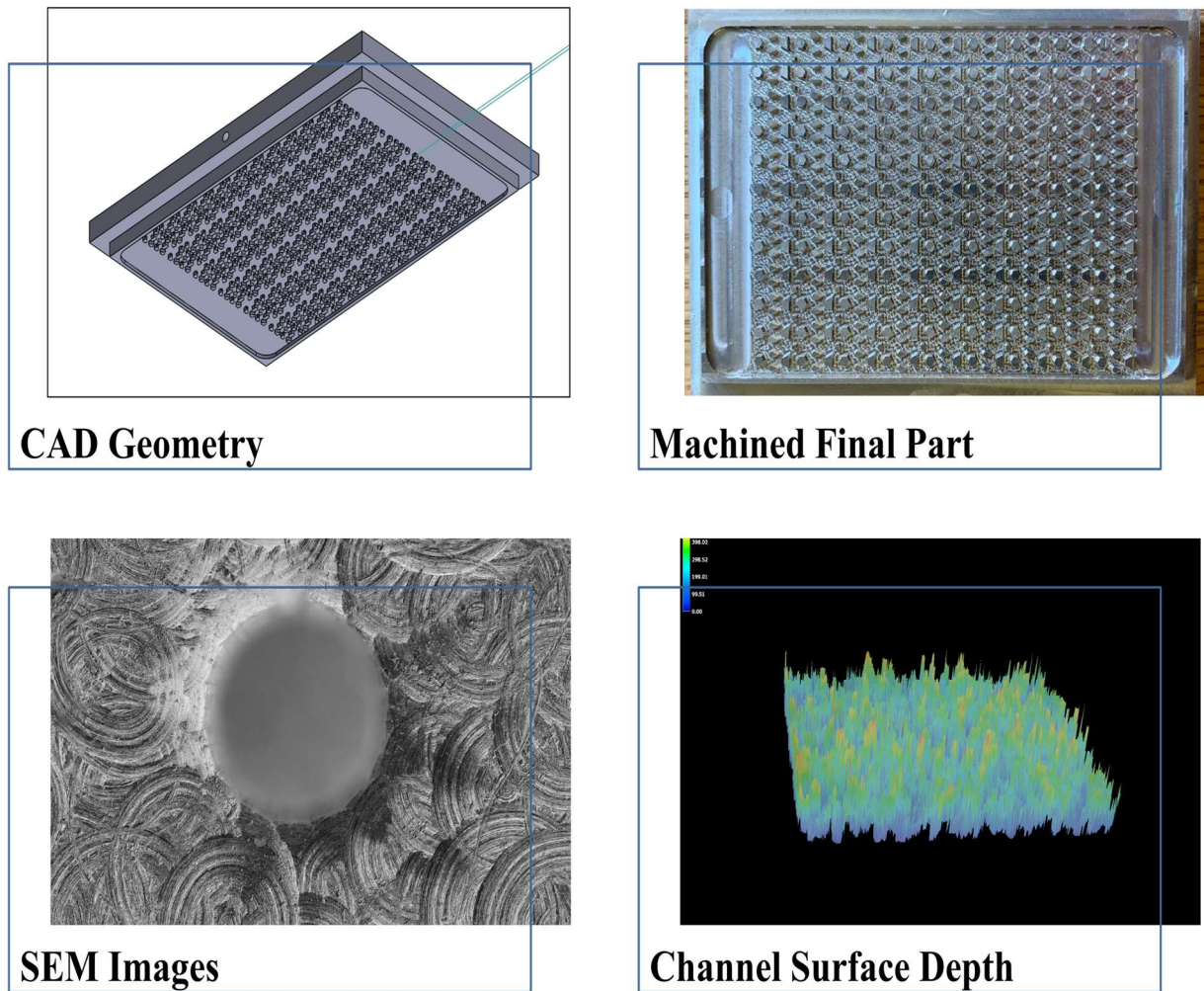


Fig. 3.5 Design quality assurance

3.4 Hybrid Manufacturing Benefits and Sustainability Analysis

To evaluate the effectiveness of the hybrid manufacturing strategy, components were divided based on complexity and produced through a combination of in-house and outsourced manufacturing processes. Simpler components, such as heating bases and straight microchannels, were fabricated using in-house facilities at the University of Hertfordshire in the UK, leveraging readily available equipment to ensure quality control and minimise costs. In contrast, more complex parts, such as micropin-fin heat sinks, were outsourced to a green manufacturing company in China. This approach not only took advantage of specialised expertise and advanced capabilities at the outsourcing facility but also aligned with sustainable manufacturing practices.

Fully producing in the UK would result in higher costs due to expensive machining and labour rates, while full production in China would lead to potential bottlenecks and extended shipping times, contradicting the principles of Just-In-Time (JIT) manufacturing. By producing

simple parts locally, we were able to leverage JIT philosophies, ensuring that only necessary quantities were manufactured without overstocking, thus reducing lead times and minimising storage costs. Additionally, the hybrid approach allowed us to retain tighter control over quality for critical components while taking advantage of green manufacturing from the manufacturer and cost benefits for more intricate parts. Another advantage of this hybrid strategy is improved flexibility in managing production changes, enabling a more agile response to market demands and design modifications without significantly disrupting the supply chain.

To ensure the accuracy and reliability of our cost assessments, we consulted with in-house manufacturing experts and external collaborators to gather precise data and obtain multiple cost estimations from both sides. We chose a neutral USD to match the internal market trading standards. This consultation provided insights into machining costs, processing times, shipping rates, and material expenses. Further, we cross-validated these findings with data from the literature and credible online sources to validate the main parameters such as machining time, energy consumption, and carbon emissions. The integration of both primary and secondary data sources helped us form a robust basis for calculating overall estimated production costs and environmental impacts, ensuring that conclusions were well-founded.

3.4.1 Main Parameters Driving Costs

Based on the expertise of local and external technicians, we identified the main factors influencing production costs. Each region's cost drivers were carefully assessed and optimised as much as possible. For example, in the UK, no shipping costs were added as components were produced and assembled locally, whereas shipping costs were factored in for complex parts produced in China. Additionally, despite adopting green manufacturing options to reduce energy usage intensity, the production in China still resulted in slightly higher CO₂ emissions per kWh compared to the UK. This discrepancy is mainly due to the region's energy grid relying on higher proportions of fossil fuels. Consequently, we finalised the following as the primary parameters driving production costs and created a Pandas data frame to model our analysis. Fig. 3.6 shows a snippet of the identified main cost-driving factors data frame, used for the study, from Python/Google Collaboratory. A 1,000-unit production benchmark was followed as a standard unit for scalability and cost assessment. This approach is commonly used in the industry to evaluate development and manufacturing costs, providing a consistent basis for comparing different production strategies [332]. These parameters provided a comprehensive view of cost dynamics, enabling us to assess the impact of varying production strategies systematically.

```

# Create a DataFrame for modeling
df = pd.DataFrame({
    'Units': units,
    'ProductionType': production_type, # 0 = Full UK, 1 = Hybrid
    'MaterialCost': material_cost, # Cost of aluminium per kg based on location
    'MachiningTime': machining_time, # Machining time (hours) required for each component
    'LabourCost': labour_cost, # Labour cost per hour in the UK and China
    'EnergyConsumption': energy_consumption, # kWh consumed based on the production type
    'ShippingCost': shipping_cost, # Shipping costs applied only for Hybrid Production
    'TotalCost': total_cost # Calculated total production cost for each production strategy
})

```

Fig. 3.6 Main cost factor parameters

3.4.2 Impact Assessment and Calculations

Appendix C shows the full breakdown of the codes, calculations, and units used to calculate costs. For brevity, only the main results are discussed here. The comparison of the Full UK Production with the Hybrid Production Strategy revealed substantial benefits. The detailed calculations showed that switching to hybrid production resulted in a cost savings of 42.76%. The energy consumption was reduced by 28.95%, corresponding to a savings of 1,100 kWh, while carbon emissions were lowered by 18.80% (150 kg CO₂). These savings were visualised using the bar chart in Fig. 3.7, which highlights the relative impact of each savings category.

The enhanced visualisation highlighted the cost savings driven by lower machining and material costs in China for complex pin-fin structures, while energy savings were achieved by utilising China's less energy-intensive processes for these parts. The carbon emissions reduction, although not as significant as the cost savings, still demonstrates the hybrid strategy's positive environmental impact, aligning with sustainable manufacturing goals. The hybrid approach thus effectively balances economic and environmental performance, making it a viable solution for the production of micro heat sinks.

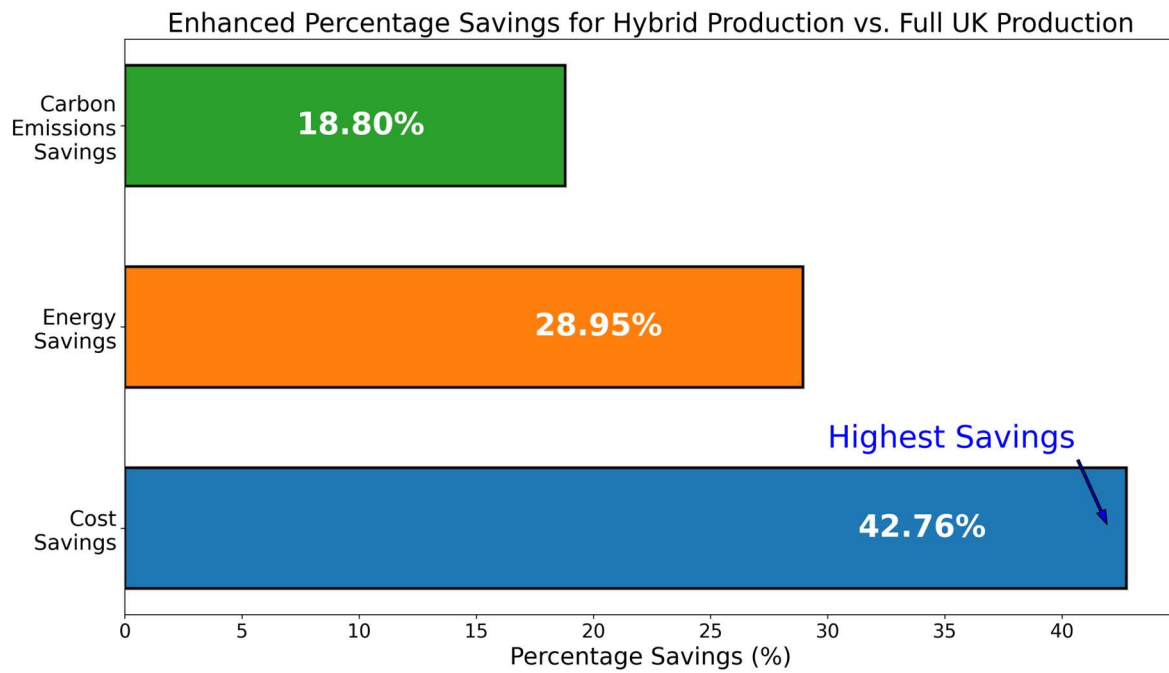


Fig. 3.7 Savings for different categories

3.4.3 Verification of the Hybrid Strategy through Machine Learning

To further verify the impact of the hybrid strategy, machine learning techniques were utilised to compare the predicted production costs with the actual costs. Using two machine learning models—Linear Regression (LR) and Random Forest (RF)—we predicted production costs based on key features such as units produced, production type, machining costs, labour rates, and shipping expenses. The models were evaluated using Root Mean Squared Error (RMSE) and R^2 (R-squared) to assess their accuracy.

The Linear Regression model achieved an RMSE of 30,983 USD and an R^2 of 0.888, indicating that it captured general cost trends but struggled to model the complex variations. In contrast, the Random Forest model showed significantly better performance, with an RMSE of 11,116 USD and an R^2 of 0.986, demonstrating its ability to account for non-linear relationships and interactions between different production factors. This high accuracy added confidence to the hybrid manufacturing strategy, as the model's predictions closely aligned with the actual cost outcomes. The initial cluster of points at the start denotes the same type of random initialisation for the type of production happening that is 0 or 1, and it is not an issue.

Fig. 3.8 shows the visualisation of “Actual vs. Predicted Costs” using both models, and it further validates the chosen hybrid approach. The Random Forest predictions were clustered closer to the perfect prediction line, confirming the model's reliability in capturing the cost dynamics of the hybrid production strategy. The strong predictive performance of the machine

learning model thus reinforces the feasibility and effectiveness of hybrid manufacturing, supporting the decision to adopt this strategy over full local or outsourced production.

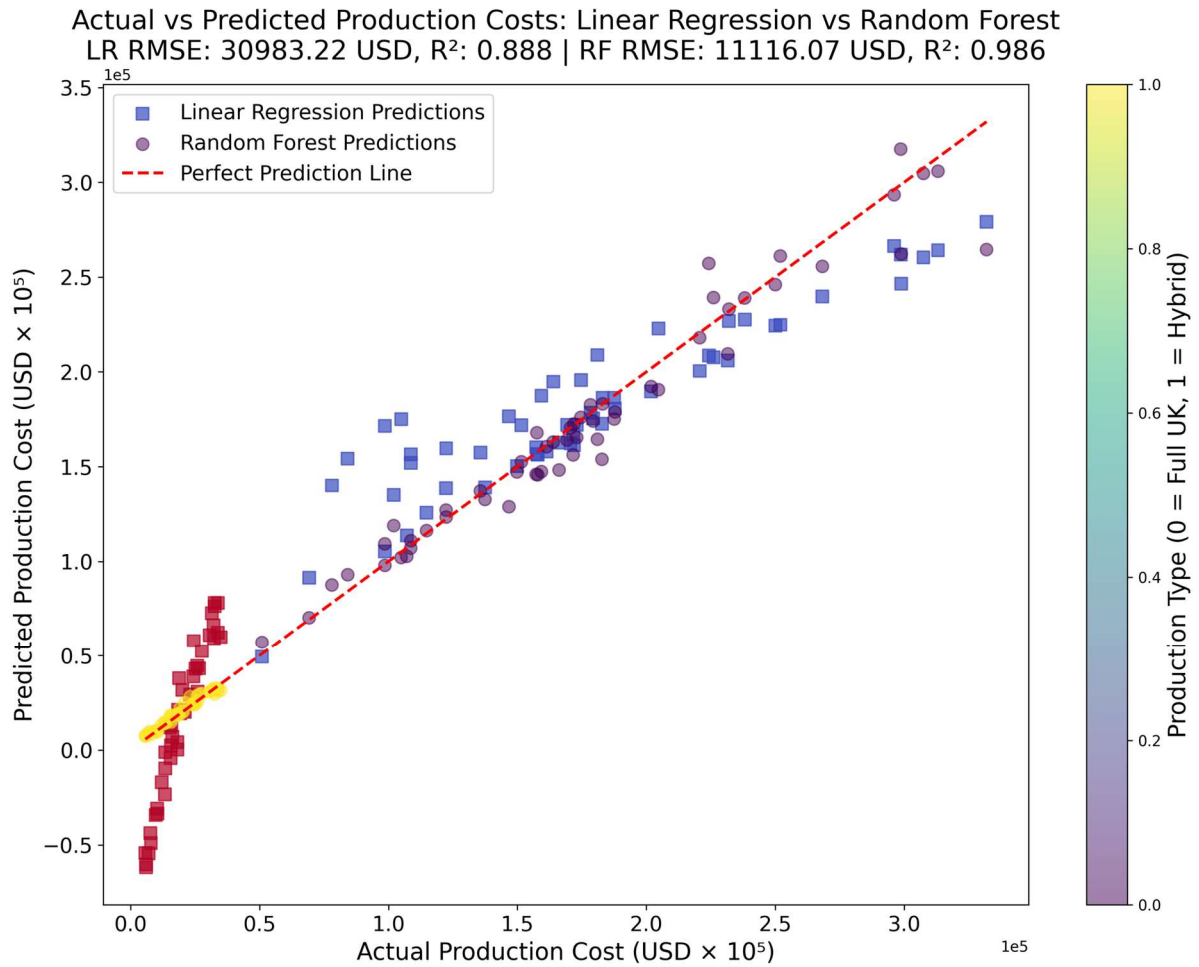


Fig. 3.8 Actual vs Predicted cost comparison

Overall, the hybrid strategy not only reduced costs and improved sustainability but also enabled agile and efficient production management. This approach leveraged data-driven insights and expert consultation, combined with rigorous verification using machine learning, to comprehensively evaluate the manufacturing process. The resulting savings and environmental benefits made the hybrid production strategy an optimal solution for micro heat sink production, aligning with both economic and sustainable manufacturing objectives.

3.5 Experimental Setup

The setup involves a closed-loop flow circulation system suitable for single-phase and two-phase flows, designed to study heat transfer and flow dynamics in mini/microchannels and micro pin-fin-based heat sinks. Key components include a Masterflex gear pump (GJ-N23-PF1SA, UK), data loggers (Thermo Fisher Scientific DT80), a flow meter (Omega FTB332D-

PVDF, USA), a pressure transducer (Omega PX2300, USA), a microscope (KERN OZM-5, Germany), thermal bath (Cole Palmer StableTemp Digital Bath, UK), and a 320W power supply. A desktop computer was the base for setup initiation, control, and data storage. The DT80 data tracker monitored temperature distribution along the heat sink and system inlet/outlet while maintaining the water bath temperature. The experimental section was positioned horizontally, with the heat sink's temperature monitored by evenly spaced K-type thermocouples (RS-397–1589, UK) to prevent localised heating effects. Table 2 summarises the major equipment, range, and accuracy.

Table 2: Experimental equipment range and accuracy

Equipment	Model	Manufacturer	Range	Accuracy
Gear Pump	GJ-N23-PF1SA	MasterFlex (UK)	--	±0.1%
Flow Meter	FTB332D-PVDF	Omega (USA)	0.1– 1 l/min	±6%
Pressure Transducer	PX2300	Omega (USA)	0 – 1 PSID	±0.25%
Power Supply	PS 2084-10B	Elektro-Automatik (Germany)	Voltage: 0 – 84 V	<0.2%
			Current: 0 – 10 A	<0.3%
Thermocouples	RS-397–1589 (K-type)	RS Components (UK)	Temperature: -75 – 260 °C	±1.5 °C

The flow originates from the thermal bath, which also serves as a storage tank. In this case, a gear pump circulates the working fluid—deionised water through the pipes to the experimental section (anticlockwise, from left to right). The fluid passes through an electromagnetic flowmeter, where the flow rate is measured along the way. A pressure transducer positioned behind the microscope records the pressure difference between the inlet (left port) and the outlet (right port). After passing through the experimental section, the fluid is cooled in an air-cooled radiator before returning to the thermal bath and then to the pump for recirculation, completing the closed-loop system. Fig. 3.9 shows the setup, instruments, and schematic diagram for a better understanding of the experimental setup's working mechanism.

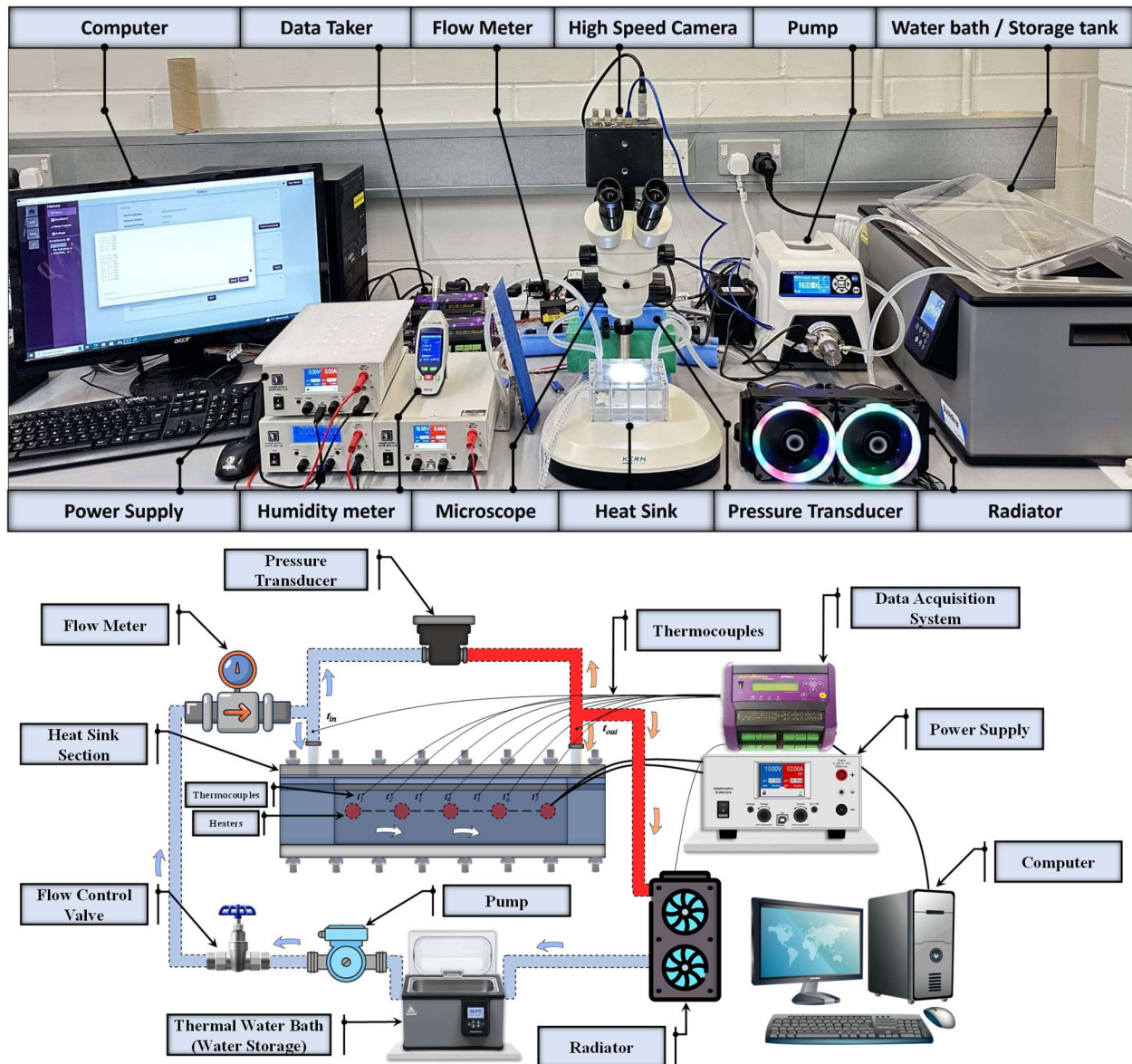


Fig. 3.9 Experimental setup and instruments

3.5.1 Heat Sink Material and Working Fluid

Aluminium was selected for the fabrication of micro heat sinks due to its distinct advantages over copper and other metals. Its primary benefit lies in cost-effectiveness, as aluminium is not only less expensive than copper but also easier to machine, particularly when handling intricate microstructures such as pin-fins and microchannels. Additionally, aluminium's lower density renders it significantly lighter, a critical consideration in applications where weight minimisation is paramount, such as aerospace engineering and portable electronic devices. Although copper boasts superior thermal conductivity, aluminium remains highly efficient at the microscale, owing to the increased surface area-to-volume ratio that is characteristic of

micro heat sinks. Moreover, aluminium naturally forms a thin oxide layer that offers superior corrosion resistance compared to copper, thus ensuring greater durability and longevity in diverse environmental conditions, including both single and two-phase flows. Its malleability further enhances its suitability, facilitating the precise fabrication of complex designs, which is crucial for the advancement of micro heat sink technologies.

Concerning the working fluid, deionised water was selected over conventional refrigerants for several compelling reasons. A review of the literature identified it as the most commonly utilised working fluid. Deionised water offers a higher specific heat capacity and thermal conductivity, making it more effective in absorbing and transferring heat. Additionally, it is environmentally friendly, as it avoids the high global warming potentials of many refrigerants and aligns with sustainable engineering principles. Furthermore, deionised water is non-toxic and non-flammable, thereby, presenting none of the chemical hazards typically associated with refrigerants, which can be dangerous to handle and store. Its high latent heat of vaporisation makes it particularly efficient in two-phase cooling systems, where rapid heat dissipation is essential. Lastly, deionised water is both inexpensive and widely available, making it ideal for experimental applications, particularly when large volumes or extended testing periods are required, following Just-In-Time (JIT) principles. In contrast, refrigerants tend to be costly and subject to strict regulatory controls.

3.5.2 Wall Temperature Variations

To improve adaptability and ensure efficient changeovers in the experimental setup, a 3D-printed housing was created to encase the heat sink/test section. The heat sinks were attached to a heating block equipped with six RSPro 300W heaters along its length. RS PRO Non-Silicone Thermal Grease ($4\text{W/m}\cdot\text{K}$) was applied at the contact interfaces to enhance heat transfer. Temperature measurements were taken using five K-type thermocouples placed equidistantly and parallel to the heating block, providing a detailed temperature profile. To assess the temperature distribution, any potential heat loss, and the impact of the thermal grease between the contact surface, an additional thermocouple was positioned 10 mm above the heating block to monitor the temperature at the centre of the heat sink wall that is attached to the heating block. The new 3D-printed casing (FormLabs Rigid 10K resin, USA) allows for quick changeovers in single-phase flow, and it is also adaptable to high-temperature two-phase boiling conditions due to its high melting point of the resin (over 170°C), heat deflection temperature at 0.45 MPa (218°C), low thermal expansion coefficient ($46\text{ }\mu\text{m/m}/^\circ\text{C}$ for $0\text{--}150^\circ\text{C}$), and ability to prevent heat loss due to low thermal conductivity ($0.83\text{ W/m}\cdot\text{K}$). Given

the resin's thermal properties, temperature gradients between the fluid-solid interface and measurement points remain minimal, ensuring accurate readings without significant need for correction. For transient states, these material characteristics maintain stable temperature measurements, confirming negligible influence. Fig. 3.10 shows the modified experimental casing and the dimensions and details of thermocouple and heater placements.

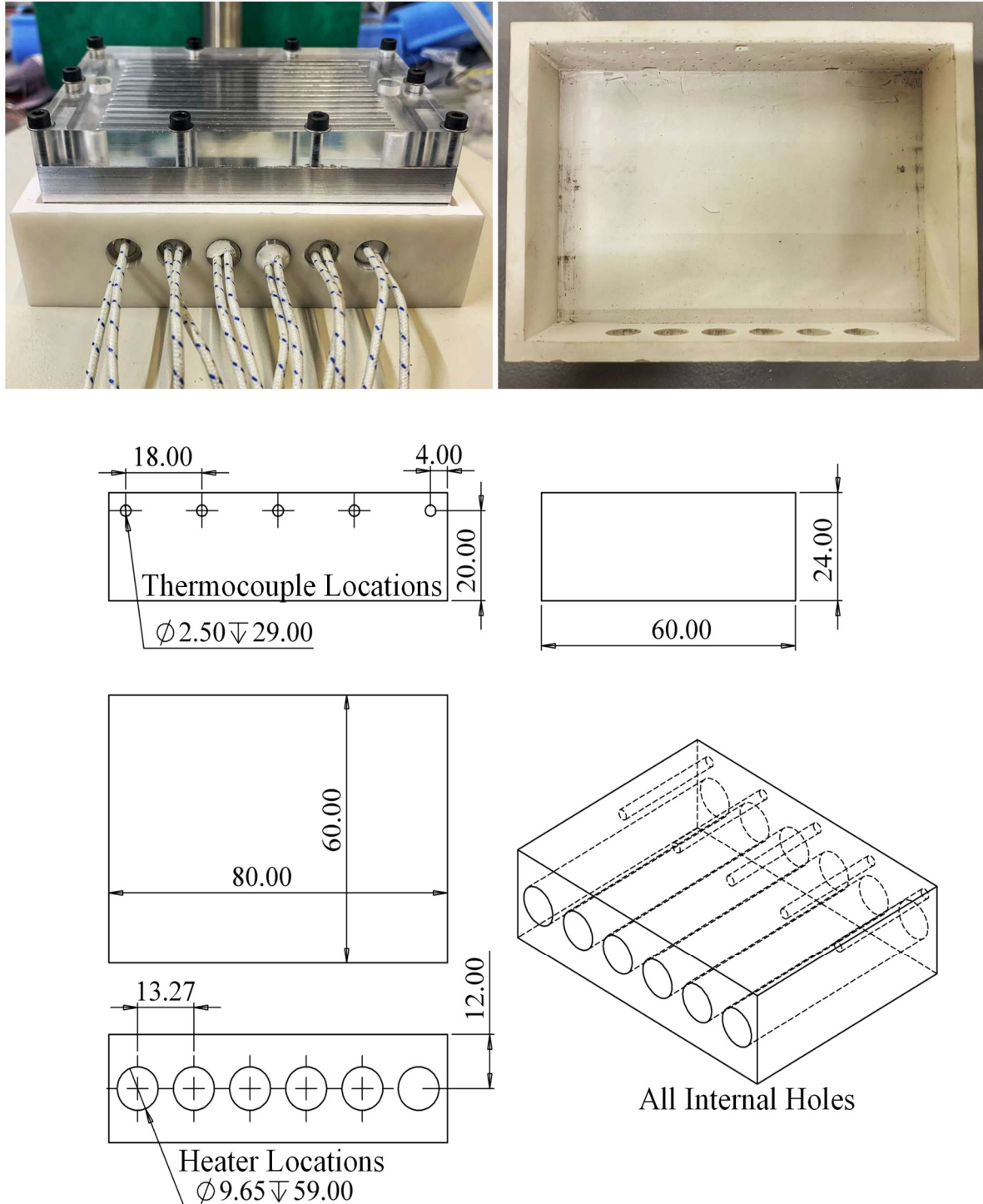


Fig. 3.10 Housing modification and dimensions for a detachable heat sink setup

The original acrylic setup was effective in minimising heat loss. Thus, due to the modification, one of the primary goals was to assess wall temperature differences and potential heat loss under various power outputs (100W, 150W, and 250W) as the heating block was heated from 20°C to 100°C under natural convection conditions; the dimension for the heating area is (80 mm x 60mm). The average temperature across the heating block wall (T_{avg}), measured by the five parallel thermocouples, as compared to the temperature at the centre of the heat sink wall (T_c) recorded by the additional thermocouple. Results showed a temperature profile difference of 2 - 3% between T_{avg} and T_c at all power levels. As we are using the T_{avg} for calculation of different thermal parameters, it was necessary to understand the effect of the thermal grease layer (between the heating block and the detachable heat sink) on the temperature difference; hence, the value of T_c was cross-checked to ensure minimal impact.

This slight 2-3% variation can be attributed to several factors: the residual thermal resistance of the thermal paste, which, despite enhancing heat transfer, still presents a minor barrier; differences in thermocouple placement, with the embedded thermocouples and the external one under the heat sink experiencing slightly different thermal environments due to height variation; and the inherent measurement accuracy of the thermocouples, which typically have a margin of error of $\pm 1.5^\circ\text{C}$; this value encompasses both the intrinsic accuracy of the thermocouples and the minor differences observed due to height variation between the embedded and external thermocouples and due to the effect of the thermal grease layer's conductivity. The 2-3% variation can be considered acceptable as it falls within the expected range of measurement uncertainty and does not significantly impact the overall thermal performance assessment. In terms of overall heat loss of the system from the housing, it varied between 11% to 16.4% for power outputs of 100W, 150W, and 250W. Fig. 3.11 shows the wall temperature distribution at different powers with times.

Along with the adaptability benefits, the detachable setup promotes efficient material and component usage by allowing the same heating block to be used with different heat sink designs, enabling quick turnover times when experimenting with various configurations. This flexibility is crucial for optimising thermal management solutions and enhances the efficiency of the experimental process — in alignment with the sustainable and agile manufacturing philosophy followed in this research. Moreover, by leveraging technologies such as additive manufacturing instead of traditional machining processes and 3D-printed resin instead of acrylic glass, this approach provides an alternative, effective, and sustainable method for experimenting with thermal management and heat dissipation under varied conditions.

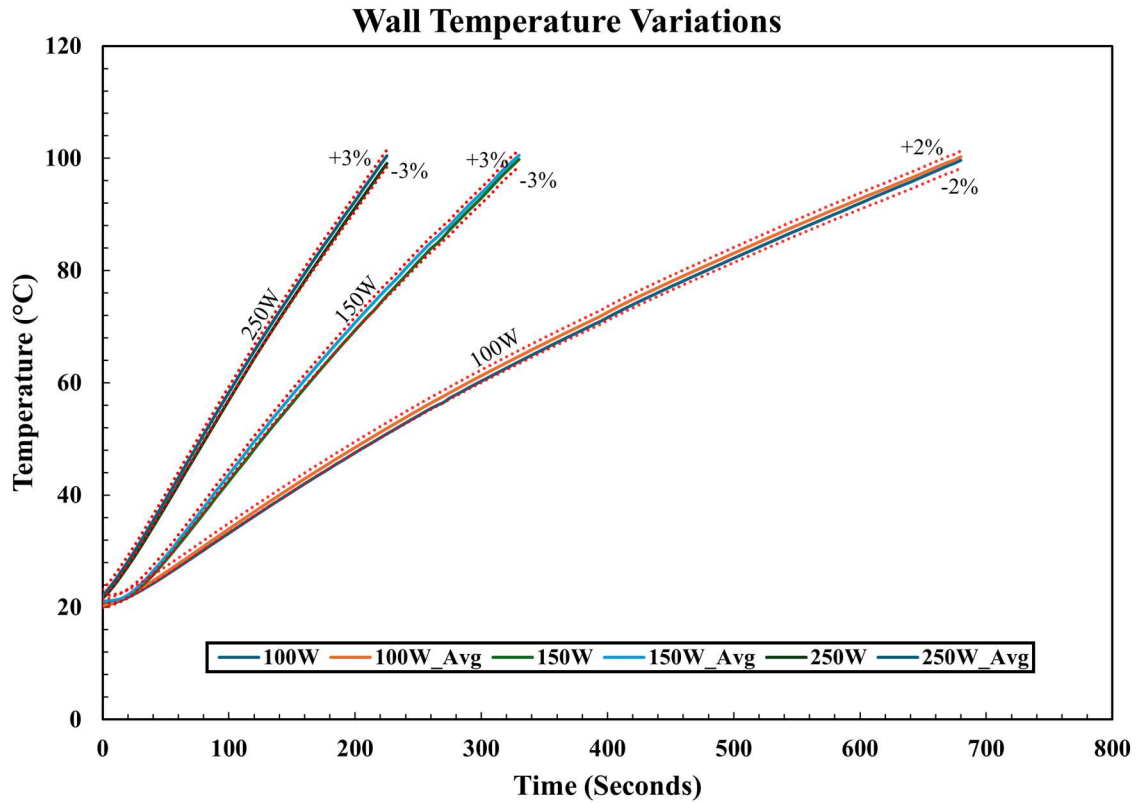


Fig. 3.11 Wall temperature variations for heating blocks and heat sinks

This slight variation can be attributed to several factors: the residual thermal resistance of the thermal paste, which, despite enhancing heat transfer, still presents a minor barrier; differences in thermocouple placement, with the embedded thermocouples and the external one under the heat sink experiencing slightly different thermal environments due to height variation; and the inherent measurement accuracy of the thermocouples, which typically have a margin of error of $\pm 1.5^{\circ}\text{C}$. The 2-3% variation can be considered acceptable as it falls within the expected range of measurement uncertainty and does not significantly impact the overall thermal performance assessment. Along with the adaptability benefits, the detachable setup promotes efficient material and component usage by allowing the same heating block to be used with different heat sink designs, enabling quick turnover times when experimenting with various configurations. This flexibility is crucial for optimising thermal management solutions and enhances the efficiency of the experimental process — in alignment with the sustainable and agile manufacturing philosophy followed in this research. Moreover, by leveraging technologies such as additive manufacturing instead of traditional machining processes and 3D-printed resin instead of acrylic glass, this approach provides an alternative, effective, and

sustainable method for experimenting with thermal management and heat dissipation in electronic and mechanical systems, ensuring reliable performance under varied conditions.

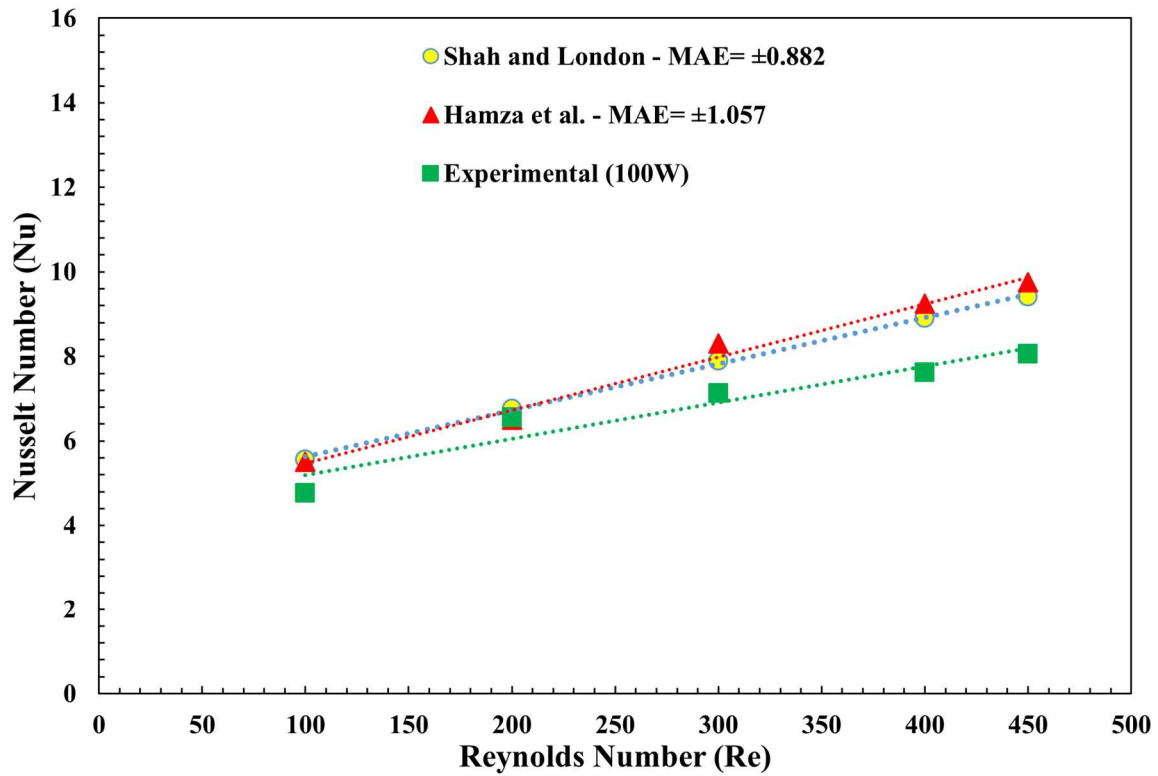
3.5.3 Experimental Validation

Experimental validation plays a critical role in establishing the accuracy and reliability of any scientific investigation. To validate our experimental test rig, the results were benchmarked against the well-recognised Shah model [333], a widely used method for predicting the Nusselt number under laminar flow conditions with constant heat flux, as outlined in Eq. (6). The Shah model has been consistently cited as a reliable reference in various studies [334,335], making it an ideal standard for validation. Additionally, for a more robust comparison, findings were evaluated against those of Babar et al. [44], who employed a similar experimental apparatus. To quantify the accuracy of our results, we calculated the mean absolute error (MAE) [229,336], as demonstrated in Eq. (7). The MAE values consistently remained below 1.5, which is deemed acceptable, thus confirming that our experimental data aligns closely with both the Shah model and Hamza et al.'s findings. Fig. 3.12 shows the experimental validation graphs at two power outputs 100W and 150W.

$$Nu = \begin{cases} 1.953 \left(\text{RePr} \frac{d_h}{l} \right)^{1/3} & \text{if } \left(\text{RePr} \frac{d_h}{l} \right) \geq 33.3 \\ 4.364 + 0.0722 \left(\text{RePr} \frac{d_h}{l} \right) & \text{if } \left(\text{RePr} \frac{d_h}{l} \right) < 33.3 \end{cases} \quad (6)$$

$$\text{Mean Absolute Error (MAE)} = \frac{1}{n} \sum_{j=1}^n \left[\frac{|x_{\text{exp.}} - x_{\text{pred.}}|}{x_{\text{exp.}}} \right] \times 100\% \quad (7)$$

Experimental Validation (100W)



Experimental Validation (150W)

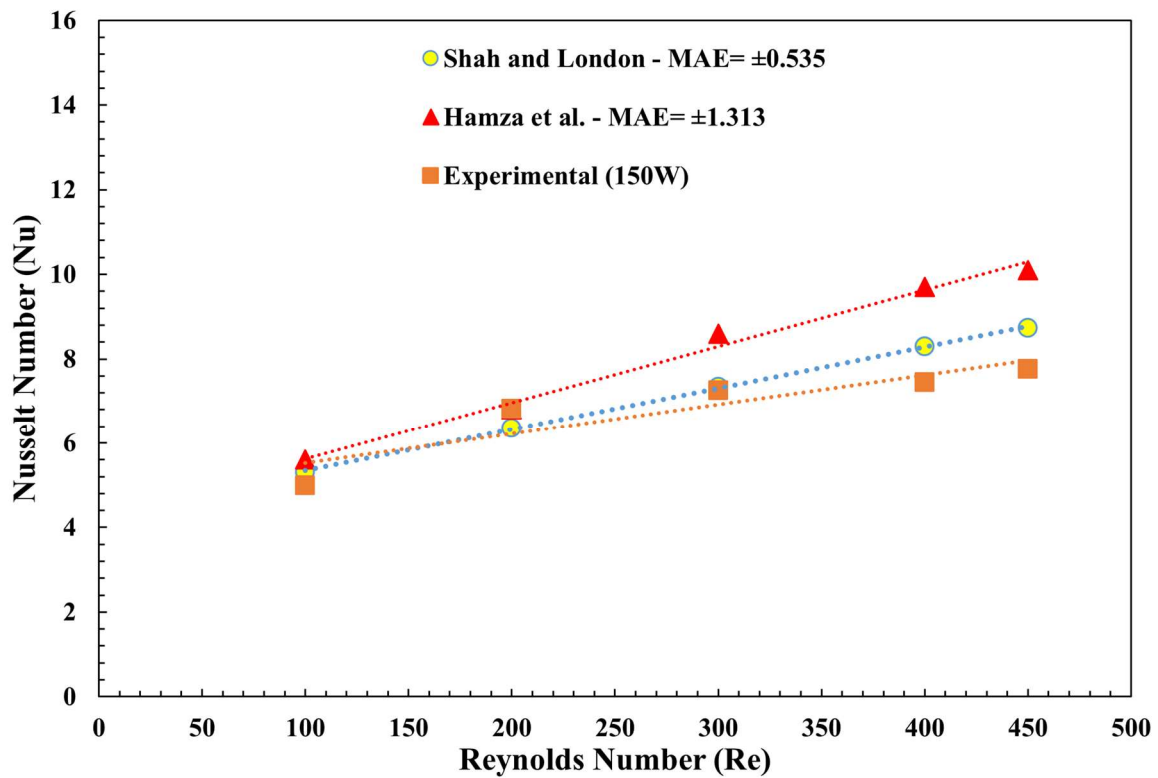


Fig. 3.12 Experimental validation

In small-scale experiments, particularly those at the micro or mini level, uncertainty analysis is essential to ensuring that the experimental results reflect reality with precision. It is not merely a matter of conducting the experiments, but of carefully accounting for potential errors arising from the measuring instruments involved. Following established methodologies employed by other researchers, an uncertainty analysis was conducted to provide a firm foundation for interpreting our experimental data and enhancing the reliability of the outcomes. Using a series of equations (Eq. 8–12), uncertainties for key parameters were determined. The highest uncertainties, observed in the hydraulic diameter, Reynolds number, and Nusselt number, were 1.41%, 6.18%, and 7.39%, respectively. Whilst these values are low, it is important to acknowledge that they do not fully negate the limitations inherent in small-scale experimental setups. A more detailed breakdown of instrument accuracy is provided in Table 3, which summarises the precision of each instrument utilised during the study.

$$\frac{U_{d_h}}{d_h} = \sqrt{\left(\frac{U_h}{h}\right)^2 + \left(\frac{U_w}{w}\right)^2} \quad (8)$$

$$\frac{U_v}{v} = \sqrt{\left(\frac{U_{d_h}}{d_h}\right)^2 + \left(\frac{U_m}{m}\right)^2 + \left(\frac{U_A}{A}\right)^2} \quad (9)$$

$$\frac{U_{Re}}{Re} = \sqrt{\left(\frac{U_\rho}{\rho}\right)^2 + \left(\frac{U_v}{v}\right)^2 + \left(\frac{U_\mu}{\mu}\right)^2} \quad (10)$$

$$\frac{U_h}{h} = \sqrt{\left(\frac{U_m}{m}\right)^2 + \left(\frac{U_{(T_w - T_i)}}{(T_w - T_i)}\right)^2 + \left(\frac{U_{(T_w - T_o)}}{(T_w - T_o)}\right)^2 + \left(\frac{U_{C_p}}{C_p}\right)^2 + \left(\frac{U_{A_{eff}}}{A_{eff}}\right)^2 + \left(\frac{U_{(T_{out} - T_{in})}}{(T_{out} - T_{in})}\right)^2} \quad (11)$$

$$\frac{U_{Nu}}{Nu} = \sqrt{\left(\frac{U_h}{h}\right)^2 + \left(\frac{U_{d_h}}{d_h}\right)^2 + \left(\frac{U_{k_f}}{k_f}\right)^2} \quad (12)$$

Table 3: Measuring apparatus range and accuracy

Instrument	Range	Accuracy
Flowmeter	0.1 – 1 l/min	±6%
Thermocouple	-75 – 260 °C	±1.5 °C
Pressure Transducer	0 – 1 PSID	±0.25%
Power Supply	0 – 84 V	Voltage < 0.2%
	0 – 10 A	Current < 0.3%

3.6 Machine Learning Setup

Machine learning algorithms are generally categorised into three types: prediction, classification, and clustering. Each type plays a crucial role in modelling and analysing complex systems. In the context of this study, a combination of supervised, semi-supervised, and unsupervised methods was employed to holistically address the challenges in the thermal management of heat sinks. These methods were applied and adapted at various stages of data analysis to enhance both predictive accuracy and system performance, contributing to the development of optimised heat transfer solutions.

3.6.1 Role of Machine Learning and Artificial Intelligence

Artificial intelligence (AI) and machine learning (ML) played a pivotal role in this research, offering advanced tools to enhance the design and analysis of micro heat sinks. These techniques were employed to provide quick performance indicators, enabling efficient identification of optimal designs. They also facilitated the prediction of key heat transfer metrics, supported the development of correlation models, and contributed to the verification and validation of results. AI-powered classification methods were used to identify flow boiling regimes, while clustering-based data pipelines were developed for effective monitoring and data analysis potential. This integration of AI and ML streamlined the research process, ensuring accurate and data-driven insights across multiple aspects of the study.

3.6.2 Data Collection and Processing

Data used in this thesis were acquired through a combination of experimental studies, numerical simulations, and external sources. Experimental data came from single-phase and two-phase flow experiments conducted as part of this research. Numerical simulations were performed using ANSYS Fluent, generating key parameters such as fluid velocity, temperature distribution, and design specifications. Additionally, external datasets from the literature were incorporated, particularly for cost and sustainability analyses. These diverse data sources were combined to generate a local dataset for machine learning.

In the pre-processing phase, outliers were identified and removed, and missing data points were imputed using either median or K-Nearest Neighbours (KNN) imputation, chosen for its ability to account for the relationship between neighbouring data points. The dataset was then normalised using either min-max scaling or standard scaling to ensure all features were within a consistent range, preventing bias from variables with larger scales (e.g. geometric dimensions versus heat transfer coefficients).

The datasets comprised various data types tailored to the specific requirements of the analyses. Numerical data, often in floating-point format, represented continuous variables such as temperature, pressure, and velocity, offering high precision for capturing intricate variations in physical processes. Boolean data represented binary conditions or classifications, such as the presence or absence of a specific feature, providing a straightforward way to encode discrete states. Image data, particularly for flow boiling experiments, captured visual characteristics critical for classification tasks and pattern recognition. Each data type contributed uniquely to the robustness and comprehensiveness of the analyses.

Measures were taken to ensure dataset robustness despite practical constraints on data availability. In Chapter 4, computational fluid dynamics (CFD) data was combined with external experimental datasets to create a reliable basis for model training and validation. Sample code and raw data outputs are provided in Appendix C2. Chapter 5 relied on in-house experimental data, which was limited due to resource constraints. To address this, the dataset was augmented to enhance its diversity and improve the model's generalisation capability; the dataset and augmentation process are detailed in Appendix C3. Chapter 6 employed over 1,500 experimental images for flow boiling classification and generated a synthetic dataset to increase model robustness and reduce dependence on real-world data; corresponding codes and datasets are included in Appendix C4. These strategies ensured the models were trained on diverse and representative datasets, mitigating potential biases and gaps arising from limited experimental data.

Furthermore, other raw data outputs, key variables, and processed results are provided in Appendix C for reference. While data availability posed challenges, the robust measures taken—including data augmentation, synthetic data generation, principal component analysis, and the integration of multiple data sources—ensured that the findings were reliable, generalisable, and reflective of real-world applications.

3.6.3 Feature Selection

The features selected for model training included fluid properties (density, viscosity, specific heat capacity), geometric configurations (fin height, fin area/volume), and thermal performance indicators (HTC, Nu). Feature selection was guided by domain knowledge and further refined using feature importance scores. This helped prioritise the most impactful features, such as fin volume and fluid velocity while discarding less relevant features that contributed noise or redundancy. Additionally, Principal Component Analysis (PCA) was

applied to reduce dimensionality and simplify the data without losing significant information, thereby improving model training efficiency and reducing computational cost.

3.6.4 Model Training and Algorithms

For prediction tasks, supervised machine learning algorithms such as Random Forest, Support Vector Machines (SVMs), and fully connected Neural Networks (NNs) were employed. The Random Forest model consisted of decision trees, and grid search was used to optimise hyperparameters such as the number of trees and the maximum depth of each tree. For the Neural Network, the architecture included two or three hidden layers with ReLU activation functions and an Adam optimiser with a variable learning rate. The choice of these algorithms was driven by their proven ability to handle high-dimensional, non-linear data, which is typical in fluid-thermal systems. To mitigate overfitting, dropout layers were introduced in the neural network to randomly disable certain neurons during training. For semi-supervised learning, self-training techniques were employed, using a small portion of labelled data combined with large unlabelled data to improve model performance where labelled data were scarce. K-means clustering, or Gaussian mixture models were applied in unsupervised learning contexts to discover patterns in fluid flow behaviours.

3.6.5 Hyperparameter Tuning and Validation

Hyperparameter optimisation was performed using grid search, adjusting parameters like the number of estimators, max features, and learning rate. For Random Forest, the number of trees was varied between 100 and 1,000 to find the optimal configuration. For the Neural Network, batch size and epochs were adjusted to ensure the model converged efficiently. Additionally, k-fold cross-validation was used to assess the generalisability of each model. This ensured that model performance was not overly dependent on a particular data split and helped detect any overfitting to the training data. The cross-validation process allowed for a more reliable assessment of performance on unseen data. To further enhance the model's robustness, early stopping was implemented to terminate training when the model's performance ceased to improve on the validation set, reducing the risk of overfitting.

3.6.6 Evaluation Metrics

The performance of the predictive models was evaluated using a combination of R-squared, Mean Absolute Error (MAE), Mean Absolute Percentage Error (MAPE), and Root Mean Square Error (RMSE). These metrics were selected because they measure the accuracy and variance of the model's predictions, which are critical for determining the thermal performance

of heat sinks. For instance, high R-squared values indicated that the model captured most of the variance in heat transfer coefficient predictions, while low MAE and RMSE values suggested minimal error between the predicted and actual values. The choice of metrics was aligned with the physical significance of heat transfer efficiency, ensuring the models could predict real-world performance accurately. Feature selection and hyperparameter tuning were revisited for models that underperformed, particularly when RMSE values were high, indicating significant error margins. In such cases, further optimisation was conducted to improve model accuracy.

3.6.7 Sample Process Flow

The flowchart in Fig. 3.13 presents a structured methodology used as a guideline for Machine Learning-driven Optimisation, incorporating both Predictive and Descriptive Models. The optimisation process begins with training Predictive models, which include General Supervised Models (such as Random Forest, SVM, KNN, and XGBoost) and Neural Networks (CNNs, ANNs). These models are trained and fine-tuned using external CFD, experimental data, or synthetic data sources. In cases where the training process fails, the models undergo a cycle of troubleshooting, refinement, and potential combination with other models to address performance issues, followed by further testing. Once the training succeeds, the Predictive models are subject to further refinement and validation to ensure that they produce acceptable results. When satisfactory results are achieved, the models' data is stored within a centralised database for future use.

On the other hand, Descriptive models, such as Computer Vision techniques, are applied for feature extraction and classification tasks. The performance of these models is similarly assessed, and if they fail, appropriate adjustments are made to improve their accuracy and effectiveness. Once these Descriptive models meet the required standards, their results are stored in the database. Finally, the optimised Predictive and Descriptive models are integrated to enhance overall system operations. This integration ensures the machine learning framework achieves optimal performance through repeated refinement, validation, and combination of model outputs. By employing this iterative and systematic approach, the process ensures robust development for both predictive analytics and feature classification.

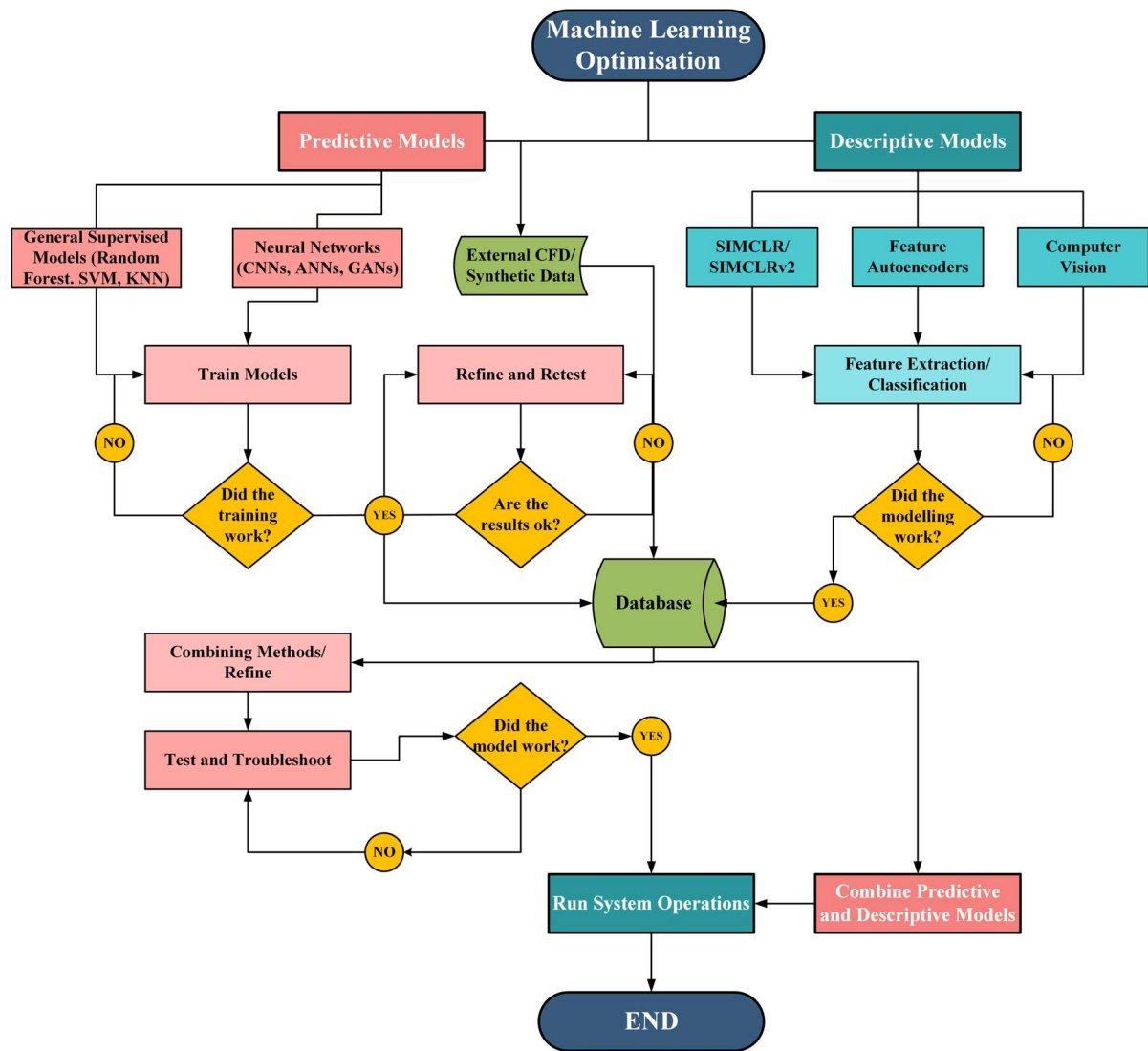


Fig. 3.13 Guideline for machine learning optimisation

3.7 Summary of Methodology Chapter

The methodology chapter begins by defining the research worldview, grounded in pragmatism, which allows for a flexible and practical approach to problem-solving. A mixed-methods design was employed, combining both qualitative and quantitative approaches to provide comprehensive insights. The research methodology integrated data from various sources, including numerical simulations (CFD), experimental investigations, literature data, and synthetic datasets, to support predictive and descriptive tasks. Machine learning models were developed to analyse and unify these diverse data sources, streamlining the process for heat transfer coefficient predictions and enhancing design exploration. The chapter also details the manufacturing process of the heat sinks, the setup of the experimental test rig, and a flow chart guide outlining the machine learning process.

Chapter 4: Evaluation of Biomorphic Extended Top Pin-Fin Heat Sinks

4.1 Background to the Chapter

The initial exploration centered on mushroom-inspired pin-fins, Air, the thermofluid, was introduced to assess the heat transfer and flow characteristics through Computational Fluid Dynamics (CFD) simulations. These simulations unveiled the key dynamics governing performance, particularly in heat transfer coefficient (HTC) and pressure drop, paving the way for further innovations. Building on these findings, a novel biomorphic design inspired by scutoid-shaped skin cells was developed. This hybrid design was evaluated using a design-for-manufacturing (DfM) philosophy to reduce weight while maintaining structural integrity. Additionally, machine learning algorithms were integrated to predict the HTC using minimal parameters such as Reynolds number (Re), surface area, and design volume. The results indicated significant improvements in thermal management efficiency, highlighting the potential for scutoid-based designs in next-generation cooling applications. Additionally, the study provided valuable insights into the underlying physical phenomena.

4.2 Initial Design Investigation

In this phase, two designs were created inspired by parasol fungus/mushrooms. The first design had smoother circular stems/pin-fins and flat tops (CSFT), but the second design maintained sharp edges, pentagonal stems, and diamond-shaped tops (PSDT). Next, a numerical study was performed to analyse the heat transfer and flow characteristics and compare the designs using CFD. The geometry of the parasol-inspired pin-fin heat sinks can be seen in Fig. 4.1. A sample of 30 pin-fins was selected to reduce simulation time and cost. Both designs had identical sizes, pin-fin spacing, and dimensions.

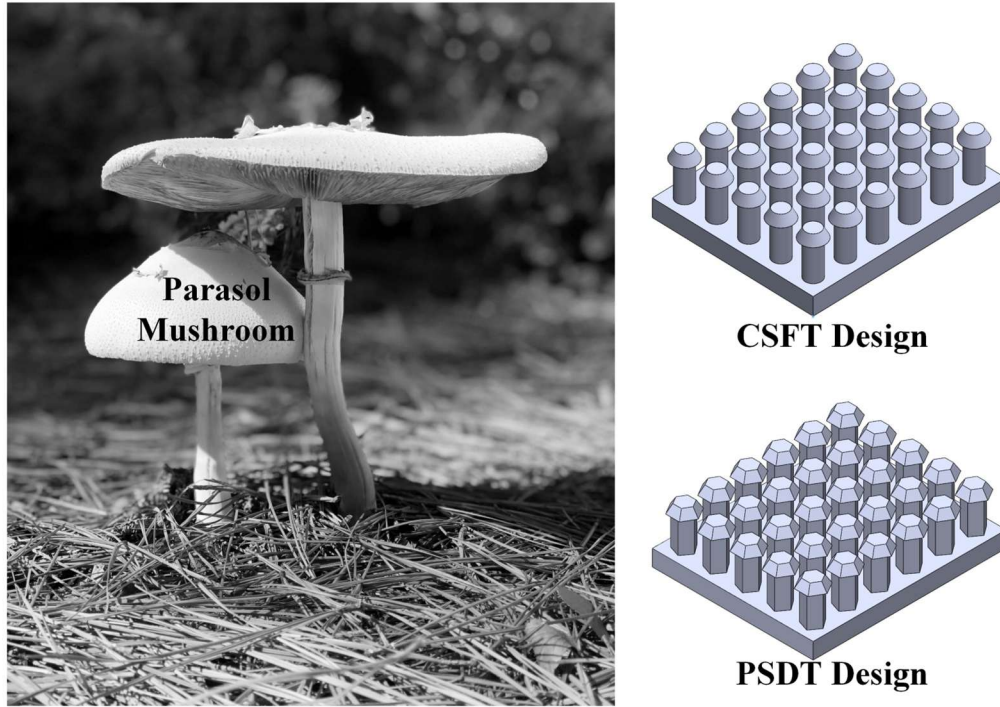


Fig. 4.1 Bio-inspired/biomorphic heat sink designs

Model Pre-processing: ANSYS Fluent Mesh software was employed to create three distinct mesh sizes for fluid and solid domains. The mesh grid independence test/validation was done using a velocity metric. Table 4 provides the mesh statistics.

Table 4: Grid independence test results

Mesh Type	Nodes	Mean Velocity	Maximum Velocity	Refinement Ratio
Mesh (I)	128016	1.349	1.494	--
Mesh (II)	278333	1.352	1.505	2.174
Mesh (III)	534609	1.352	1.496	1.921

Based on the minimal deviations between the velocity results, Mesh (I) was chosen as the suitable option; Mesh (I) orthogonal quality ranged from 0.75 on average to 1 at its highest. Furthermore, the refinement ratio of Mesh (II)/(I) and (III)/(II) were both above 1.3 providing additional validation to the grid independence results [337].

Equations: flow on the micro-scale exhibits dissimilar properties from the flow on the macro scale; albeit, some disagreements amongst researchers exist regarding this. Nevertheless, the governing equations used for modelling the simulation of the novel heat sinks and standard k-epsilon flow turbulence assumptions were adapted from previous works [338,339].

$$\text{Continuity equation: } \frac{\partial u}{\partial x} + \frac{\partial v}{\partial y} + \frac{\partial w}{\partial z} = 0 \quad (13)$$

$$\begin{aligned} \text{Energy equation (fluid): } & \rho_f \left(u \frac{\partial T}{\partial x} + v \frac{\partial T}{\partial y} + w \frac{\partial T}{\partial z} \right) \\ & = \mu \cdot \text{Pr} \left(\frac{\partial^2 T}{\partial x^2} + \frac{\partial^2 T}{\partial y^2} + \frac{\partial^2 T}{\partial z^2} \right) + S_t(\text{fluid}) \end{aligned} \quad (14)$$

$$\text{Nusselt Number: } Nu = \left(\frac{D_h}{k} \right) \ln \left[\frac{(T_s - T_i)}{(T_s - T_o)} \right] (m C_p / A_{ht}) \quad (15)$$

Where, u, v, w - velocity components; x, y, z - directions; ρ_f - fluid density; μ - dynamic viscosity; Pr - Prandtl number; S_t - energy equation source term; T, T_s, T_i, T_o are fluid, bottom wall, inlet, and outlet temperatures, respectively; m - mass flow rate; A_{ht} - base area where heat is applied; D_h - hydraulic diameter; k - thermal conductivity; C_p - specific heat.

4.2.1 Discussion of Findings

Fig. 4.2 exhibits the findings from the CFD simulations. The initial temperature and inlet velocity were 300 K and 1 m/s. For exploratory purposes, the initial heat source term was given a high value of 100 MW/m^3 . PSDT had a higher temperature saturation region/heat distribution near the outlet with some low temperature region on the bottom right edge. However, due to the potential influence of the laminar boundary layer, CSFT design showed lower temperature saturation regions but had a small high temperature zone on the bottom right edge — in contrast to the other design.

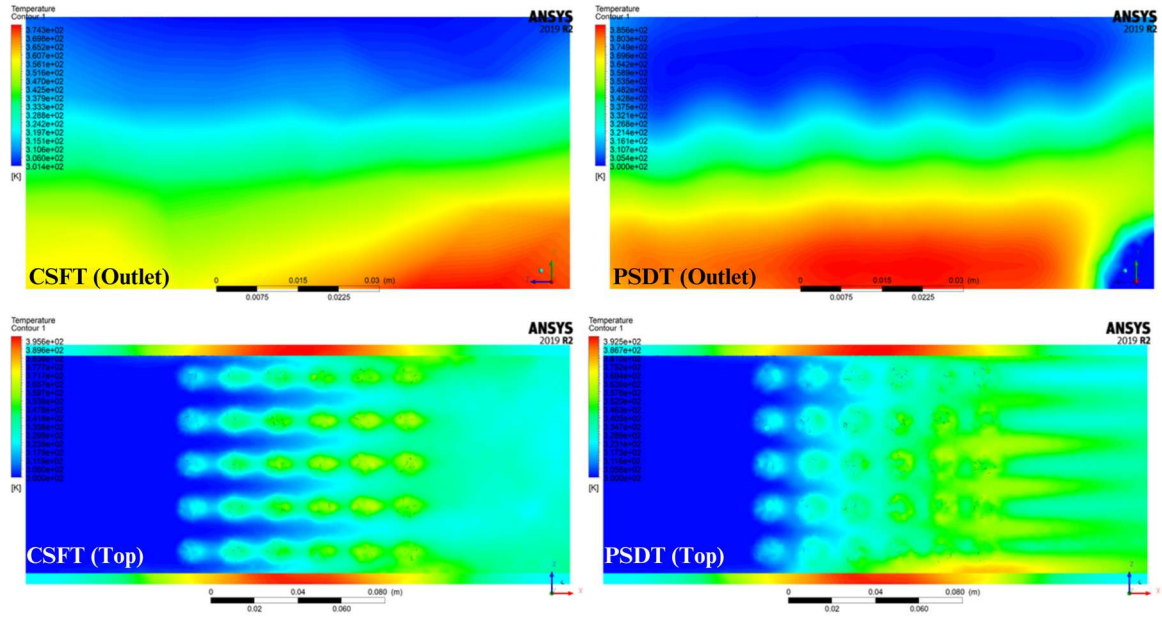


Fig. 4.2 Temperature distribution from the top view and outlets

Fig. 4.3 shows the pressure distribution of CSFT and PSDT. Compared to CSFT, the sharp-edged PSDT had a lower pressure zone at the outlet. Nevertheless, the difference between the inlet and outlet pressure in both designs was minimal.

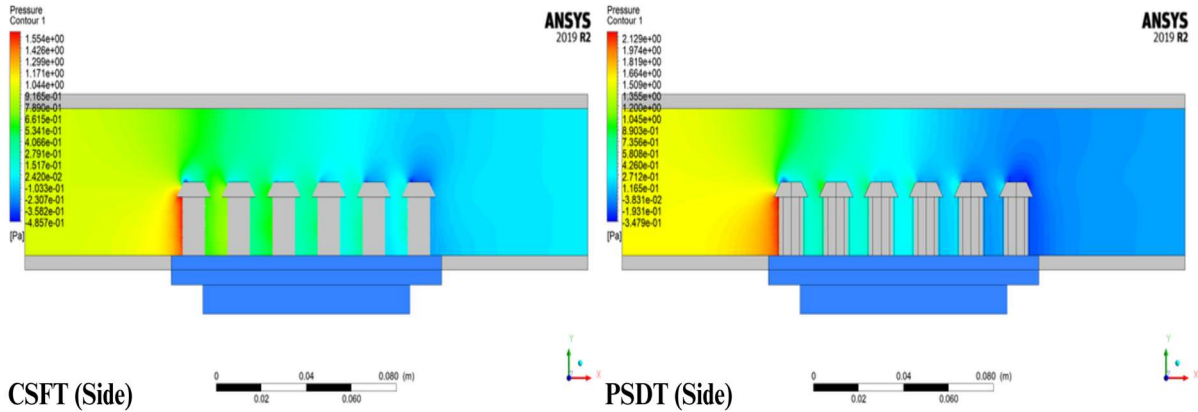


Fig. 4.3 Pressure distribution in the heat sinks

Fig. 4.4 shows localised Nu variation using points along the pin-fin tops. PSDT had an average of approximately 14% higher Nu — the highest Nu coming at both designs' first row/set of pin-fins. The model simulations were validated against previous work [340]; the Nu and pressure change values were in acceptable ranges. Nevertheless, further investigation and verification were required to assess the feasibility of such sharp-edged pin-fin designs. Therefore, subsequent experiments needed optimisation and expansion of the initial designs. It should be noted that it was challenging to utilise past experimental data from the literature due

to the vastly different geometrical configurations and setup. Hence, the author acknowledges the limitations of the findings. However, the current research output was arguably still valuable to build the final prototype design.

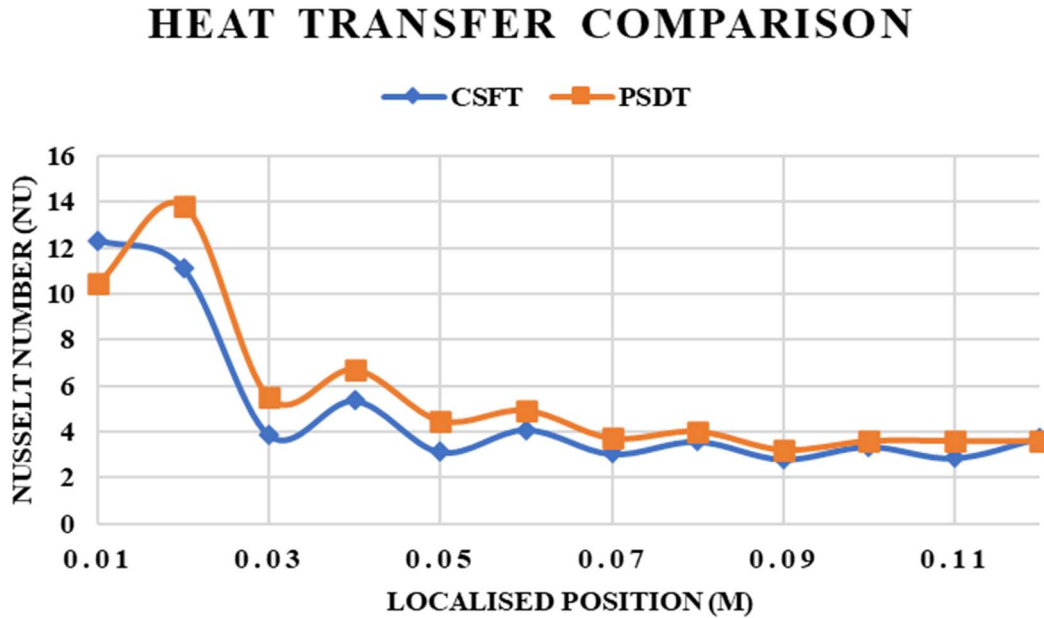


Fig. 4.4 Heat transfer comparison

4.3 Finalised Prototype Heat Sink Design

Building on the initial investigation, further analysis and designs were developed. The use of air-cooled pin-fin heat sinks for electronic devices remains a research hotspot [187,341–343]. For heat transfer enhancement, it is necessary to increase the contact/surface area between the pin-fins and working fluid and induce flow disturbances—while minimising the resulting rise in flow resistance. Therefore, a trade-off of different parameters needs consideration depending on the application. Additionally, adhering to the design for manufacturing (DfM) philosophy, designs must be replicable with reduced cost, materials, and manufacturing complexities. Consequently, an additive manufacturing strategy is required to manufacture pin-fins with complex shapes but with a reduced volume of material to save manufacturing costs [241].

Therefore, this study aimed to provide the following major novel contributions: 1) design of a new type of hybrid pin-fins with non-conventional geometries that can be produced using additive manufacturing; this innovation could expand the current design space and offer advantages over traditional pin-fin designs. 2) appraisal of the effects of combined features with different pin-fin “top” geometries via numerical simulations to gain new insights into fluid flow and heat transfer characteristics, adding further domain knowledge to this area. 3)

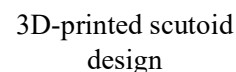
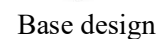
heat transfer performance optimisation via manipulating design properties that can lead to improved performance with reduced volume and material usage — whilst considering the trade-off between design complexity and performance. 4) propose a simplistic machine learning model to predict heat transfer and provide quick performance indicators and reduce design development and exploration times.

4.3.1 Biomorphic Design for Manufacturing (DfM) Philosophy

Nature and organisms have developed various survival strategies and shapes to adapt to their environments. The authors' previous works briefly explored the thermodynamics and thermal performance of nature-inspired biomorphic pin-fin designs [244,253]. Therefore, adopting a similar biomorphic approach, which involves designing inspired by nature, organisms, or naturally occurring shapes, a shape existing in skin cells (Scutoid) [344] was used as a baseline to propose four new pin-fin structures. While skin cells are linked together for material delivery, the biomorphic analogy to skin cells emphasises the efficient utilisation of surface area and generating flow disturbances for enhanced heat transfer, rather than a direct imitation of their mechanism and arrangement, which would be the case in biomimetic design philosophy and is outside the scope of this work.

Moreover, the pin-fin utilises two geometries in a unique shape; thus, there is scope to save materials in the new designs compared to the base fin design — whilst still producing the desired results. The proposed pin-fin structure consists of arrays of staggered pin-fins, in comparison to the in-lined base rectangular/square pin-fin design (SPF). The "top features" of the biomorphic pin-fin structures are designed with specific characteristics, such as sharp edges, faces, and curvatures, aimed at enhancing heat transfer, inducing flow disturbances, and manipulating the volume of material used in the design. In other words, the "top features" are engineered protrusions strategically placed on the pin-fin structures. The design philosophy behind these features involves manipulating their shape/dimensions for maximum effectiveness in heat transfer enhancement while considering the constraints of manufacturing feasibility and cost of the material.

By aligning with DfM principles, the proposed pin-fin designs aim to strike a balance between enhanced heat transfer performance, reduced product development time, and practical manufacturing considerations of complex pin-fin geometries via additive manufacturing or metal 3D-printing; this holistic approach offers efficient and sustainable air-cooled pin-fin heat sinks. Furthermore, in the existing literature, hexagonal, pentagonal, twisted, protrusions, etc.,



113

The new designs followed the same heat sink dimensions as the base design — such as the same internal fin-occupied width (Wb_i), height of the base (H_b), source/heat flux height (H_f), etc. However, the new designs incorporated different shaped "top" features with a scutoid base geometry. Moreover, they vary in the surface area of the "top" geometry, aiming to manipulate the volume of materials used and comprehend the impact of different shapes. For detailed geometrical information, refer to Table 5, which outlines the dimensions of each design. The material usage (%M) shows a reduction of weight in comparison to the base design (SPF).

Table 5: Details of geometrical data for all designs

Model	Top-fin Geometry	Fin-Height (H_f , mm)	No. of Fins (N)	Surface Area (m^2)	Volume (m^3)	Mass (M , g)	Material (%M)
SPF	Square	60	25	80000	271500	271.5	-
PHT	Hexagon	63	23	70646	232542	232.5	-14%
CT	Cone	60	23	73540	250542	250.5	-8%
DT	Tetrahedral	60	23	71590	245093	245.1	-10%
MT	Hexaprism	60	23	75419	254437	254.4	-6%

As mentioned in the earlier paragraphs, the base geometry of the pin-fins utilised a combination of pentagonal and hexagonal shapes to save materials and introduce twists to generate flow disturbances. Additionally, alterations in the top geometry enable the manipulation of boundary layers, providing insights into the flow characteristics of these novel shapes. Given that the proposed designs are intended for additive manufacturing, the critical goal is to save material/weight while ensuring efficient heat transfer. A reduced surface area hampers heat transfer, while an increased surface area adds more volume — contributing to higher material usage and costs. Therefore, the volume of the new pin-fins was constrained within a $\pm 15\%$ range from the base design SPF to strike a balance between reduced material usage and increased heat transfer efficiency. Maintaining a $\pm 15\%$ range in the volume of the new pin-fins relative to the SPF design ensures a reasonable degree of flexibility in design modifications without deviating significantly from the original parameters. Moreover, this range arguably aligns with industry standards and current engineering and design practices.

In the initial paragraphs, the existing literature suggested that hexagons, tetrahedrons, cones, and mushroom/prism shapes can enhance heat transfer. Consequently, a combination of various

pin-fin strategies was investigated to get a more robust understanding of underlying flow characteristics and physical processes. While the PHT and DT designs focused on altering the flow through a change in the height of the top fins, the CT and MT designs elongated the lateral surfaces of the fins. The first PHT design featured a plain hexagon top with 5% more pin height and 0.5mm more side width than the other scutoid pin fins. This adjustment aimed to maintain the reduction in volume/surface area of PHT within the initially discussed $\pm 15\%$ acceptable range. The plain surface of PHT could potentially enable boundary layer formations on top while inducing turbulence between and around the fins. All the other designs had 4.5mm sides/60mm fin height. However, there are minor variations between the spacing distances of the fins due to the difference in the fin-top geometry, to avoid interactions, and leave a reasonable amount of gap between the extended surfaces, especially for the CT and MT.

The second design, CT, featured a cone-shaped pointed top geometry, where the pointed shape was expected to cause flow separations, while the smooth surface of the cone can lead to flow attachments. The third design, DT, incorporated an extended tetrahedral diamond-shaped structure inside the top geometry of the fins, with sharp edges capable of generating turbulence. The last design, a sharp biomorphic mushroom-shaped prism, covered the top of the fins extensively in an attempt to increase the heat transfer area. In addition to these design modifications, there was a 90-degree twist and a vertex within the fin-base geometry converting the pentagonal shape into a hexagon and causing the designs to have a slight curve. Thus, all the combinations existing within these design modifications produced a new type of novel hybrid pin-fins. Despite the complexity of the pin-fin shapes, as illustrated in Fig. 4.6 for the 3D printed prototype, they represent a feasible option for future manufacturing through additive manufacturing and casting process, if needed. Fig. 4.6 displays the 3D geometry of all the new pin-fins designed for this study.

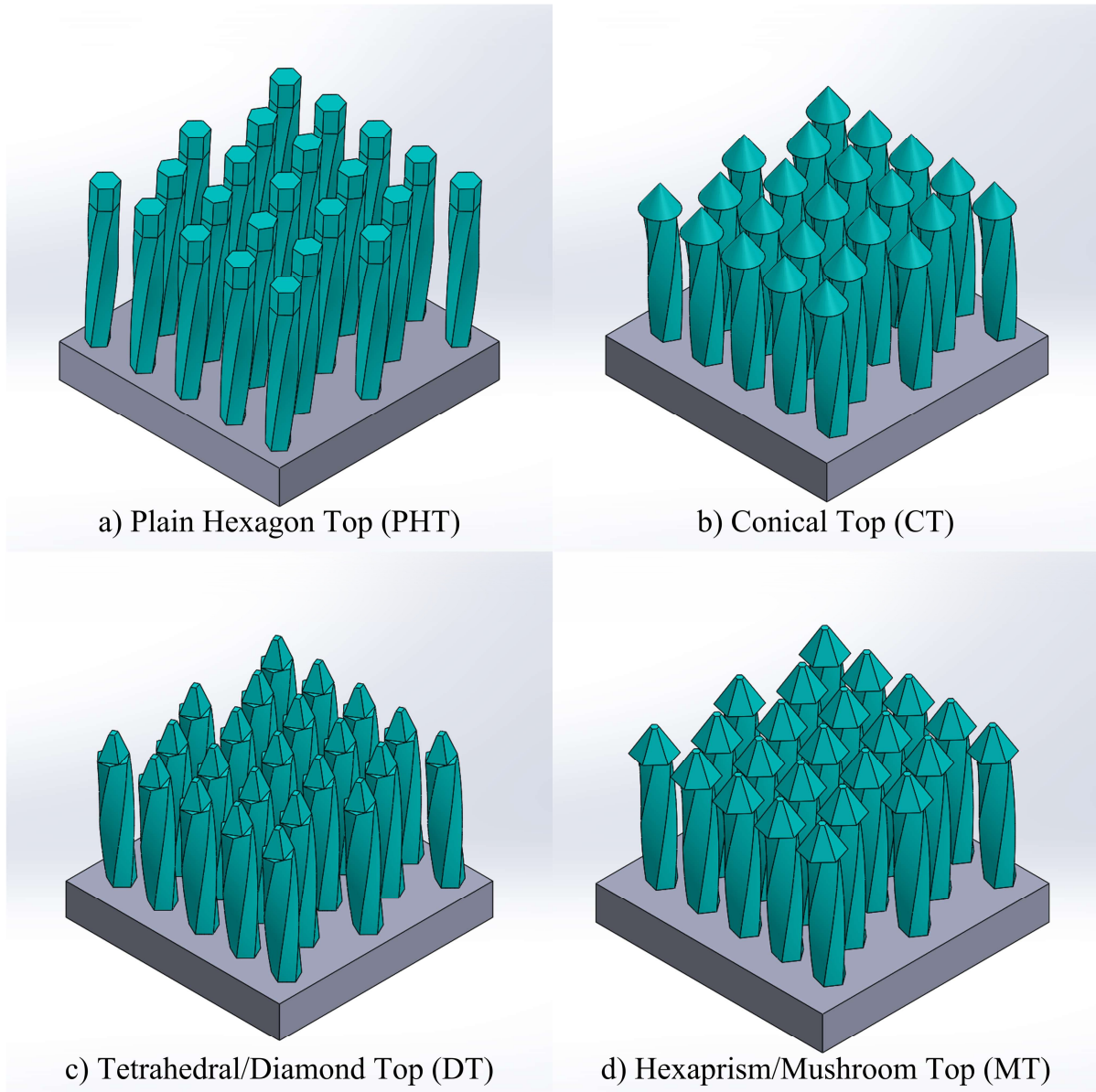


Fig. 4.6 All biomorphic scutoid pin-fin designs: a) Plain Hexagon Top (PHT), b) Conical Top (CT), c) Diamond Top (DT), d) Mushroom Top (MT)

4.3.2 Numerical Simulation Setup and Validation

4.3.2.1 Physical and Mathematical Model

The initial numerical simulations were validated using the experimental findings of El-said et al. [240]. One of the primary motivations behind this research was to minimise computational time and cost on a holistic level. To achieve this, certain methods allow conducting simulations with half designs or geometries, assuming setups exhibit symmetry. However, the current study deals with non-symmetrical shapes and complex geometries, which may result in non-symmetrical flow characteristics. Therefore, the experimental setup was replicated for validation purposes to ensure more reliable and robust findings. Therefore, achieving an

optimised number of meshing and nodes was preferred to save on computational time and cost. In the experiments of El-said et al. [240], an extended area of 200 mm exists on either side of the test section; therefore, the inlet effect or outlet reflux is avoided by default. The pressure drop in the system was also relatively minimal due to the extended length of the fluid domain, no flow re-circulation, and the outlet being exposed to atmospheric pressure. Conventionally, Reynolds Number (Re) < 2000 tends to be laminar flow; transition region, $2000 < Re < 4000$; turbulent flow is $Re > 4000$ [345]. However, for flows in micro scales, diverse and conflicting characteristics are reported. Extant research reported transition and turbulent flow regions within micro-scale flows for $300 < Re < 2000$ [346]. Therefore, in this paper, flows with $Re > 3000$ were assumed as turbulent. Consequently, a standard $k - \epsilon$ model was chosen for turbulence modelling. The simulations were performed with single-phase phenomena considerations, as the working fluid is air. Additionally, adapting and modifying previous research [26,246,338,339,347,348], the simulations considered the following assumptions:

- 1) The working fluid (air) is incompressible;
- 2) Gravity can be ignored due to the low mass of air;
- 3) The material properties are isotropic;
- 4) Surface radiation and viscous heat dissipation are negligible.

The baseline governing equations for simulations, validation, and data reduction were:

Continuity equation:

$$\frac{\partial U}{\partial X} + \frac{\partial V}{\partial Y} + \frac{\partial W}{\partial Z} = 0 \quad (16)$$

Energy equations:

$$\rho_f \left(u \frac{\partial T}{\partial x} + v \frac{\partial T}{\partial y} + w \frac{\partial T}{\partial z} \right) = \mu \cdot \text{Pr} \left(\frac{\partial^2 T}{\partial x^2} + \frac{\partial^2 T}{\partial y^2} + \frac{\partial^2 T}{\partial z^2} \right) + S_t(\text{fluid}) \quad (17)$$

$$k_s \left(\frac{\partial^2 T_s}{\partial u^2} + \frac{\partial^2 T_s}{\partial y^2} + \frac{\partial^2 T_s}{\partial z} \right) = 0 \text{ (solid)} \quad (18)$$

Dimensionless parameters: $X = \frac{x}{D_h}$, $Y = \frac{y}{D_h}$, $Z = \frac{z}{D_h}$, $U = \frac{u}{u_{in}}$, $V = \frac{v}{u_{in}}$, $W = \frac{w}{u_{in}}$

Conductive heat transfer/Fourier's law

$$Q = -kA \frac{\partial T}{\partial x} \quad (19)$$

Where, thermal conductivity (k) is a thermophysical constant, $K = \frac{Qd_p}{A\Delta T}$

Mean convective heat transfer coefficient (HTC):

$$h = \frac{\dot{m}_a c_{p,a} (T_{out,a} - T_{in,a})}{A_s [T_b - \left(\frac{T_{in,a} + T_{out,a}}{2} \right)]} \quad (20)$$

Nusselt Number (Nu):

$$Nu = \frac{hL_b}{k_a} \quad (21)$$

Thermal Resistance (R_{th}):

$$R_{th} = \frac{T_b - T_{a,in}}{\dot{m}_a c_{p,a} (T_{out,a} - T_{in,a})} \quad (23)$$

Fin efficiency (η_F):

$$\eta_f = \frac{\tanh(M \times H_a)}{M \times H_a} \quad (24)$$

$$\text{Where, } M = \sqrt{\left(\frac{4h}{k_f D_h} \right)}$$

Pressure drops (ΔP):

$$\Delta P = (P_{inlet} - P_{outlet}) \quad (25)$$

Performance Improvement Factor (PIF):

$$PIF = \left(\frac{h_{(nc)}}{h_{(bc)}} \right) / \left(\frac{\eta_{f(nc)}}{\eta_{f(bc)}} \right)^{\frac{1}{3}} \quad (26)$$

4.3.2.2 Grid Independence and Numerical Validation

ANSYS Fluent's Finite Volume Method (FVM) was used for simulations and meshing. A mixture of hybrid and rectangular-grid type meshing was implemented to increase the overall mesh quality whilst reducing computational time and meshing nodes. The mesh independence test was conducted and compared with the experimental data for rectangular pin-fins for validation of the simulation setup; this was the base design (SPF). The element sizes of the

solid domain were 0.004 mm, 0.0035 mm, and 0.003 mm; the element size of the fluid domain varied from 0.002 to 0.001 mm. The three different meshes (with varying element count) were *Mesh I* (164269), *Mesh II* (255186), *Mesh III* (530970), respectively. The element sizes were chosen and adjusted based on a target average orthogonal quality. The average orthogonal quality of the mesh was over 0.75 (very good). Refinement ratios between two different mesh types were above 1.3. The grid validation considered two variables: maximum velocity at the outlet, $V_{max(out)}$, and average temperature of the outlet, $T_{avg(out)}$. The numerical validation considered the heat transfer coefficient, HTC (h), from $Re = 3182$ to 9971. The grid independence results are summarised in Fig. 4.7; it shows that deviations between the corresponding mesh qualities are minimal. Furthermore, to complement the visualisation in Fig. 4.7 and Fig. 4.8, Table 6 displays a sample of the mesh and grid independence results, providing a quantitative assessment of the values obtained for accuracy and uncertainty.

Table 6: Sample grid independence test accuracy results

Re, V_{in}	$T_{avg(out)}$	$V_{max(out)}$	h	% <i>Deviation</i> (h)
(3182, 0.3 m/s)	(K)	(m/s)	(W/m^2k)	[240]
Mesh I	306.98	0.47	54.96	12%
Mesh II	306.85	0.46	53.00	8%
Mesh III	306.88	0.46	56.66	16%
Re, V_{in}	$T_{avg(out)}$	$V_{max(out)}$	h	% <i>Deviation</i> (h)
(3182, 0.3 m/s)	(K)	(m/s)	(W/m^2k)	[240]
Mesh I	300.70	1.34	107.64	12%
Mesh II	300.72	1.36	108.48	10%
Mesh III	300.68	1.34	111.93	8%

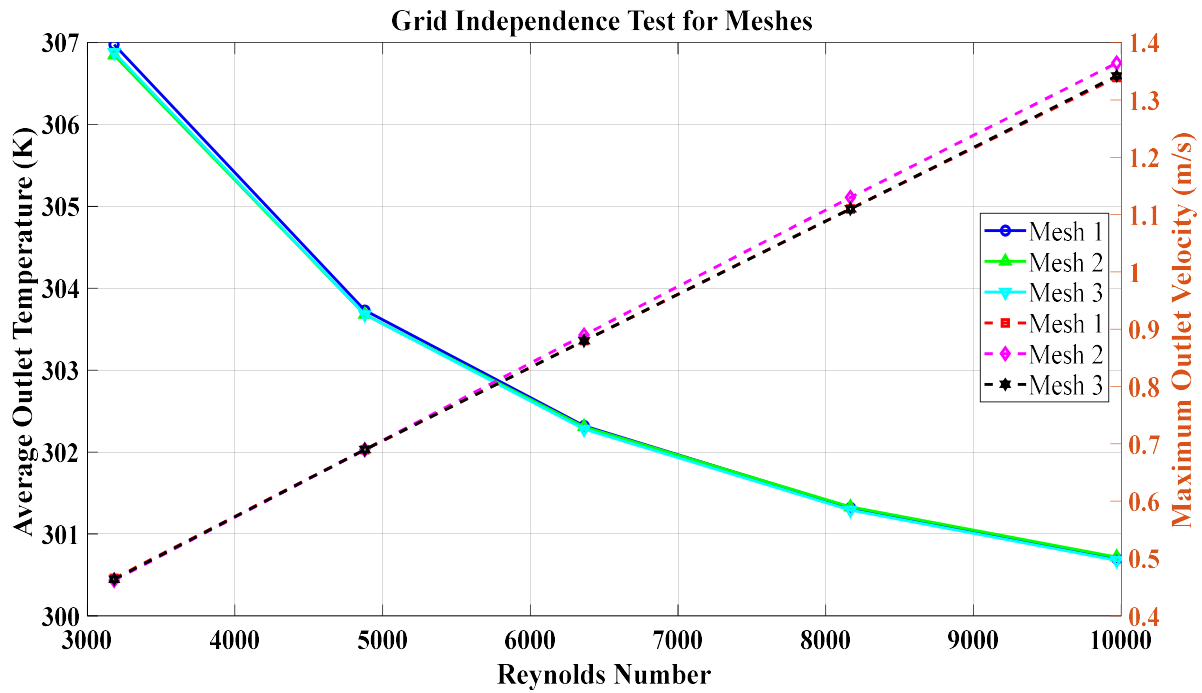


Fig. 4.7 Grid independence test results

After considering all the findings and computational time, Mesh II was taken as the preferred option for simulations. Fig. 4.8 shows the deviation between the simulations and experimental data [240]. As mentioned earlier, $Re < 4000$ values are generally in the transitional range before turbulent flow conditions occur. Therefore, using the $k - \epsilon$ model, the initial value overshoots by 10%, but, in higher Re values, the data points are relatively consistent.

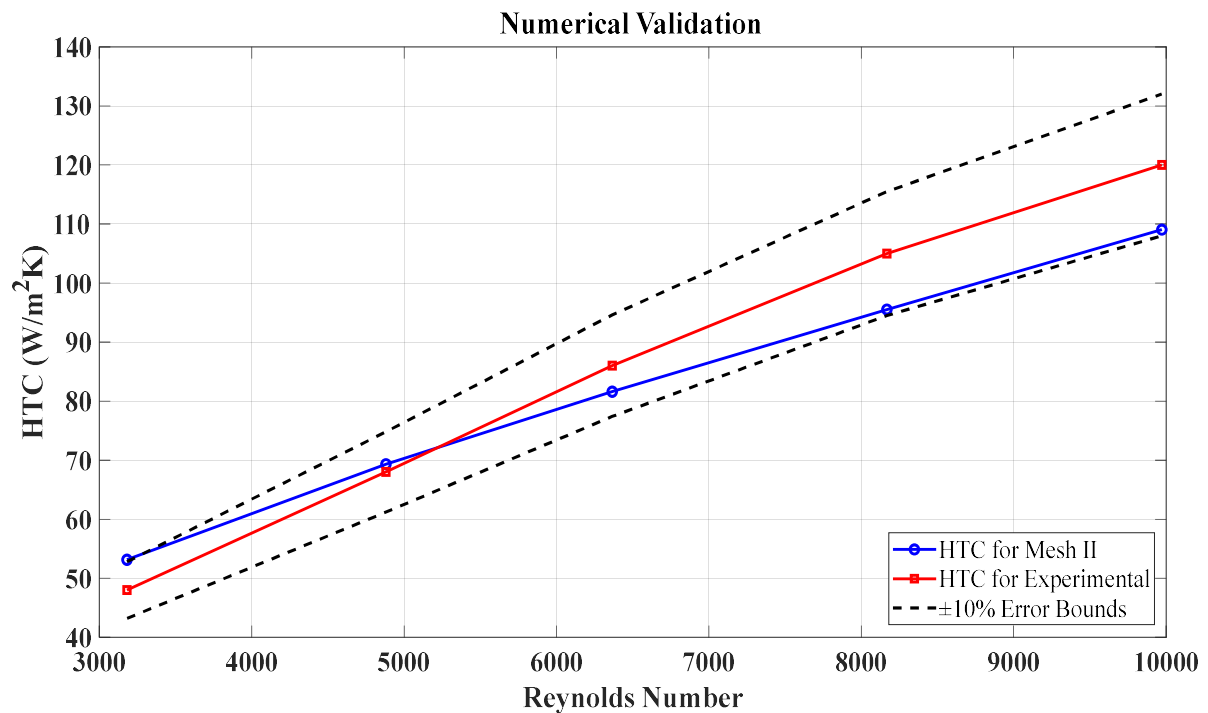


Fig. 4.8 Numerical validation of the simulation

4.3.2.3 Meshing and Boundary Conditions

One of the objectives of our research was to appraise different volume and implement machine learning. Hence, after the numerical validation, to avoid overfitting of the data and enable a more broader data analysis, the operating conditions were slightly changed to investigate higher Reynolds Numbers not examined in the available literature for similar designs. Therefore, the simulations were set up with the following boundary condition: a uniform velocity and constant temperature at the inlet, with values of $u = u_{in}$, $v = 0$, $w = 0$, $T = T_{in} = 298\text{ K}$; zero pressure at the outlet, and scalable wall function for the near-wall treatment. The heat flux value was 15500 W/m^2 .

The mesh interaction boundary was coupled at the fluid-solid contact surface, while all other surfaces were adiabatic. The momentum and energy equations used second-order upwind schemes, and the velocity-pressure coupling was selected using the SIMPLE algorithm having monitors' residual value set to 10^{-5} and 10^{-7} , respectively. Lastly, hybrid initialisation was chosen for the calculations. Fig. 4.9 illustrates the simulation setup, including the fluid domain, solid domain (pin-fins), and meshing. The simulation fluid and solid domains are depicted with a sliced plane, revealing 3D mesh blocks to provide a more three-dimensional perspective of the mesh employed — the sliced view utilises the base design SPF. Next to the simulation domains, the meshes for the scutoid pin-fins are also presented, with the PHT design view intentionally rotated to offer an alternative perspective of the mesh within the designs. In certain regions or cases, minor or local face refinements were employed to minimise the number of elements or improve the average orthogonal mesh quality.

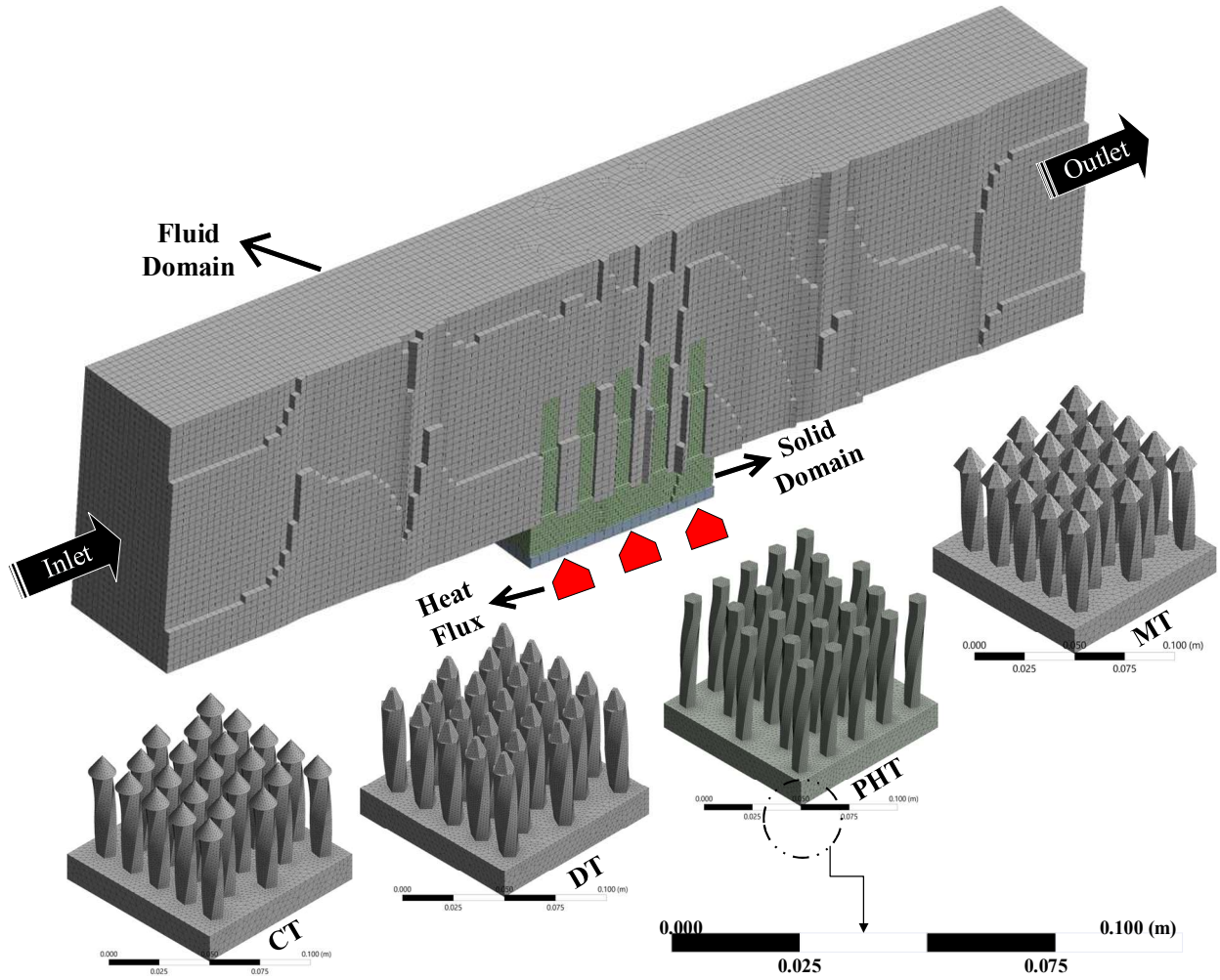


Fig. 4.9 3D Mesh visualisation of fluid and solid domains for the pin-fins

4.3.3 Results

4.3.3.1 Heat Transfer Performance

Figs. 5.10-5.13 illustrate the performance metrics to evaluate the pin-fins. Firstly, Fig. 4.10 presents a graph that plots the Heat Transfer Coefficient (HTC) against the Reynolds Number (Re). The HTC is significant in thermal management research as it quantifies heat transfer efficiency between a solid surface and a fluid medium. HTC represents the rate at which heat is convectively transferred from the solid metal surface to the surrounding air — in this case. The results reveal that the plain hexagon top (PHT), showcases the highest overall HTC, despite having the lowest volume and surface area ($volume (V) = 232541.53 \text{ mm}^3$, $surface area (SA) = 70646.26 \text{ mm}^2$). In comparison, the hexaprism or mushroom-inspired top (MT) design showed, on average, 5% lower HTC values whilst having the highest material usage among all pin-fin designs ($V = 254437.03 \text{ mm}^3$, $SA = 75418.77 \text{ mm}^2$). The diamond/tetrahedral top (DT) and conical top (CT) were the two least-performing pin-fin

shapes, with CT demonstrating the worst HTC performance ($96.6 \text{ W/m}^2\text{K}$ at $Re = 5500$). The DT and CT designs might suffer from boundary layer separation or inadequate mixing of the fluid flow. In the case of the conical top (CT) design, its particularly poor HTC performance can be attributed to its geometry, which might induce strong separation of the boundary layer and hinder effective heat transfer.

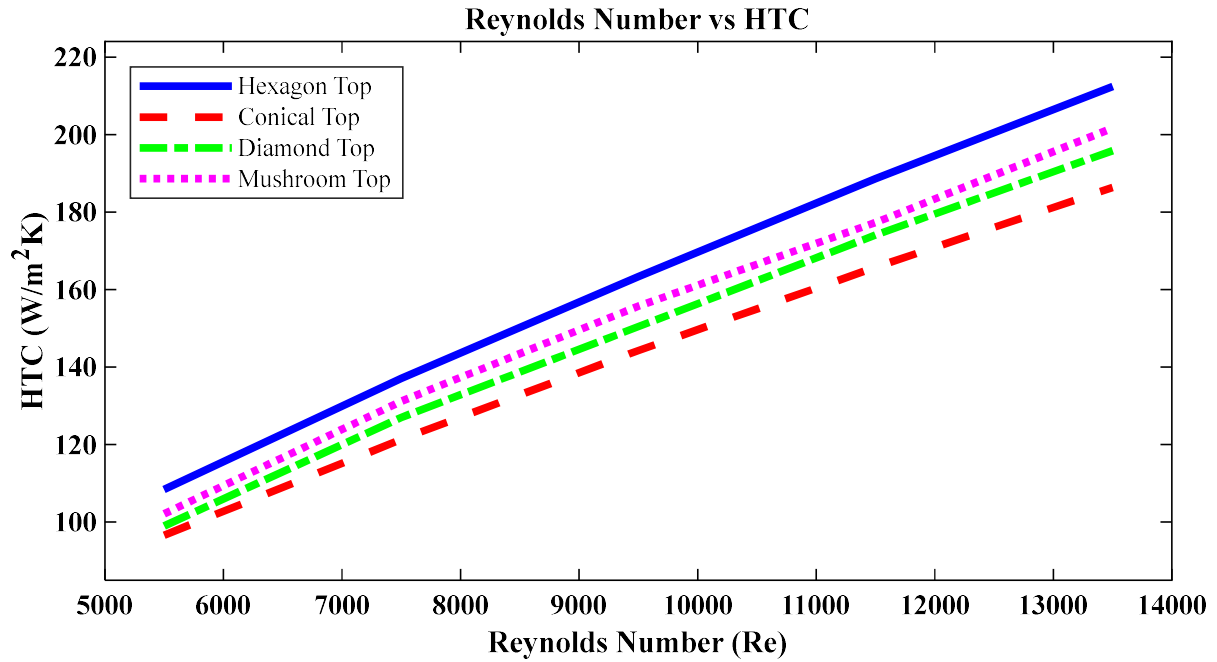


Fig. 4.10 Heat transfer coefficient comparison with different Re

The Nusselt Number (Nu), similar to the HTC, is a critical metric for assessing heat transfer and insights into convective heat transfer properties of systems. By comparing the conductive heat transfer to the convective heat transfer at the surface, the Nu quantifies the convective heat transfer rate. Fig. 4.11 shows the Nu comparison; since the Nu is directly proportional to the HTC, it exhibits a similar trend. In this study, the plain hexagon top (PHT) design consistently exhibited the highest Nu across different Reynolds Numbers (Re). In contrast, the conical top (CT) design showed the lowest Nu value. The Nu performance of different pin-fin shapes, just like the HTC, can be influenced by flow reversal and recirculation phenomena. Pin-fin shapes that promote flow reversal or recirculation might experience reduced heat transfer rates due to inefficient removal of the heated fluid and replacement with cooler fluid.

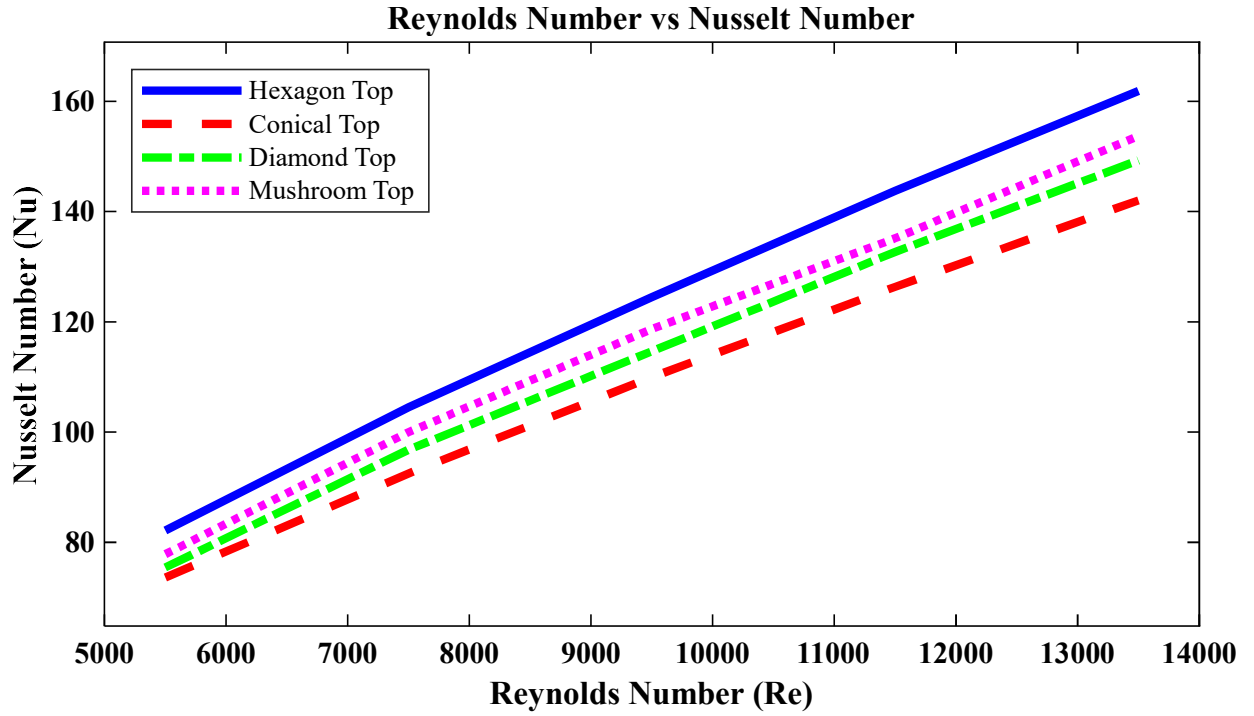


Fig. 4.11 Nusselt Number comparison with different Re

Fig. 4.12 illustrates the thermal resistance (R_{th}) of the pin-fins. Thermal resistance represents the obstruction to heat flow in a material or system, serving as a fundamental parameter in heat transfer analysis and thermal management. It enables the evaluation and optimisation of the overall thermal performance of heat sinks. Notably, in this case, both the PHT and MT designs, which feature hexagonal bases, exhibited the lowest R_{th} values, indicating their superior heat dissipation capabilities compared to other designs. On the other hand, the DT and CT designs displayed the highest R_{th} , with CT demonstrating the most resistance. The thermal resistance of a pin-fin design is influenced by the thickness of the thermal boundary layer surrounding the fins. Designs that effectively reduce the boundary layer thickness can achieve lower thermal resistance. The PHT and MT designs may minimise boundary layer thickness more effectively compared to other designs, leading to lower R_{th} .

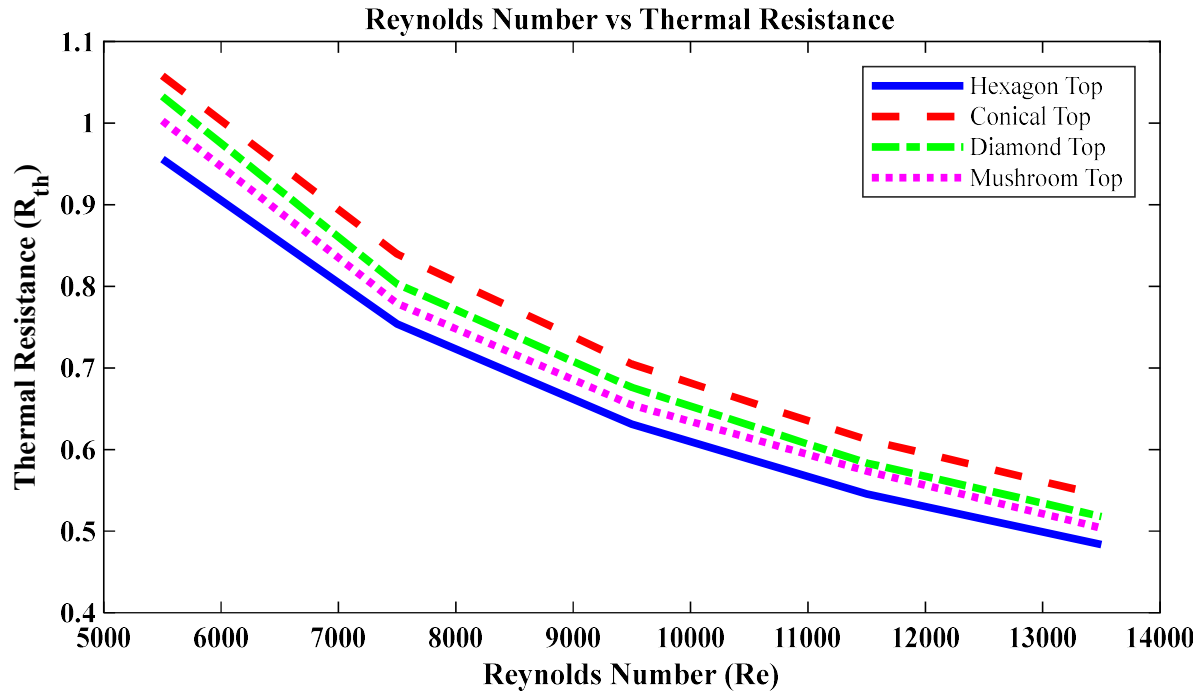


Fig. 4.12 Thermal resistance comparison with different Re

Interestingly, the findings and trends diverged when considering the fin efficiency values depicted in Fig. 4.13. Fin efficiency (η_f) is a parameter used to assess the effectiveness of a fin in enhancing heat transfer; it quantifies how efficiently a fin transfers heat from the solid surface to the surrounding fluid medium. Fin efficiency is particularly relevant in heat transfer applications involving extended surfaces or fins, where the primary objective is to increase heat dissipation capacity. Based on the values in Fig. 4.13, the CT design demonstrated the highest η_f , followed by the DT, while the MT and PHT designs exhibited the lowest η_f . However, it is noted that the differences in fin efficiency among the pin-fin designs were minimal ($\leq 1\%$). Therefore, a marginally lower fin efficiency as a trade-off can be acceptable. The CT design could benefit from smoother flow attachment and detachment along its streamlined shape; this reduces flow separation and enhances the effectiveness of the fin in transferring heat to the surrounding fluid.

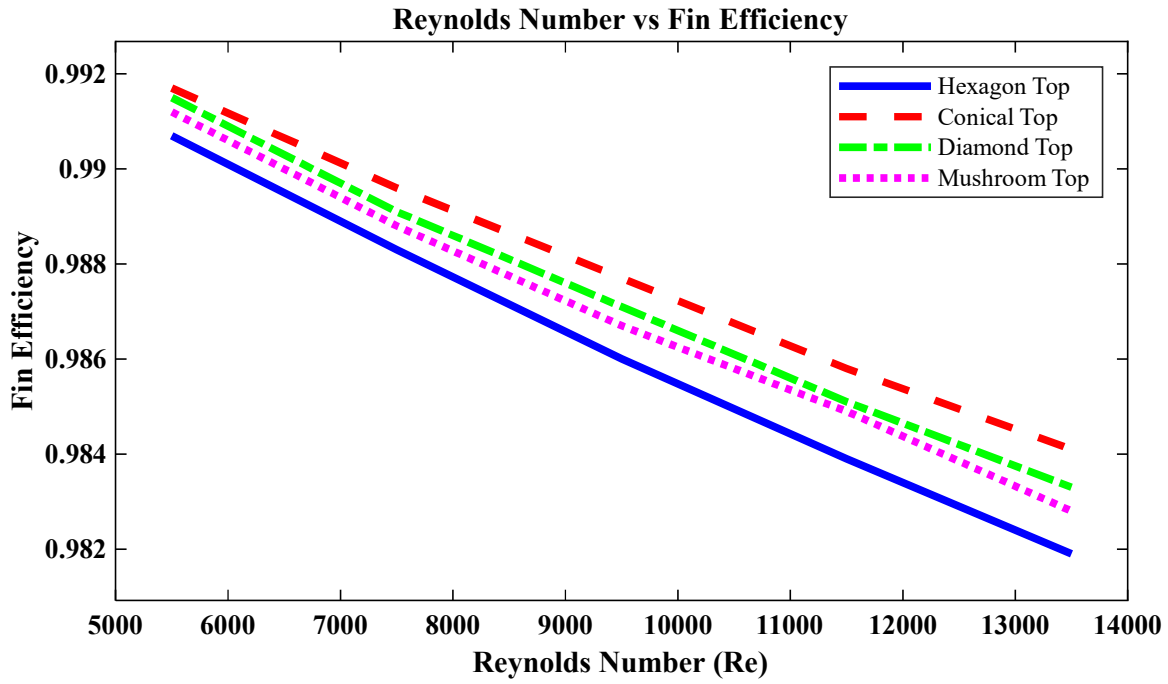


Fig. 4.13 Fin efficiency comparison with different Re.

4.3.3.2 Pressure Drop and Pumping Power

In the design and optimisation stage for heat sinks, one of the key considerations includes pressure drop and pumping power expenses [349]. However, as previously mentioned, the reference system exhibited minimal pressure drops mainly due to its open outlet (exposed to atmospheric pressure) and the absence of flow recirculation. Thus, the focus of this study was on enhancing heat transfer and fluid flow characteristics — with the understanding that any trade-offs in pressure drop would remain within acceptable limits. Fig. 4.14 shows the pressure drop comparisons. In this investigation, the highest value of $Re = 13500$ was chosen for comparison for two reasons: i) existing literature lacks experimental/numerical values for similar designs within the Re range of $10000 - 15000$; ii) $Re = 13500$ corresponds to the point of maximum heat transfer in the new designs, implying that it will also lead to the conditions with the highest-pressure drops. Consequently, the highest pressure drop was associated with PHT fins, and the lowest pressure drop was observed in SPF fins.

The pressure drop trend is consistent with the heat transfer coefficient (HTC), as PHT had the highest HTC. Furthermore, the simulated pressure drops values closely matched the ranges from previous numerical validations with similar Reynolds Numbers [206,350]. It is important to note that a system's pumping power is directly related to the pressure drop. When comparing the pressure drop values between PHT and SPF, even when factoring in a pump with 70% efficiency, the resulting increase in pumping power is approximately 55 mW, which remains

relatively low. As a result, this trade-off is deemed acceptable in exchange for achieving superior heat transfer rates. Additionally, it can be remarked that the extended flow build-up region length employed in the initial experiment had a role in achieving these low pressure drops and pumping power.

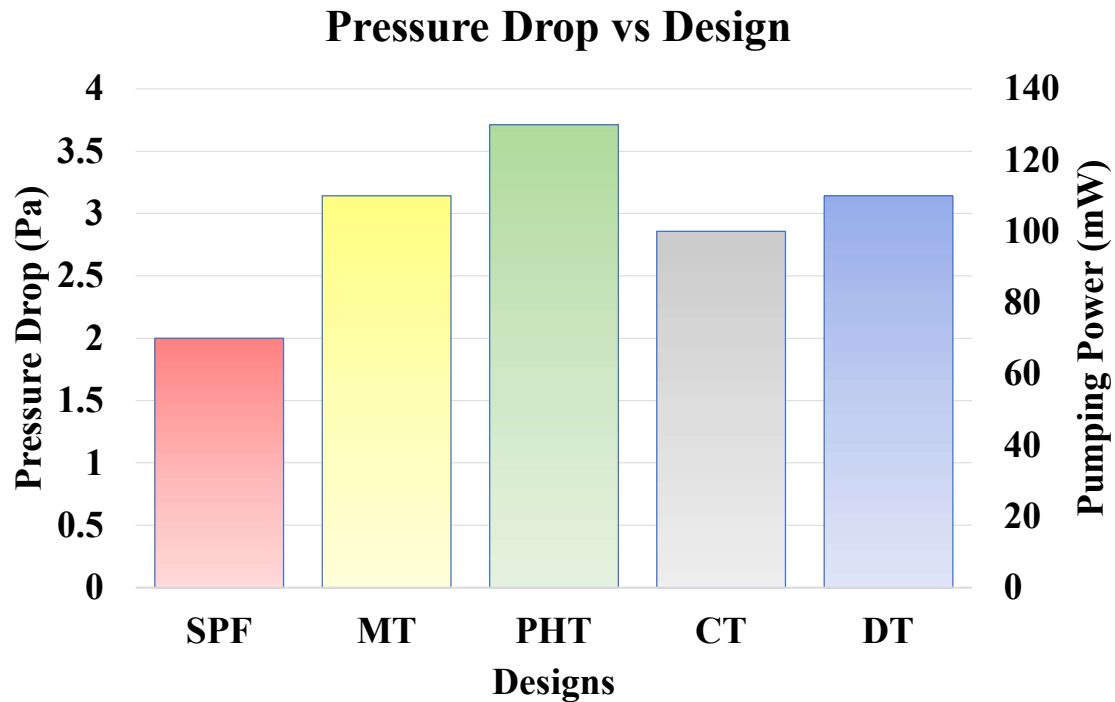


Fig. 4.14 Pressure drop comparisons

4.3.3.3 Machine Learning Predictions

In this study, one of the points of interest was investigating the influence and relationship between the design volume, surface area, and heat transfer in a system. The data indicated that volume manipulation via different geometrical adjustments can help to achieve enhanced heat transfer with material savings. Therefore, this led to the assessment of a prediction model to determine HTC whilst incorporating design properties such as volume and surface area. Accordingly, a combination of four independent variables (IV) — volume, surface area, Reynolds number (Re), and inlet velocity — was used to predict the dependent variable (DV) — heat transfer coefficient (HTC). The rationale behind this idea was that developing a simplistic model that relates volume to the HTC would have significant implications, as it would provide a quick performance indicator and assessment of heat transfer effectiveness without the need for extensive experiments, CFD simulations, or requiring vast datasets.

Consequently, six different types of machine learning models were compared for predicting the HTC: Multiple Linear Regression (MLR), K-nearest Neighbours (KNN), Random Forest (RF), Gradient Boosting Regression (GBR), and ensemble methods such as Bagging and Stacking. The description and mechanics of all the machine learning models go beyond the scope of this work and have been extensively detailed in existing literature. While MLR, KNN, and RF have been commonly used [351], GBR and ensemble methods like Bagging and Stacking are relatively unexplored, compared to the popular algorithms such as MLR and RF, especially in heat transfer analysis; thus, these algorithms could produce promising results. GBR employs a boosting technique to create an ensemble of weak predictive models, typically in decision trees [352], while Bagging (also referred to as bootstrap aggregation) and Stacking are ensemble methods that combine multiple models to improve predictions [353]. Regression models generally do not require many data points compared to neural networks; hence, two distinct datasets were created for the machine learning predictions (CFD and Combined).

The first dataset consisted solely of data points from CFD — gained from the novel pin-fins produced in this investigation. The second dataset combined CFD simulation and experimental results to form a broader dataset and enhance accuracy or avoid overfitting. The experimental data consisted of rectangular and hexagonal pin-fins' best and worst performing designs from El-said et al. [240]; the volume and surface area information was gained via the SolidWorks evaluation tool. It should be noted that even though the dataset has a limited number of points, due to the different types of data considered, it can arguably provide good predictions. Additionally, recent research suggests that condensing datasets and using reduced data can potentially provide better predictions for thermal analysis [354].

The performance of each model was calculated using Root Mean Squared Error (RMSE) and Mean Absolute Percentage Error (MAPE). RMSE measured the average deviation between predicted and actual HTCs, while MAPE assessed the relative errors in percentages. Table 7 shows the data of the model performances. RMSE and MAPE metrics enabled a thorough comparison and ranking of the models' performance. To exhibit the results clearly, a grouped bar graph in Fig. 4.15 compares the model's predictive capabilities. The evaluation process using RMSE and MAPE ensured an objective assessment of the predictive models and aided in determining the most suitable approach for predicting HTCs in heat sinks.

The results showed that Bagging and Stacking methods had the best performance, with an average MAPE value of 4.6% and 4.4% and RMSE values of 8.7 and 8.4, closely followed by

MLR at 4.7% and 8.4. RF and KNN had a poorer performance, with KNN performing the worst among all models. Although GBR had slightly higher errors than the top-performing models, the percentage deviation between the two datasets for GBR was the lowest; this shows that GBR is less sensitive to the differences in datasets. In forced air convection, the HTC values can range between 10 to 500 (W/m²k) [355]. Therefore, considering the range for prediction, mean MAPE <5% and RMSE <10 can arguably be considered relatively good and acceptable; this is especially valid considering the original experiments and the CFD simulations had approximately $\pm 10\%$ margin for error.

Table 7: Data for machine learning model performance

Model Type	RMSE (CFD)	MAPE (CFD)	RMSE (Combined)	MAPE (Combined)
MLR	6.09	4.3%	10.72	5.0%
GBR	7.37	5.5%	9.32	4.9%
RF	6.99	4.4%	15.71	9.0%
KNN	13.97	11.3%	15.36	7.2%
Bagging	6.55	4.9%	10.77	4.2%
Stacking	6.28	4.5%	10.56	4.3%

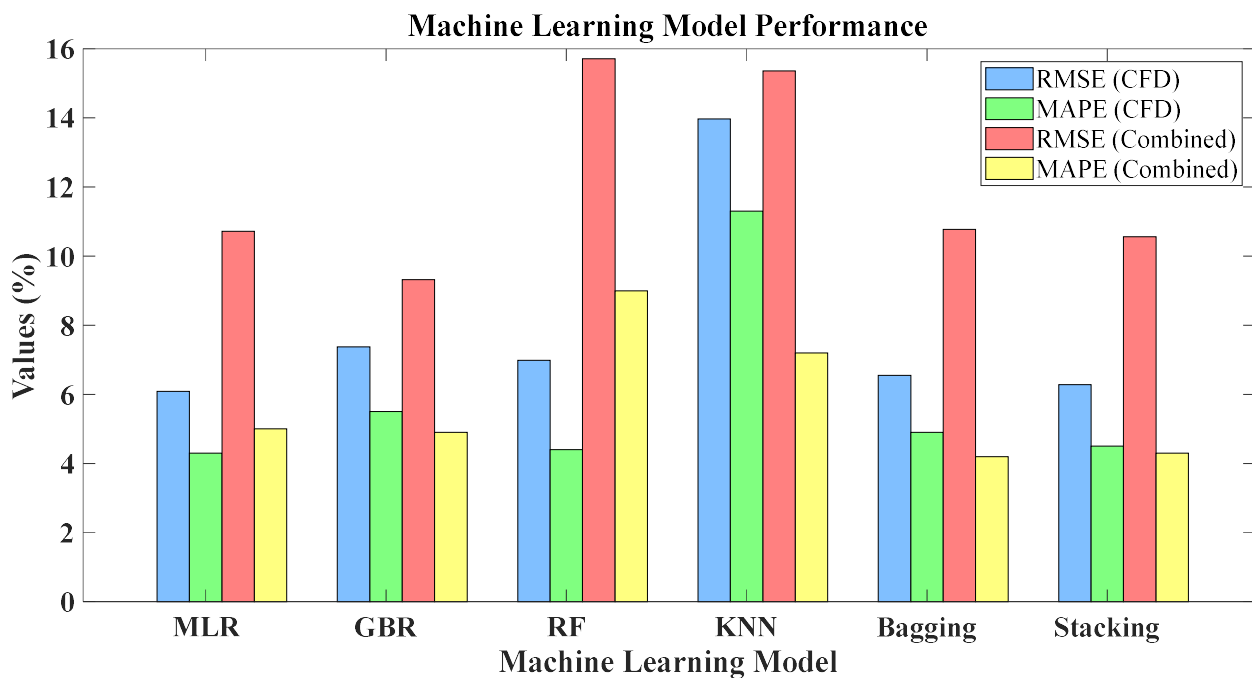


Fig. 4.15 Comparison of machine learning model performance

4.3.3.4 Fluid Flow Characteristics

Fig. 4.16 (a)-(d) showcases the temperature contours across three planes at $Re = 13500$ — where the highest heat transfer occurs. The first plane is positioned in the mid-section of the heat sink, the second plane is 0.1m from the first plane, and the third plane is at the outlet position. Temperature contours provide visualisation of temperature variations across specific regions, enabling interpretation of thermal and flow behaviour.

In Fig. 4.16a, hotter temperature spots near the bottom portion of the fins are observed, while no apparent similar features are evident at the tops. In the middle/second plane, a thin high-temperature (red colour zone) thermal boundary layer is present; thinner boundary layers can promote better heat transfer performance as seen in Fig. 4.10. However, the dominant temperature range in the second plane consists of mid-temperature (300K – 306K) values. Fig. 4.16b illustrates the temperature distribution in the CT design. One primary difference between CT and PHT is the presence of localised hotter regions around the conical tops, extending beyond the solely bottom portion that was observed in Fig. 4.16a; this indicates that the contact between air and the pin-fins are more prominent compared to the other design and validates the initial assumption of better flow attachments leading to higher fin efficiency in Fig. 4.13. At the outlet, a high-temperature region appears, and it is broader compared to PHT, forming sinusoidal-shaped thermal layers; this denotes the presence of uneven flow distribution.

Fig. 4.16c depicts the temperature contours for DT. Akin to Fig. 4.16a, there is no region of high temperature (red zones) at the top of the fins, but the bottom portion exhibits higher temperatures (1K to 1.2K more) than the surrounding air. Interestingly, a localised cold spot or anomaly is present at the bottom-right position of the outlet, due to uneven flow distribution and inefficient flow mixing; hence, this will be further investigated in the next sections to assess the flow characteristics and turbulence buildup in DT. Lastly, Fig. 4.16d shows the temperature distribution of the MT fins. The temperature contours of MT are similar to those of CT; however, some notable differences exist. In the middle plane, the temperature regions showed distinct thermal boundary layers, more pronounced than CT; thus, showing a more even flow distribution/less turbulence compared to CT. Nevertheless, the outlet section displays a sinusoidal distribution of thermal boundary layers, similar to CT, but with a slightly lower maximum outlet temperature — 0.5K less than CT.

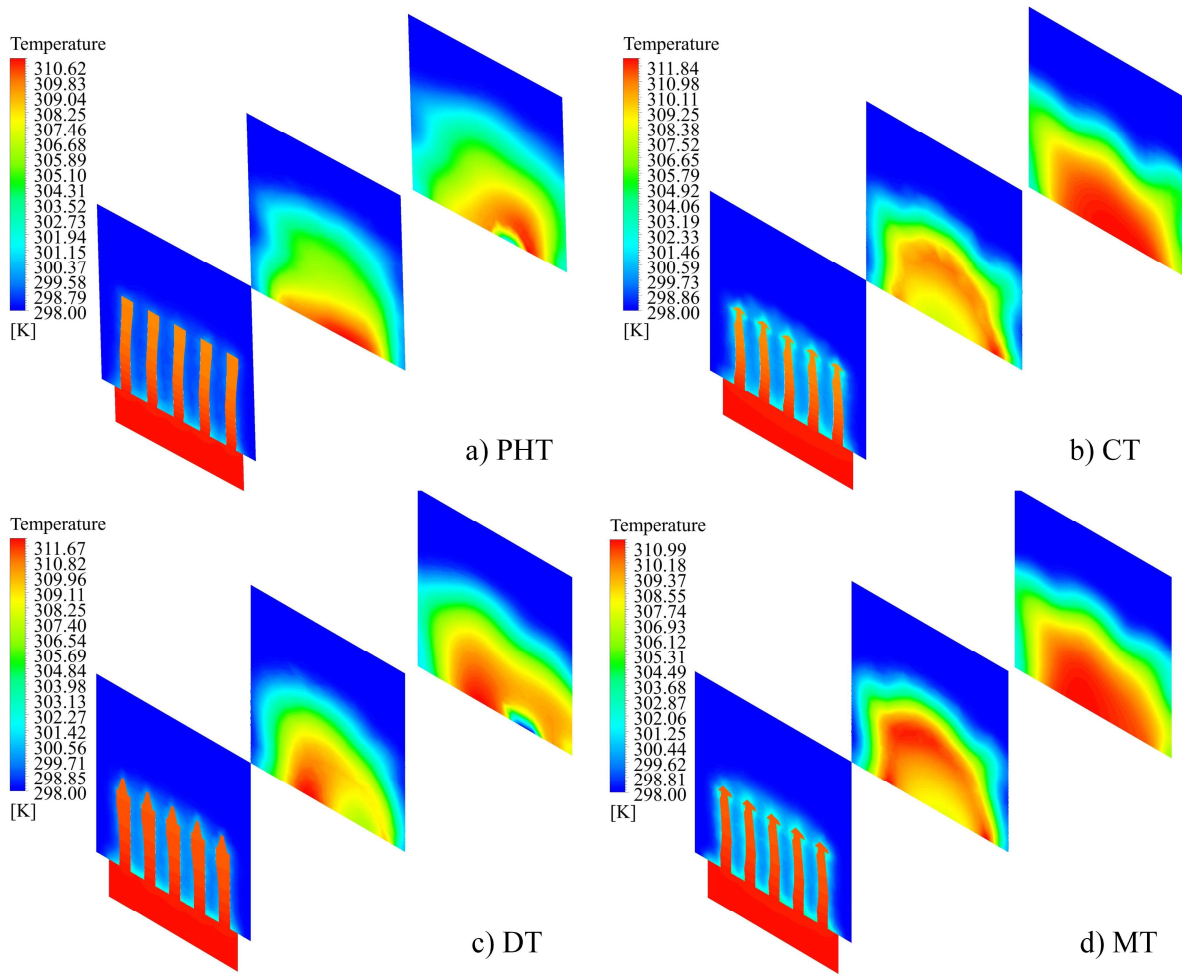


Fig. 4.16 (a)-(d). Temperature contours of all scutoid pin-fins (planar views).

Fig. 4.17 (a)-(d) depicts the velocity contours at $Re = 13500$. Velocity contours are valuable tools for understanding fluid flow patterns and dynamics. They provide visualisation of fluid velocities across specific regions or objects, such as heat sinks. In this study, for a more thorough understanding of heat transfer and fluid flow characteristics, various parameters were evaluated from distinct points of interest across multiple perspectives. Fig. 4.16 showed temperature contours, emphasising the diverse temperature distribution across three important regions. Meanwhile, the velocity contours concentrated on delineating the velocity and its boundary layers between and behind the pin fins, ultimately guiding the flow toward the outlet. This visualisation of flow features from different viewpoints, using different metrics or parameters, provided a deeper insight into the underlying flow characteristics and physics. The contours were drawn in the exact mid-plane of the heat sinks; as mentioned earlier, due to the minor differences pin-fin spacing and geometry, the pins (white cavities) are not identical.

Fig. 4.17a illustrates the velocity distribution within the PHT fins region. Notably, PHT exhibited no significant dead (blue) zones alongside the pin-fins compared to the other designs,

where such zones are apparent in distinct points, such as the bottom of the fins (DT) or the last row (CT). Concerning "top" features, designs with pointed tops like CT, DT, and MT show noticeable flow separation, forming thick boundary layers of rapidly moving air above the pin fins; the varying thick boundary layers ultimately reduce the heat transfer efficiency. The most pronounced velocity hotspot for flow separation was observed on the first row of pin-fins in the CT design (maximum velocity = 2.86 m/s), due to the pointed tops. Since all the pin-fins shared an identical base design and thickness, the base contributed minimal variation to the thermal boundary layer flow. However, the varying top designs resulted in a visual difference of 10–15% in the thermal boundary layers at the top of the pin-fins. Notably, in the PHT design, the boundary layer (red) on top of the fins appears comparatively thinner than the other designs; this was primarily due to the 5% increased height, showcasing positive implications of the height increase. PHT also recorded the second highest maximum velocity among the designs (2.84 m/s), while DT exhibited the lowest (2.74 m/s).

Observing the wake profile behind the pin fins, it becomes evident that PHT fins had a steady and widespread wake compared to other designs, hinting at a steady or slow-moving flow. Conversely, other designs displayed a relatively larger gap between fast-moving red regions and slow-moving thick dead regions (dark blue). Therefore, such a difference between fast and slow-moving fluids will lead to high-pressure and low-pressure zones. Although there is a relationship between pressure drop and wake profiles behind objects, the geometrical variations led to an acceptable level of minimal overall system pressure drop as shown in Fig. 4.14, and the differences in pressure changes within that region were not significant enough (cross-checked using a data probe point and pressure contours, yielding values less than 1 Pa). As mentioned earlier, such minor pressure differences were expected in these systems. Thus, to better comprehend the differences in flows and turbulence, the next sections focused on streamline velocity and turbulent kinetic energy.

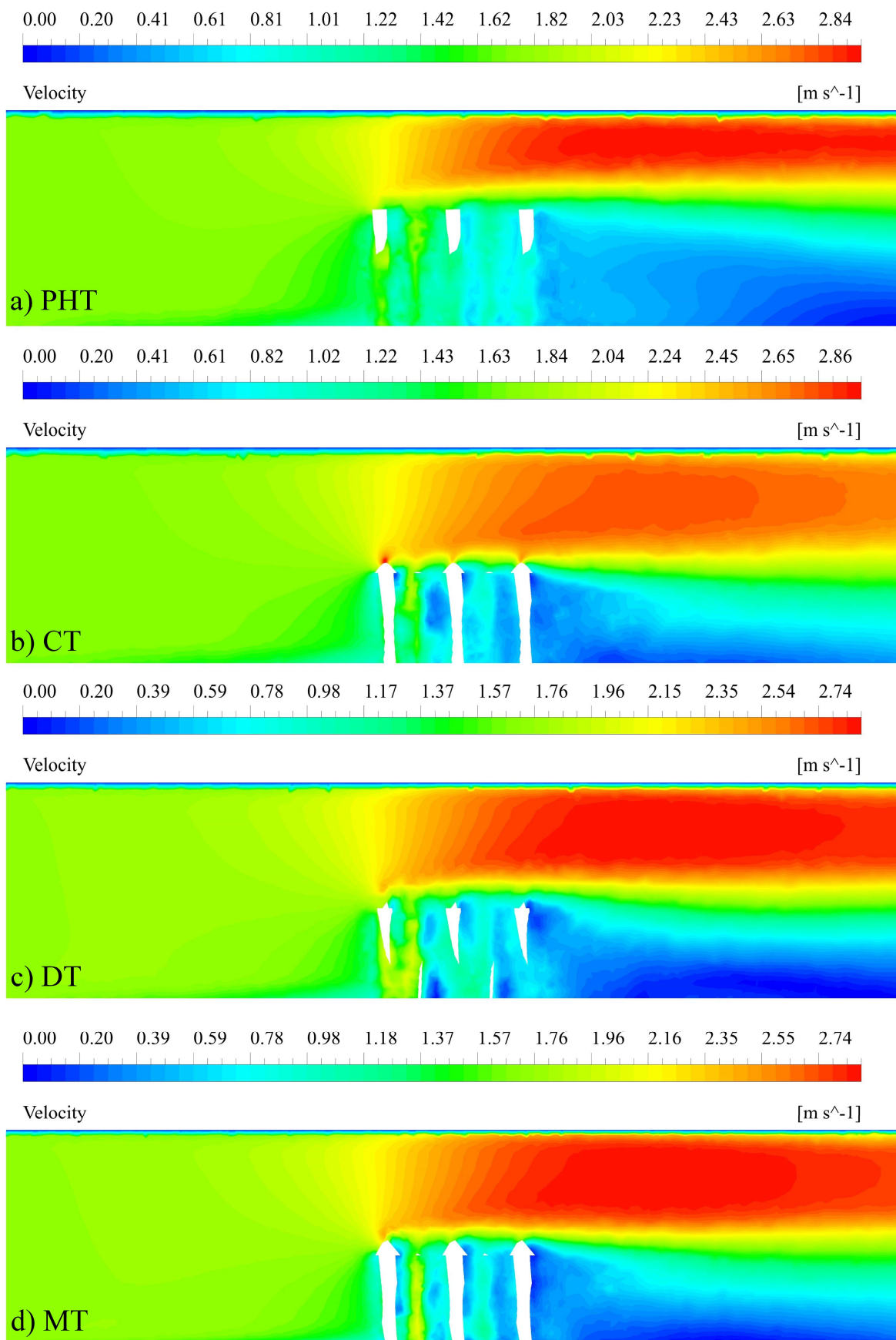


Fig. 4.17 (a)-(d). Velocity contours of all scutoid pin-fins (side view).

Fig. 4.18 (a)-(d) displays the Turbulent Kinetic Energy (TKE) contours for the pin-fins at $Re = 13500$. It can be remarked that TKE parameters are not commonly used in thermal analyses of pin-fin-based heat sinks, primarily due to the complexities associated with turbulent flows. However, TKE patterns can offer crucial insights for comparing the fluid dynamics of a system. TKE involves the conversion of kinetic energy from chaotic eddy motion into thermal energy [356]. Moreover, TKE contours provide valuable insights into the spatial distribution and intensity of turbulence within flows. In Fig. 4.18, the TKE contours visually represent dissipation patterns and aid in identifying turbulent hotspots, offering a top-down perspective of the designs.

The figures revealed that, compared to other designs, PHT fins displayed a more evenly distributed TKE within the pin-fins at the centre of the heat sinks. Furthermore, the PHT designs exhibited some turbulence throughout all the fins. In other designs, TKE intensity diminished after the initial rows of pin-fins, with a wake profile immediately behind the last row; this suggests a transition to laminar flow or turbulence not contributing to thermal energy conversion. In CT and MT, the second row of pins generated the two highest maximum turbulence values (7.13 Joules and 8.84 Joules) due to top features acting as a restrictor between the pin fins, compressing airflow into thinner lanes, promoting faster fluid movement and higher energy conversion and efficient flow mixing.

Conversely, PHT featured no such flow restrictors, resulting in less intense and spread-out turbulence wake profiles; thus, it contained reduced maximum TKE (4.89 Joules). In DT, a turbulence hotspot, notably in the lower second row of fins, created an asymmetrical wake profile that leans slightly left, potentially contributing to localised hotspots observed in Fig. 4.16c's temperature contours. Despite CT and MT having the highest turbulence values, turbulence intensity decreased after the third row of fins, evident in small localised blue regions; this indicates flow separation and recirculation. Consequently, evaluating velocity streamlines around the pin-fins and turbulence near the outlet in the following section is crucial for understanding flow development before reaching the outlet.

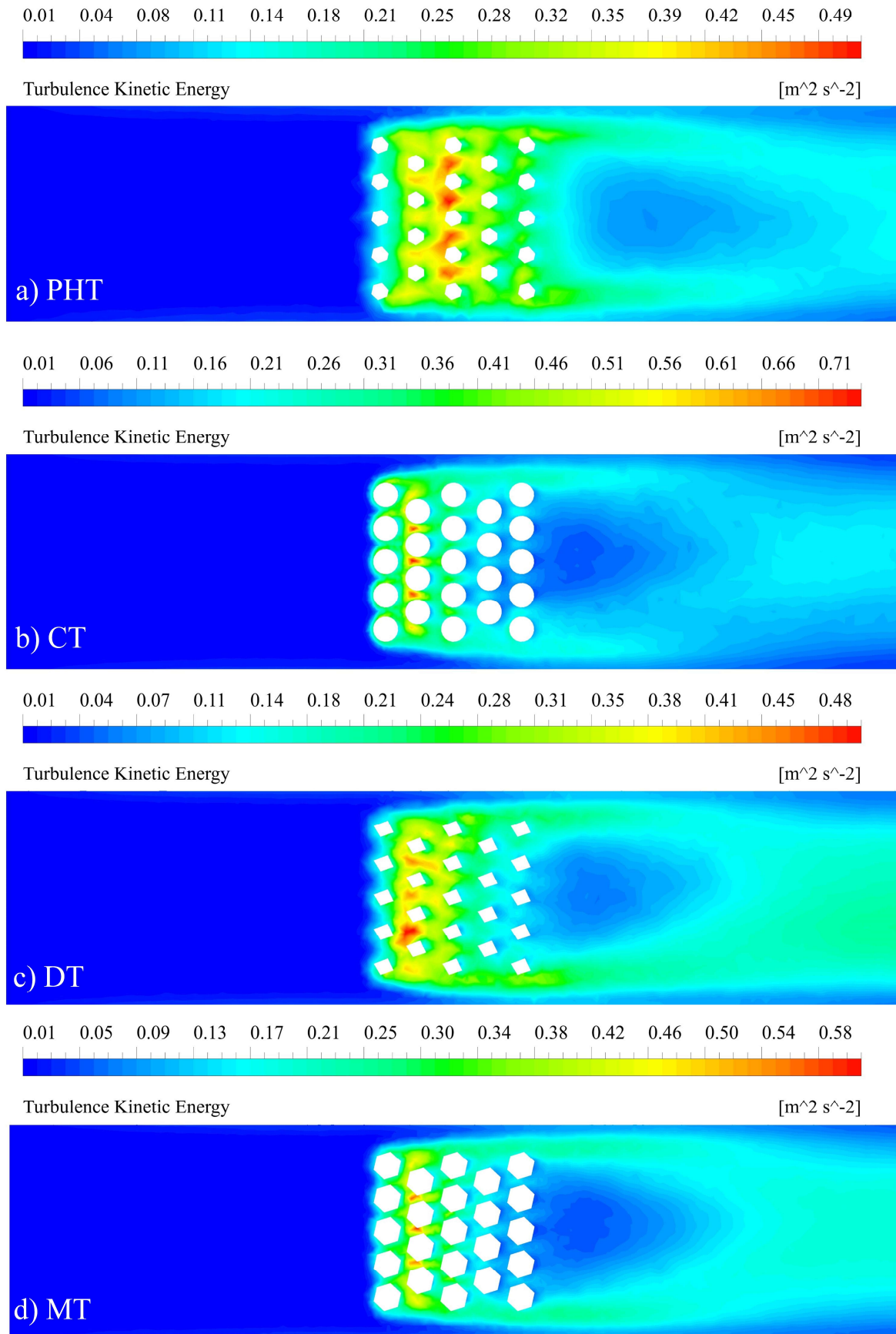


Fig. 4.18 (a)–(d). Turbulent kinetic energy contours of all pin-fins (top view)

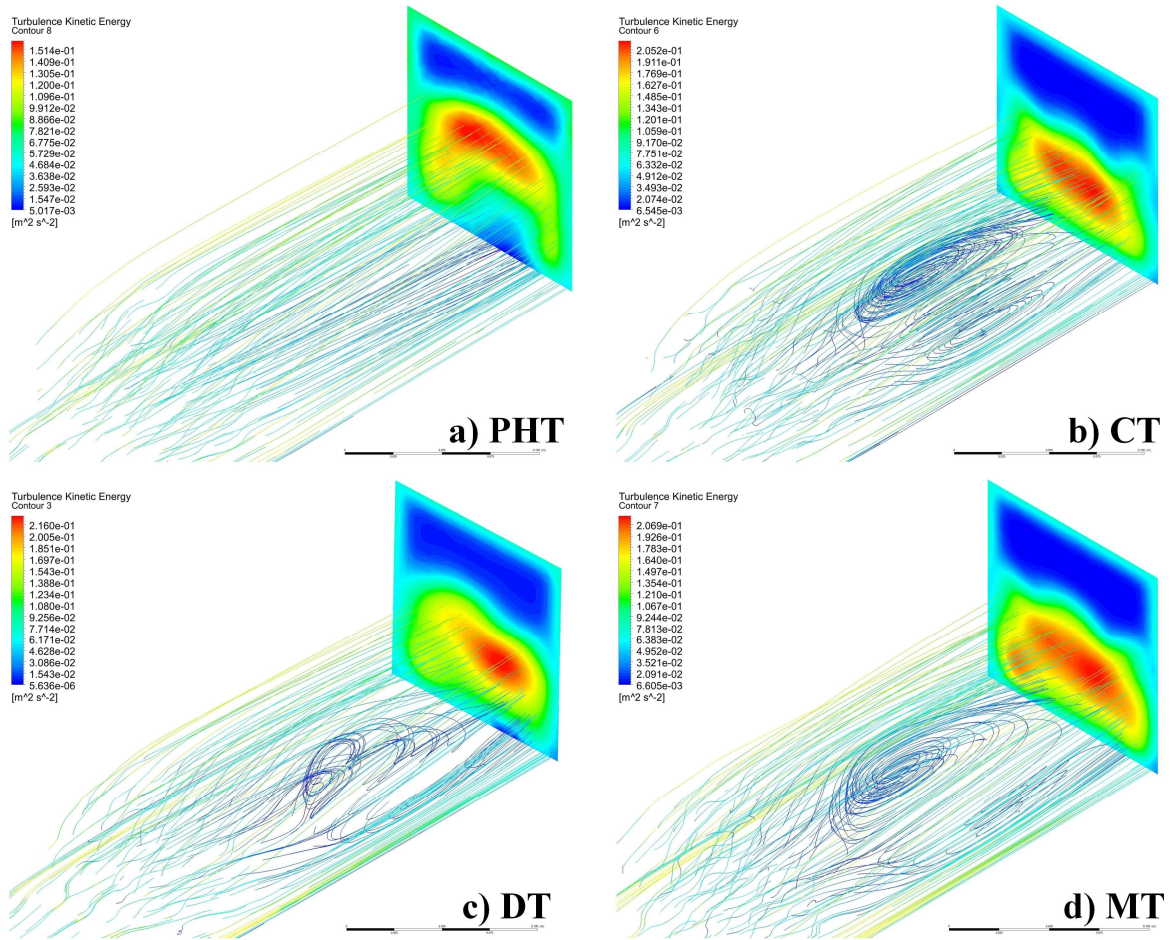


Fig. 4.19 (a)-(d) Velocity streamlines with TKE outlet contours (isometric view)

Fig. 4.19 (a)-(d) offers insights into the underlying mechanisms by combining velocity streamlines and TKE contours (outlet). Except for PHT, all other designs showed flow instability and vortex formations behind the pin-fins. The extended top features caused these flow disturbances and detachments that resulted in flow recirculation, eddy formation, and reversed flow behind the fins, contributing to the dead zones observed in the previous figures' contours. The difference between fast and slow-moving fluid layers, combined with pressure differences, played contributing roles in vortex formation. However, the geometry's shape and pin-tops appeared to have a greater influence, as shown in Figs. 5.19b and 5.19d depict CT and DT, respectively. Flow separation leading to localised cold spots in temperature contours was also influenced by vortex formation in DT — depicted in Fig. 4.19c. Additionally, CT and DT showed the most intense vortices, resulting in the highest turbulent kinetic energy at the outlet, while PHT displayed minimal or no vortex formations due to the lack of turbulent flow mixing and the geometry causing efficient flow movement. Active and passive vortex formations have

been shown to enhance heat transfer efficiency [357]. However, studying vortex-related heat transfer goes beyond the scope of this work.

4.3.4 Discussion of Findings

The findings from this study on heat transfer and fluid flow provide insights into the performance, underlying mechanisms, and limitations of various pin-fin designs. The combination of CFD, experimental data, and machine learning helps bring a fresh perspective in the development of hybrid bio-inspired pin-fin designs, along with the possible reduction in manufacturing time and costs. Evaluating performance metrics such as heat transfer coefficient (HTC), Nusselt Number (Nu), thermal resistance, fin efficiency, velocity, temperature, and turbulent kinetic energy (TKE) allows for a critical assessment of the heat transfer characteristics and thermal performance of the novel scutoid-based pin-fins having non-conventional geometry.

The results presented in Figs. 5.10 and 5.11 highlight the dominant performance of the plain hexagon top (PHT) design in terms of HTC and Nu. Surprisingly, despite having the lowest volume and surface area, the PHT design consistently demonstrates the highest heat transfer efficiency. For reference, the base geometry (SPF) had a volume of $V = 275000 \text{ mm}^3$, $\text{mass} = 275 \text{ g}$. Thus, this raises questions about the prevailing understanding of the correlation between enlarging geometry and heat transfer performance. On the other hand, the Mushroom Top (MT) design, with its larger volume and surface area, exhibits slightly lower HTC values, indicating a potential trade-off between geometric complexity and heat dissipation capability. Fig. 4.20 presents a comparison of the designs at $\text{Re} = 13500$. By comparing the best-performing PHT design (in terms of HTC) against the worst and second best-performing alternatives, it was observed that PHT had approximately 8.6% and 7.2% less mass/volume than MT and CT. Despite its lower mass/volume, PHT demonstrates around 5.2% and 14% higher HTC than MT and CT, respectively. Furthermore, with 1.6% more mass/volume than CT, MT exhibits approximately 8.3% higher HTC than CT; however, this is to be expected due to the larger surface area.

Based on the graphical values and simulation results, the variation in heat transfer coefficients (HTC) and Nu among the different pin-fin designs can be attributed to different factors. Despite having the lowest volume and surface area, the PHT design exhibits the highest HTC, due to its geometry promoting better fluid flow and heat transfer. Conversely, the hexaprism or mushroom-inspired top (MT) design, with higher material usage and surface area,

shows slightly lower HTC values because of flow reattachment and separation around its protruding elements. The least-performing designs, diamond/tetrahedral top (DT) and conical top (CT), suffer from boundary layer separation and inadequate mixing, especially the CT design, which demonstrates the worst performance due to its geometry inducing strong boundary layer separation and intense vortex formations.

All these factors interacted to influence heat transfer performance, with turbulence enhancement, flow reversal, and thermal boundary layer thickness also playing roles in determining the HTC of each pin-fin design. The underperformance of the conical top (CT) and diamond/tetrahedral Top (DT) designs in HTC and Nu further emphasises the need for critical evaluation of the assumptions and design principles underlying conventional and non-conventional pin-fin configurations. This is because a shape which had positive impacts previously may negatively affect heat transfer based on modifications, as shown in this study.

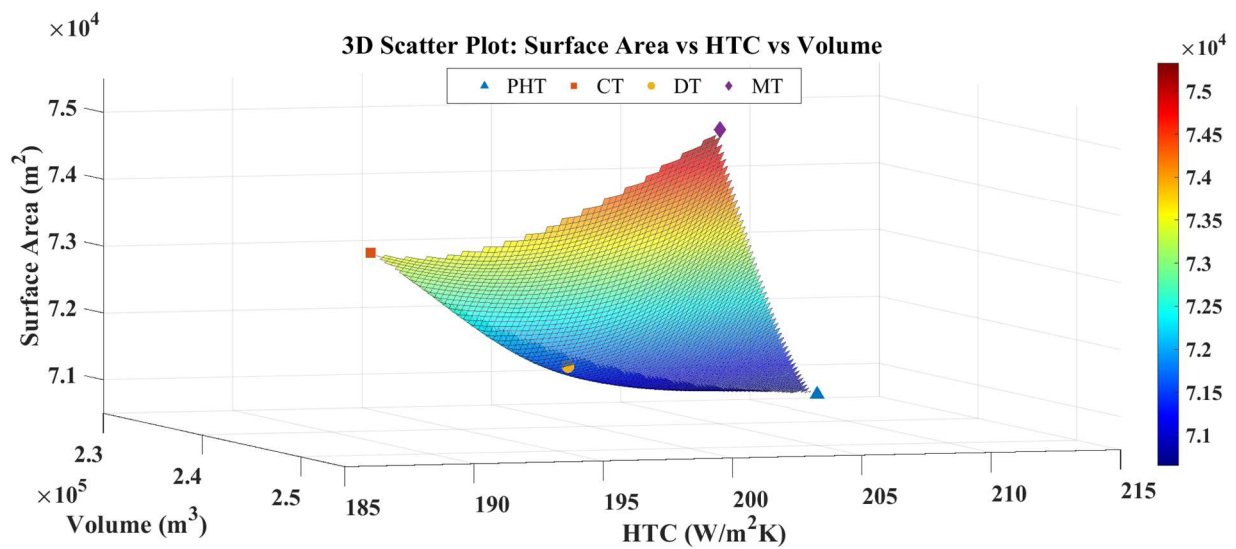


Fig. 4.20 Mass, volume, and heat transfer performance comparison at $Re = 13500$

With increasing Re , the thermal resistance (R_{th}) decreases due to the increased velocity. Examining the thermal resistance results presented in Fig. 4.12, it is evident that the PHT and MT designs, featuring hexagonal bases for their top features, outperform other designs relating to thermal resistance. Comparing the range of R_{th} , PHT had 7.2% and 7.4% lower range than CT and DT; similarly, MT had 2.9% and 3.1% lower range of R_{th} than CT and DT. This potentially suggests that the pin-fin tops' base shape and the resulting flow characteristics play a crucial role in determining the overall thermal performance of the heat sinks. The variation in thermal resistance among the different pin-fin designs can be attributed to several physical factors related to heat transfer and fluid dynamics. Notably, the PHT and MT designs, both

featuring hexagonal top features, promote better heat transfer, minimised boundary layer thickness, efficient heat conduction paths, and adequate flow mixing. Conversely, the diamond/tetrahedral top (DT) and conical top (CT) designs suffer from boundary layer separation and lower heat transfer rates due to their geometrical features. These findings underscore the importance of optimising pin-fin designs to minimise thermal resistance for improved thermal management efficiency. Therefore, the higher thermal resistance observed in the CT and DT designs, particularly in the CT design, raises concerns about their suitability for high-performance heat dissipation applications.

The assessment of fin efficiency in Fig. 4.13 reveals slightly different trends among the pin-fin designs. While the CT design demonstrates the highest fin efficiency, the differences among the designs are minimal; thus, a potential trade-off can be considered if other heat transfer parameters give superior results. The surface shape/roughness, from edges or sharp features, of the fin structures can influence turbulence levels in the fluid flow, affecting heat transfer efficiency. The specific configurations of the CT and DT designs promote turbulence enhancement, contributing to their higher fin efficiency values; nevertheless, the sharp hexagonal tops promote better overall heat transfer. Therefore, adding chamfers or smooth edges can strike a balance within these designs. The marginal differences in fin efficiency underscore the need to explore alternative design approaches that prioritise overall thermal performance and heat dissipation capability over specific geometric characteristics. The minimal pressure drops and pumping power is another metric where the trade-off can be arguably deemed acceptable for this case due to the superior heat transfer performance of the hexagon-top-based designs.

To further understand the heat performance enhancements of the new pin-fins alongside their trade-offs, the Performance Improvement Factor (PIF) was compared between the new design and the base design. The PIF calculations revealed that, compared to the base design, the heat transfer performance was improved by 1.70, 1.50, 1.56, and 1.60 times using the designs PHT, CT, DT, and MT, respectively. Moreover, this investigation presented a variety of parameters for comparison. Therefore, Fig. 4.21 consolidates and synthesises the findings of this research to highlight which designs exhibit the best performance. However, due to the significant differences in parameter ranges and their units (e.g., R_{th} values are 200 times smaller than HTC values), the heatmap/colourmap was generated using normalised and scaled data, often used in machine learning-related data analysis, to make it dimensionless [358]. Linear scaling of the original data was employed to convert it into values ranging between 0

and 100, where dark green indicates minimum values and yellow indicates maximum values (as shown by the colourmap legend). The heatmap visualisation offers a mixed-method (qualitative and quantitative) approach to gain a condensed understanding of heat transfer performance improvements and comparisons between the base and new designs within this study. The best-performing designs can be inferred using either colour alone or both colour and data. The heatmap, illustrating six parameters [Heat Transfer Coefficient (HTC), Pressure Drop (PD), Thermal Resistance (RTH), Performance Improvement Factor (PIF), Fin Efficiency (FE), and Mass], consistently demonstrates that PHT and MT designs are the overall optimal designs and outperform the conventional designs and geometries.

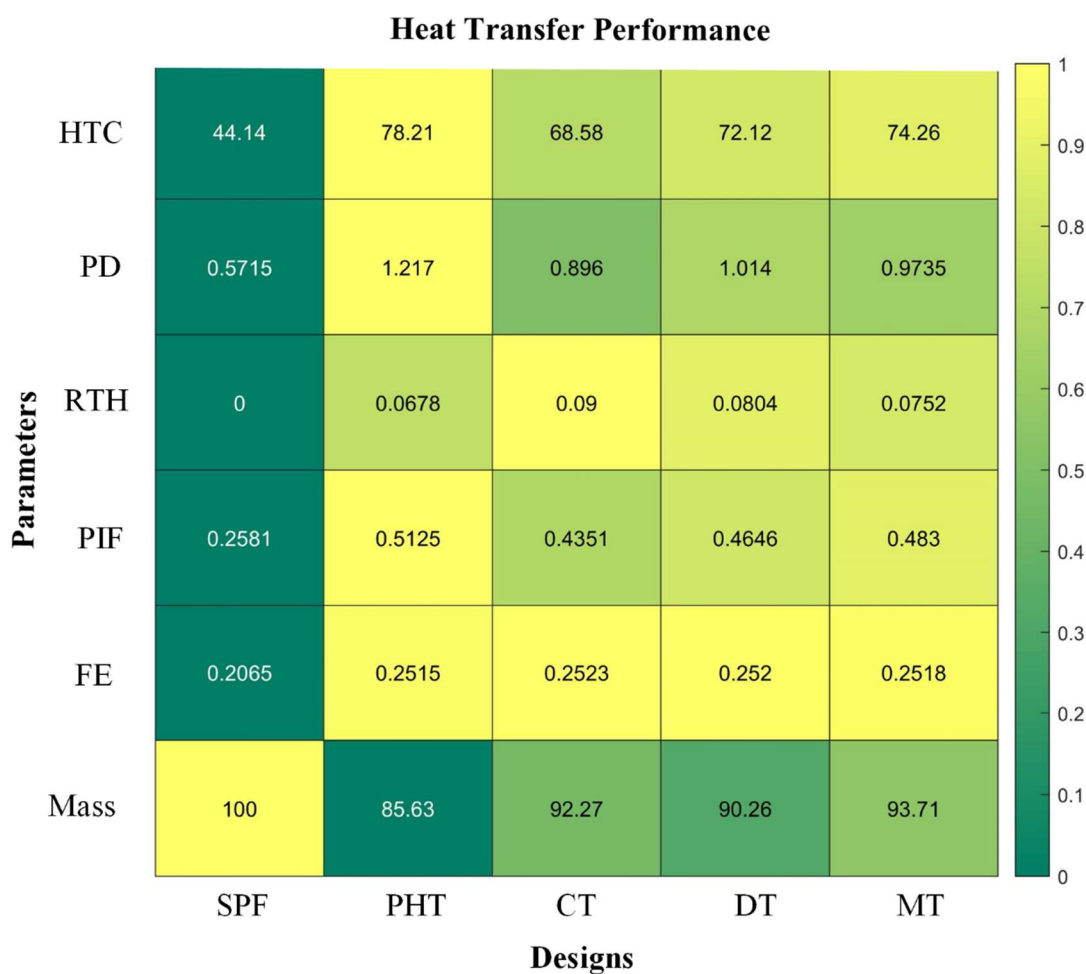


Fig. 4.21 Colourmap and summary of heat transfer performance of all design

The assessment of velocity and temperature contours, along with TKE and velocity streamlines, offered insights into fluid flow behaviour, temperature distributions, and energy dissipation within pin-fin structures. The PHT design exhibited relatively even velocity distribution and efficient heat dissipation, while the CT design shows concerns regarding flow separation and turbulence hotspots. In contrast, the DT design presented challenges in

achieving efficient heat transfer due to the asymmetrical wakes and the presence of cold spots. The presence of hotspots and variations in TKE across designs underscore the complexity of turbulent flows and highlight the need for comprehensive analysis for heat transfer effectiveness throughout the fin structure. As one of the primary objectives of this study was to investigate the underlying physical mechanisms in air-cooled heat transfer strategies, several key insights were observed:

1) Utilising complex fin geometries manufactured through additive manufacturing can enhance heat performance while reducing weight. The data and numerical simulations verified the initial assumptions that these intricate geometries can effectively disrupt airflow without inducing significant flow instability and offer improved heat dissipation, demonstrating the potential for improved heat transfer beyond the traditional surface area relationship;

2) The incorporation of twisted scutoid geometry and various hybrid pin-fin topologies can augment heat transfer by manipulating boundary formation above the pin-fins and controlling wake region formation between and behind the fins. However, careful monitoring of pin-fin spacing, and height is crucial for optimal heat transfer performance within acceptable trade-off limits. Greater pin-fin height can promote thinner boundary layers and uniform flow distribution;

3) Sharp-edged top designs tend to outperform pointed or curved surfaces. While pointed or conical surfaces may induce flow separations, they result in the formation of intense passive vortices and increased wake or dead zones. Further investigation into passive vortex manipulation is warranted in air-cooled heat sinks to refine heat transfer strategies;

4) Pin-fin geometry not only influences heat transfer but also impacts thermal resistance and pressure drop within the system, particularly under varying operating conditions. Previous studies showed that conical and tetrahedral geometries have promising results, yet their effects on temperature distribution along the fins and behind the pins can be significant, influenced by factors such as velocity boundary layers and turbulent kinetic energy, leading to non-uniform and unstable flow patterns. All these factors combined ultimately reduced their heat transfer.

Moreover, moving on to the machine learning model predictions, determining whether volume and surface area could predict the HTC while employing underutilised algorithms such as Gradient Boosting Regressor and ensemble methods in heat transfer analysis, holds several key motivations and advantages. The HTC is a critical factor in determining the efficiency of

heat transfer processes. Thus, through understanding the relationship between volume, surface area, and HTC, heat sink designs and other thermal management systems can be optimised.

Also, current prediction models can be further utilised via transfer learning methods to help researchers, engineers, and designers develop more efficient and effective cooling solutions, leading to improved performance and energy savings. The current dataset can also be augmented with more experimental and numerical simulations in the future via an open-source database. Additionally, by predicting the HTC based on volume and surface area, the need for extensive and costly experimental testing can be avoided in the design development stage. Instead, these easily measurable geometric parameters can estimate the HTC, significantly reducing both time and resource requirements during the design and evaluation phases. In this era of Industry 4.0, with a continuous reduction in product development times [67], finding innovative solutions via technology is warranted to trigger continuous improvement.

Furthermore, if design properties such as volume and readily available heat transfer parameters prove to be effective predictors of the HTC, as highlighted by the findings of this investigation, it simplifies the modelling process. Instead of relying on complex and computationally expensive simulations, a simpler model could make dependable predictions using available geometric parameters or operating conditions. Following this approach can lead to a 60-70% reduction in development times by using key parameters like Reynolds number, volume, and surface area for rapid pre-screening. For example, while a single high-fidelity simulation or a physics-informed neural network can take up to 5 to 6 hours per configuration, the proposed method reduces this to just 1-2 hours by narrowing down the design options early on, significantly cutting the total optimisation time when testing multiple designs.

This simplicity can streamline the design process and facilitate agile analysis of different heat sink configurations. Additionally, this allows flexibility and scalability as the knowledge and predictions can be applied to various applications, providing valuable insights for different engineering scenarios. Moreover, the relationship between volume, surface area, and the HTC contributes to a deeper understanding of the underlying physics and mechanisms involved in heat transfer processes. It enables the study of complex shapes, and new configurations of pin-fin heat sink via additive manufacturing methods, and it allows researchers and engineers to gain insights into how these geometric parameters impact the convective heat transfer characteristics, enhancing their comprehensive knowledge base.

Comparing new designs and setups with multiple existing literature findings can often pose challenges due to differences in operating conditions, characteristic dimensions, and design applications. Furthermore, in some instances, authors may withhold critical data from simulations or experiments due to confidentiality concerns. This research reveals that the hybrid pin-fins with top geometries can outperform traditional shapes and conventional designs in terms of HTC performance, as reported in prior related studies [240,350]. However, it's crucial to recognise that, depending on the acceptable trade-offs in the application and HTC, our design may or may not also excel or underperform at extremely high Reynolds numbers employed in other investigations. Hence, the availability of future rapid performance indicators, facilitated by machine learning and based on readily available parameters such as volume or surface area, will aid both the design and optimisation stages of heat transfer research and beyond.

Moving forward, the critical findings from this study call for a paradigm shift in pin-fin heat sink design. The traditional reliance on simplistic geometric configurations may limit the potential for optimal heat dissipation. Instead, a holistic approach that considers the intricate balance between flow dynamics, heat transfer efficiency, and energy dissipation patterns should be pursued, especially given the availability of advanced manufacturing techniques. Similarly, advanced techniques and combined approaches involving machine learning, multi-objective optimisation algorithms [359], CFD simulations and experimental investigations can drive the next generation of heat sinks and enable a broader design choice to identify novel configurations that offer enhanced thermal performance. Furthermore, future research should focus on integrating advanced materials and surface enhancements into complex pin-fin designs to amplify cooling and heat transfer, but with reduced cost [360]. Integrating combined innovative approaches, such as surface coatings, micro/nanostructured surfaces, and additive manufacturing techniques, have the potential to significantly alter flow characteristics and enhance convective heat transfer, thereby overcoming the limitations of conventional designs.

The discussion of the findings emphasises the need for a comprehensive re-evaluation of pin-fin heat sink designs. The dominant performance of the biomorphic PHT and MT design in most metrics, coupled with the limitations observed in other designs, highlights the potential for significant improvements. By embracing a multidisciplinary approach that combines insights from fluid dynamics, heat transfer, machine learning, and design for manufacturing considerations, researchers can unlock the full potential of pin-fins and develop next-generation heat sink solutions with superior thermal performance, reduced size and cost, and

improved energy efficiency. Nonetheless, despite ensuring different measures and robust methods to ensure the reliability of this study, it is also important to acknowledge the limitations of this study. The findings rely on a specific set of experimental and simulation conditions and limited data points, and therefore, generalisability to other scenarios needs further assessment. Additionally, while advanced materials and additive manufacturing were discussed as potential avenues for improvement, their practical implementation and scalability need to be explored [241,361]. Future research should address these limitations to ensure the practicality and real-world applicability of the proposed design strategies. Therefore, although the study produces valuable findings, the author accepts the limitations for this analysis.

4.3.5 Summary of Chapter

In conclusion, this chapter provides valuable insights into the performance and limitations of various novel pin-fin designs for heat transfer and fluid flow. The combination of computational fluid dynamics (CFD), experiments, and machine learning techniques offers a fresh perspective in the development of hybrid biomorphic pin-fins, with potential reductions in manufacturing time and costs. The key findings include:

- Dominant performance of the plain hexagon top (PHT) design in heat transfer coefficient (HTC) and Nusselt Number (Nu), challenging the conventional understanding of the correlation between surface area and heat transfer. The novel scutoid-based designs produce 1.5 to 1.7 times better heat transfer performance with a 6% to 14% weight reduction compared to the base rectangular/square fin design;
- Numerical thermal analysis demonstrates the superiority of hexagon-based designs (PHT and MT) and raises concerns about the suitability of conical (CT) and tetrahedral (DT) designs for high-performance heat dissipation. Fin efficiency shows minimal differences among designs, with the CT design having the highest efficiency.
- Temperature, velocity, and turbulent kinetic energy contours highlight the importance of geometry and even velocity distribution within the pin-fin region for efficient convective heat transfer, with the PHT design excelling in this aspect. The CT and DT designs exhibit flow separation regions, compromising heat dissipation uniformity due to intense vortex formation, leading to uneven heat distribution. Turbulent energy dissipation patterns further emphasise the complexity of heat transfer but gives insights into the underlying mechanism;

- Machine learning predictions demonstrate the potential of using volume and surface area as predictors of the HTC, simplifying design optimisation and exploration, and providing quick performance indicators. Ensemble methods and multiple linear regression perform the best among the compared models (mean absolute percentage error <5%).

In summary, this study contributes to the knowledge of pin-fin heat sink designs, highlighting the dominance of non-conventional designs and the importance of combining multiple strategies. Integrating advanced design and manufacturing techniques and utilising machine learning can unlock the full potential of pin-fins, leading to next-generation heat sink solutions with superior performance, reduced size, cost, product development times, and improved energy efficiency.

Chapter 5: Thermohydraulic Assessment of Bio-inspired Hybrid Micro Pin-Fins

5.1 Background to the Chapter

In this chapter, water was employed as the working fluid to investigate the hydrodynamic behaviour of bio-inspired micro pin-fins. The research initially focused on numerical simulations to evaluate the pressure distribution and thermal performance under wall heating conditions. The analysis revealed the impact of bio-inspired geometries on the pressure distribution, heat, and fluid flow characteristics of micro heat sinks.

Afterwards, this study then evolved to include four newly developed hybrid micro pin-fin designs, combining various pin-fin optimisation strategies, and incorporating agile manufacturing and cost-feasibility assessments. These designs aimed to balance hydraulic performance (such as pressure drops) and heat transfer improvements (Nu number). Existing correlations were found inadequate for these complex geometries, and new machine-learning-driven correlation models were developed to fill this gap. These models enhanced prediction accuracy, enabling more efficient design optimisations.

5.2 Initial Design Investigation

Initially, for this study, two designs were compared. The first base design featured traditional inline rectangular pin fins (RF) and was used for numerical validation from the works of [362]; The second design, containing pentagonal-hexa-prism fins (SF), drew inspiration from a skin cell shape called scutoid, similar to the previous case. The SF combined the effects of two different shapes and offered new insights. Then, a CFD study analysed heat transfer and flow characteristics to understand the underlying physics. The micro pin-fin geometries, heat sink design, along with the different wall heating setup, are depicted in Fig. 5.1; the heat sinks had identical dimensions and number of pin fins (17×34).

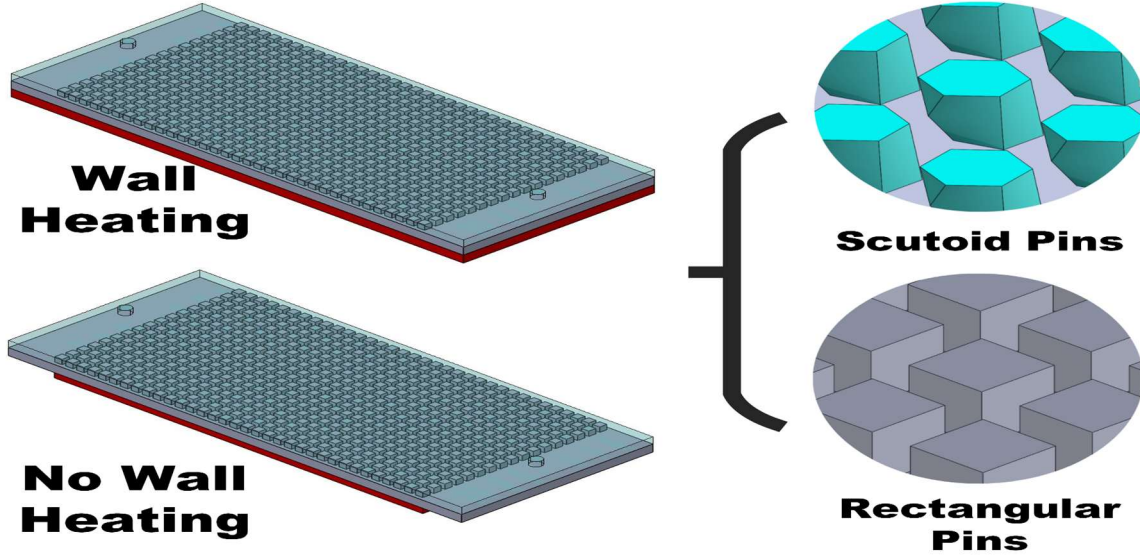


Fig. 5.1 Initial micro pin-fin heat sink designs

Governing Equations: There are some disagreements between authors regarding the flow characteristics and Reynolds Number (Re) at which turbulent flow occurs at the microscale. However, $550 \geq Re \geq 400$ generally fall in the laminar region. The governing equations and assumptions used for modelling were adapted/modified from previous works [281,338]:

$$\text{Continuity equation: } \frac{\partial u}{\partial x} + \frac{\partial v}{\partial y} + \frac{\partial w}{\partial z} = 0 \quad (27)$$

$$\text{Energy equation: } \left(u \frac{\partial T}{\partial x} + v \frac{\partial T}{\partial y} + w \frac{\partial T}{\partial z} \right) = \frac{1}{Re \cdot Pr} \left(\frac{\partial^2 T}{\partial x^2} + \frac{\partial^2 T}{\partial y^2} + \frac{\partial^2 T}{\partial z^2} \right) \quad (28)$$

$$\text{Heat transfer coefficient (HTC): } h = \frac{\dot{m}_a c_p (T_o - T_i)}{A_s [T_b - \left(\frac{T_i + T_o}{2} \right)]} \quad (29)$$

Where, u, v, w - velocity components; x, y, z - directions; ρ_f - fluid density; μ - dynamic viscosity; Pr - Prandtl number; S_t - energy equation source term; T, T_b, T_i, T_o are fluid, base, inlet, and outlet temperatures, respectively; \dot{m} - mass flow rate; A_s - base area where heat is applied; C_p - specific heat.

Model pre-processing and numerical validation: ANSYS Fluent Mesh software helped to create three mesh sizes for fluid (water) and solid (aluminium) domains. One of the goals whilst using CFD is to improve mesh/accuracy and reduce the time and cost of simulation. Therefore, the mesh grid independence test was done using a velocity metric (V_{max}) at the

outlet; the numerical validation was done using the base temperature (T_b) from [362]. Table 8 provides the mesh statistics and related data for the pre-processing.

Table 8: Numerical validation and grid independence test results

Mesh (No. of Nodes)	V_{max} (Re = 550)	T_b (CFD)	%Error, T_b [362]	V_{max} (Re = 400)	T_b (CFD)	%Error, T_b [362]
Mesh I (58443)	0.246 m/s	329.3 K	2%	0.179 m/s	337.6 K	18%
Mesh II (76000)	0.240 m/s	325.6 K	13%	0.178 m/s	337.5 K	18%
Mesh III (143695)	0.245 m/s	328.5 K	4%	0.174 m/s	334.0 K	7%

The minimal difference between the V_{max} values and acceptable %error for T_b highlights the success in numerical validation. Mesh (III) was preferred for simulations, with orthogonal quality above 0.70 (considered good). The refinement ratio of Mesh (II)/(I) and (III)/(II) were both above 1.3, further supporting the grid independence and CFD simulation results [337].

5.3 Discussion of Results

Fig. 5.2 presents CFD simulation results for temperature variations and velocity streamlines. Boundary conditions included an initial inlet temperature of 298 K, zero outlet pressure, and $Re = 550$, with a system heat flux of 37.2 kW/m^2 . NWH designs (RF, SF) lacked extended heat flux, while SFX and RFX designs had heated inlet and outlet regions. WH designs exhibited higher temperature saturation near the outlet, contrasting with NWH designs, showing cold spots near the inlet. Due to the geometric influences and potential laminar boundary layers, the RF design displayed thick boundary layers, but generally, there were no significant difference between NWH and WH. Overall, WH designs had more evenly distributed distinct temperature regions and higher base temperatures than NWH designs. Also, SF and SFX designs showed potential flow recirculation and turbulence near the right side of the inlet, influencing boundary layer formations.

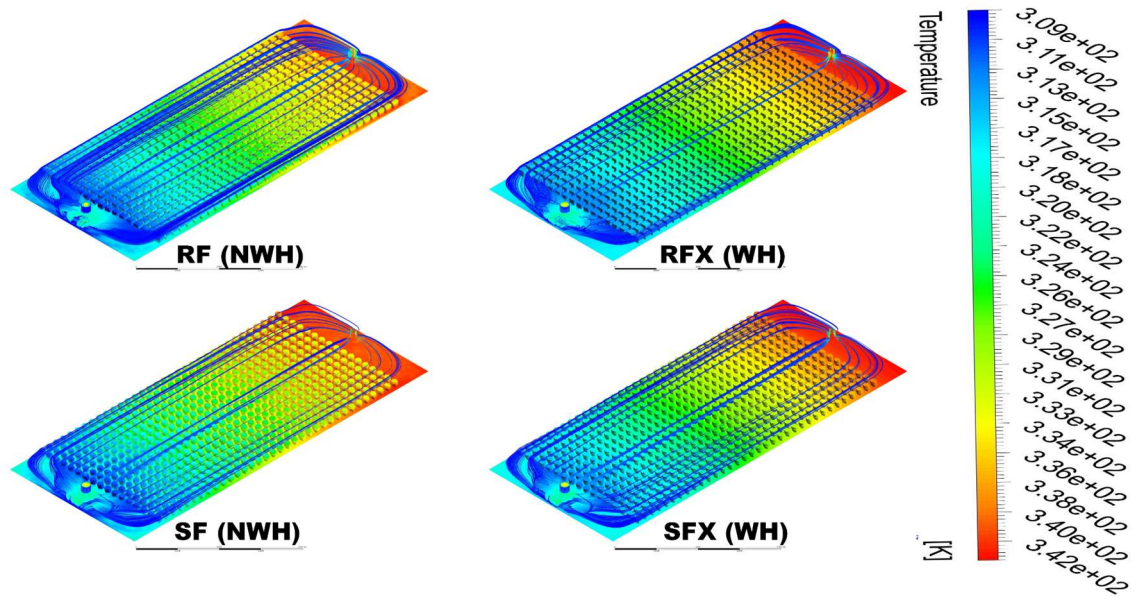


Fig. 5.2 Temperature distribution from the top view

It can be said that the three of the most important considerations for heat sink designs include pressure drop, HTC, and the base operating temperature. Fig. 5.3 shows the 3D surface plot used for visualising the data and comparing the designs.

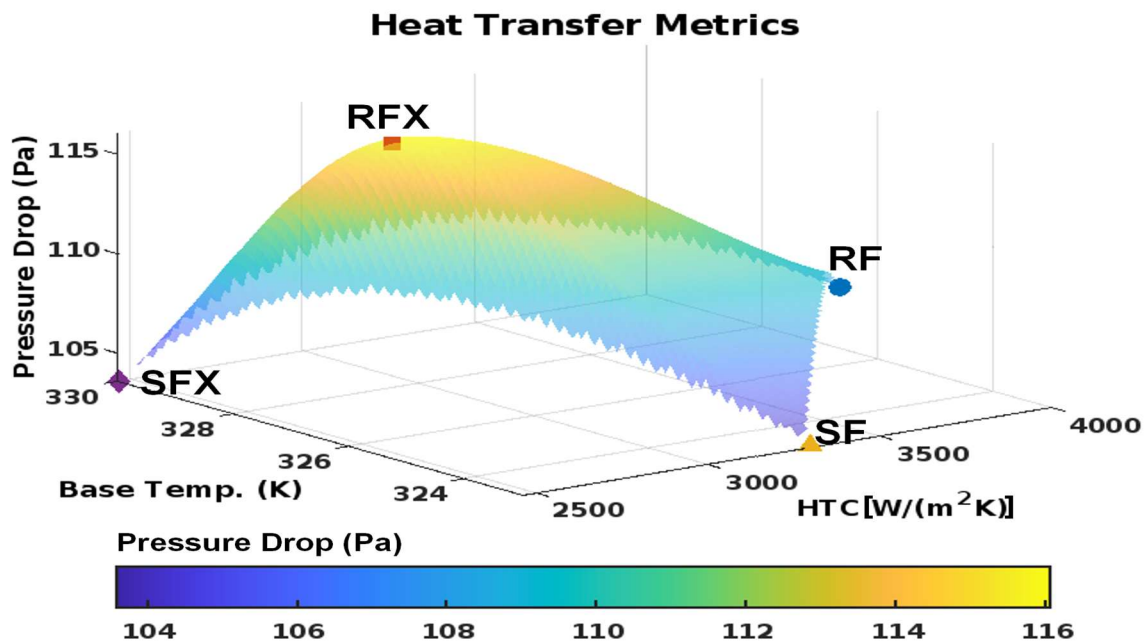


Fig. 5.3 Pressure distribution in the heat sinks

In analysing the performance metrics of the four designs—RF, RFX, SF, and SFX—several observations are made. While RF boasts the highest Heat Transfer Coefficient (HTC) at $3892 \text{ W/m}^2\text{K}$, the slightly elevated operated Base Temperature (BT) of 326 K and pressure

drop values may impact its overall performance. SF demonstrated a commendable HTC of $3298 \text{ W/m}^2\text{K}$ and, notably, the lowest operating base temperature at 323 K, suggesting superior continuous heat dissipation. Additionally, when considering the Pressure Drop (PD), SFX emerges with the lowest value at 103.6 Pa, closely followed by SF at 103.65 Pa. Despite RF's impressive HTC, the combination of SF's substantial HTC, lowest base temperature, and lowest pressure drop makes SF as the overall best option, striking a balance between efficient heat transfer and fluid dynamics. Also, it should be noted that the WH designs showed lower HTC values and higher BT for both types of pins.

The study explored the influence of wall heating conditions, particularly the impact of extended heat flux and new micro pin-fin geometries on heat distribution and fluid dynamics. The extended heat flux resulted in distinct and uniformly distributed heat regions. However, in wall-heated (WH) designs, the absence of pin-fins in the heated inlet and outlet areas affected heat dissipation, leading to a higher overall operating base temperature than non-wall-heated (NWH) designs. Notably, the data indicated that pressure drop values were predominantly influenced by pin-fin geometry rather than wall heating conditions, as evidenced by the lower pressure drop values in designs like SF and SFX. Despite SF operating at a lower base temperature with approximately 4% less pressure drop than RF, its HTC was roughly 15% less than RF. Therefore, this discrepancy was due to the reduced surface area/volume of SF pins.

Additionally, the complex geometry may have induced turbulence, potentially disrupting the flow and thermal resistance, which could have been better computed using different turbulence models; some research has indicated turbulent transition regions in microscale flows for $\text{Re} > 400$ under various operating conditions [346]. Nonetheless, the study's significance lies in giving insights into design optimisations, understanding trade-offs between operating parameters, and researching future assessments of complex pin-fins under different operating conditions to advance sustainable cooling technology.

5.4 Finalised Prototype Micro Pin-Fin Heat Sink

The scutoid-based pin-fin simulations showed promising results due to their unique incorporation of a mixture of shapes. However, manufacturing constraints required modifications to the original design, leading to adopting a mixed geometry and strategy approach that still retained the bio-inspired philosophy derived from the numerical simulations. The literature further revealed additional advantages linked to the inclusion of secondary lanes or splitters within microchannels, which were subsequently factored into the design process.

As a result, four innovative hybrid heat sinks were developed for manufacturing, evolving from the initial scutoid-based concept to a more versatile approach, driven by the dual goals of overcoming manufacturing challenges and maximising thermal performance and efficiency.

Consequently, this case aimed to advance the understanding and optimisation of micro pin-fin (MPF) heat sink technologies by designing and experimentally analysing four distinct biomorphic hybrid MPF geometries. The research uses an agile manufacturing approach, including a detachable and quickly reconfigurable heat sink setup with a 3D-printed case to explore various designs efficiently. By integrating experimental data with machine learning models, this research also endeavours to develop predictive tools and design strategies that enhance thermohydraulic performance across various high-demand applications, thereby contributing to academic knowledge and practical solutions. To achieve our research aim, we established a series of objectives. First, we designed and experimentally evaluated four innovative micro pin-fin (MPF) geometries to appraise their performance across important thermal metrics. Second, we investigated the impact of design shape and geometry on MPF performance to assess how the design variations influence overall heat transfer. Third, we created new empirical correlations for the best-performing hybrid biomorphic MPF heat sink (MPFHHS) to predict the Nusselt number and pressure drops. Fourth, we analysed machine learning regression models using experimental data to evaluate the viability of predicting thermohydraulic performance in future heat sinks. Finally, we critically analysed insights from both experimental and machine learning models to propose optimised MPF-based thermal management solutions, all while incorporating an agile manufacturing philosophy.

5.4.1 New Heat Sink Designs, Rationale, and Manufacturing

In this study, four distinct biomorphic micro pin-fin heat sink designs were developed and manufactured. Each design was inspired by biological forms and tailored to optimise thermal performance by enhancing flow dynamics and mixing. By manipulating thermohydrodynamic properties such as turbulence, thermal resistance, and heat transfer efficiency, these designs aim to improve the overall thermohydraulic performance of the heat sinks. The key features and underlying thermohydrodynamic rationale for each design are detailed below.

5.4.1.1 Cruciform Flower-inspired Designs

Cruciform Flower with Astroid Splitters (CFAS): The first design features a cruciform flower pattern, characterised by a cross-shape at the centre of the heat sink. To enhance flow mixing and redistribution, petal-shaped and astroid-shaped splitters are integrated between the

cruciform sections. These splitters are strategically placed to redirect the coolant flow into the surrounding pin-fin sections. From a thermohydrodynamic perspective, the design intends to:

- **Increase Turbulence:** By introducing obstructions in the flow path, the splitters induce turbulence, disrupting the laminar boundary layer and enhancing heat transfer;
- **Enhance Mixing:** The splitters promote coolant mixing, leading to a more uniform temperature distribution and reducing thermal resistance;
- **Optimise Flow Distribution:** Redirecting the flow ensures that all pin-fin surfaces are effectively utilised, preventing hotspots and improving overall heat transfer efficiency.

This design aims to balance flow distribution and mixing efficiency, potentially improving the interaction between flow redirection and pin-fin cooling surfaces to improve performance.

Cruciform Flower with Secondary Microchannels (CFSM): Building upon the cruciform shape, this design omits the astroid splitters. The absence of splitters allows the gaps between the sections to act as secondary microchannels, providing additional and unrestricted pathways for coolant flow. Thermohydraulic considerations for this design include:

- **Reduced Pressure Drop:** The open microchannels decrease flow resistance, lowering the overall system pressure drop compared to designs with flow obstructions;
- **Laminar Flow Maintenance:** The additional channels may promote laminar flow conditions, which can be beneficial for certain operating regimes;
- **Optimised Flow Distribution:** The secondary lanes facilitate more uniform coolant distribution, potentially enhancing thermal performance by ensuring consistent cooling.

This configuration evaluates the effect of secondary flow lanes on overall system pressure drop and heat transfer, aiming to find an optimal balance between enhanced mixing and effective flow distribution, as previous literature has reported potential benefits of having secondary lanes.

5.4.1.2 Exocoetidae-inspired Designs

Exocoetidae-Inspired Shape with Sharp Edges (ESE): The third design draws inspiration from the morphology of Exocoetidae (flying fish), with pins shaped to emulate this natural form. Key features include: 1) **Hexagonal Base:** each pin fin has a hexagon base, a shape that offers favourable thermal performance due to increased surface area and ability to induce turbulence; 2) **Kite or Diamond-Shaped Fins:** extending from the base are fins reminiscent of wings, to compress and expand the coolant flow, enhancing mixing and promoting turbulence; 3) **Trapezoidal Tail:** designed to expand the flow further, ensuring effective utilisation of all pin fins and minimising areas of stagnant flow; 4) **Interspersed**

Circular Pins: placed between the kite-shaped fins, these contribute to additional flow mixing by continuous expansion and convergence zones. Thermohydrodynamic rationale includes:

- **Controlled Flow Expansion and Compression:** By manipulating the flow pathways, the design increases turbulence intensity, disrupting thermal boundary layers and enhancing convective heat transfer coefficients;
- **Maximised Surface Area:** The complex geometry increases the contact area between the coolant and the heat sink, reducing thermal resistance;
- **Enhanced Turbulence:** Sharp edges and abrupt changes in flow direction induce turbulence, potentially improving heat transfer; albeit, pressure may also increase.

This design focuses on leveraging complex geometry to optimise thermal management by controlling flow expansion, convergence, and mixing.

Exocoetidae-Inspired Shape with Filleted Edges (EFE): Retaining the overall geometry of the third design, the fourth design introduces filleted edges to the pin fins instead of sharp edges. From a thermohydraulic and thermohydrodynamic performance consideration, the filleted-edged designs are intended to:

- **Reduce Flow Resistance:** Streamlining the geometry decreases pressure drop across the heat sink by minimising frictional losses;
- **Alter Turbulence Levels:** Smoother edges may reduce turbulence intensity, potentially lower levels of turbulence;
- **Improve Thermal Efficiency:** By decreasing flow resistance, the coolant can flow more freely, which may enhance heat transfer efficiency under certain conditions;
- **Balance Between Turbulence and Pressure Drop:** The design seeks to maintain sufficient turbulence for effective heat transfer while reducing the pressure losses associated with high turbulence levels;
- **Thermal Resistance Reduction:** Smoother flow paths may lower thermal resistance by facilitating more efficient heat exchange between the coolant and heat sink surfaces.

By comparing the ESE and EFE designs, the study assesses the impact of edge geometry on flow dynamics and thermal performance, aiming to find an optimal balance between enhanced mixing and reduced flow resistance.

Fig. 5.4 shows the drawing and dimensions of the pin-fins. Note that all the heat sinks have the same base dimensions and cover the same effective heating area (80 mm × 60 mm); therefore, for brevity, the ESE design is shown as the base design.

CFSM	72 (12×6)	792	Curved Arcs;(90° angled segments); petaloid rectangle	lanes (2mm) Total = (5×1)	3122
CFAS	72 (12×6)	852	Curved Arcs (90° angled segments); petaloid rectangle	Astroids Total = (12×5)	3410

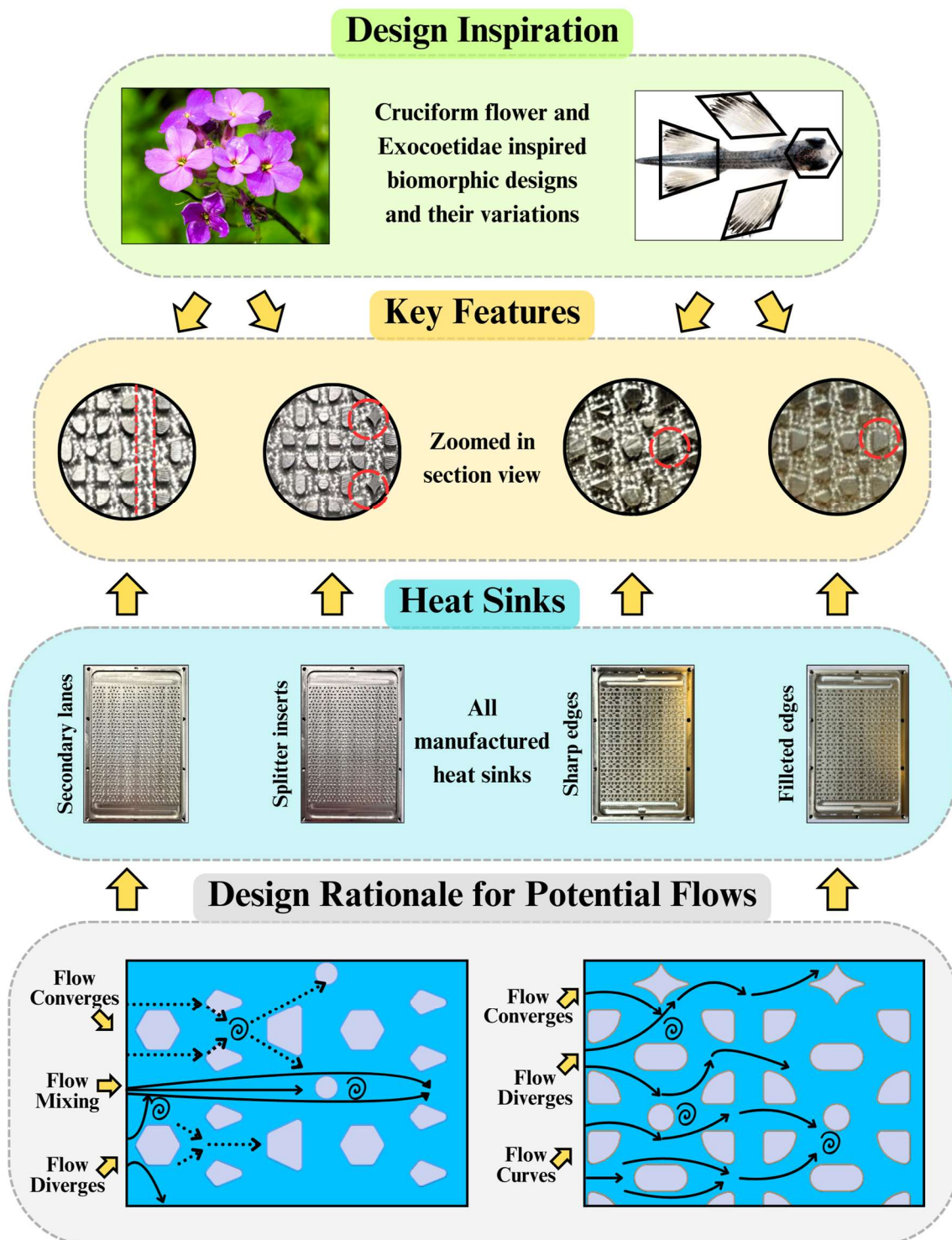


Fig. 5.5 New heat sink designs and inspirations

5.4.2 Data Reduction

During the experimental run, data was recorded at timed intervals to examine the thermal performance of single-phase heat transfer. The recorded data included the inlet and outlet temperatures of the deionised water as a working fluid, along with temperatures at five equally spaced points within the heat sink. Parameters such as flow rate, pressure drop, and heat dissipation were also monitored. Additionally, various equations were employed to study the experimental results, enabling the calculation of crucial performance parameters related to heat transfer and thermal characteristics, including thermal resistance, Reynolds number, Nusselt number, and pressure drops. As mentioned in the earlier section, the test section was well insulated to minimise heat loss, therefore adapting previous works [8,44,362,363], the baseline governing equations for data reduction were as follows:

Convective heat transfer rate (Q):

$$Q = \dot{m}c_p(T_{out} - T_{in}) \quad (30)$$

where T_{in} and T_{out} , \dot{m} , and c_p refers to the inlet and outlet temperature, mass flow rate, and coolant's specific heat capacity respectively

To calculate density, specific heat, and the mean fluid temperature (T_m) is given by:

$$T_m = \left(\frac{T_{in} + T_{out}}{2} \right) \quad (31)$$

Although the current designs have some degree of developing flow due to the inlet entrance, Eq. (2) provides reliable calculations with minimal errors, as highlighted in past research [229,362,364].

Characteristics Length (L) or Hydraulic diameter (D_h):

$$L = D_h = \frac{4A}{P} \quad (32)$$

where A is the cross-section area and P is the perimeter of the inlet

Reynolds Number (Re):

$$Re = \frac{\rho v L}{\mu} \quad (33)$$

where ρ , v , μ are fluid density, velocity, and viscosity, respectively

Wall Temperature (T_w):

$$T_w = T_b - \left(\frac{QL_x}{k_s A_w} \right) \quad (34)$$

$$A_w = L_{ts} \times W_{ts} \quad (35)$$

where T_b temperature below the channel wall (cw); L_x is the distance from the base to cw; k_s is the thermal conductivity of the heat sink; A_w is the surface area of the cw given as a product of the length (L_{ts}) and width (W_{ts}) of the test section covered by the pin fins.

The logarithmic mean temperature difference (LMTD):

$$LMTD = \frac{(T_w - T_{in}) - (T_w - T_{out})}{\ln \left[\frac{(T_w - T_{in})}{(T_w - T_{out})} \right]} \quad (36)$$

The LMTD approach provides a representative average driving force for heat transfer across the length of the heat sink, capturing the effects of this temperature variation more accurately than a constant wall-to-fluid temperature difference.

Effective fin area (A_{eff}):

$$A_{eff} = NA_f H_f + A_w \quad (37)$$

where N is the number of fins or fin sections

Convective heat transfer coefficient (h)

$$h = \frac{Q}{A_{eff} \times LMTD} \quad (38)$$

Nusselt Number (Nu)

$$Nu = \frac{h \times D_h}{k_f} \quad (39)$$

where k_f is the thermal conductivity of the fluid

Thermal Resistance (R_{th}):

$$R_{th} = \frac{LMTD}{Q} \quad (40)$$

Pressure drops (ΔP):

$$\Delta P = (P_{inlet} - P_{outlet}) \quad (41)$$

Pumping Power Usage (P_u):

$$P_u = \frac{\Delta P \times \dot{m}}{\rho} \quad (42)$$

5.4.3 Results

5.4.3.1 Nusselt Number

The Nusselt number (Nu) is an important dimensionless parameter that helps to quantify convective heat transfer between fluid and solid surfaces. Nu varies with fluid flow conditions, providing insights into fluid behaviour. When Nu equals 1, heat transfer by conduction equals that by convection. Nu values of >1 imply more efficient heat transfer by convection, highlighting effective cooling mechanisms. The study evaluated the heat transfer efficiency of four micro pin-fin heat sink designs — EFE, ESE, CFSM, CFAS — by calculating their Nusselt numbers (Nu) across Reynolds numbers (Re) ranging from 101 to 507, with a power output of 150W and 250W. Fig. 5.6 (a)-(d) shows the Nu performance of the designs.

Looking at Fig. 5.6(a) and (b), the results show that the filleted design (EFE) steadily increased in Nusselt number from 8.4-8.9 at Re 101 to a maximum of 12.4-12.9 at Re 507, indicating improved heat transfer efficiency with higher flow velocities. However, the overall Nu values at 250W are around 4-5% lower than at 150W. In comparison, the edged design (ESE) shows a more moderate increase in Nusselt number, from 7.6-7.9 at Re 101 to 9.6-10.2 at Re 507, suggesting that the sharp edges provide less significant improvement in heat transfer compared to the filleted design. For ESE, the overall Nu is also lower at 250W than 150W. The CFSM design demonstrated the lowest Nusselt numbers, increasing from 5.2-5.3 at Re 101 to 8.0-9.1 at Re 507, indicating lower effectiveness in enhancing heat transfer. For CFSM, the heat transfer efficiency shows a different trend than other designs, with the overall Nu being more effective at 250W than 150W. The CFAS design, featuring astroid splitters, achieves the second-highest Nu overall and the highest Nu at lower Re values, ranging from 8.8 to 9.8 at Re 101. At max Re value, the Nu ranges from 12.1-12.5 at Re 507, indicating superior heat transfer performance relative to the two other designs. As observed with the other two designs, the heat transfer efficiency is slightly better at 150W than at 250W.

Overall, across both power outputs, the EFE and CFAS designs consistently demonstrated the highest Nusselt numbers, confirming them as the most efficient designs for heat transfer. The CFAS design performs well initially but shows signs of a gradual decrease in heat transfer

efficiency at higher Reynolds numbers and power outputs. The ESE design provides moderate performance with steady but limited improvements, while the CFASM is the least effective.

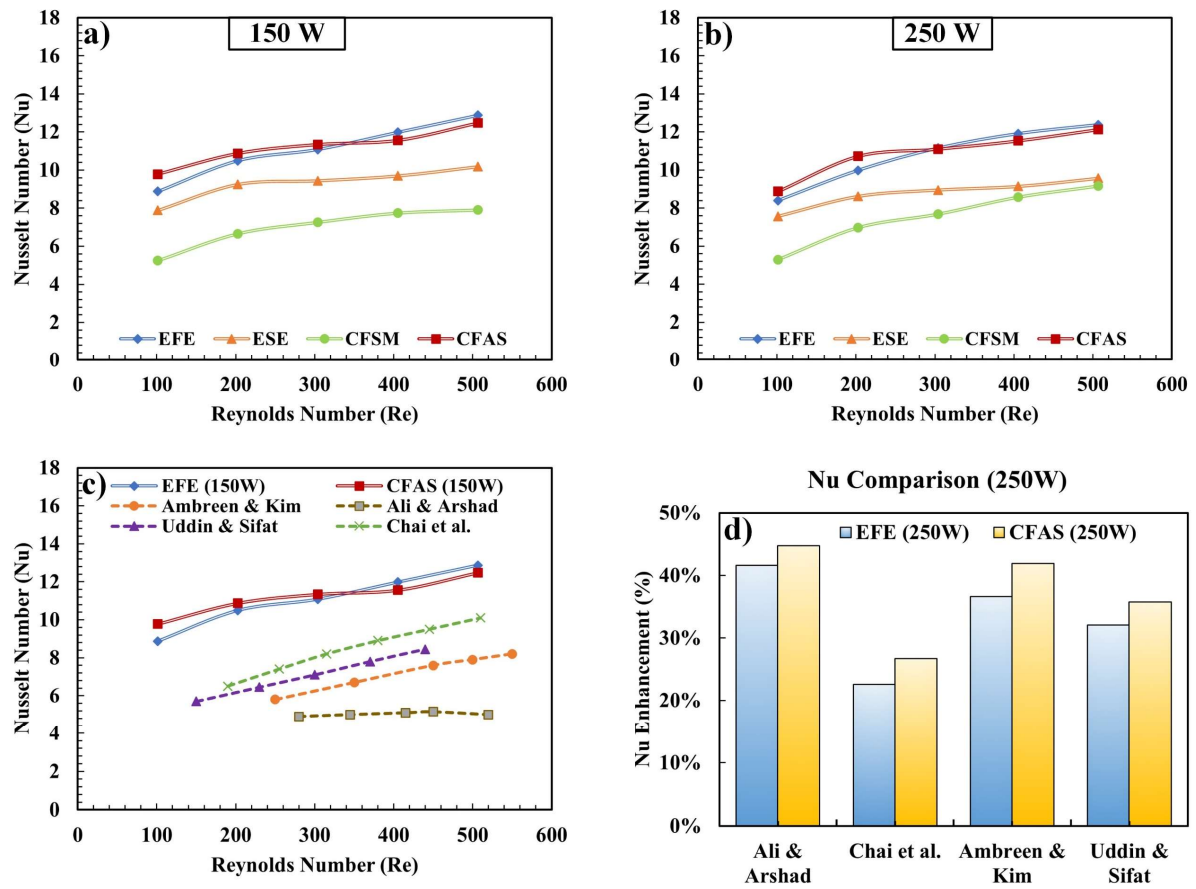


Fig. 5.6 (a)-(d) Nusselt Number comparison

To further evaluate the performance of the new designs, the Nusselt number (Nu) results of the two best-performing designs at 150W were compared with those reported in the existing literature, as shown in Fig. 5.6(c). Also, to gain a more comprehensive understanding, different setup strategies were considered. For instance, Ali and Arshad examined conventional square pin fins arranged in inline and staggered configurations using both water and nanofluids. Their experiments were conducted at a power output of 192 W within a Reynolds number (Re) range similar to this study. However, since this current research focused on an inline configuration and did not involve nanofluids, the first comparison was limited to their inline square fin setup with water as the working fluid. The second study considered micro pin fins from the research of Ambreen and Kim, who experimented with hexagonal pin fins—a key feature of ESE and EFE designs—and conducted within a Re range of 250 to 550. However, because they did not provide Nu performance values using water, their use of nanofluids for performance enhancement was taken as an additional basis for comparison.

Moreover, Chai et al. [365] investigated a three-dimensional numerical model of a non-conventional interrupted microchannel heat sink with mixed geometries. They explored the effects of pressure drop and heat transfer characteristics resulting from various dimensions and positions of rectangular ribs within transverse microchambers. Although their research focused on microchannels, the presence of interrupted and varied geometries makes it a valuable basis for comparison with this study. Additionally, the mixed geometry with interruptions in Chai et al.'s [365] design can be appraised against the new designs, which also feature mixed geometry with asteroid splitters/cylindrical interrupters. Lastly, Uddin and Sifat [366] analysed the thermo-hydraulic characteristics of Mini-Channel Heat Sinks (MnCHS) featuring different secondary channel shapes—rectangular, oblique, and curvy—across a Re range of 150 to 1050; however, for a more like-for-like comparison, their Re values will be limited to 550 as the current research investigates Re values between 100 to 500. In summary, the four studies with comparable strategies implemented in various types of heat sink setups provided a solid foundation for performance evaluation.

Additionally, to focus on both the maximum and minimum performances, Fig. 5.6(d) shows the performance comparison of the EFE and CFAS designs with those from extant literature at the lowest Reynolds number (requiring the least pumping power) at 250W. The findings were:

- **EFE Design:** The EFE design shows a significant enhancement in performance, with improvements ranging from 23% to 42% over the designs presented in the literature. The highest enhancement (42%) is observed when compared with the design by Ali and Arshad, suggesting that the design offers substantially better heat transfer efficiency. Additionally, when comparing at the highest Re Number and pumping power, the EFE and CFAS designs show over 140% Nu enhancement compared to the inline rectangular pin-fins of Ali & Arshad. Even the lowest enhancement of 23% against Chai et al. [365] still represents a meaningful improvement, highlighting the efficacy of the EFE design.
- **CFAS Design:** At lower Re, the CFAS design performs slightly better than the EFE design, with enhancements ranging from 27% to 45% compared to the literature. The maximum improvement of 45% over Ali and Arshad demonstrates that the CFAS design is particularly effective, likely due to its ability to manage fluid flow and surface interaction more efficiently. The lowest improvement of 27% against Chai et al. [365] still exceeds the performance, reaffirming the superior performance of the CFAS.

The performance comparison with existing literature indicates that the EFE and CFAS designs developed in this study offer substantial enhancements in Nusselt number at 250 W compared to previously reported designs. The CFAS design, in particular, outperforms the EFE design at lower Re , but the EFE design outperforms CFAS overall, making it the most effective in enhancing heat transfer efficiency. This comparative analysis further validates the effectiveness of these innovative heat sink designs and suggests that they could offer significant advantages in practical applications where efficient thermal management is critical.

5.4.3.2 Thermal resistance

Thermal resistance, a key factor in heat transfer analysis, defines the resistance a system presents to heat flow. Reducing thermal resistance is crucial for improving heat transfer efficiency and ensuring electronic devices and other heat-generating systems operate safely. This study measured thermal resistance across different heat sink designs—EFE, ESE, CFSM, and CFAS—under various flow rates (Reynolds numbers) and heating powers (150 W and 250 W). Fig. 5.7 (a)-(b) shows the thermal resistance trend for 150W and 250W.

As anticipated, thermal resistance generally decreased with increasing Reynolds numbers, signifying enhanced heat dissipation at higher flow rates. At 150 W, the CFAS design consistently exhibited the lowest thermal resistance, recording a minimum value of 0.0333 K/W at $Re = 507$. This superior performance can be attributed to the CFAS design's optimised surface area and fluid flow channels, which likely promote more effective heat transfer. In contrast, the CFSM design showed the highest thermal resistance, reaching 0.0821 K/W at $Re = 101$. The higher resistance in CFSM could be due to less efficient fluid flow patterns, leading to reduced surface heat removal.

The EFE and ESE designs displayed thermal resistance values between CFAS and CFSM data, with EFE generally outperforming ESE. This suggests that the EFE design may have better thermal contact or more favourable flow characteristics than ESE but is not optimised as CFAS.

At 250 W, a similar pattern was observed: CFAS continued to outperform the other designs, achieving a thermal resistance of 0.0343 K/W at $Re = 507$, while CFSM again showed the highest resistance, especially at lower flow rates, with 0.0815 K/W at $Re = 101$. The slightly higher thermal resistance across all designs at 250 W compared to 150 W could be due to the increased heat load, which might exacerbate the inefficiencies in heat transfer, particularly in designs like CFSM.

The results highlight that among the tested configurations, CFAS is the most effective in minimising thermal resistance, particularly at higher flow rates. This efficiency likely stems from its design, which facilitates better fluid distribution and heat removal. Conversely, the CFSM design's higher thermal resistance suggests potential areas for improvement in its thermal management strategy, such as enhancing flow uniformity or increasing surface contact.

The apparent dependence of thermal resistance on heat input (Q) in the pin-fin heat sinks likely results from slight temperature-induced variations in fluid properties, which can affect convective heat transfer. Additionally, some effect arises from the thermal properties of the thermal grease layer used, as its conductivity and thickness can influence overall thermal resistance, particularly at higher heat fluxes. Regarding the potential for mixed convection, we calculated the Grashof and Rayleigh numbers. We found them to be relatively low, indicating that natural convection effects were negligible in our single-phase flow setup. Consequently, mixed convection was not a contributing factor, and the system remains governed by forced convection.

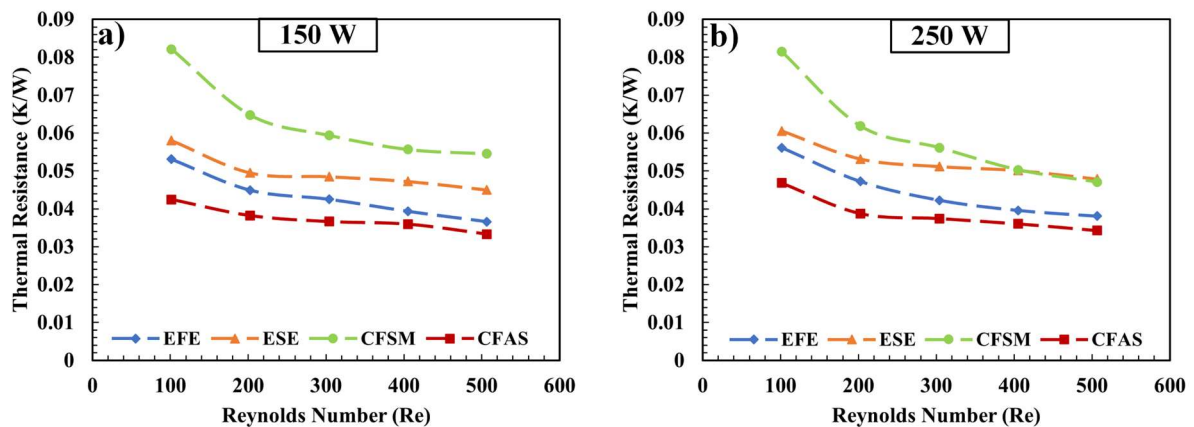


Fig. 5.7 Thermal resistance performance

5.4.3.3 Pressure drop and energy consumption

In the design and evaluation of heat sinks, understanding pressure drop values, pumping power requirements, and energy consumption is essential for optimising performance and operational costs. Pressure drop measures the resistance to fluid flow through the heat sink, which affects the amount of pumping power needed to maintain adequate coolant circulation. Higher pressure drops usually result in greater energy consumption, influencing the overall efficiency and cost-effectiveness of the cooling system. Thus, balancing these trade-off factors is important for selecting the most appropriate heat sink design for a given application.

The analysis of heat sink designs—EFE, ESE, CFSM, and CFAS—was conducted at both 150 W and 250 W heating powers. Fig. 5.8 (a)-(d) presents the data related to pressure drops and associated parameters. Although the values were assessed for both power outputs, the differences between them were minimal, as seen from Fig. 5.8(a) and (b), so the results primarily focus on the higher heat flux/power output of 250 W data for brevity purposes.

The ESE design, with sharp-edged micro pin-fins, demonstrates the second highest pressure drop among the designs, measuring 350.6 Pa at $Re = 101$ and reaching 4001 Pa at $Re = 507$. This significant resistance to fluid flow translates into a high pumping power requirement of 60.1 mW. Consequently, the ESE design has one of the lowest energy efficiencies, consuming 1 kWh of energy in 692.8 days. The sharp edges create substantial turbulence and flow disruption, potentially leading to increased pressure drop and operational costs.

Conversely, the CFSM design features a secondary flow lane between the pin fins, which helps to alleviate some of the flow resistance. This results in a moderate pressure drop of 220 Pa at $Re = 101$ and 3340 Pa at $Re = 507$. Despite this moderate pressure drop, the CFSM design requires a lower pumping power of 50.2 mW. It demonstrates the longest energy consumption time of 830.3 days for 1 kWh, indicating better overall energy efficiency.

The EFE and CFAS designs excel in heat transfer performance, as indicated by their high Nusselt numbers (Nu). The EFE design, with its curved filleted edges, achieves a pressure drop of 160 Pa at $Re = 101$ and 3463 Pa at $Re = 507$. This design strikes a balance by minimising flow separation and turbulence, requiring 52 mW of pumping power and consuming 1 kWh of energy in 800.6 days. The energy consumption is relatively low, considering its effective thermal performance. Similarly, the CFAS design incorporates splitter inserts between the flow lanes to enhance heat transfer efficiency. However, this design leads to the highest pressure drop of 216 Pa at $Re = 101$ and 4224 Pa at $Re = 507$. It requires 63.5 W of pumping power and consumes 1 kWh of energy in 656.3 days. Although CFAS has a higher resistance than EFE, its energy consumption remains manageable and justifiable due to its thermal performance.

While designs like EFE and CFAS exhibit higher pressure drops, their overall performance justifies these trade-offs. The EFE design offers an effective balance between heat transfer efficiency and energy consumption, making it a cost-effective choice despite its moderate pressure drop. The CFAS design, although it incurs a higher pressure drop and pumping power, provides good thermal performance, and its overall energy consumption remains relatively low as shown in Figs. 6.7(c) and 6.7(d). Thus, despite the higher pressure drops, the energy

consumption metrics of both EFE and CFAS align well with their heat transfer benefits, making them acceptable choices depending on the specific needs of the application.

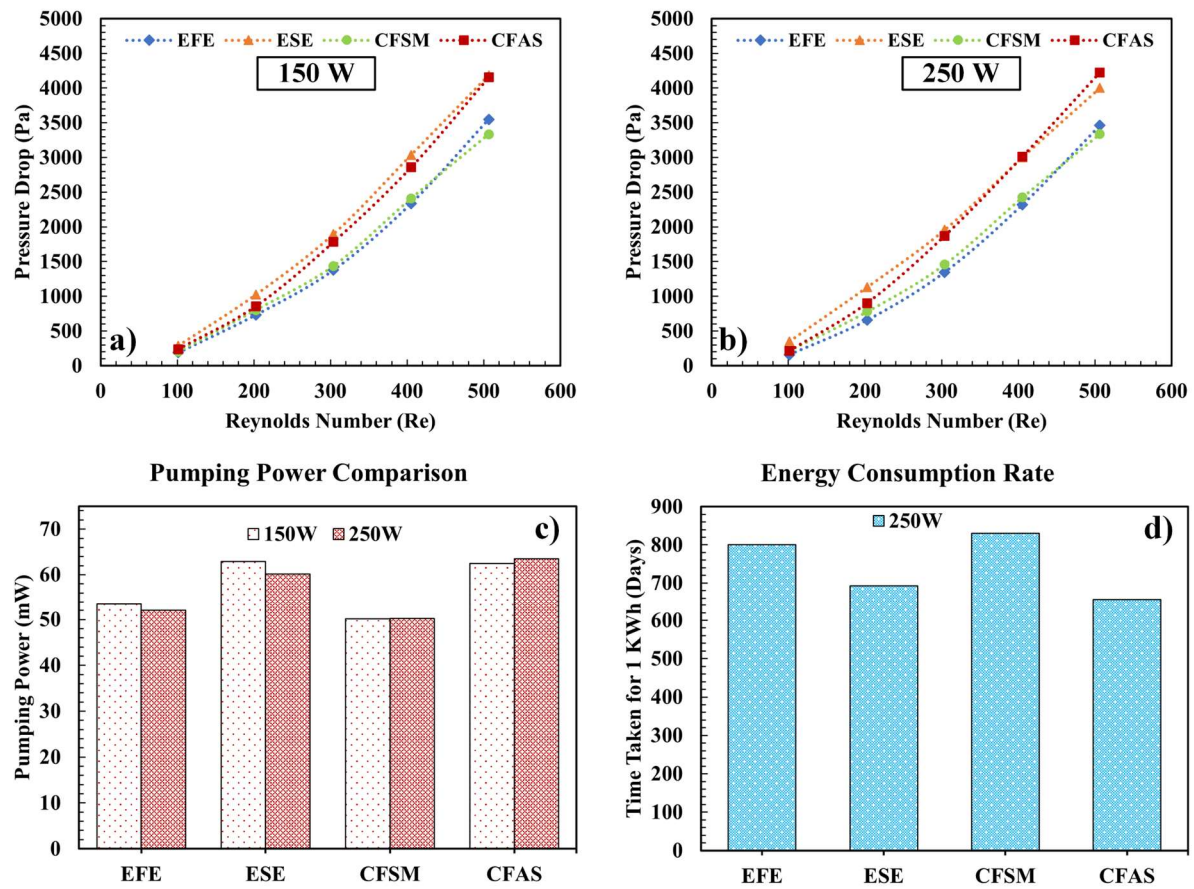


Fig. 5.8 (a)-(d) Pressure drop and pumping power comparison

5.4.3.4 Effect of fin shape on thermohydraulic performance

The thermohydraulic performance of heat sinks is closely tied to the geometric design of the fins, which influences the flow dynamics, heat transfer efficiency, and pressure characteristics of the system. This section discusses how different micro pin-fin heat sink designs—EFE, ESE, CFMS, and CFAS—affect key performance metrics such as the Nusselt number, thermal resistance, and pressure drop, offering insights into the underlying physics for these outcomes.

In this study, the EFE design, which features filleted (curved) edges, consistently achieved the highest Nu values across a range of Reynolds numbers (Re). The rounded edges in the EFE design likely facilitate smoother fluid flow over the fin surfaces, reducing the formation of turbulent wake regions that can disrupt the thermal boundary layer. By maintaining a more stable and attached flow, the EFE design enhances convective heat transfer by maximising the effective surface area exposed to the fluid and minimising thermal resistance at the interface.

In contrast, the ESE design, characterised by sharp-edged fins, demonstrated lower Nu values. The sharp edges likely induce early flow separation, creating vortices and turbulent wake regions that, while increasing local heat transfer, disrupt the overall flow pattern and reduce the effective surface area available for heat exchange. The increased turbulence can lead to higher localised heat transfer. It also introduces inefficiencies by causing larger pressure gradients and non-uniform heat transfer distribution, resulting in a less effective overall convective HTC than the EFE design.

The CFSM design, which incorporates secondary flow lanes, exhibited the lowest Nu values among the designs. The secondary lanes led to less direct fluid interaction with the fin surfaces, reducing the overall heat transfer coefficient. These lanes might cause the fluid to bypass certain areas of the fins, leading to lower surface area utilisation and weaker convective heat transfer. The design may also create a more complex flow path, increasing the residence time of the fluid without significantly enhancing heat transfer, resulting in a lower Nu.

The CFAS design, with its innovative astroid splitters, achieved the second-highest Nu values, particularly at lower Re. The splitters likely act to increase turbulence in a controlled manner, enhancing mixing and ensuring that cooler fluid is continually brought into contact with the hot surfaces. This design likely improves the surface interaction of the fluid, increasing the effective convective heat transfer area and leading to higher Nu values. However, at higher Re, the increase in turbulence might lead to diminishing returns, as excessive turbulence could disrupt the flow too much, reducing the overall heat transfer efficiency.

Thermal resistance measures a heat sink's ability to dissipate heat, with lower values indicating better performance. The CFAS design consistently exhibited the lowest thermal resistance, particularly at higher Re. The design's astroid splitters likely optimise the flow paths within the heat sink, ensuring a more even distribution of the fluid over the surface area. This enhanced fluid distribution reduces hotspots and maximises the contact between the fluid and the fin surfaces, leading to more efficient heat removal and, consequently, lower thermal resistance. The complex geometry increases the effective surface area without significantly impeding fluid flow, which helps in maintaining low thermal resistance.

In contrast, the CFSM design showed the highest thermal resistance, particularly at lower Re. The design's secondary flow lanes might cause non-uniform flow distribution, leading to areas of stagnant flow where heat builds up. The reduced surface area contacts due to the flow bypassing certain regions result in inefficient heat removal, thereby increasing thermal

resistance. Additionally, the potential for flow recirculation within the secondary lanes could further impede heat transfer by trapping hot fluid in certain regions, worsening the thermal resistance.

The EFE and ESE designs exhibited intermediate thermal resistance values, with the EFE generally outperforming the ESE. The filleted edges of the EFE design likely promote smoother fluid flow and better surface contact, reducing thermal resistance compared to the ESE design. The sharper edges in the ESE design may cause flow disruptions that limit the effectiveness of heat removal, leading to higher thermal resistance. These flow disruptions could cause uneven temperature distribution on the fin surfaces, further contributing to increased thermal resistance.

Pressure drop is a critical factor in the design of heat sinks, as it influences the energy required to pump the coolant through the system. The ESE design, with its sharp-edged fins, exhibited one of the highest pressure drops. The sharp edges likely cause significant turbulence and flow separation, which increases the resistance to fluid flow. This increased resistance requires more pumping power to maintain the desired flow rate, leading to higher energy consumption. The substantial pressure gradients created by the sharp edges increase the energy required to overcome these resistances, making the ESE design less energy-efficient in long-term operation.

On the other hand, the CFSM design, featuring secondary flow lanes, demonstrated a moderate pressure drop and the lowest pumping power requirement. The secondary lanes likely help streamline the flow by providing alternate paths, reducing the overall resistance to fluid flow. This design, while not maximising heat transfer, offers better energy efficiency due to the lower pressure drop, which translates to reduced pumping power and lower operational costs. The trade-off here is between reduced heat transfer and improved energy consumption.

The EFE design, with its filleted edges, achieved a balance between pressure drop and thermal performance. The rounded edges minimise flow separation and reduce turbulence, leading to a moderate pressure drop. This design's ability to maintain efficient heat transfer while also reducing the pressure drop makes it a cost-effective option, as it requires less energy for pumping while still providing good thermal performance.

The CFAS design, though resulted in the highest pressure drop, maintained an acceptable energy consumption due to its superior thermal performance. The complex geometry with astroid splitters enhances heat transfer but at the cost of increased flow resistance. The high-

pressure drop indicates that the design creates substantial flow disruptions, likely due to the intricate flow paths around the splitters. However, the improved heat transfer efficiency justifies the higher pumping power required, making it suitable for applications where maximising heat dissipation is critical, even at the expense of higher energy use.

Therefore, the shape of the fins plays a crucial role in determining the thermohydraulic performance of micro pin-fin heat sinks. Designs like EFE, which offers a balance between smooth fluid flow and efficient heat transfer, tend to perform well across all metrics, while more complex designs like CFAS can push the limits of heat transfer at the cost of higher pressure drops. Understanding the interplay between these factors is essential for optimising heat sink design to meet specific thermal management needs.

While a comprehensive comparison including thermal resistance and pumping power is beneficial, it is challenging to produce a direct, like-for-like comparison with conventional heat sinks from the literature due to the varying flow rate, leading to massively different Re and pumping power, and configurations across studies. Additionally, most studies in the literature do not compare thermal resistance across different investigations; instead, they typically compare thermal resistance between designs within the same study. Many comparative studies also do not consistently report values for parameters like pressure drop, further complicating direct comparisons. However, to provide a combined thermohydraulic comparison, we have incorporated a performance improvement factor (Eq. 14) relying on Nusselt number and pressure drop to provide relevant heat transfer enhancement; to achieve this we have used the experimental values of [246]. The results show that compared to circular pin-fins, the new designs EFE and CFAS, show a combined improvement of 1.30 and 1.33 respectively. Therefore, this further highlights the effectiveness of the mixed geometries in providing a balanced thermohydraulic improvements.

Performance Improvement Factor (PIF):

$$PIF = \frac{\left(\frac{Nu_{(nc)}}{Nu_{(bc)}}\right)}{\left(\frac{\Delta P_{(nc)}}{\Delta P_{(bc)}}\right)^{\frac{1}{3}}} \quad (43)$$

Where nc refers to the new case, and bc is the base case (circular fins) gained from the experimental results of [246].

5.4.4 Building empirical correlation models

The currently available empirical correlation models, including classical models developed by Shah [333] or London or Kosar, et al. [367], are not suitable for the new types of hybrid micro pin fin geometries, even if they initially show good agreement at lower Reynolds numbers. These traditional models, designed for simpler microchannel or pin-fin configurations, fail to account for the complex flow dynamics introduced by the intricate geometries of hybrid micro pin setups. While Xu et al.'s correlation, tailored for petaloid geometries, demonstrated reasonable accuracy at lower Reynolds numbers, its applicability diminishes as the flow approaches the transitional regime. In this study, the flow transition occurs between Reynolds numbers 300 and 400, a range where flow behaviour becomes unstable and difficult to model accurately. Xu et al.'s [246] correlation, developed for a broader range of 300 to 1500, reports turbulence around a Reynolds number of 900. However, existing literature suggests that transitional regimes can begin at Reynolds numbers greater than 300 [346]. This transitional behaviour is evident in the graphs of Nusselt number (Nu) and thermal resistance, where the values show only limited increases or massive fluctuations.

Although MSE is a commonly used metric, this research primarily focuses on R^2 and MAPE values due to the different data scales between Rth, Nu, and pressure drops. MAPE values are more generalisable when the data ranges vary significantly in magnitude. Hence, the breakdown of the equations for calculating MSE, MAPE, and R^2 are as follows:

The R^2 (R-squared) is a statistical measure that represents the proportion of the variance in the dependent variable that is predictable from the independent variables given by this equation:

$$R^2 = 1 - \frac{\sum_{i=1}^n (y_i - \hat{y}_i)^2}{\sum_{i=1}^n (y_i - \bar{y})^2} \quad (44)$$

Where:

- n is the number of data points.
- y_i is the real value for i^{th} data point.
- \hat{y}_i is the prediction for i^{th} data point.
- \bar{y} is the average of the real values.
- $\sum_{i=1}^n (y_i - \hat{y}_i)^2$ is the sum of squared errors.

- $\sum_{i=1}^n (y_i - \bar{y})^2$ is the total sum of squares (the total variance in the actual values).

The Mean Absolute Percentage Error (MAPE) is a measure of prediction accuracy in a model. The equation calculates the average of the absolute percentage errors between actual and predicted values, expressed as a percentage. The equation for MAPE is:

$$\text{MAPE} = \frac{1}{n} \sum_{i=1}^n \left| \frac{y_i - \hat{y}_i}{y_i} \right| \times 100 \quad (45)$$

Where:

- y_i is the real value for i^{th} data point.
- $\left| \frac{y_i - \hat{y}_i}{y_i} \right|$ is the absolute percentage error for the i^{th} data point.

The Mean Squared Error (MSE) is used as a quality measure for a model estimator; it calculates the average of the squared differences between actual and predicted values, given by:

$$\text{MSE} = \frac{1}{n} \sum_{i=1}^n (y_i - \hat{y}_i)^2 \quad (46)$$

- $(y_i - \hat{y}_i)^2$ is the squared error for the i^{th} data point.

Despite the limitations of existing correlations, the experimental values from this research remain robust, with the Mean Absolute Percentage Error (MAPE) between Nu, thermal resistance (Rth), and pressure drops ranging between 2.5% to 7.5% for power levels of 250W and 150W. This indicates that the experimental data are consistent and reliable. Notably, the Nusselt number is slightly lower at 250W compared to 150W, which can be attributed to the increased thermal load at higher power levels. This higher thermal load may lead to elevated fluid temperatures and reduced heat transfer efficiency due to changes in fluid properties or boundary layer effects under these conditions. Therefore, while existing correlations fall short in predicting the behaviour of hybrid micro pin-fins, the experimental results are robust and give valuable performance insights.

Nonetheless, to develop new correlation models, the data and parameters were combined to assess the Pearson correlation between various dependent and independent variables (DVs and IVs). Fig. 5.9 shows the correlation matrix, where it is evident that Nu, Re, pressure drop (PD), and power (Pu) have strong positive correlations, while Rth has a strong negative correlation. In many empirical correlation models, Nu is calculated using Reynolds number (Re) and

Prandtl number (Pr). The Pr for the flows were calculated depending on the temperature; however, the Pr values vary inconsistently across different models, with only the EFE model showing any significant correlation between Nu and Pr. This inconsistency further highlights the complexity of the dataset and the intricate underlying physics. To determine if Pr significantly influences the dataset, a principal component analysis (PCA) was conducted for feature engineering and to ensure that any power law correlation equations developed are robust and generalisable.

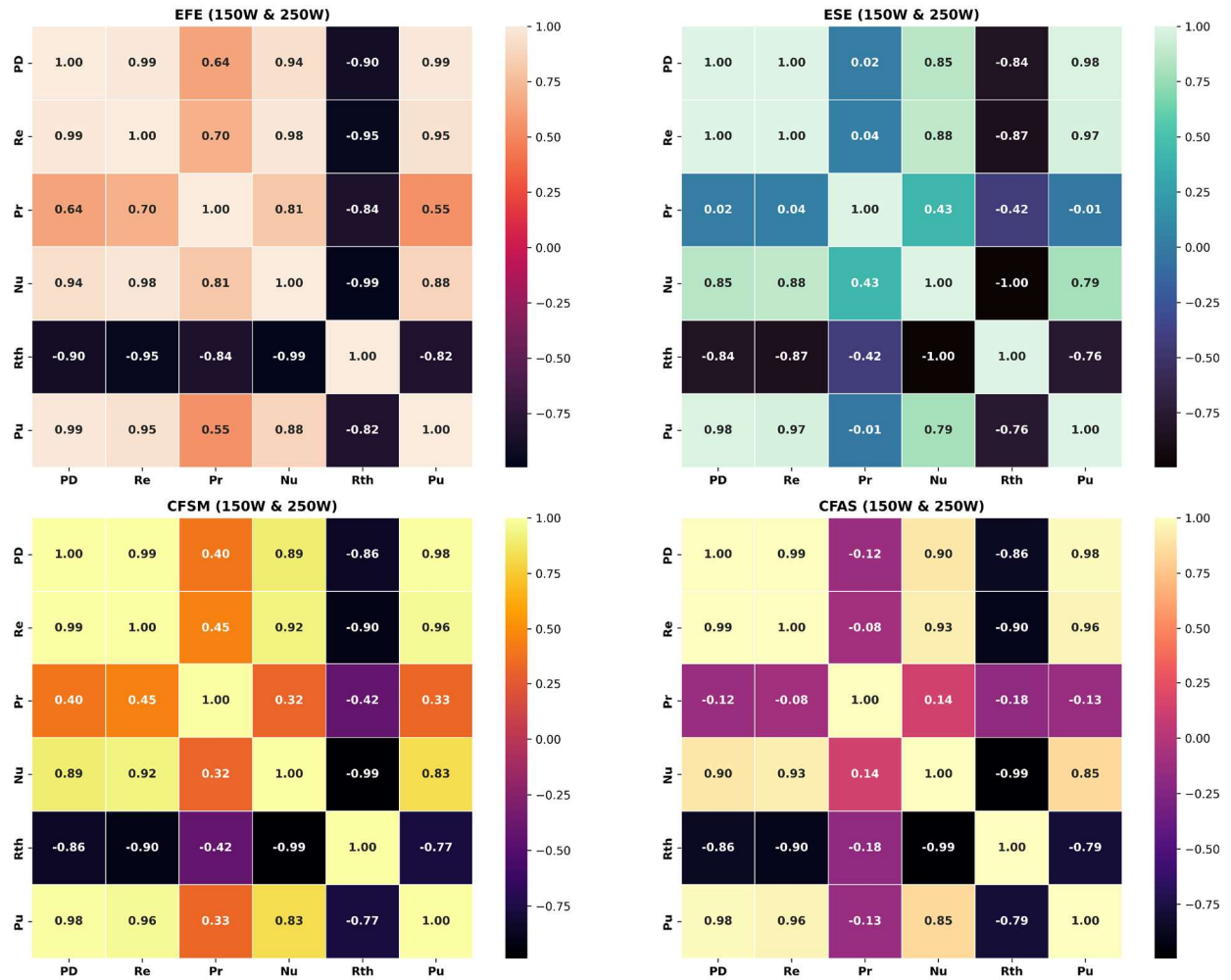


Fig. 5.9 Correlation matrix for parameters

Principal Component Analysis (PCA) is a dimensionality reduction technique used to identify key parameters which influence variability in the original dataset. Although domain knowledge suggested that Nu, PD, Re, and Pr are key variables, the irregularity and weak correlations of Pr warranted the application of PCA as an additional confirmation. PCA was applied to identify the key variables that contribute most to the variability in the dataset, which is composed of different power configurations and thermal performance metrics. The strategy involved

standardising the data to ensure each feature contributed equally to the PCA. PCA was then performed, and the first two principal components were analysed, as they typically capture the most variance in the data. The loadings of the variables were examined to determine which had the most influence on these principal components. Generally, variables with the highest absolute loading values in the first two components are considered the most impactful, providing insight into the underlying structure of the data and allowing for a more focused analysis of the key factors driving the observed patterns.

In this case, R_{th} and Nu were the most influential. Nevertheless, the other three factors— Re (0.77), PD (0.76), and Pr (0.74)—showed strong and closely matched loading values to Nu (0.80). Therefore, the PCA confirmed the inclusion of Pr as a parameter in forming empirical correlations for the new hybrid micro pin-fins. However, since CFAS and EFE were the two best-performing configurations from the two types of MPFHS setups, power law empirical equations were derived for them, along with their MAPE and R^2 values, to demonstrate the model's accuracy and variations. Table 10 presents the new empirical correlation equations created using Python and power law equations for the best-performing Cruciform and Exocoetidae-inspired biomorphic heat sinks

Table 10: Empirical correlation equations

Design	Equation	Accuracy
EFE	$Nu = 1.9434 \times Re^{0.2126} \times Pr^{0.3517}$	MAPE = 1.34%; $R^2 = 0.987$
	$\Delta P = 0.0283 \times Re^{1.8120} \times Pr^{0.2866}$	MAPE = 3.11%; $R^2 = 0.99$
CFAS	$Nu = 3.4822 \times Re^{0.1602} \times Pr^{0.1466}$	MAPE = 1.63%; $R^2 = 0.957$
	$\Delta P = 0.1737 \times Re^{1.6626} \times Pr^{-0.1492}$	MAPE = 7.06%; $R^2 = 0.98$

5.4.5 Machine learning-driven analysis

This research employs machine learning algorithms for investigative data analysis and to enhance validation of the dataset; thus, providing an in-depth description of each algorithm goes beyond the scope of this paper. Furthermore, these algorithms have been extensively discussed in the existing literature [8,351,352,368]. The experimental data results and subsequent empirical correlations yielded high R^2 values. Therefore, a key point of interest was determining whether machine learning algorithms could provide more accurate Nu predictions

using Re and Pr and if they can better capture the complex data patterns to show the existence of meaningful relationships and valid patterns in the dataset. As a result, 10 different types of regression models were used.

Firstly, Linear Regression (LR) models the relationship between dependent and independent variables (DV and IV) by fitting a straight line. On the other hand, Polynomial Regression (PLR) extends LR by modelling non-linear trends through polynomial relationships. XGBoost (XGB) is an optimised version of a gradient boosting algorithm that enhances prediction accuracy via ensemble learning, and it is highly efficient for structured data. Random Forest (RF) is another ensemble learning method that improves prediction accuracy and robustness by averaging outputs from multiple decision trees.

On a different note, Support Vector Regression (SVR) leverages support vector machines to make predictions by finding the optimal hyperplane to minimise errors. K-Nearest Neighbours (KNN) predicts values by averaging the outputs of the closest data points, offering a simple yet effective approach. Ridge Regression (RR) is a regularised version of linear regression that adds a penalty on high coefficients to reduce overfitting; Elastic Net (EN) combines the penalties of Ridge and Lasso regression, balancing variance and bias. MLP Regression, based on a multi-layer perceptron, uses neural networks to model complex, non-linear relationships in data. Lastly, a Combined Model (CML) blends multiple models to enhance prediction accuracy by leveraging their strengths — in this case, it combines MLP, KNN, and LR. The reason multiple different models are compared against each other is to assess and address any overfitting issues. Table 11 shows the initial model performances.

Table 11: Different regression algorithm performance

Model	MSE	MAPE	R ²
XGBoost	0.000	0.07%	1
Polynomial Regression	0.010	0.72%	0.995
Random Forest	0.050	1.67%	0.9748
Support Vector Regression	0.209	3.17%	0.894
K-Nearest Neighbors	0.099	2.72%	0.8026
Linear Regression	0.108	2.95%	0.7833

Ridge Regression	0.110	2.79%	0.7808
Combined Model	0.134	2.26%	0.7317
Elastic Net	0.262	3.30%	0.4762
MLP Regression	0.388	5.21%	0.2225

The performance of various predictive models for Nusselt number (Nu) based on Reynolds number (Re) and Prandtl number (Pr) revealed significant differences in accuracy and reliability. They were categorised into four different categories discussed in the following.

Very High Accuracy Models, Possible Overfitting ($R^2 > 0.95$), include XGBoost, Polynomial Regression, and Random Forest. XGBoost stands out with a perfect R^2 of 1.00, therefore there is overfitting. However, its near-zero MSE and MAPE indicate that it effectively minimises prediction errors and handles the non-linearity and interactions between Re and Pr adeptly, and, thus, is too reliant on this dataset. Polynomial Regression also performs exceedingly well with an R^2 of 0.9950, leveraging polynomial terms to capture intricate relationships between the variables. This model's high performance is due to its flexibility in fitting complex patterns, despite a slight increase in error metrics compared to XGBoost. Random Forest achieves an R^2 of 0.9748, demonstrating strong predictive power with an ensemble of decision trees that reduces overfitting and captures a broad range of interactions between Re and Pr. The slightly higher MSE and MAPE compared to XGBoost and Polynomial Regression suggest it might not model the data's most intricate patterns as precisely.

High Accuracy Models ($0.95 > R^2 > 0.80$) consist of Support Vector Regression (SVR). SVR, with an R^2 of 0.8940, shows effective performance but with higher MSE and MAPE, which might be due to its sensitivity to the choice of kernel and hyperparameters. Although SVR handles non-linearities well, its performance is slightly less robust than very high-accuracy models. KNN, with an R^2 of 0.8026, offers reasonable predictions but struggles with higher MSE and MAPE due to its reliance on local data and sensitivity to the choice of k-neighbours.

Good Accuracy Models ($0.80 > R^2 > 0.70$) included Linear Regression and Ridge Regression, with R^2 values of 0.7833 and 0.7808 respectively, show basic predictive capabilities but are limited by their assumptions of linear relationships. Ridge Regression improves upon Linear Regression by adding regularisation to handle multicollinearity. Yet,

both models fail to capture the non-linear interactions as effectively as more advanced techniques, resulting in higher errors. The combined model produces even lower accuracies than a single model.

Low Accuracy Models ($R^2 < 0.70$) are represented by Elastic Net and MLP Regression. Elastic Net, with R^2 of 0.4762, demonstrates poor performance due to the challenges of balancing L1 and L2 regularisation, which may not suit the complex relationships in the dataset. The high MSE and MAPE suggest that the regularisation terms are not effectively tuning the model. MLP Regression also exhibits the lowest R^2 of 0.2225, attributed to its complexity potential underfitting issues and limited data. The model's architecture might not be well-suited for this problem, leading to significant inaccuracies in prediction.

Overall, XGBoost and Polynomial Regression are the most reliable models for predicting Nu, offering the highest accuracy and lowest errors due to their ability to handle non-linearity and complex interactions. Nevertheless, these show signs of overfitting too. Models in the high accuracy category are effective but may not provide the same level of precision due to their inherent limitations. The lower accuracy models show notable deficiencies in capturing the data's nuances, indicating a need for different modelling approaches or further optimisation to improve performance. Therefore, to cross-validate the results and alleviate overfitting issues for better data generalisation. The original dataset was synthetically augmented with large Gaussian noise to distort the dataset and further analyse if the models can still make robust predictions. The reason Gaussian noise was used for regularisation over other methods is due to its versatility and continuity in handling data. Additionally, gaussian methods have previously yielded good performance results [31]. As in the original code, Re and Pr data were standardised using 'StandardScaler' so the features have mean 0 and standard deviation 1 after scaling, a noise of scale of 0.5 of standard deviation is added which is quite significant. The specific equation for generating Gaussian noise would be:

$$\text{Noise} = \sigma \cdot Z \quad (47)$$

Where:

- Z is a random variable sampled from the standard normal distribution $N(0,1)$
- $\sigma = 0.5$ is the standard deviation.

So, for each data point y_i , the noisy version would be:

$$\text{Noisy } y_i = y_i + \sigma \cdot Z_i$$

Where: Z_i is sampled from $N(0,1)$ independently for each data point.

Gaussian noise was chosen for its effectiveness in replicating minor variations commonly observed in experimental measurements, helping to prevent overfitting by introducing controlled random variability. Compared to standard scaling, which uniformly adjusts data, Gaussian noise allows for more realistic, small-scale fluctuations that align with natural measurement uncertainties, thereby better simulating the variability in experimental conditions. By simulating realistic measurement uncertainties, Gaussian noise enhances the model's robustness, making it less sensitive to minor discrepancies and improving predictive accuracy across diverse conditions in the dataset.

The addition of Gaussian noise had an interesting impact on the performance of various regression models used to predict Nu based on Re and Pr. Fig. 5.10 shows the comparison between the original and augmented datasets. Initially, the models trained on the original dataset demonstrated near-perfect performance metrics, with XGBoost achieving an MSE of 0.0001, a MAPE of 0.07%, and an R^2 of 1. These metrics, while impressive, suggest a potential risk of overfitting, where the model might be capturing noise and specificities of the training data rather than generalisable patterns. Hence, introducing substantial noise allowed assessment of the model's ability to generalise beyond the overly specific patterns of the original data. The augmentation showed that models could better handle data variability, leading to improvements.

Model Performance

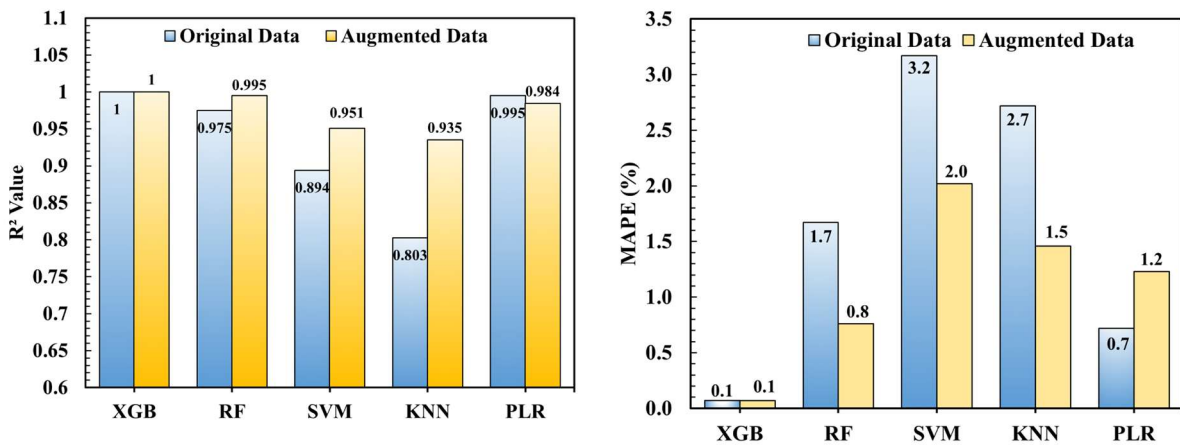


Fig. 5.10 Model comparison for original and augmented synthetic data

Nonetheless, such perfect predictions shown by XGB are unrealistic in a real-world scenario, therefore further assessment of XGB is required. Random Forest's performance improved from an MSE of 0.0498, a MAPE of 1.67%, and an R^2 of 0.9748 to an MSE of 0.0096, a MAPE of 0.76%, and an R^2 of 0.9951. Similarly, SVR's metrics improved from an MSE of 0.2093 to 0.0973, with MAPE decreasing from 3.17% to 2.02%, and R^2 increasing from 0.8940 to 0.9507. The KNN and Polynomial Regression models also exhibited enhanced performance, reflecting a robust generalisation ability after augmentation. Therefore, based on the overall performance of aR^2 and MAPE and considering potential overfitting issues, PLR and RF are perhaps the most suitable models for future predictions of Nu.

These results underscore the utility of data augmentation in capturing complex relationships. The substantial noise introduced in the augmentation process helped simulate real-world variability, making the models more adept at handling noise and less prone to overfitting. This process is particularly valuable for predicting Nu from Re and Pr, as it helps in modelling the intricate and often non-linear relationships between these variables. Moreover, using augmented data is beneficial in the context of empirical correlation models, where complex relationships might be oversimplified. Traditional empirical models often rely on limited data or simplistic correlations, which may not capture the true dynamics of the system. By contrast, regression models trained with augmented data can explore a broader range of relationships and interactions, providing more accurate and reliable predictions.

It is important to acknowledge that the dataset used is limited, and acquiring more experimental data is both expensive and impractical. Thus, data augmentation becomes a crucial technique to enhance the robustness and accuracy of the models without the need for extensive new data collection. This approach supports agile manufacturing concepts by offering a time-efficient method to improve model performance and adaptability. Therefore, the augmentation of data with a large Gaussian noise scale has proven to be a powerful technique in improving model performance, capturing complex relationships, and aligning with agile manufacturing principles. The enhanced generalisation, reflected in improved MAPE and R^2 values, demonstrates the practical benefits of this approach in handling real-world data variability and refining predictions. However, this data-driven approach for exploration is aligned with the ethos of continuous improvement via technology in advancing manufacturing efficiency [369] and provides a good baseline for future predictions of thermohydraulic performance without using extensive datasets.

5.4.6 Summary of Chapter

In summary, this research illustrates the effectiveness and limitations of various innovative micro pin-fin configurations in assessing the thermohydraulic performance of biomorphic heat sinks. By integrating different design strategies, agile manufacturing, experimental methods, and machine learning approaches, the study offers a novel perspective on the design and production of hybrid biomorphic pin-fins, potentially reducing production time, development costs, and manufacturing expenses. The key conclusions were:

- The Exocoetidae-inspired pin-fins with filleted edges (EFE) and Cruciform-inspired pin-fins with a novel type of astroid splitters (CFAS) outperformed other designs in terms of Nusselt Number (Nu), thermal resistance, and pressure drops. These new designs achieve a 23% to 45% enhancement in heat transfer at lower Reynolds numbers compared to existing designs in the literature, with manageable increases in pumping power and energy consumption.
- Further thermal assessments reveal that adding secondary lanes or sharp-edged features results in uneven heat distributions, leading to increased turbulence and less efficient heat transfer. However, secondary lanes do help reduce system pressure drop.
- New empirical correlations and machine learning predictions demonstrate high accuracy in forecasting Nusselt Numbers, streamlining design optimisation and providing rapid performance assessments. Among the tested models, ensemble methods such as XGBoost, Random Forest, and Polynomial Regression produced the most accurate results, with a mean absolute percentage error of less than 3% and high R^2 values.

Overall, this study enhances our understanding of pin-fin heat sink designs by highlighting the advantages of unconventional designs and the benefits of integrating diverse approaches. Combining advanced design techniques with machine learning can significantly improve pin-fin performance, reduce size, cost, and development time, and enhance energy efficiency in next-generation heat sink solutions. Future research should focus on optimising the distribution of pin-fin segments and developing more robust methods for using limited datasets to provide more accurate predictions of thermohydraulic parameters.

Chapter 6: Flow Boiling Regime Classification in Microchannel Heat Sinks

6.1 Background to the Chapter

The chapter focused on accurately predicting and classifying flow boiling regimes in straight microchannels using a custom semi-automated data pipeline. A combined Convolutional Neural Network (CNN) and clustering algorithm approach was utilised to streamline data capture, analysis, and processing. This method not only improved the interpretability of the results but also significantly reduced the time and manual handling required for analysis. The CNN-clustering method was found to align well with sustainable manufacturing philosophies, as it facilitated continuous improvement in both data analysis efficiency and the overall development process. Furthermore, the implementation of this technology demonstrated a clear link to sustainable design, reducing resource waste in testing and manufacturing while providing accurate, scalable insights for future heat sink development and a working data pipeline that can be used for further investigations.

6.2 Research Scope

The flow boiling mechanism involves intricate interactions between liquid and vapour phases, resulting in varied flow patterns and heat transfer dynamics within microchannel heat sinks. However, due to the complex interchange and physical phenomena involved, flow boiling classification contains many challenges related to subjectivity, interpretability, generalisability, and accuracy, amongst other issues [30]. Therefore, understanding and accurately categorising these flow patterns is crucial for enhancing heat transfer efficiency and ensuring dependable thermal management. Furthermore, classifying flow boiling regimes helps engineers to tailor microchannel designs to specific operational conditions, thereby maximising heat dissipation while minimising thermal resistance, pressure drops, or energy consumption.

Consequently, this study conducted a comparative assessment of flow boiling classification in micro/mini channel heat sinks, employing neural network-based classification and pattern recognition via clustering algorithms under varying mass flow rate conditions (ranging from 180 mL/min to 600 mL/min using 1600 images). The research aimed to offer a new perspective and evaluate different algorithms via a custom dataset gained from experimental findings; thus, the focus lies in assessing machine learning-based approaches, specifically clustering methods,

for accurately recognising and labelling boiling patterns in microchannel heat sinks. Thus, the research provides the following major contributions:

- A streamlined, generalisable flow boiling image segmentation pipeline;
- A semi-automated system to generate data and classify images for flow boiling;
- A baseline boiling regime classifier using a combined CNN-clustering that can be expanded/built upon;
- A methodological comparative analysis of clustering algorithms not reported in similar preceding works;
- Furthermore, the system considers a mixture of different bubble formations and regimes with data augmentations, so there is the generalisability of the proposed work in real-world applications such as different lighting conditions, backgrounds, and orientations.

6.3 Overview of available technologies

Reviewing the literature shows that boiling heat transfer classification, particularly in micro/mini channels, has various implications for diverse engineering applications. Flow boiling patterns directly impact heat transfer efficiency, system stability, and energy usage. In micro/mini channels, where space constraints and high heat fluxes prevail, precise classification becomes even more critical for effective thermal management. Therefore, accurate classification of boiling heat transfer regimes is integral for optimising heat transfer processes, enhancing system performance, and ensuring operational safety. However, achieving robust classification methodologies in such intricate systems presents many challenges, warranting a critical review of existing techniques and further research.

The current flow pattern classification and recognition strategies encompass a spectrum of approaches ranging from traditional empirical correlations, computer vision and advanced ML algorithms [297]. Flow pattern detection methods can mainly be categorised into direct and indirect techniques. Direct methods like high-speed photography, X-ray computed tomography, provide insights into flow patterns, but can be subjective in their interpretation and often require manual feature extraction or data labelling. On the other hand, indirect methods, such as time-frequency analysis methods (TFA), can analyse fluctuation signals (such as pressure drop, flow, or electrical impedance) to identify flow patterns [370]. While TFA is popular, other techniques include statistical analysis like probability density function (PDF). One of the main limitations of indirect methods like TFA is their sensitivity to noise and signal

interference, making them unsuitable for accurately capturing the dynamics of complex systems such as flow boiling, ultimately leading to incorrect results.

Moreover, relying on traditional methods and empirical correlations may struggle to capture the intricate dynamics/changes of flow boiling phenomena, leading to limitations in accuracy and generalisation. The prospect of machine learning and deep learning algorithms has revamped flow boiling classification by offering data-driven, automated, and scalable solutions. Techniques like K-nearest neighbours (KNN), Random Forest, Support Vector Machine (SVM), and Multilayer Perceptron (MLP) have demonstrated promising results in classifying flow patterns based on diverse input parameters [298]. These algorithms leverage large datasets to uncover intricate patterns and relationships, enhancing classification accuracy and generalisation across different operational conditions. Nevertheless, the effectiveness of machine learning or deep learning-related pattern recognition or classification relies on several critical factors, including training data quality, feature selection, data labelling, and model robustness. Furthermore, the interpretability of machine learning models remains a concern, particularly in safety-critical applications where classification decisions are crucial.

Clustering methods, such as K-means, Gaussian Mixture Models (GMM), and Hierarchical Clustering, are widely recognised unsupervised learning techniques extensively employed in pattern recognition tasks like image analysis [371]. Despite their popularity, they remain underutilised in flow boiling research, particularly in microchannel/minichannel studies. Recent research in this field has predominantly focused on bubble dynamics in flow boiling via chord lengths and bubble diameters [302]. However, boiling dynamics within a generalised system may significantly differ in micro-scale systems, necessitating more targeted investigations for a comprehensive analysis. Moreover, experimental data acquisition is costly, and large dataset-based artificial intelligence models demand considerable computational power and expenses. Therefore, there is a growing need for robust yet agile methods that address the current demands of rapid product development times — while minimising complexity and data requirements. Recent reports suggest that smaller datasets, especially in the thermal management area, can yield superior results [354]. Additionally combining different strategies and technologies can further improve the continuous improvement of diverse processes in heat sinks [8]. Accordingly, clustering techniques combined with CNNs are a worthwhile strategy to extract meaningful insights from such datasets, potentially enhancing the understanding of flow boiling phenomena in microchannel and minichannel.

6.4 Clustering Algorithms for Flow Boiling

While the definitions and intricacies of these methods are well-documented in existing literature [371–373] a brief overview of their underlying mechanics and equations is provided in the following:

K-means Clustering: The objective function for k-means can be expressed as:

$$\arg \min_S \sum_{i=1}^k \sum_{x \in S_i} \|x - \mu_i\|^2 \quad (48)$$

where: $S = \{S_1, S_2, \dots, S_k\}$ represents the partitioning of the dataset into k clusters; μ_i is the centroid (mean) of cluster S_i ; $\|x - \mu_i\|^2$ denotes the squared Euclidean distance between a data point x and the centroid μ_i . The goal is to find the optimal partitioning S and centroid positions $\{\mu_1, \mu_2, \dots, \mu_k\}$ that minimise the objective function. The algorithm iterates between two steps: assigning each data point to the nearest centroid to form clusters and updating the centroids based on the mean data points in each cluster. The rationale behind choosing the k-means algorithm is that it can group similar patterns or features extracted from flow-boiling images. For instance, it can cluster images based on pixel intensities, texture features, or other image descriptors, helping identify different flow regimes or anomalies.

Gaussian Mixture Models (GMM): The probability density function (PDF) of a GMM is given by this equation:

$$p(x) = \sum_{i=1}^k \phi_i \cdot \mathcal{N}(x|\mu_i, \Sigma_i) \quad (49)$$

Where: x represents the observed data point; k is the number of mixture components; ϕ_i is the mixing coefficient associated with the i th Gaussian component, satisfying $\sum_{i=1}^k \phi_i = 1$ and $\phi_i > 0$; μ_i is the mean vector of the i th Gaussian component; Σ_i is the covariance matrix of the i th Gaussian component; $\mathcal{N}(x|\mu_i, \Sigma_i)$ denotes the multivariate Gaussian PDF with mean μ_i and covariance Σ_i . As GMM can model complex distributions in flow boiling images, it potentially enables the identification of different patterns or regions of interest. It can be applied to segment images into distinct regions based on pixel intensities or texture features (such as bubble formation or coalescence), aiding in feature extraction and subsequent recognition tasks.

Hierarchical Clustering: There are two main types of hierarchical clustering: agglomerative and divisive. This study investigated agglomerative hierarchical clustering as it is more commonly used. The linkage criterion defines the distance between two clusters A and B as:

$$d(A, B) = \min_{x \in A, y \in B} \text{dist}(x, y) \quad (50)$$

where: A and B are two clusters being considered for merging; $\text{dist}(x, y)$ is the distance between data points x and y . Based on this linkage criterion, different distance measures such as Euclidean distance, Manhattan distance, or cosine similarity can be used to calculate $\text{dist}(x, y)$. The dendrogram generated by hierarchical clustering visually represents the merging process and can be cut at different heights to obtain the desired number of clusters. Hierarchical clustering can reveal hierarchical structures in flow boiling images, identifying both macroscopic and microscopic patterns. Additionally, it can help understand relationships between different features or segments in the images, aiding in the interpretation and analysis of flow boiling phenomena.

Therefore, based on the discussion regarding the three chosen algorithms, it can be remarked that in flow boiling image pattern recognition, these clustering methods can preprocess data by segmenting images into meaningful regions, extracting features, or reducing dimensionality. They can enable distinct flow regimes' identification, anomalies, or critical patterns, facilitating further analysis or decision-making processes in flow boiling systems.

6.5 Strategic Process Plan

This image analysis and pattern recognition study was done using a custom dataset derived from experimental findings. The process involves creating a data pipeline and synthetic datasets, detailed across subsequent sections covering data collection, augmentation, model construction, and evaluation. While other studies explored pattern recognition with custom datasets to create data pipelines for other applications [374], this research addresses challenges like subjectivity, feature extraction, and data labelling by comparing the performance of manually labelled flow boiling data and unlabelled clustering algorithm data through a clustering-based convolutional neural network (CNN) classification. Given the high costs of experimental investigations and diverse behaviours of flow boiling systems, custom datasets play a critical role in enhancing future pattern recognition techniques. Therefore, while ResNet50 or CIFAR10 datasets may yield good results elsewhere, using a custom dataset for

training flow boiling images offers unique advantages: ensuring the model learns relevant features, adapts to image characteristics, and enables fine-tuning for optimal performance.

Measurement and monitoring were achieved through a suite of instruments. Temperature measurements utilize K-type thermocouples with an accuracy exhibiting an error margin of $\pm 0.5^{\circ}\text{C}$. Five thermocouples were evenly spaced across the heating base to ensure no heating hot spots were present that could affect the flow of boiling bubble formations, ultimately leading to incorrect results. An image acquisition system, consisting of a high-speed camera, and an optical microscope with an LED background light source was deployed. This entire system captured the evolution of various gas-liquid two-phase flow patterns during the experiment; four distinctive flow patterns were observed: dispersed bubbly flow (jets), bubble-slug flow, annular-like flow, and mist flow (local dry-out), shown in Fig. 6.1.

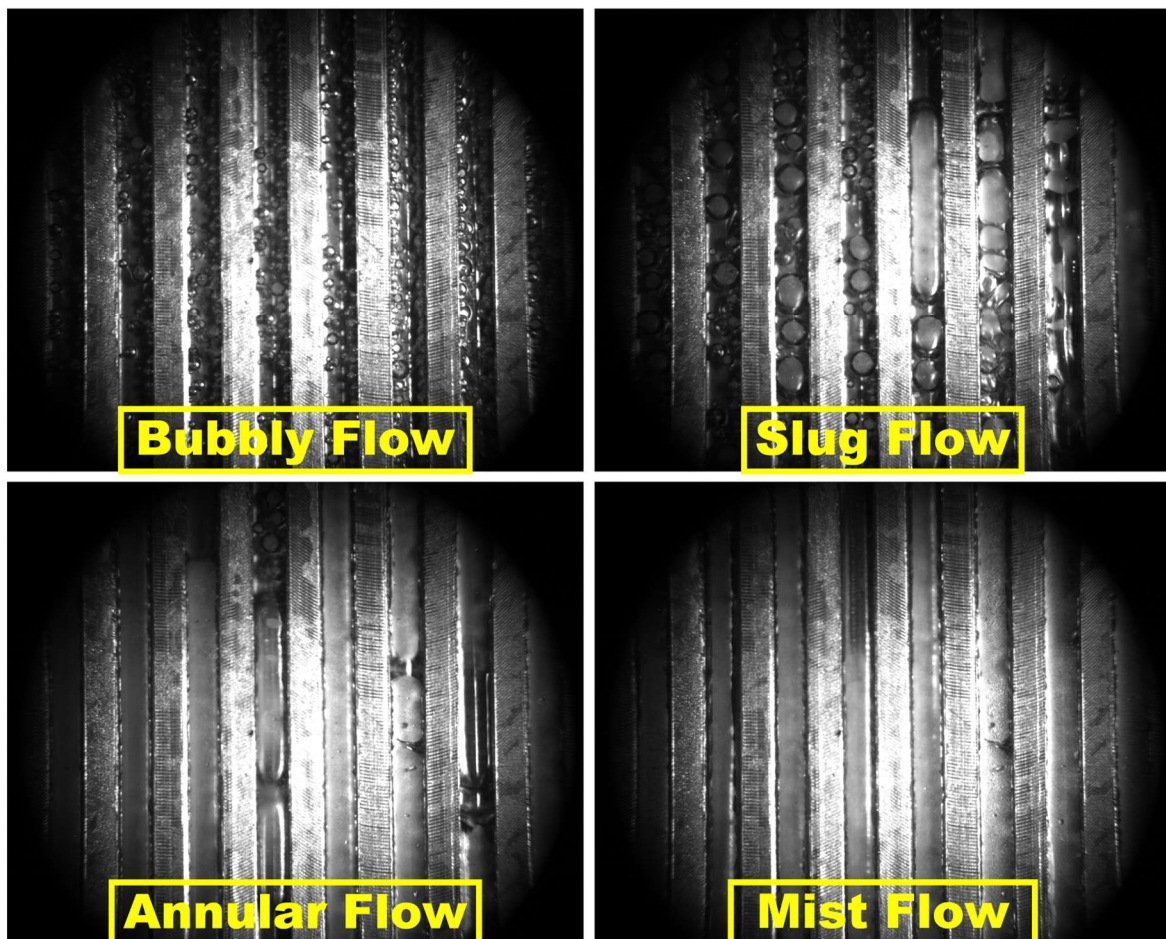


Fig. 6.1 Different flow regimes

6.5.1 Dataset Description

In the classification of flow boiling regimes, several criteria are utilised to delineate distinct patterns and behaviours within the boiling process. These criteria encompass factors such as bubble size and distribution, the thickness of the liquid film surrounding bubbles, the presence of dry-out regions, and the overall flow dynamics observed. By analysing these parameters, researchers can categorise flow boiling regimes into different phases, each characterised by unique thermal and hydrodynamic properties. Identifying different flow regimes within a flow boiling system involves careful observation and analysis of several key characteristics unique to each regime as highlighted in section 2.3.

In general, flow boiling can be categorised into four broad categories [30]. Jet flow is typically characterised by the presence of small, dispersed bubbles resembling jets within the liquid phase, while slug flow is marked by the alternating presence of elongated bubbles (slugs) and liquid slugs moving through the flow channel. Annular flow is distinguished by the formation of a continuous vapour phase surrounding a thin liquid film along the walls of the flow channel, and mist flow occurs when the liquid film becomes thin enough to expose patches of the wall directly to the vapour phase. In practice, distinguishing between these flow regimes often involves a combination of visual observation, analysis of flow patterns, measurement of bubble or slug sizes and velocities, and monitoring changes in local heat transfer rates.

The high-speed camera utilised in this study initially recorded videos capturing the entire duration of the boiling process. However, to focus on the analysis and extract meaningful insights, the authors specifically selected the first phase of boiling, spanning from the initiation of the jet-like dispersed bubbly flow to the occurrence of local dry-out regions. This selective approach allowed for a detailed examination of the critical transitional stages within the flow boiling process, shedding light on the mechanisms underlying heat transfer and vapour-liquid interactions. From the videos, 1600 images were extracted for further investigation, Appendix C4 shows a portion of the dataset. However, subtle changes in flow regime dynamics proved challenging to follow, emphasising the complexity of flow boiling phenomena and the necessity for advanced visualisation techniques and detailed analysis. Hence, through this targeted investigation, a deeper understanding of flow boiling and its practical implications in various engineering applications can be achieved.

6.5.2 Data Pipeline

The experimental setup generated data and was stored in a local dataset, stored in the computer as part of the experimental setup. To aid analysis, manual data labelling was performed to distinguish between flow boiling regimes. Initially, the labelled datasets were used to construct the base Convolutional Neural Network (CNN) model, enabling an assessment of its accuracy. Following this, the base CNN model acted as a foundation for analysis and classification using clustering techniques. The raw data undergoes augmentation and progresses through feature mapping stages such as convolutional, pooling, flattening, and ultimately resulting in fully connected layers capable of enabling multi-class classification of flow boiling regimes.

In the **Feature Extraction stage**, before augmentation, the images underwent resizing from 1280x1024 to 500x500. However, this reduction in dimensions resulted in a deterioration of image lighting. Thus, to rectify this issue and improve contrast, a histogram equalization was applied. Regarding the convolutional layers, the initial layer comprised 64 filters, with each subsequent layer containing 32 filters. The stride size for each step was set to 2, and a max pooling of 2 was utilised. The image preprocessing phase was initiated with an image size of 224 and a batch size of 64. Following this, the images underwent augmentation, which included rescaling, zooming, shearing, and horizontal flipping (Appendix C4 shows the sample code for this process). Given the significance of preserving bubble features, extensive noise or Gaussian augmentation was intentionally omitted. Fig. 6.2 shows a sample data augmentation process.

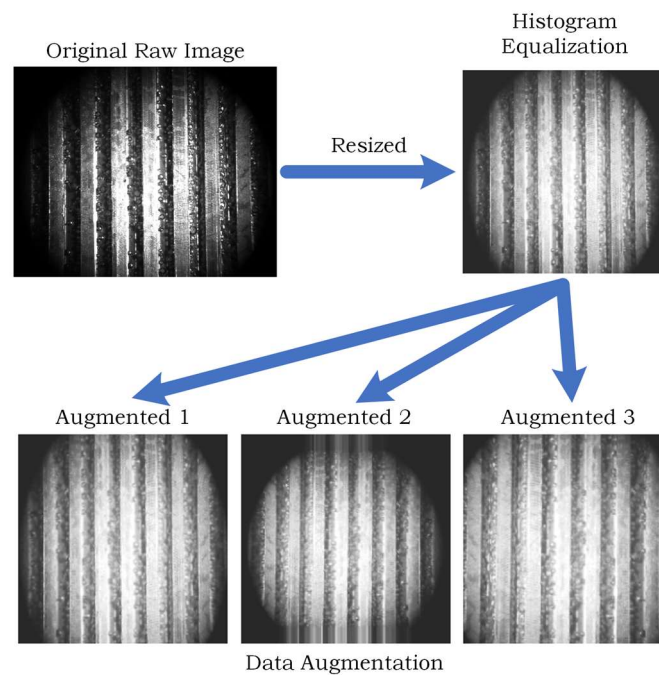


Fig. 6.2 Sample data augmentations

Furthermore, in the **Classification Stage**, the dataset had a 90% training and 10% test split. This division aimed to maximise the effective utilisation of the dataset for training whilst ensuring reliable results on the test sets [375]. In real-life applications, test datasets often tend to be small — hence the rationale behind this choice. Additionally, the division ensures reliable evaluation by maintaining a separate test set to enable a realistic assessment of the model's generalisation to unseen data; thus, replicating limited testing scenarios helps simulate real-world conditions. Moreover, a smaller test set reduces the risks of overfitting, where the model may memorise training data. To address overfitting, techniques such as regularisation, dropout, or adjustment of model complexity can be employed later to optimise the best-performing model. The accuracy of the models and the loss function was assessed using the categorical cross-entropy loss (softmax loss) [376], which is typically defined as follows:

Given:

- y_i : the true label (ground truth) for sample i
- p_i : the predicted probability distribution over all classes for sample i
- N : the total number of samples
- C : the total number of classes

Then, the categorical cross-entropy loss L is calculated as:

$$L = -\frac{1}{N} \sum_{i=1}^N \sum_{c=1}^C y_{i,c} \cdot \log(p_{i,c}) \quad (51)$$

where:

- $y_{i,c}$ is the indicator function, which is 1 if the true label of sample i is class c , and 0 otherwise.
- $p_{i,c}$ is the predicted probability of sample i belonging to class c according to the model's output.

This loss function penalises models based on the difference between predicted probabilities and true labels across all classes, encouraging the model to assign high probabilities to the correct class labels.

The evaluation of the base CNN model was then carried out using the initial labelled data. Simultaneously, unlabelled data was fed into three distinct clustering algorithms, segmenting

and classifying images into four distinct clusters for the four different flow regimes, with results stored in a desired local directory. The coding of the data pipeline facilitates clustering analysis and saves data, requiring minimal preprocessing and fostering agile analysis from experiments, leading to agile product development. With each iteration or data capture, new data seamlessly integrates to train clustering algorithms, allowing for semi-supervised generation and storage of synthetic data, pattern recognition, and organisation into four directories. This streamlined process significantly reduced the need for manual data handling, ensuring consistency between the root and save directories. The data pipeline loop, illustrated in Fig. 6.3, underscores the iterative nature of the process. Subsequently, in the **Post Processing Stage**, the clustered data was reintegrated into the base CNN setup to assess training and validation accuracy, thereby evaluating the feasibility and effectiveness of employing clustering-based pattern recognition to ultimately reduce the need for extensive manual labelling of future datasets.

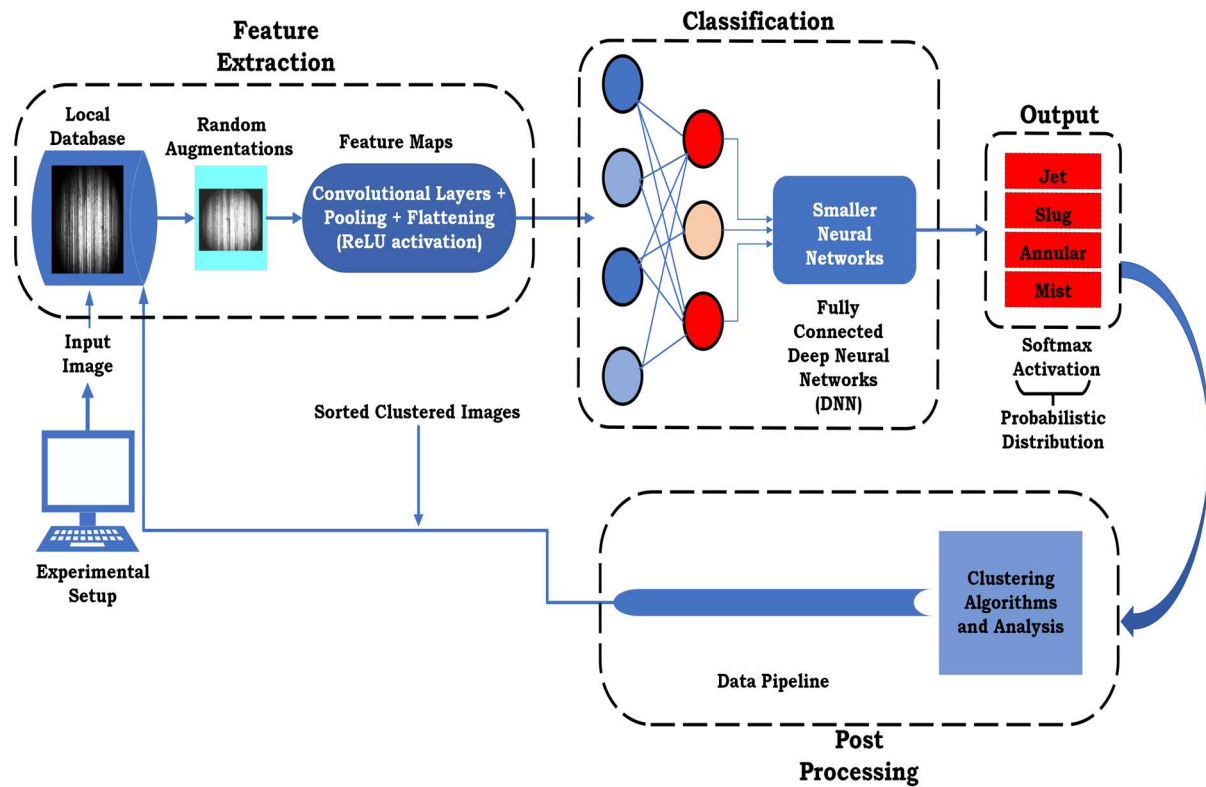


Fig. 6.3 Architecture for data pipeline and model implementations

6.6 Results and Discussion

6.6.1 CNN Classification

The experiment and images from Fig. 6.1 highlighted how the confined space within narrow channels restricts bubble development, altering bubble morphology compared to traditional

tubes or pipes. The deformation or bursting of bubbles under different wall flow conditions significantly influences flow patterns and can produce mixed patterns. Consequently, labelling the data and flow patterns poses challenges and is subject to interpretability issues, affecting the accuracy of classification models and the usability of datasets for generalisation or specific applications. To further assess these challenges, initially, a convolutional neural network (CNN) was trained on the dataset, incorporating a fully connected layer along with two additional layers, and the model was further fine-tuned with additional epochs. Fig. 6.4 illustrates the comparison of classification accuracy achieved by the CNN.

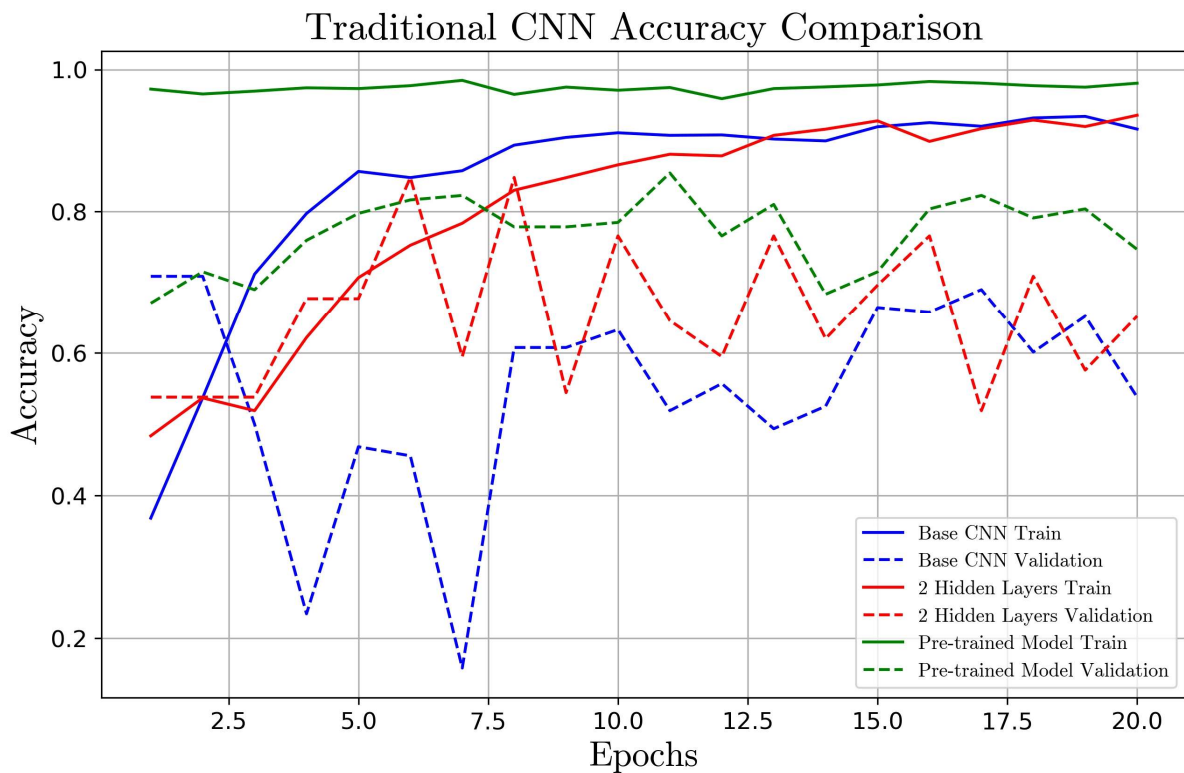


Fig. 6.4 CNN classification accuracy

The results from the CNN indicate significant variations between each epoch, ranging from 10-50% for the base CNN model. Although the addition of extra layers or epochs improves the accuracy of the validation on test sets, the overall variation across different epochs keeps the reliability of the classification below 75%, dropping to lower than 70% for the other two models. These substantial variations or the zigzag pattern suggest the challenge for neural networks to consistently identify flow patterns accurately, indicating potential subjectivity and complexity issues in labelling datasets where one image could belong to multiple categories visually. While high accuracy values of 90% to 95% seem promising, they also imply

overfitting problems based on the validation results, highlighting the need for a more objective assessment and methodology to enhance the classification robustness.

6.6.2 Clustering Results

Three different types of clustering algorithms were implemented. It can be seen that K-means has a relatively even distribution of cluster points where Hierarchical clustering classifies one type of cluster more than the others. For the Gaussian model, cluster 3 contains the most points. The cluster outputs were fed into the same base CNN model for classification comparison. The comparative analysis of flow boiling regimes across clustering algorithms yields interesting findings. Despite consistent total input counts of data points assigned to each algorithm, variations exist in how these points are distributed across clusters, as seen in Fig. 6.5 (a)-(c).

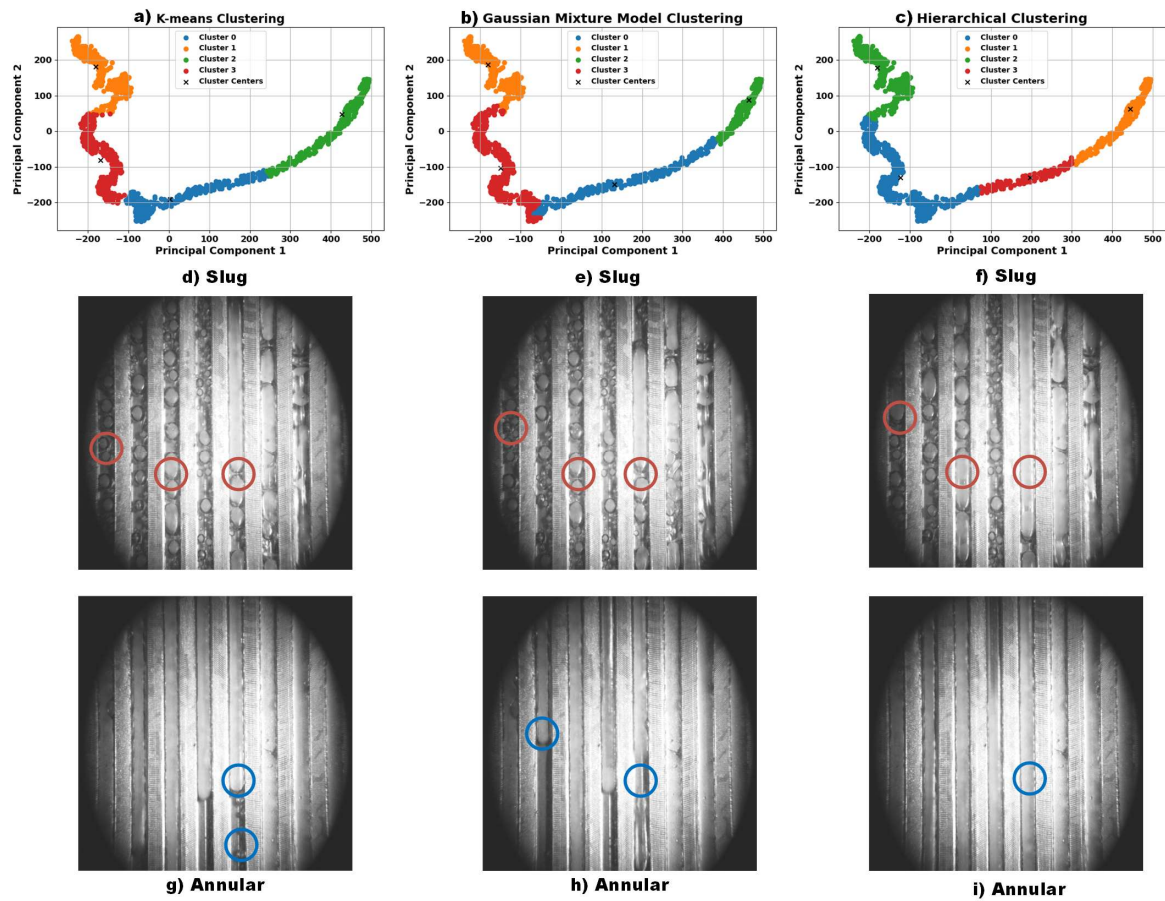


Fig. 6.5 (a)-(i) comparative analysis for algorithms

Notably, Hierarchical clustering demonstrates the greatest diversity in cluster sizes, with the highest cluster containing 689 data points for the slug flow regime, while K-means and Gaussian clustering exhibit more uniformity. Specifically, K-means allocates 458 data points to Cluster 1, Gaussian assigns 440, and Hierarchical only 158, indicating disparities in their

categorization approach. Moreover, Hierarchical clustering assigns 491 data points to Cluster 2, while Gaussian assigns 273 and K-means 365, further accentuating distinctions. Gaussian clustering tends to allocate more points to the annular flow cluster, with 580 data points, compared to K-means (442). These disparities underscore the importance of selecting an appropriate clustering algorithm based on the specific characteristics of the flow boiling regimes under study. While the total counts remain consistent, understanding the nuances of cluster distribution offers valuable insights into the underlying structure of the data and facilitates informed decision-making in analysing flow boiling regimes.

Examining the two different flow types in the slug [red spots, (d)-(f)] and annular (blue spots, [(g)-(i)], which are often the most desired flow regimes for high heat transfer. For K-means at the same image and instance, it focuses more on the bubble separations, whilst GMM categorises the region between bubble separation and coalescence efficiently, but Hierarchical considers merging bubbles into the same category as during dry out. Although the differences in the overall images are minimal, these small differences compound and ultimately lead to the distinctions of clusters overall and affect the efficacy of the algorithms.

6.6.3 Comparative Analysis

For a detailed quantitative discussion of the findings based on the training and validation accuracy of the four different models, the trends and data insights are presented in Table 12 (best values bolded). Table 13 compares the key findings and differences between the datasets.

Table 12: Model metrics

Model	Metric	Mean	Median	SD
KMeans	Training Accuracy	0.8788	0.8879	0.0432
	Validation Accuracy	0.6198	0.6226	0.1232
Base CNN	Training Accuracy	0.9743	0.9749	0.0061
	Validation Accuracy	0.7706	0.7816	0.0504
GMM	Training Accuracy	0.9142	0.9195	0.0323
	Validation Accuracy	0.8837	0.8994	0.0538

Model	Metric	Mean	Median	SD
Hierarchical	Training Accuracy	0.9013	0.9088	0.0310
	Validation Accuracy	0.7364	0.7166	0.0796

Table 13: Key highlights and differences

Dataset	Key Points
Dataset 1 (Base CNN, manually labelled data)	<ul style="list-style-type: none"> - High training accuracy suggests potential overfitting. - Minimal SD and variance in validation accuracy indicate good generalisation. - Quick convergence to high accuracy implies dataset suitability for the model architecture.
Dataset 2 (K-means, unlabelled data)	<ul style="list-style-type: none"> - Discrepancy between training and validation accuracy indicates potential overfitting. - Low training accuracy and poor generalisation suggest model complexity issues. - High variance in validation accuracy indicates instability.
Dataset 3 (GMM, unlabelled data)	<ul style="list-style-type: none"> - Close training and validation accuracy (less than 5%) suggest minimal overfitting. - Consistently high validation accuracy indicates good generalisation. - Slight fluctuations suggest the potential for further optimisation.
Dataset 4 (Hierarchical, unlabelled data)	<ul style="list-style-type: none"> - Moderate overfitting with consistently higher training accuracy. - Wide variation in validation accuracy indicates sensitivity to hyperparameters or dataset characteristics. - Decent validation accuracy (over 70%) despite overfitting.

In terms of overall performance, the Gaussian Mixture Model offers the most stable and promising performance, with both high training and validation accuracy. The manually labelled base CNN also shows decent performance, although slight fluctuations suggest room for improvement. Hierarchical clustering exhibits overfitting but still achieves decent validation accuracy, indicating that the model might be capturing relevant features despite the noise. K-means shows the most erratic behaviour with a significant gap between training and validation accuracy, suggesting issues with model generalisation and potential overfitting. Nevertheless, while GMM appears to be the most promising based on the provided metrics, further analysis was done regarding the data splitting performance to cross validate the initial decision for the 90/10 data split, which is 90% train data and 10% test data. Fig 7.6 shows the data split performance comparison.

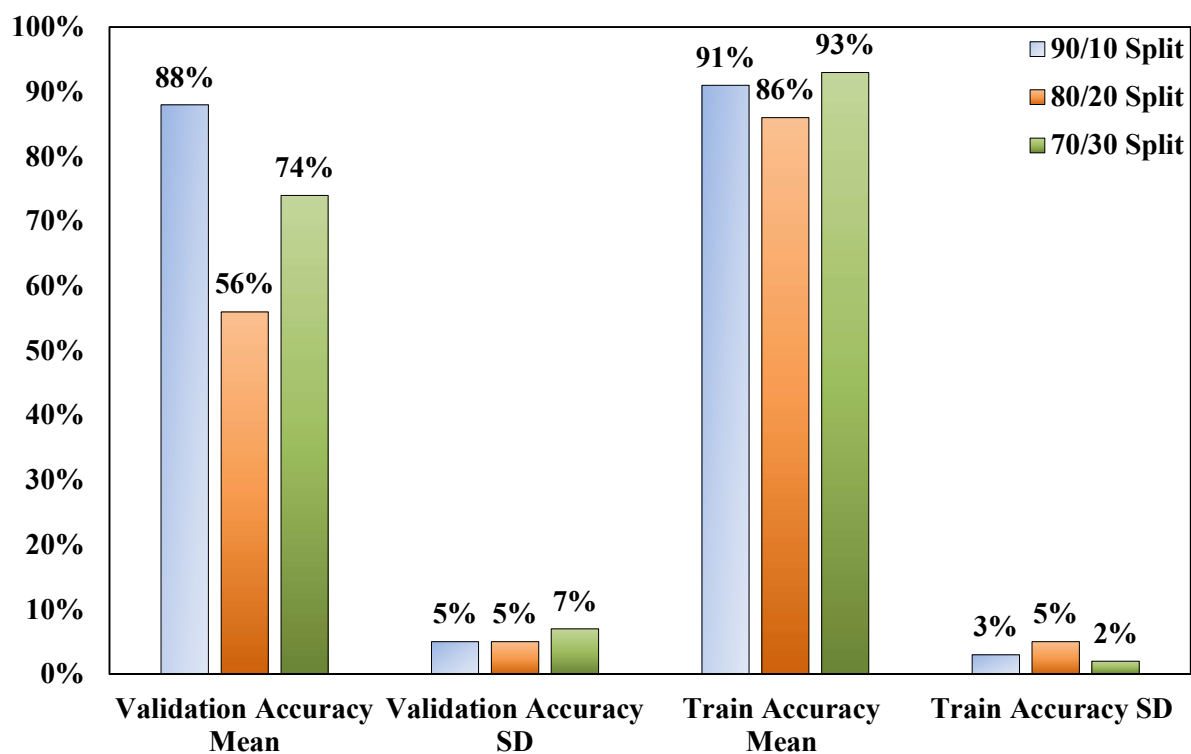


Fig. 6.6 Data split performance comparison

The data split performance comparison graph demonstrates the model's performance across three data split ratios: 90/10, 80/20, and 70/30. For the 90/10 split, the model achieves high validation accuracy (88%) with a low standard deviation (5%), alongside a strong training accuracy of 91% with minimal variation (3%), indicating stable and generalised performance. In contrast, the 80/20 split shows a significant drop in validation accuracy to 56%, though training accuracy remains reasonably high at 86%. The similar standard deviations for both

training and validation (5%) suggest increased variability and a possible struggle to generalise with a larger validation set. The 70/30 split reveals the highest training accuracy (93%), but validation accuracy dips to 74%, with a higher standard deviation of 7% for validation performance, hinting at overfitting and increased instability as the model is trained on less data.

The observed trend can be attributed to the fact that smaller validation sets (like in the 90/10 split) allow the model to be trained on more data, improving its ability to generalise while also retaining high performance in validation. However, as the validation set increases (in the 80/20 and 70/30 splits), the model has less data to train on, which can lead to overfitting or underfitting. In the case of the 80/20 split, the model might not have enough capacity to generalise well, resulting in poor validation accuracy. For the 70/30 split, overfitting could occur as the model becomes too specialised to the training set, resulting in higher training accuracy but lower validation accuracy due to poorer generalisation. Therefore, based on the results, the initial 90/10 split was justified as it provided the best balance between training and validation performance with minimal variability.

6.7 Research Impact and Limitations

The flow boiling classification developed in this research offers a highly effective method for predicting critical heat flux (CHF), a key parameter in ensuring safe and efficient thermal management in boiling systems. By employing a clustering-based Convolutional Neural Network (CNN) approach, the model can accurately classify flow regimes and detect the onset of CHF by tracing back the point of clustering separation. This feature provides an intuitive way to identify critical transition points that signal performance limits, allowing engineers to monitor these shifts in real time. Unlike conventional methods reported earlier and in Chapter 2 that rely on high-frequency data or complex imaging techniques like x-ray tomography, which require extensive computational resources and are costly, the proposed method achieves comparable accuracy using significantly less data. Traditional approaches can take several hours to process, especially when using detailed time-frequency analysis, whereas the developed pipeline reduces the entire data processing time to just a few minutes, making it highly efficient for real-time monitoring. This reduction in time and resource demand enables faster decision-making and makes it feasible to implement the technique in practical systems, providing a reliable and cost-effective solution for CHF prediction and flow monitoring.

This research significantly advances thermal management in microchannel heat sinks by addressing the challenge of flow boiling pattern recognition and streamlining inefficient data

handling. It illuminates effective classification techniques and presents practical approaches to enhance accuracy, offering invaluable insights for the industry. These findings enable the development of more efficient cooling systems and facilitate rapid, precise pattern recognition in real-world scenarios. Moreover, this quick flow boiling identification technique aligns well with agile product development principles and continuous improvement through technology, reducing the need for manual data analysis and handling.

However, it's crucial to acknowledge the limitations of this study. The reliance on a specific dataset underscores the need for additional experimental data to validate the efficacy of similar, efficient data pipeline creations and accurate flow boiling recognition. Additionally, traditional clustering algorithms, such as k-means, can be sensitive to the initial placement of cluster centres [377]. Enhancing performance through robust initialization methods like K-means++ or multiple random starts could yield more consistent and accurate clustering results. Future research should explore further comparisons to fine-tune and optimise current models, presenting a promising avenue for advancement.

In complex heat sink designs, such as those presented in Chapter 6, accurately identifying flow boiling regimes poses a significant challenge. The variability in geometries leads to the absence of a singular onset of bubble formation that can be distinctly labelled as a jet, slug, or annular regime. Instead, multiple phenomena can coincide at different locations, complicating holistic labelling. For instance, Fig. 6.7 illustrates the diverse flow boiling patterns observed across the new types of heat sinks, highlighting that various patterns emerge around different geometries. This underscores the necessity of establishing a comprehensive ground truth dataset, which remains critical for future research. Furthermore, exploring machine learning techniques capable of handling unlabelled data with minimal ground truth information presents another promising avenue for investigation. These approaches could enhance the classification of flow regimes, even without extensive labelled datasets, thereby advancing the understanding and optimisation of complex heat sinks.

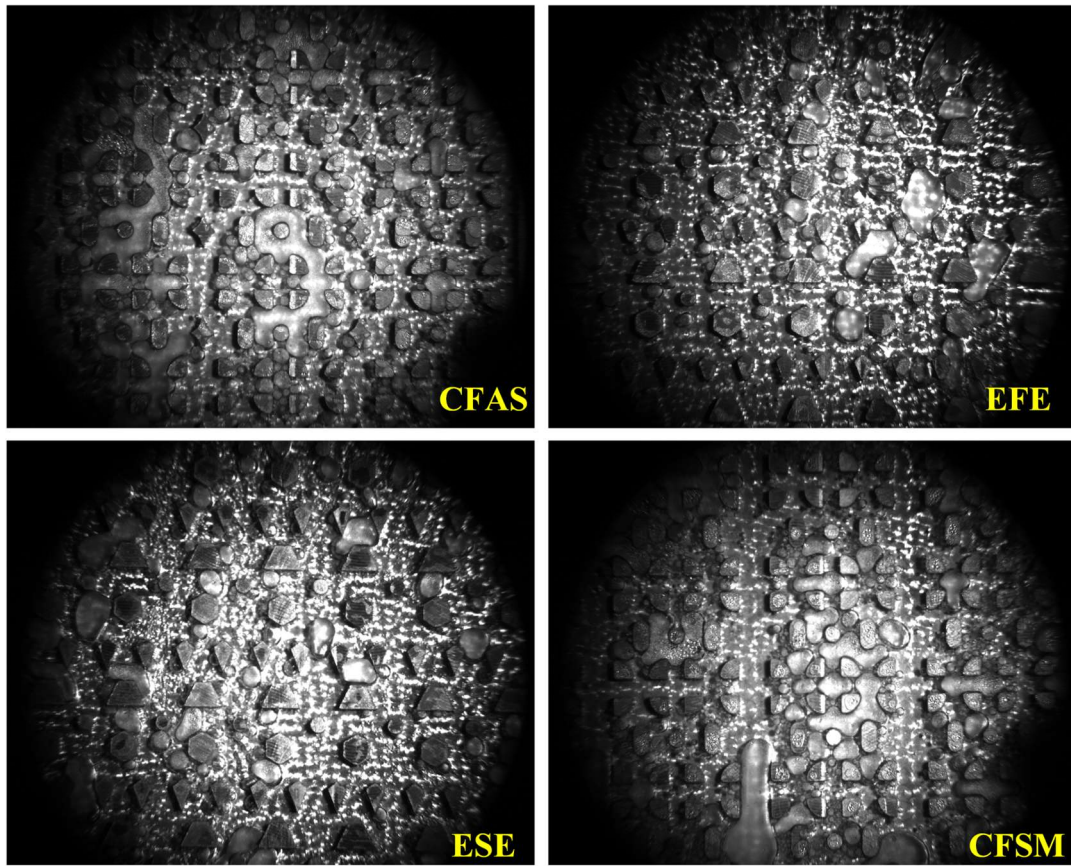


Fig. 6.7 Complex boiling patterns

6.8 Summary of Chapter

In conclusion, this research provided valuable insights into recognising flow boiling patterns within rectangular micro/mini channel heat sinks. Through systematic analysis and methodological refinement, the Gaussian Mixture Model clustering-based CNN approach demonstrated superior performance, achieving a mean accuracy of 91.4% on the training, and 88.4% on the test set, with minimal overfitting. Conversely, the K-means clustering approach exhibited the poorest performance, with a mean validation accuracy dropping as low as 62% and the highest variations, underscoring its inability to identify complex underlying patterns. Additionally, the research methodology facilitated the creation of an agile semi-automatic data pipeline, aiding accurate classification and expediting product development processes. Consequently, these findings advance the heat transfer and thermal management research space, and the study findings also provide opportunities for enhancing predictive analytics, safety protocols, and real-time monitoring in industrial settings — whilst reducing subjectivity and interpretability issues. Thus, this study laid the groundwork for further exploration and innovation in advancing thermal management practices. Future research can focus on conducting extensive comparative analyses of similar algorithms and data pipelines.

Chapter 7: Conclusion

Chapter Precursor: Arabic

“So, surely with hardship comes ease.”

فَإِنَّ مَعَ الْعُسْرِ يُسْرًا

القرآن, الانشراح ٩٤:٦

This Arabic quotation from the Holy Quran encapsulates the essence of the conclusion chapter. Facing numerous challenges—be it initial experiments that didn't yield expected outcomes, simulations that posed difficulties, or just waiting to submit my thesis—I reminded myself that perseverance through hardship leads to ease. This mindset helped me persist, ultimately achieving meaningful results and valuable insights. Additionally, engaging with my Arabic-speaking colleagues and friends provided profound perspectives that enriched the thesis, demonstrating how overcoming obstacles can lead to significant academic growth and contributions.

7.1 Advancing the Next Generation of Thermal Management Strategies

The need for effective thermal management in modern electronics has become increasingly critical due to the rapid miniaturisation and escalating power densities of devices. Conventional micro heat sink designs, such as straight and rectangular channels, face inherent limitations, including high thermal resistance, increased pressure drops, and manufacturing complexities. These issues are compounded by a lack of integration with sustainable design philosophies, which has hindered the development of next-generation micro heat sinks that can balance performance, cost, and environmental responsibility. This thesis addresses these challenges by systematically exploring bioinspired micro heat sink geometries, applying machine learning to optimise performance and process efficiency, and integrating sustainable manufacturing strategies to enhance these designs' scalability and environmental impact. The study is structured around four core research questions, each corresponding to a specific objective to overcome the limitations of conventional heat sinks to build and advance the next generation of thermal management technologies.

7.2 Summary of Key Findings

7.2.1 RQ1: What are the key recent advancements and limitations in micro heat sink technologies for heat transfer and thermal management?

Objective 1 (OB1): To comprehensively review recent advancements and limitations in micro heat sink (MCHS) technologies, identifying current gaps and opportunities in heat transfer and thermal management. This objective aims to serve as a foundational reference for newcomers to the field and a valuable resource for industry professionals seeking an updated overview of emerging trends. The key highlights are:

1. Design Opportunities: The prevalence of conventional rectangular and square channels (totalling 72%) in MCHS underscores a significant opportunity for innovation. Exploring non-conventional structures, such as pin-fin and bio-inspired geometries, can achieve performance improvements exceeding 30%, presenting a compelling case for adoption;

2. Material Considerations: A heavy reliance on materials like PLM and copper (50% combined) necessitates immediate attention to refining their thermal properties, manufacturability, and cost. There is a need to prioritise mixed-material approaches that enhance performance and identify alternatives capable of high heat transfer efficiency while minimising environmental impact;

3. Emerging Fabrication Techniques: The widespread use of micromachining, alongside the growing interest in additive manufacturing (9% of studies) for intricate geometries, marks a shift in fabrication strategies. A more focused effort is needed to integrate these methods, balancing precision and cost challenges to fully unlock the potential of these technologies for complex and novel heat sink designs;

4. Fluid Dynamics and Flow Boiling: Despite being a heavily researched area, there is still a lack of clarity on the optimal strategies for managing flow boiling dynamics. There is a need to utilise advanced working fluids (e.g., green refrigerants, stable hybrid nanofluids), introduce flow disturbances through novel geometries, and leverage surface treatments like biphilic coatings to further enhance flow boiling heat transfer effectiveness;

5. Global Research Landscape: China's substantial contribution—accounting for nearly 50% of research output in MCHS technologies—solidifies its leadership. This dominance should prompt EU countries to step up their efforts (18%), promote cross-border collaboration and remain competitive to meet the EU 2050 sustainability goals;

6. Integration of Advanced Technologies: The gradual integration of cutting-edge Industry 4.0 technologies such as machine learning and artificial intelligence is transforming the field. However, these tools must be adaptable and less data-intensive, and alternative methods are urgently needed to enhance the efficiency of the overall process. Without robust strategies to refine and integrate these technologies, the field risks lagging in meeting the evolving demands of thermal management systems while addressing sustainability and cost.

7.2.2 RQ2: What insights can experimental and numerical investigations provide into the performance of bioinspired heat sinks, and how can these findings contribute to improved thermal efficiency?

Objective 2 (OB2): To carry out investigations on bioinspired heat sinks, analysing their performance under various thermal conditions and extracting insights that contribute to improved design and heat transfer efficiency. This research question involved developing and evaluating eight novel bioinspired heat sinks—four for air-cooled systems, and four for liquid-cooled systems. The main findings are summarised as follows:

1. Significant Heat Transfer Gains: Air-cooled heat sink designs featuring a novel twisted base and extended top surface, inspired by mushrooms and scutoids, **achieved a 1.5 to 1.7 times heat transfer efficiency** compared to traditional square or rectangular pin-fin configurations. Liquid-cooled heat sink geometries inspired by cruciform flowers and

flying fish showed a **20%-30% increase in Nusselt number at lowest Re** compared to existing designs, even when combined with other techniques such as nanofluids;

2. Reduced Thermal Resistance: All bioinspired heat sinks demonstrated minimal thermal resistance, ensuring uniform temperature distribution. This performance was attributed to the optimised hybrid geometries, which enhanced heat dissipation and maintained lower temperature gradients across the surface;

3. Enhanced Flow Manipulation: Air-cooled pin-fin designs having extended pin-fin top surfaces induced turbulence and generated vortices, disrupting boundary layers and improving convective heat transfer. Liquid-cooled micro pin-fins, featuring multiple flow disruptors, facilitated the **early transition to turbulent flow** at Reynolds numbers between 300 and 400, enhancing mixing and promoting efficient heat transfer at lower flow rates;

4. Material Efficiency and Energy Consumption: The combined approach led to a 14% reduction in material usage without sacrificing performance in air-cooled systems. Moreover, both systems showed an acceptable raise in pressure drops and strategies to reduce pressure drops for future research, making these bioinspired designs suitable for sustainable heat transfer solutions.

7.2.3 RQ3: How can machine learning approaches be applied to optimise heat sink design and enhance thermal management in light of current limitations in traditional methods?

Objective 3 (OB3): To develop and apply machine learning algorithms for optimising the design and thermal performance process of micro heat sinks, addressing the limitations of traditional design methods and improving overall efficiency. The research integrated various machine learning techniques into developing micro heat sinks to enhance development efficiency, improve predictive accuracy, and reduce the need for time-intensive simulations. The key insights and contributions are summarised below:

1. Accurate Predictions for Air-Cooled Systems: The machine learning model, using ensemble learning like the bagging and stacking algorithm, predicted the heat transfer coefficient (HTC) with a Mean Absolute Percentage Error (MAPE) of 5-10% for air-cooled systems. This precision allowed for quick pre-screening of different design configurations, eliminating the need for extensive CFD simulations in the initial stages.

2. Reliable Correlation Models for Liquid-Cooled Systems: For liquid-cooled systems, Principal Component Analysis (PCA) identified the main factors affecting Nusselt number and pressure drop. **The XGBoost, polynomial regression, and random forest models achieved R^2 scores above 0.97**, resulting in new correlation equations for these bioinspired heat sinks that can be used for rapid design validation evaluations;

3. Informed Decision-Making through Data Integration: By incorporating domain knowledge, external datasets, and synthetic data, throughout the research project, the ML models produced acceptable results even with limited experimental data. This not only improved decision-making by highlighting promising designs, but it also validated the results against traditional methods, ensuring reliability and accuracy;

4. Facilitating Flow Regime Classification: A custom data pipeline was developed using a clustering-convolutional neural network (CNN) approach to classify flow boiling regimes with **over 90% prediction accuracy**. This pipeline can be built upon to enable real-time monitoring of flow patterns and provide a robust tool for predicting critical heat flux, which is essential for optimising thermal management;

5. Significant Time Savings and Enhanced Analysis: Pre-screening designs using machine learning models helped select the most promising candidates for detailed CFD simulations, reducing the overall optimisation time by 60-70%. Additionally, manual image analysis time for flow boiling regimes was decreased from around 2 hours to minutes, using the pipeline, which significantly sped up experimental analysis and enabled faster insights.

7.2.4 RQ4: How can sustainable design principles and manufacturing philosophies be integrated into developing next-generation heat sinks, ensuring performance optimisation and environmental responsibility?

Objective 4 (OB4): Objective 4 (OB4): To critically appraise and integrate sustainable design principles and manufacturing approaches into developing next-generation heat sinks, ensuring a balance between performance optimisation, cost, and environmental responsibility. The research followed a structured seven-stage development process guided by a manufacturing philosophy integration flowchart, incorporating specific philosophies at each stage:

Stage 1: Research and Design – Design Thinking and Sustainable Engineering

- Design Thinking: Enabled understanding of cooling issues and facilitated innovation via iterative prototyping, ensuring designs addressed real-world requirements.

- Sustainable Engineering: Focused on minimising the environmental impact from the beginning by selecting low-carbon footprint materials and identifying trade-offs between thermal efficiency and environmental responsibility using MEDS framework.

Stage 2-4: Prototype Development, Design Optimisation, and Production Planning

- Agile Manufacturing: Supported rapid prototyping and iterative testing, reducing the development cycle and enabling quick validation of new configurations.
- Design for Manufacturing and Assembly (DFMA): Simplified geometries, optimised assembly, and ensured compatibility with existing manufacturing lines, **reducing costs by ~43%.**
- Just-In-Time (JIT): Implemented a hybrid approach, manufacturing simpler parts in-house and outsourcing complex geometries, which reduced lead times, minimised inventory costs, and supported efficient resource allocation.

Stage 5-6: Manufacturing and Quality Assurance

- Lean Manufacturing: Identified and eliminated waste via detailed process audits, causing a 14% reduction in material usage without compromising thermal performance.
- Six Sigma: Maintained precision and dimensional accuracy for micro pin-fin structures, minimising performance variability and ensuring consistent quality.
- Total Quality Management (TQM): Fostered Continuous Improvement, using expert feedback and real-time quality checks to refine processes and ensure high standards.

Stage 7: Testing and Continuous Improvement

- Agile Manufacturing: Enabled rapid feedback loops, allowing the design to evolve quickly in response to real-time testing data.
- Green Manufacturing: Employed sustainable production methods, such as energy-efficient micromachining and eco-friendly materials, **reducing overall carbon emissions by an estimated 20% and energy consumption by approximately 30%.**
- Continuous Improvement: Integrated real-time performance data and expert feedback to refine designs, ensuring that the final heat sinks achieved an optimal balance between thermal efficiency and sustainability.

7.3 Cross-case Synthesis

This thesis employed distinct methodologies across three cases to address specific challenges in micro heat sink research, with a focus on prioritising sustainable and agile manufacturing

philosophies. The strategic application of machine learning was pivotal in reducing reliance on computational fluid dynamics (CFD), traditional experimental methods, and highly intensive dataset usage, thereby enhancing the overall efficiency of the designs and product cycle.

Chapter 4 (Case 1) explored mushroom-inspired pin-fins and scutoid geometries, utilising CFD simulations to evaluate thermal performance with air as the working fluid. While CFD provided critical insights into fluid dynamics and thermal behaviour, incorporating machine learning algorithms facilitated the development of predictive models for heat transfer coefficients (HTC) based on minimal input parameters. This shift aimed to reduce dependency on CFD, allowing for faster iterations and adaptations in design while aligning with agile manufacturing principles.

Building on the insights from Case 1, Chapter 5 (Case 2) transitioned to a stronger emphasis on experimental methods, focusing on the hydrodynamic performance of liquid-cooled micro pin-fins. This case aimed to gather crucial performance data using water as the working fluid under real-world conditions by prioritising empirical validation rather than CFD. This approach supported agile manufacturing practices and provided robust evidence of how innovative geometries perform in practical applications. Furthermore, machine learning was employed to develop new correlation models, effectively combining empirical data with predictive insights. This integration minimised reliance on CFD, traditional experimental setups, and the need for highly intensive datasets, reinforcing the applicability of the designs and heat transfer while maximising efficiency.

Chapter 6 (Case 3) advanced this progression by introducing a machine learning framework that utilised convolutional neural networks (CNNs) to classify flow boiling regimes in straight microchannels. This case also marked a methodological shift, minimising reliance on traditional analytical methods, data-intensive machine learning models, and extensive experimental data. By leveraging smarter datasets and synthesising domain knowledge with external data, it was demonstrated that high prediction accuracy could be achieved even with smaller sample sizes. This innovation enhanced operational efficiencies and real-time monitoring capabilities, illustrating how advanced analytics can effectively address the complexities of flow boiling phenomena while reducing the burden of intensive data or expensive analytical requirements.

Therefore, the cases collectively reflect a strategic progression towards minimising reliance on specific methodologies, including highly intensive dataset usage, while building on the

findings from each stage. This research not only underscores the importance of integrating machine learning and empirical validation to foster innovation in micro heat sink technologies but also advances the field of thermal management and heat transfer. By optimising the design and performance of micro heat sinks, the findings contribute to enhanced thermal efficiency, operational effectiveness, and sustainability in thermal management systems. Ultimately, this multifaceted approach represents a significant step forward in developing advanced solutions that meet the growing demands for efficient and effective heat transfer technologies.

7.4 Research Limitations and Future Recommendations

Despite the significant contributions, this research is not without limitations, which provide opportunities for further refinement and expansion. Addressing these limitations in future studies could enhance the applicability and robustness of the proposed methodologies.

- 1. Scope of Working Fluids and Boundary Conditions:** The experimental and numerical evaluations were primarily conducted using water and air as the working fluids under controlled boundary conditions. This narrow scope may not fully capture the performance variations under more complex multi-phase flow regimes, such as flow boiling or refrigerant-based systems. Extending the investigation to include diverse working fluids and dynamic conditions would provide a more comprehensive understanding of heat sink performance.
- 2. Scalability and Manufacturing Constraints:** Due to manufacturing constraints and limitations, alternative designs were explored to ensure feasibility within the scope of this research. Although the study introduced novel hybrid manufacturing strategies, challenges related to fabrication precision and scalability for mass production remained. The complex bioinspired pin-fin structures, while demonstrating excellent thermal characteristics, presented significant manufacturing challenges. These structures may require advanced techniques, such as additive manufacturing, which were not fully explored in this study. As a result, alternative design approaches were considered to balance performance with manufacturability. Future research should focus on improving the scalability of these designs, refining the fabrication processes, and maintaining the performance benefits of the bioinspired structures.
- 3. Generalisation of Machine Learning Models:** While the machine learning models used in this research achieved high accuracy for the specific dataset and geometric configurations, their generalisation capability for other types of heat sinks and

manufacturing scenarios has not been fully established. A broader dataset encompassing a wider range of designs, materials, and operating conditions is needed to validate the robustness of the predictive models.

4. **Lack of Full Life Cycle Assessment (LCA):** The sustainability analysis was limited to evaluating energy consumption, carbon emissions, and material usage. A full LCA, encompassing the environmental impact from material extraction to end-of-life recycling, was not conducted. Incorporating a complete LCA would provide deeper insights into the environmental footprint of the proposed designs.
5. **Simplification of Complex Flow Patterns:** The use of simplified flow patterns in the CFD simulations and machine learning classification models might overlook the nuances of real-world flow dynamics, particularly in turbulent or transitional flow regimes. This simplification could affect the accuracy of performance predictions under highly dynamic conditions. Future work should include more detailed turbulence models and experimental validation under varying Reynolds numbers.

7.5 Concluding Remarks and Research Impact

The research presented in this thesis contributes significantly to the fields of thermal management and micro heat sink technology by introducing novel bioinspired designs, integrating machine learning for enhanced design optimisation, and applying sustainable manufacturing philosophies. The work addresses critical limitations in traditional microchannel geometries and provides a comprehensive framework for the development of next-generation thermal management systems that are both efficient and sustainable. The impact of this research extends beyond academic contributions, offering practical solutions for industries that require advanced cooling technologies. The major impacts on industry and research domains are highlighted in the following sections.

7.5.1 Innovation in Bioinspired Geometries

Developing hybrid bioinspired pin-fin heat sinks establishes a new paradigm for heat sink design by moving away from conventional geometries and embracing nature-inspired structures. The unique configurations demonstrated significant performance improvements in both air-cooled and liquid-cooled systems, **achieving up to 70% higher heat transfer performance compared to traditional designs.** These findings can be leveraged in sectors

such as high-performance electronics cooling, automotive thermal management, and renewable energy systems, where efficient heat dissipation is critical.

7.5.2 Application of Machine Learning for Design and Development:

By integrating machine learning models into the design process, this research demonstrated how data-driven techniques can enhance the efficiency and accuracy of thermal performance predictions. The ability to quickly identify optimal designs using smaller datasets and minimal computational resources is a transformative approach that can shorten development cycles and reduce costs. This methodology directly applies to industries seeking to implement rapid prototyping and agile product development, offering a scalable solution for complex designs.

7.5.3 Sustainability Integration in High-Performance Cooling Solutions:

The adoption of sustainable design and manufacturing philosophies, such as Lean, JIT, and Agile, showcased the feasibility of achieving high thermal efficiency while minimising environmental impact. The research demonstrated that it is possible to balance performance with sustainability, achieving significant reductions in production costs, energy usage, and carbon emissions. This has implications for companies aiming to align with Industry 4.0 and environmental regulations, providing a practical model for sustainable production in the field of thermal management.

7.5.4 Framework for Next-Generation Thermal Management Systems

The comprehensive framework developed in this thesis—spanning bioinspired geometries, machine learning integration, and sustainable manufacturing—can serve as a blueprint for future research and development in thermal management technologies. By combining innovative design methodologies with robust validation techniques, this research sets a new standard for creating heat sink systems that are adaptable, efficient, and environmentally responsible. This can inspire further research into more complex multi-phase cooling systems and smart materials for adaptive thermal control, pushing the boundaries of what is achievable in thermal management.

7.5.5 Overall Impact

The research's Knowledge Contribution Areas—spanning Design, Application, Development, and Research—demonstrate a holistic approach to advancing micro heat sink technologies. The innovative bioinspired designs, integration of machine learning for HTC predictions, sustainable manufacturing practices, and application of agile concepts ensure that this work is

academically robust and highly applicable to industries aiming to improve thermal performance while meeting sustainability goals. This multi-disciplinary framework offers a comprehensive toolkit for designing and optimising next-generation thermal management solutions, bridging the gap between research and scalable practical industrial implementation. Fig. 7.1 summarises the key research and knowledge contributions of this PhD Thesis.

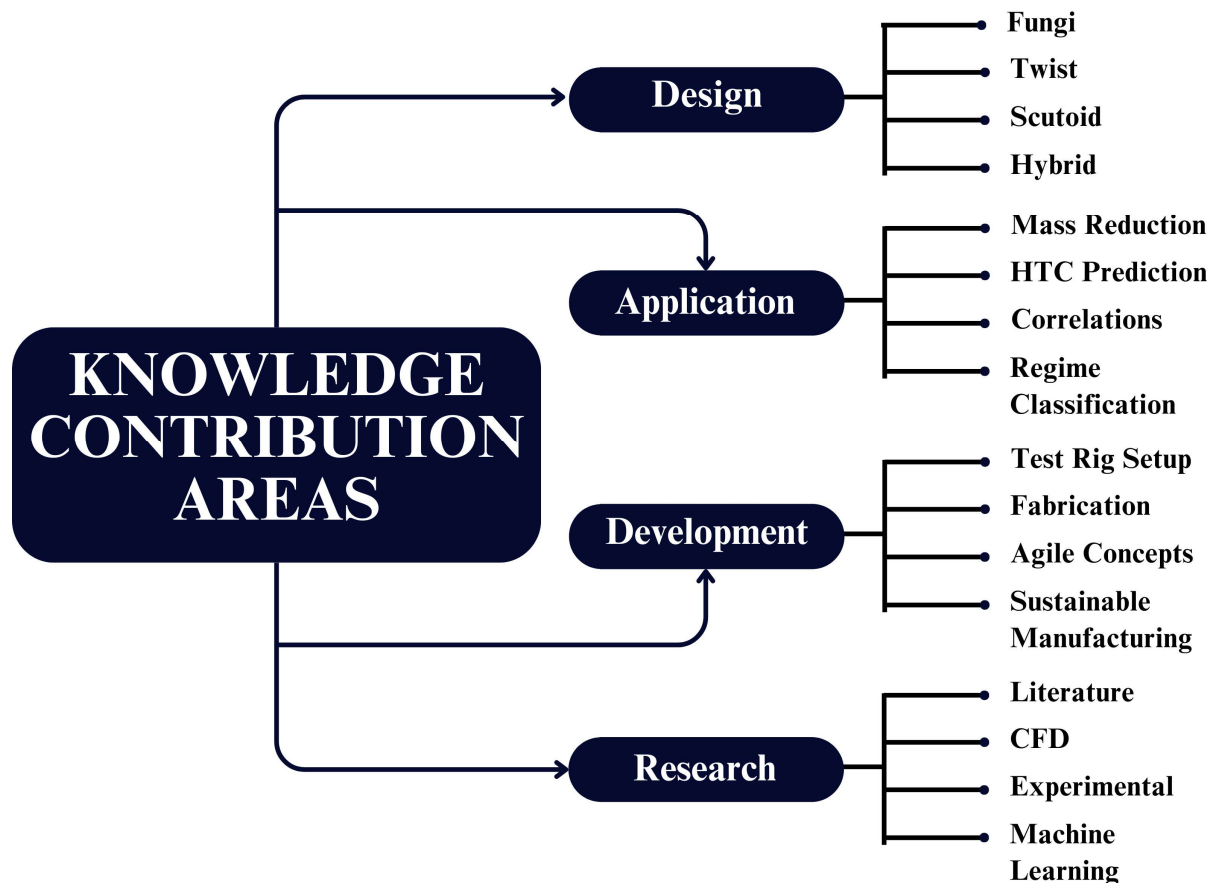


Fig. 7.1 Summary of knowledge contributions arising from this research

References

- [1] Statista, Consumer Electronics, Technology & Telecommunications (2024). <https://www.statista.com/markets/418/topic/485/consumer-electronics/#overview> (accessed September 26, 2024).
- [2] A. Datta, D. Sanyal, A. Agrawal, A.K. Das, A review of liquid flow and heat transfer in microchannels with emphasis to electronic cooling, *Sādhanā* 44 (2019) 234. <https://doi.org/10.1007/s12046-019-1201-2>.
- [3] B. Parizad Benam, A.K. Sadaghiani, V. Yağcı, M. Parlak, K. Sefiane, A. Koşar, Review on high heat flux flow boiling of refrigerants and water for electronics cooling, *International Journal of Heat and Mass Transfer* 180 (2021) 121787. <https://doi.org/10.1016/j.ijheatmasstransfer.2021.121787>.
- [4] Z. He, Y. Yan, Z. Zhang, Thermal management and temperature uniformity enhancement of electronic devices by micro heat sinks: A review, *Energy* 216 (2021) 119223. <https://doi.org/10.1016/j.energy.2020.119223>.
- [5] B. Chang, T. Yuan, Y. Wang, H. Guo, Z. Li, L. Zhao, C. Zhang, S. Peng, J. Deng, Cooling performance enhancement of electric vehicle film capacitor for ultra-high temperatures using micro-channel cold plates thermal management system, *International Journal of Heat and Mass Transfer* 233 (2024) 126037. <https://doi.org/10.1016/j.ijheatmasstransfer.2024.126037>.
- [6] D.B. Tuckerman, R.F.W. Pease, Z. Guo, J.E. Hu, O. Yildirim, G. Deane, L. Wood, Microchannel Heat Transfer: Early History, Commercial Applications, and Emerging Opportunities, in: *ASME 2011 9th International Conference on Nanochannels, Microchannels, and Minichannels*, Volume 2, ASMEDC, Edmonton, Alberta, Canada, 2011: pp. 739–756. <https://doi.org/10.1115/ICNMM2011-58308>.
- [7] M. Ghassemi, A. Shahidian, *Nano and Bio Heat Transfer and Fluid Flow*, Academic Press, 2017.
- [8] M. Harris, H. Wu, A. Angelopoulou, W. Zhang, Z. Hu, Y. Xie, Heat transfer optimisation using novel biomorphic pin-fin heat sinks: An integrated approach via design for manufacturing, numerical simulation, and machine learning, *Thermal Science and Engineering Progress* 51 (2024) 102606. <https://doi.org/10.1016/j.tsep.2024.102606>.
- [9] L. Du, W. Hu, An overview of heat transfer enhancement methods in microchannel heat sinks, *Chemical Engineering Science* 280 (2023) 119081. <https://doi.org/10.1016/j.ces.2023.119081>.
- [10] M. Harris, H. Wu, W. Zhang, A. Angelopoulou, Overview of recent trends in microchannels for heat transfer and thermal management applications, *Chemical Engineering and Processing - Process Intensification* 181 (2022) 109155. <https://doi.org/10.1016/j.cep.2022.109155>.
- [11] B. Dash, J. Nanda, S.K. Rout, The role of microchannel geometry selection on heat transfer enhancement in heat sinks: A review, *Heat Transfer* 51 (2022) 1406–1424. <https://doi.org/10.1002/htj.22357>.
- [12] R.S.J. Tol, Europe's Climate Target for 2050: An Assessment, *Intereconomics* 56 (2021) 330–335. <https://doi.org/10.1007/s10272-021-1012-7>.
- [13] The European Green Deal - European Commission, (2021).

https://commission.europa.eu/strategy-and-policy/priorities-2019-2024/european-green-deal_en (accessed September 26, 2024).

- [14] P. Bhandari, K.S. Rawat, Y.K. Prajapati, D. Padalia, L. Ranakoti, T. Singh, Design modifications in micro pin fin configuration of microchannel heat sink for single phase liquid flow: A review, *Journal of Energy Storage* 66 (2023) 107548. <https://doi.org/10.1016/j.est.2023.107548>.
- [15] C.A. Mack, Fifty Years of Moore's Law, *IEEE Transactions on Semiconductor Manufacturing* 24 (2011) 202–207. <https://doi.org/10.1109/TSM.2010.2096437>.
- [16] M. Ahmadian-Elmi, A. Mashayekhi, S.S. Nourazar, K. Vafai, A comprehensive study on parametric optimization of the pin-fin heat sink to improve its thermal and hydraulic characteristics, *International Journal of Heat and Mass Transfer* 180 (2021) 121797. <https://doi.org/10.1016/j.ijheatmasstransfer.2021.121797>.
- [17] M. Mohammadilooy, B. Parizad Benam, A. Ateş, V. Yagcı, M. Çaglar Malyemez, M. Parlak, A. Sadaghiani, A. Koşar, Multiple hot spot cooling with flow boiling of HFE-7000 in a multichannel pin fin heat sink, *Applied Thermal Engineering* (2024) 123077. <https://doi.org/10.1016/j.applthermaleng.2024.123077>.
- [18] M.W. Alam, S. Bhattacharyya, B. Souayeh, K. Dey, F. Hammami, M. Rahimi-Gorji, R. Biswas, CPU heat sink cooling by triangular shape micro-pin-fin: Numerical study, *International Communications in Heat and Mass Transfer* 112 (2020) 104455. <https://doi.org/10.1016/j.icheatmasstransfer.2019.104455>.
- [19] J. Ning, X. Wang, H. Huang, S. Wang, W. Yan, Topology optimized novel additively manufactured heat sink: Experiments and numerical simulations, *Energy Conversion and Management* 286 (2023) 117024. <https://doi.org/10.1016/j.enconman.2023.117024>.
- [20] G. Chen, X. Jiang, Y. Li, J. Bai, S. Waqar Ali Shah, Y. Gao, Y. Tang, S. Zhang, C. Pan, A highly efficient and sustainable heat sink via liquid film boiling in hybrid mesh with active liquid supply, *Energy Conversion and Management* 277 (2023) 116688. <https://doi.org/10.1016/j.enconman.2023.116688>.
- [21] N. Van Toan, K. Ito, T.T.K. Tuoi, M. Toda, P.-H. Chen, M.F.M. Sabri, J. Li, T. Ono, Micro-heat sink based on silicon nanowires formed by metal-assisted chemical etching for heat dissipation enhancement to improve performance of micro-thermoelectric generator, *Energy Conversion and Management* 267 (2022) 115923. <https://doi.org/10.1016/j.enconman.2022.115923>.
- [22] J. Lin, X. Liu, S. Li, C. Zhang, S. Yang, A review on recent progress, challenges and perspective of battery thermal management system, *International Journal of Heat and Mass Transfer* 167 (2021) 120834. <https://doi.org/10.1016/j.ijheatmasstransfer.2020.120834>.
- [23] B. Yu, Z. Lu, B. Wang, X. Wang, J. Lou, L. Yang, W. Li, A bioinspired programmable Self-Organization approach for designing additively manufactured heat sinks, *Energy Conversion and Management* 286 (2023) 116996. <https://doi.org/10.1016/j.enconman.2023.116996>.
- [24] K. Nilpueng, M. Mesgarpour, L.G. Asirvatham, A.S. Dalkılıç, H.S. Ahn, O. Mahian, S. Wongwises, Effect of pin fin configuration on thermal performance of plate pin fin heat sinks, *Case Studies in Thermal Engineering* 27 (2021) 101269. <https://doi.org/10.1016/j.csite.2021.101269>.

- [25] J. Jaseliūnaitė, M. Šeporaitis, Performance optimisation of microchannel pin-fins using 2D CFD, *Applied Thermal Engineering* 206 (2022) 118040. <https://doi.org/10.1016/j.applthermaleng.2022.118040>.
- [26] R. Singupuram, T. Alam, M.A. Ali, S. Shaik, N.K. Gupta, N. Akkurt, M. Kumar, S.M. Eldin, D. Dobrotă, Numerical analysis of heat transfer and fluid flow in microchannel heat sinks for thermal management, *Case Studies in Thermal Engineering* 45 (2023) 102964. <https://doi.org/10.1016/j.csite.2023.102964>.
- [27] W.M.A.A. Japar, N.A.C. Sidik, R. Saidur, Y. Asako, S.N.A. Yusof, A review of passive methods in microchannel heat sink application through advanced geometric structure and nanofluids: Current advancements and challenges, *Nanotechnology Reviews* 9 (2020) 1192–1216. <https://doi.org/10.1515/ntrev-2020-0094>.
- [28] A. Taheri, M. Ghasemian Moghadam, M. Mohammadi, M. Passandideh-Fard, M. Sardarabadi, A new design of liquid-cooled heat sink by altering the heat sink heat pipe application: Experimental approach and prediction via artificial neural network, *Energy Conversion and Management* 206 (2020) 112485. <https://doi.org/10.1016/j.enconman.2020.112485>.
- [29] V.Y.S. Lee, T.G. Karayiannis, Influence of system pressure on flow boiling in microchannels, *International Journal of Heat and Mass Transfer* 215 (2023) 124470. <https://doi.org/10.1016/j.ijheatmasstransfer.2023.124470>.
- [30] B. Yang, X. Zhu, B. Wei, M. Liu, Y. Li, Z. Lv, F. Wang, Computer Vision and Machine Learning Methods for Heat Transfer and Fluid Flow in Complex Structural Microchannels: A Review, *Energies* 16 (2023) 1500. <https://doi.org/10.3390/en16031500>.
- [31] M. Harris, A. Angelopoulou, H. Wu, W. Zhang, Comparative Analysis of Micro/Minichannel Flow Boiling Pattern Recognition and Classification using Clustering Algorithms, in: *IEEE 14th International Conference on Pattern Recognition Systems*, Institute of Electrical and Electronics Engineers (IEEE), 2024. <https://researchprofiles.herts.ac.uk/en/publications/comparative-analysis-of-microminichannel-flow-boiling-pattern-rec> (accessed August 14, 2024).
- [32] M.A.A. Rehmani, S.A. Jaywant, K.M. Arif, Study of Microchannels Fabricated Using Desktop Fused Deposition Modeling Systems, *Micromachines* 12 (2021) 14. <https://doi.org/10.3390/mi12010014>.
- [33] W. Wan, D. Deng, Q. Huang, T. Zeng, Y. Huang, Experimental study and optimization of pin fin shapes in flow boiling of micro pin fin heat sinks, *Applied Thermal Engineering* 114 (2017) 436–449. <https://doi.org/10.1016/j.applthermaleng.2016.11.182>.
- [34] H.E. Ahmed, B.H. Salman, A.Sh. Kherbeet, M.I. Ahmed, Optimization of thermal design of heat sinks: A review, *International Journal of Heat and Mass Transfer* 118 (2018) 129–153. <https://doi.org/10.1016/j.ijheatmasstransfer.2017.10.099>.
- [35] J. Gao, Z. Hu, Q. Yang, X. Liang, H. Wu, Fluid flow and heat transfer in microchannel heat sinks: Modelling review and recent progress, *Thermal Science and Engineering Progress* 29 (2022) 101203. <https://doi.org/10.1016/j.tsep.2022.101203>.
- [36] H. Ehsani, F.N. Roudbari, S.S. Namaghi, p. Jalili, D.D. Ganji, Investigating thermal performance enhancement in perforated pin fin arrays for cooling electronic systems through integrated CFD and deep learning analysis, *Results in Engineering* 22 (2024) 102016. <https://doi.org/10.1016/j.rineng.2024.102016>.

- [37] E.M. Mihalko, A. Basak, Optimizing thermal performance of pin-fin arrays using Bayesian methods for turbine cooling, *International Journal of Heat and Mass Transfer* 225 (2024) 125355. <https://doi.org/10.1016/j.ijheatmasstransfer.2024.125355>.
- [38] A. Sikirica, L. Grbčić, L. Kranjčević, Machine learning based surrogate models for microchannel heat sink optimization, *Applied Thermal Engineering* 222 (2023) 119917. <https://doi.org/10.1016/j.applthermaleng.2022.119917>.
- [39] P. Farrell, F. Sherratt, A. Richardson, *Writing Built Environment Dissertations and Projects: Practical Guidance and Examples*, John Wiley & Sons, 2016.
- [40] G.P. Peterson, Heat Transfer Fundamentals, in: *Mechanical Engineers' Handbook*, John Wiley & Sons, Ltd, 2015: pp. 1–64. <https://doi.org/10.1002/9781118985960.meh405>.
- [41] O.A. Ezekoye, Conduction of Heat in Solids, in: M.J. Hurley, D. Gottuk, J.R. Hall, K. Harada, E. Kuligowski, M. Puchovsky, J. Torero, J.M. Watts, C. Wiecezorek (Eds.), *SFPE Handbook of Fire Protection Engineering*, Springer, New York, NY, 2016: pp. 25–52. https://doi.org/10.1007/978-1-4939-2565-0_2.
- [42] D.M. Gates, Conduction and Convection, in: D.M. Gates (Ed.), *Biophysical Ecology*, Springer, New York, NY, 1980: pp. 268–306. https://doi.org/10.1007/978-1-4612-6024-0_9.
- [43] G.B. Arfken, D.F. Griffing, D.C. Kelly, J. Priest, chapter 23 - HEAT TRANSFER, in: G.B. Arfken, D.F. Griffing, D.C. Kelly, J. Priest (Eds.), *International Edition University Physics*, Academic Press, 1984: pp. 430–443. <https://doi.org/10.1016/B978-0-12-059858-8.50028-5>.
- [44] H. Babar, H. Wu, W. Zhang, Investigating the performance of conventional and hydrophobic surface heat sink in managing thermal challenges of high heat generating components, *International Journal of Heat and Mass Transfer* 216 (2023) 124604. <https://doi.org/10.1016/j.ijheatmasstransfer.2023.124604>.
- [45] H. Ma, Z. Duan, X. Ning, L. Su, Numerical investigation on heat transfer behavior of thermally developing flow inside rectangular microchannels, *Case Studies in Thermal Engineering* 24 (2021) 100856. <https://doi.org/10.1016/j.csite.2021.100856>.
- [46] S. Nukiyama, The maximum and minimum values of the heat Q transmitted from metal to boiling water under atmospheric pressure, *International Journal of Heat and Mass Transfer* 9 (1966) 1419–1433. [https://doi.org/10.1016/0017-9310\(66\)90138-4](https://doi.org/10.1016/0017-9310(66)90138-4).
- [47] M.C. Vlachou, J.S. Lioumbas, T.D. Karapantsios, HEAT TRANSFER ENHANCEMENT IN BOILING OVER MODIFIED SURFACES: A CRITICAL REVIEW, *IPHT* 3 (2015). <https://doi.org/10.1615/InterfacPhenomHeatTransfer.2016014133>.
- [48] S.K. Singh, D. Sharma, Review of pool and flow boiling heat transfer enhancement through surface modification, *International Journal of Heat and Mass Transfer* 181 (2021) 122020. <https://doi.org/10.1016/j.ijheatmasstransfer.2021.122020>.
- [49] B. Stutz, M. Lallemand, F. Raimbault, J. Passos, Nucleate and transition boiling in narrow horizontal spaces, *Heat Mass Transfer* 45 (2009) 929–935. <https://doi.org/10.1007/s00231-007-0325-9>.
- [50] S.G. Kandlikar, Fundamental issues related to flow boiling in minichannels and microchannels, *Experimental Thermal and Fluid Science* 26 (2002) 389–407. [https://doi.org/10.1016/S0894-1777\(02\)00150-4](https://doi.org/10.1016/S0894-1777(02)00150-4).
- [51] M. Shojaeian, A. Koşar, Pool boiling and flow boiling on micro- and nanostructured

- surfaces, *Experimental Thermal and Fluid Science* 63 (2015) 45–73. <https://doi.org/10.1016/j.expthermflusci.2014.12.016>.
- [52] L.S. Tong, BOILING CRISIS AND CRITICAL HEAT FLUX., Westinghouse Electric Corp., Pittsburgh, Pa., 1972. <https://doi.org/10.2172/4629988>.
- [53] V.S. Devahdhanush, I. Mudawar, Review of Critical Heat Flux (CHF) in Jet Impingement Boiling, *International Journal of Heat and Mass Transfer* 169 (2021) 120893. <https://doi.org/10.1016/j.ijheatmasstransfer.2020.120893>.
- [54] V. Talari, P. Behar, Y. Lu, E. Haryadi, D. Liu, Leidenfrost drops on micro/nanostructured surfaces, *Front. Energy* 12 (2018) 22–42. <https://doi.org/10.1007/s11708-018-0541-7>.
- [55] M.W. Nazar, N. Iqbal, M. Ali, H. Nazir, M.Z.B. Amjad, Thermal management of Li-ion battery by using active and passive cooling method, *Journal of Energy Storage* 61 (2023) 106800. <https://doi.org/10.1016/j.est.2023.106800>.
- [56] K. Xiong, T. Yang, Z. Sun, C. Ma, J. Wang, X. Ge, W. Qiao, L. Ling, Modified graphene film powder scraps for re-preparation of highly thermally conductive flexible graphite heat spreaders, *Carbon* 219 (2024) 118827. <https://doi.org/10.1016/j.carbon.2024.118827>.
- [57] H.M. Ali, A. Arshad, M. Jabbal, P.G. Verdin, Thermal management of electronics devices with PCMs filled pin-fin heat sinks: A comparison, *International Journal of Heat and Mass Transfer* 117 (2018) 1199–1204. <https://doi.org/10.1016/j.ijheatmasstransfer.2017.10.065>.
- [58] T.C. Werner, Y. Yan, T. Karayiannis, V. Pickert, R. Wrobel, R. Law, Medium temperature heat pipes – Applications, challenges and future direction, *Applied Thermal Engineering* 236 (2024) 121371. <https://doi.org/10.1016/j.applthermaleng.2023.121371>.
- [59] Y. Zhao, Z. Liu, Z. Quan, M. Yang, J. Shi, W. Zhang, Thermal management and multi-objective optimization of an air-cooled heat sink based on flat miniature-heat-pipe arrays, *J Therm Anal Calorim* 149 (2024) 2443–2462. <https://doi.org/10.1007/s10973-023-12799-6>.
- [60] H. Wang, Y. Gan, R. Li, F. Liu, Y. Li, Experimental study on the thermal performance of a liquid-cooled heat sink integrating heat pipes for dual CPU servers, *Applied Thermal Engineering* 236 (2024) 121851. <https://doi.org/10.1016/j.applthermaleng.2023.121851>.
- [61] L. Zhou, F. Meng, Y. Sun, Numerical study on infrared detectors cooling by multi-stage thermoelectric cooler combined with microchannel heat sink, *Applied Thermal Engineering* 236 (2024) 121788. <https://doi.org/10.1016/j.applthermaleng.2023.121788>.
- [62] K. Iranshahi, T. Defraeye, R.M. Rossi, U.C. Müller, Electrohydrodynamics and its applications: Recent advances and future perspectives, *International Journal of Heat and Mass Transfer* 232 (2024) 125895. <https://doi.org/10.1016/j.ijheatmasstransfer.2024.125895>.
- [63] W. Dong, X. Zhang, B. Liu, B. Wang, Y. Fang, Research progress on passive enhanced heat transfer technology in microchannel heat sink, *International Journal of Heat and Mass Transfer* 220 (2024) 125001. <https://doi.org/10.1016/j.ijheatmasstransfer.2023.125001>.
- [64] G. Narendran, N. Gnanasekaran, D.A. Perumal, A Review on Recent Advances in Microchannel Heat Sink Configurations, *MENG* 11 (2018) 190–215. <https://doi.org/10.2174/2212797611666180726124047>.

- [65] S.S. Bhosale, A.R. Acharya, Review on Applications of Micro Channel Heat Exchanger, *International Research Journal of Engineering and Technology* 07 (2020) 4.
- [66] R.J. Trent, *Strategic Supply Management: Creating the Next Source of Competitive Advantage*, J. Ross Publishing, 2007.
- [67] M. Harris, M. Ndiaye, P. Farrell, Integration of Industry 4.0 and Internet of Things in the Automotive and Motorsports Sectors: An Empirical Analysis, *SAE Technical Papers* 5079 (2020) 1–12. <https://doi.org/10.4271/2020-01-5079>.
- [68] Sample Size Calculator: Understanding Sample Sizes, SurveyMonkey (n.d.). <https://www.surveymonkey.com/mp/sample-size-calculator/> (accessed March 28, 2022).
- [69] R.F. Fellows, A.M.M. Liu, *Research Methods for Construction*, 4th ed., Wiley, London, 2015.
- [70] E. Chiriac, A.M. Bran, C. Voitincu, C. Balan, Experimental Validation of VOF Method in Microchannel Flows, in: *2021 12th International Symposium on Advanced Topics in Electrical Engineering (ATEE)*, IEEE, Bucharest, Romania, 2021: pp. 1–4. <https://doi.org/10.1109/ATEE52255.2021.9425121>.
- [71] C.H. Hoang, S. Rangarajan, S. Khalili, B. Ramakrisnan, V. Radmard, Y. Hadad, S. Schiffres, B. Sammakia, Hybrid microchannel/multi-jet two-phase heat sink: A benchmark and geometry optimization study of commercial product, *International Journal of Heat and Mass Transfer* 169 (2021) 120920. <https://doi.org/10.1016/j.ijheatmasstransfer.2021.120920>.
- [72] S. Mukherjee, I. Mudawar, Pumpless Loop for Narrow Channel and Micro-Channel Boiling, *Journal of Electronic Packaging* 125 (2003) 431–441. <https://doi.org/10.1115/1.1602708>.
- [73] A.S. Dalkılıç, C. Özman, K. Sakamatapan, S. Wongwises, Experimental investigation on the flow boiling of R134a in a multi-microchannel heat sink, *International Communications in Heat and Mass Transfer* 91 (2018) 125–137. <https://doi.org/10.1016/j.icheatmasstransfer.2017.12.008>.
- [74] W. Guo, A.J.T. Teo, A.M. Gañán-Calvo, C. Song, N.-T. Nguyen, H.-D. Xi, S.H. Tan, Pressure-Driven Filling of Closed-End Microchannel: Realization of Comb-Shaped Transducers for Acoustofluidics, *Phys. Rev. Applied* 10 (2018) 054045. <https://doi.org/10.1103/PhysRevApplied.10.054045>.
- [75] H.A. Abdulbari, F.W.M. Ling, Z. Hassan, H.J. Thin, Experimental investigations on biopolymer in enhancing the liquid flow in microchannel, *Adv Polym Technol* 37 (2018) 3136–3145. <https://doi.org/10.1002/adv.22084>.
- [76] E. Chiriac, M. Avram, C. Balan, Investigation of Multiphase Flow in a Trifurcation Microchannel—A Benchmark Problem, *Micromachines* 13 (2022) 974. <https://doi.org/10.3390/mi13060974>.
- [77] M.M. Sarafriz, M. Arjomandi, Thermal performance analysis of a microchannel heat sink cooling with copper oxide-indium (CuO/In) nano-suspensions at high-temperatures, *Applied Thermal Engineering* 137 (2018) 700–709. <https://doi.org/10.1016/j.applthermaleng.2018.04.024>.
- [78] H.E. Ahmed, M.I. Ahmed, I.M.F. Seder, B.H. Salman, Experimental investigation for sequential triangular double-layered microchannel heat sink with nanofluids, *International Communications in Heat and Mass Transfer* 77 (2016) 104–115.

- <https://doi.org/10.1016/j.icheatmasstransfer.2016.06.010>.
- [79] C. Anbumeenakshi, M.R. Thansekhar, On the effectiveness of a nanofluid cooled microchannel heat sink under non-uniform heating condition, *Applied Thermal Engineering* 113 (2017) 1437–1443. <https://doi.org/10.1016/j.applthermaleng.2016.11.144>.
 - [80] V.A. Martínez, D.A. Vasco, C.M. García-Herrera, R. Ortega-Aguilera, Numerical study of TiO₂-based nanofluids flow in microchannel heat sinks: Effect of the Reynolds number and the microchannel height, *Applied Thermal Engineering* 161 (2019) 114130. <https://doi.org/10.1016/j.applthermaleng.2019.114130>.
 - [81] M. Ding, C. Liu, Z. Rao, Experimental investigation on heat transfer characteristic of TiO₂-H₂O nanofluid in microchannel for thermal energy storage, *Applied Thermal Engineering* 160 (2019) 114024. <https://doi.org/10.1016/j.applthermaleng.2019.114024>.
 - [82] M.M. Sarafraz, M. Arjomandi, Demonstration of plausible application of gallium nano-suspension in microchannel solar thermal receiver: Experimental assessment of thermo-hydraulic performance of microchannel, *International Communications in Heat and Mass Transfer* 94 (2018) 39–46. <https://doi.org/10.1016/j.icheatmasstransfer.2018.03.013>.
 - [83] M.M. Sarafraz, V. Nikkhah, M. Nakhjavani, A. Arya, Thermal performance of a heat sink microchannel working with biologically produced silver-water nanofluid: Experimental assessment, *Experimental Thermal and Fluid Science* 91 (2018) 509–519. <https://doi.org/10.1016/j.expthermflusci.2017.11.007>.
 - [84] M.M. Sarafraz, V. Nikkhah, M. Nakhjavani, A. Arya, Fouling formation and thermal performance of aqueous carbon nanotube nanofluid in a heat sink with rectangular parallel microchannel, *Applied Thermal Engineering* 123 (2017) 29–39. <https://doi.org/10.1016/j.applthermaleng.2017.05.056>.
 - [85] E. Şimşek, S. Coskun, T. Okutucu-Özyurt, H.E. Unalan, Heat transfer enhancement by silver nanowire suspensions in microchannel heat sinks, *International Journal of Thermal Sciences* 123 (2018) 1–13. <https://doi.org/10.1016/j.ijthermalsci.2017.08.021>.
 - [86] Y. Wang, W. Li, C. Qi, J. Yu, Thermal management of electronic components based on hierarchical microchannels and nanofluids, *Thermal Science and Engineering Progress* 42 (2023) 101910. <https://doi.org/10.1016/j.tsep.2023.101910>.
 - [87] V.E. Ahmadi, A. Aboubakri, A.K. Sadaghiani, K. Sefiane, A. Koşar, Effect of Functional Surfaces with Gradient Mixed Wettability on Flow Boiling in a High Aspect Ratio Microchannel, *Fluids* 5 (2020) 239. <https://doi.org/10.3390/fluids5040239>.
 - [88] W. Zhang, Y. Chai, J. Xu, G. Liu, Y. Sun, 3D heterogeneous wetting microchannel surfaces for boiling heat transfer enhancement, *Applied Surface Science* 457 (2018) 891–901. <https://doi.org/10.1016/j.apsusc.2018.07.021>.
 - [89] K.-Y. Law, Definitions for Hydrophilicity, Hydrophobicity, and Superhydrophobicity: Getting the Basics Right, *J. Phys. Chem. Lett.* 5 (2014) 686–688. <https://doi.org/10.1021/jz402762h>.
 - [90] Y. Yin, X. Zhang, C. Zhu, T. Fu, Y. Ma, Formation characteristics of Taylor bubbles in a T-junction microchannel with chemical absorption, *Chinese Journal of Chemical Engineering* (2021) S1004954121002627. <https://doi.org/10.1016/j.cjche.2021.06.002>.
 - [91] M. Venegas, N. García-Hernando, M. de Vega, Experimental evaluation of a membrane-based microchannel desorber operating at low desorption temperatures, *Applied Thermal*

- Engineering 167 (2020) 114781. <https://doi.org/10.1016/j.applthermaleng.2019.114781>.
- [92] P. Jayaramu, S. Gedupudi, S.K. Das, Influence of heating surface characteristics on flow boiling in a copper microchannel: Experimental investigation and assessment of correlations, *International Journal of Heat and Mass Transfer* 128 (2019) 290–318. <https://doi.org/10.1016/j.ijheatmasstransfer.2018.08.075>.
- [93] E. Roumpea, N.M. Kovalchuk, M. Chinaud, E. Nowak, M.J.H. Simmons, P. Angeli, Experimental studies on droplet formation in a flow-focusing microchannel in the presence of surfactants, *Chemical Engineering Science* 195 (2019) 507–518. <https://doi.org/10.1016/j.ces.2018.09.049>.
- [94] C.P. Liang, F. Ture, Y.J. Dai, R.Z. Wang, T.S. Ge, Experimental investigation on performance of desiccant coated microchannel heat exchangers under condensation conditions, *Energy and Buildings* 231 (2021) 110622. <https://doi.org/10.1016/j.enbuild.2020.110622>.
- [95] X. Jiang, S. Waqar Ali Shah, J. Liu, Y. Li, S. Zhang, Z. Wang, C. Pan, Design of micro-nano structures for counter flow diverging microchannel heat sink with extraordinarily high energy efficiency, *Applied Thermal Engineering* 209 (2022) 118229. <https://doi.org/10.1016/j.applthermaleng.2022.118229>.
- [96] S.R. Kumar, S. Singh, Experimental Study on Microchannel with Addition of Microinserts Aiming Heat Transfer Performance Improvement, *Water* 14 (2022) 3291. <https://doi.org/10.3390/w14203291>.
- [97] H. Wang, Y. Yang, Y. Wang, C.Y.H. Chao, H. Qiu, Effects of non-wetting fraction and pitch distance in flow boiling heat transfer in a wettability-patterned microchannel, *International Journal of Heat and Mass Transfer* 190 (2022) 122753. <https://doi.org/10.1016/j.ijheatmasstransfer.2022.122753>.
- [98] X. Zhang, R. Tiwari, A.H. Shooshtari, M.M. Ohadi, An additively manufactured metallic manifold-microchannel heat exchanger for high temperature applications, *Applied Thermal Engineering* 143 (2018) 899–908. <https://doi.org/10.1016/j.applthermaleng.2018.08.032>.
- [99] W.C. Yameen, N.A. Piascik, R.C. Clemente, A.K. Miller, S.A. Niknam, J. Benner, A.D. Santamaria, M. Mortazavi, Experimental Characterization of a Manifold-Microchannel Heat Exchanger Fabricated Based on Additive Manufacturing, in: 2019 18th IEEE Intersociety Conference on Thermal and Thermomechanical Phenomena in Electronic Systems (ITherm), IEEE, Las Vegas, NV, USA, 2019: pp. 621–625. <https://doi.org/10.1109/ITHERM.2019.8757306>.
- [100] D.G. Bae, R.K. Mandel, S.V. Dessiatoun, S. Rajgopal, S.P. Roberts, M. Mehregany, M.M. Ohadi, Embedded two-phase cooling of high heat flux electronics on silicon carbide (SiC) using thin-film evaporation and an enhanced delivery system (FEEDS) manifold-microchannel cooler, in: 2017 16th IEEE Intersociety Conference on Thermal and Thermomechanical Phenomena in Electronic Systems (ITherm), IEEE, Orlando, FL, 2017: pp. 466–472. <https://doi.org/10.1109/ITHERM.2017.7992511>.
- [101] N. Mohammad, C. Chukwudoro, S. Bepari, O. Basha, S. Aravamudhan, D. Kuila, Scale-up of high-pressure F-T synthesis in 3D printed stainless steel microchannel microreactors: Experiments and modeling, *Catalysis Today* 397–399 (2022) 182–196. <https://doi.org/10.1016/j.cattod.2021.09.038>.

- [102] Q. Lv, T. Yan, Y. Feng, H. Huang, J. Qin, Experimental and numerical study of flow boiling heat transfer characteristics in rectangular groove-wall microchannels, *International Journal of Heat and Mass Transfer* 220 (2024) 124999. <https://doi.org/10.1016/j.ijheatmasstransfer.2023.124999>.
- [103] L.S. Tong, Y.S. Tang, Flow Boiling, in: *Boiling Heat Transfer and Two-Phase Flow*, Routledge, 1997.
- [104] C.E. Okon, A. Turan, Flow boiling heat transfer characteristics using the modified eulerian and wall heat balance model, *Heat Mass Transfer* 56 (2020) 2425–2443. <https://doi.org/10.1007/s00231-020-02854-5>.
- [105] J. Wang, J. Wang, J. Li, N. Liu, Pressure drop of R134a and R1234ze(E) flow boiling in microchannel arrays with single- and double-side heating, *International Journal of Heat and Mass Transfer* 161 (2020) 120241. <https://doi.org/10.1016/j.ijheatmasstransfer.2020.120241>.
- [106] K. Panda, T. Hirokawa, L. Huang, Design study of microchannel heat exchanger headers using experimentally validated multiphase flow CFD simulation, *Applied Thermal Engineering* 178 (2020) 115585. <https://doi.org/10.1016/j.applthermaleng.2020.115585>.
- [107] G. Xia, Y. Lv, D. Ma, Y. Jia, Experimental investigation of the continuous two-phase instable boiling in microchannels with triangular corrugations and prediction for instable boundaries, *Applied Thermal Engineering* 162 (2019) 114251. <https://doi.org/10.1016/j.applthermaleng.2019.114251>.
- [108] Y.T. Jia, G.D. Xia, L.X. Zong, D.D. Ma, Y.X. Tang, A comparative study of experimental flow boiling heat transfer and pressure drop characteristics in porous-wall microchannel heat sink, *International Journal of Heat and Mass Transfer* 127 (2018) 818–833. <https://doi.org/10.1016/j.ijheatmasstransfer.2018.06.090>.
- [109] Y. Lin, Y. Luo, W. Li, J. Li, Z. Sun, Y. Cao, W.J. Minkowycz, Numerical study of flow reversal during bubble growth and confinement of flow boiling in microchannels, *International Journal of Heat and Mass Transfer* 177 (2021) 121491. <https://doi.org/10.1016/j.ijheatmasstransfer.2021.121491>.
- [110] G. Oudebrouckx, D. Nieder, T. Vandenryt, S. Bormans, H. Möbius, R. Thoelen, Single element thermal sensor for measuring thermal conductivity and flow rate inside a microchannel, *Sensors and Actuators A: Physical* 331 (2021) 112906. <https://doi.org/10.1016/j.sna.2021.112906>.
- [111] Y. Li, Y. Yao, H. Wu, Experimental investigation of flow boiling characteristics in counter-flow microchannels with different mass flux distributions, *International Journal of Heat and Mass Transfer* 190 (2022) 122768. <https://doi.org/10.1016/j.ijheatmasstransfer.2022.122768>.
- [112] J. Tang, Y. Liu, B. Huang, D. Xu, Enhanced heat transfer coefficient of flow boiling in microchannels through expansion areas, *International Journal of Thermal Sciences* 177 (2022) 107573. <https://doi.org/10.1016/j.ijthermalsci.2022.107573>.
- [113] B.E. Rapp, *Microfluidics: Modeling, Mechanics and Mathematics*, William Andrew, 2016.
- [114] M. Habibi Matin, S. Moghaddam, Mechanism of transition from elongated bubbles to wavy-annular regime in flow boiling through microchannels, *International Journal of*

- Heat and Mass Transfer 176 (2021) 121464. <https://doi.org/10.1016/j.ijheatmasstransfer.2021.121464>.
- [115] L. Lei, Y. Zhao, W. Chen, H. Li, X. Wang, J. Zhang, Experimental Studies of Droplet Formation Process and Length for Liquid–Liquid Two-Phase Flows in a Microchannel, *Energies* 14 (2021) 1341. <https://doi.org/10.3390/en14051341>.
- [116] F. Ronshin, E. Chinnov, Experimental characterization of two-phase flow patterns in a slit microchannel, *Experimental Thermal and Fluid Science* 103 (2019) 262–273. <https://doi.org/10.1016/j.expthermflusci.2019.01.022>.
- [117] J. Qian, M. Chen, Z. Wu, Z. Jin, B. Sunden, Effects of a Dynamic Injection Flow Rate on Slug Generation in a Cross-Junction Square Microchannel, *Processes* 7 (2019) 765. <https://doi.org/10.3390/pr7100765>.
- [118] C. Zhang, C. Shen, Y. Chen, Experimental study on flow condensation of mixture in a hydrophobic microchannel, *International Journal of Heat and Mass Transfer* 104 (2017) 1135–1144. <https://doi.org/10.1016/j.ijheatmasstransfer.2016.09.029>.
- [119] A.V. Kovalev, A.A. Yagodnitsyna, A.V. Bilsky, Flow hydrodynamics of immiscible liquids with low viscosity ratio in a rectangular microchannel with T-junction, *Chemical Engineering Journal* 352 (2018) 120–132. <https://doi.org/10.1016/j.cej.2018.07.013>.
- [120] P. Pontes, I. Gonçalves, M. Andredaki, A. Georgoulas, A.L.N. Moreira, A.S. Moita, Fluid flow and heat transfer in microchannel devices for cooling applications: Experimental and numerical approaches, *Applied Thermal Engineering* 218 (2023) 119358. <https://doi.org/10.1016/j.applthermaleng.2022.119358>.
- [121] C. Wang, M. Tian, G. Zhang, J. Zhang, Experimental analysis on the heat transfer performance of gas-liquid Taylor flow in a square microchannel, *Applied Thermal Engineering* 228 (2023) 120537. <https://doi.org/10.1016/j.applthermaleng.2023.120537>.
- [122] A. Kravtsova, P. Ianko, Y. Meshalkin, A. Bilsky, Influence of external periodic perturbation on the flow in T-microchannel, in: Novosibirsk, Russia, 2018: p. 040084. <https://doi.org/10.1063/1.5065358>.
- [123] R. Garg, A. Agrawal, Delay of subsonic choking in slip regime by structured roughness in microchannel, *Physics of Fluids* 32 (2020) 052002. <https://doi.org/10.1063/5.0004855>.
- [124] V. Bertram, Chapter 2 - Propellers, in: V. Bertram (Ed.), *Practical Ship Hydrodynamics* (Second Edition), Butterworth-Heinemann, Oxford, 2012: pp. 41–72. <https://doi.org/10.1016/B978-0-08-097150-6.10002-8>.
- [125] R. Garg, A. Agrawal, Poiseuille number behavior in an adiabatically choked microchannel in the slip regime, *Physics of Fluids* 32 (2020) 112002. <https://doi.org/10.1063/5.0023929>.
- [126] T. Wang, Q. Ni, N. Crane, R. Guldiken, Surface acoustic wave based pumping in a microchannel, *Microsyst Technol* 23 (2017) 1335–1342. <https://doi.org/10.1007/s00542-016-2880-9>.
- [127] Y. Ji, J. Bellettre, A. Montillet, P. Massoli, Fast oil-in-water emulsification in microchannel using head-on impinging configuration: Effect of swirl motion, *International Journal of Multiphase Flow* 131 (2020) 103402. <https://doi.org/10.1016/j.ijmultiphaseflow.2020.103402>.
- [128] Q. Jin, Z. Yin, Q. Dai, Numerical and experimental study of feedforward and feedback control for microchannel cooling system, *International Journal of Thermal Sciences* 179

- (2022) 107643. <https://doi.org/10.1016/j.ijthermalsci.2022.107643>.
- [129] I. Al Siyabi, S. Khanna, S. Sundaram, T. Mallick, Experimental and Numerical Thermal Analysis of Multi-Layered Microchannel Heat Sink for Concentrating Photovoltaic Application, *Energies* 12 (2018) 122. <https://doi.org/10.3390/en12010122>.
- [130] I. Al Siyabi, K. Shanks, T. Mallick, S. Sundaram, Indoor and outdoor characterization of concentrating photovoltaic attached to multi-layered microchannel heat sink, *Solar Energy* 202 (2020) 55–72. <https://doi.org/10.1016/j.solener.2020.03.101>.
- [131] Y. Zhai, G. Xia, Z. Li, H. Wang, Experimental investigation and empirical correlations of single and laminar convective heat transfer in microchannel heat sinks, *Experimental Thermal and Fluid Science* 83 (2017) 207–214. <https://doi.org/10.1016/j.expthermflusci.2017.01.005>.
- [132] Z. Tian, Z. Huang, S. Xu, K. Li, W. Gao, Direct liquid cooling heat transfer in microchannel: Experimental results and correlations assessment, *Applied Thermal Engineering* 223 (2023) 120020. <https://doi.org/10.1016/j.applthermaleng.2023.120020>.
- [133] J.C. Han, S. Ou, J.S. Park, C.K. Lei, Augmented heat transfer in rectangular channels of narrow aspect ratios with rib turbulators, *International Journal of Heat and Mass Transfer* 32 (1989) 1619–1630. [https://doi.org/10.1016/0017-9310\(89\)90044-6](https://doi.org/10.1016/0017-9310(89)90044-6).
- [134] M.R. Özdemir, M.M. Mahmoud, T.G. Karayiannis, Flow Boiling of Water in a Rectangular Metallic Microchannel, *Heat Transfer Engineering* 42 (2021) 492–516. <https://doi.org/10.1080/01457632.2019.1707390>.
- [135] Y. Luo, W. Li, K. Zhou, K. Sheng, S. Shao, Z. Zhang, J. Du, W.J. Minkowycz, Three-dimensional numerical simulation of saturated annular flow boiling in a narrow rectangular microchannel, *International Journal of Heat and Mass Transfer* 149 (2020) 119246. <https://doi.org/10.1016/j.ijheatmasstransfer.2019.119246>.
- [136] W. Li, Z. Chen, J. Li, K. Sheng, J. Zhu, Subcooled flow boiling on hydrophilic and super-hydrophilic surfaces in microchannel under different orientations, *International Journal of Heat and Mass Transfer* 129 (2019) 635–649. <https://doi.org/10.1016/j.ijheatmasstransfer.2018.10.003>.
- [137] W. Li, Y. Lin, K. Zhou, J. Li, J. Zhu, Local heat transfer of saturated flow boiling in vertical narrow microchannel, *International Journal of Thermal Sciences* 145 (2019) 105996. <https://doi.org/10.1016/j.ijthermalsci.2019.105996>.
- [138] V.S. Duryodhan, R. Chatterjee, S. Govind Singh, A. Agrawal, Mixing in planar spiral microchannel, *Experimental Thermal and Fluid Science* 89 (2017) 119–127. <https://doi.org/10.1016/j.expthermflusci.2017.07.024>.
- [139] L. Yin, R. Xu, P. Jiang, H. Cai, L. Jia, Subcooled flow boiling of water in a large aspect ratio microchannel, *International Journal of Heat and Mass Transfer* 112 (2017) 1081–1089. <https://doi.org/10.1016/j.ijheatmasstransfer.2017.05.028>.
- [140] X. Cheng, Y. Yao, H. Wu, An experimental investigation of flow boiling characteristics in silicon-based groove-wall microchannels with different structural parameters, *International Journal of Heat and Mass Transfer* 168 (2021) 120843. <https://doi.org/10.1016/j.ijheatmasstransfer.2020.120843>.
- [141] P. Cui, Z. Liu, Experimental study on flow boiling in ultrahigh-aspect-ratio copper microchannel heat sink, *Applied Thermal Engineering* 223 (2023) 119975. <https://doi.org/10.1016/j.applthermaleng.2023.119975>.

- [142] G. Marseglia, M.G. De Giorgi, D.S. Carvalho, P. Pontes, R.R. Souza, A.L.N. Moreira, A.S. Moita, Experimental investigation on the effects of the geometry of microchannels based heat sinks on the flow boiling of HFE-7100, *Applied Thermal Engineering* 236 (2024) 121479. <https://doi.org/10.1016/j.applthermaleng.2023.121479>.
- [143] A. Abdo, T. Saito, S. Ookawara, A. Radwan, M. Ahmed, Experimental study of the performance of concentrator photovoltaic/thermoelectric generator system integrated with a new 3D printed microchannel heat sink, *Int J Energy Res* 45 (2021) 7741–7763. <https://doi.org/10.1002/er.6359>.
- [144] H. Ringkai, K.F. Tamrin, N.A. Sheikh, S. Mohamaddan, Evolution of Water-in-Oil Droplets in T-Junction Microchannel by Micro-PIV, *Applied Sciences* 11 (2021) 5289. <https://doi.org/10.3390/app11115289>.
- [145] R. Vinoth, B. Sachuthanathan, Flow and heat transfer behavior of hybrid nanofluid through microchannel with two different channels, *International Communications in Heat and Mass Transfer* 123 (2021) 105194. <https://doi.org/10.1016/j.icheatmasstransfer.2021.105194>.
- [146] T. Hou, Y. Chen, Pressure drop and heat transfer performance of microchannel heat exchanger with different reentrant cavities, *Chemical Engineering and Processing - Process Intensification* 153 (2020) 107931. <https://doi.org/10.1016/j.cep.2020.107931>.
- [147] X. Ye, T. Hao, Y. Chen, X. Ma, R. Jiang, Liquid film transport around Taylor bubble in a microchannel with gas cavities, *Chemical Engineering and Processing - Process Intensification* 148 (2020) 107828. <https://doi.org/10.1016/j.cep.2020.107828>.
- [148] D. Nadaraja, N. Kamaruzaman, U. Abidin, M. Sies, Experimental Study on the Effect of Multilayer Microchannel, *Journal of Advanced Research in Fluid Mechanics and Thermal Sciences* 57 (2019) 23–31.
- [149] Y. Li, G. Xia, Y. Jia, Y. Cheng, J. Wang, Experimental investigation of flow boiling performance in microchannels with and without triangular cavities – A comparative study, *International Journal of Heat and Mass Transfer* 108 (2017) 1511–1526. <https://doi.org/10.1016/j.ijheatmasstransfer.2017.01.011>.
- [150] R. Vinoth, D. Senthil Kumar, Channel cross section effect on heat transfer performance of oblique finned microchannel heat sink, *International Communications in Heat and Mass Transfer* 87 (2017) 270–276. <https://doi.org/10.1016/j.icheatmasstransfer.2017.03.016>.
- [151] A. Walunj, A. Sathyabhama, Comparative study of pool boiling heat transfer from various microchannel geometries, *Applied Thermal Engineering* 128 (2018) 672–683. <https://doi.org/10.1016/j.applthermaleng.2017.08.157>.
- [152] X. Ge, X. Huang, S. Huang, H. Zhang, X. Wang, C. Ye, T. Qiu, K. Xu, Enhanced solvent extraction in a serial converging-diverging microchannel at high injection ratio, *Chemical Engineering Science* 259 (2022) 117845. <https://doi.org/10.1016/j.ces.2022.117845>.
- [153] Y. Li, H. Wu, Y. Yao, Enhanced flow boiling heat transfer and suppressed boiling instability in counter-flow stepped microchannels, *International Journal of Heat and Mass Transfer* 194 (2022) 123025. <https://doi.org/10.1016/j.ijheatmasstransfer.2022.123025>.
- [154] Q. Han, Z. Liu, C. Zhang, W. Li, Enhanced single-phase and flow boiling heat transfer performance in saw-tooth copper microchannels with high L/D_h ratio, *Applied Thermal Engineering* 236 (2024) 121478. <https://doi.org/10.1016/j.applthermaleng.2023.121478>.

- [155] C. Liu, J. Zhou, K. Cheng, Q. Zhao, M. Lu, X. Chen, Flow thermohydraulic characterization of open diverging microchannel heat sink for high heat flux dissipation, *Applied Thermal Engineering* 227 (2023) 120396. <https://doi.org/10.1016/j.applthermaleng.2023.120396>.
- [156] Y. Saffar, D.S. Nobes, R. Sabbagh, Experimental Investigation of the Motion and Deformation of Droplets in Curved Microchannel, *Ind. Eng. Chem. Res.* 62 (2023) 17275–17286. <https://doi.org/10.1021/acs.iecr.3c01623>.
- [157] Y. Wang, J. Yu, C. Qi, W. Zhang, L. Liang, Secondary vortex drag reduction and heat transfer enhancement of nanofluids in hierarchical microchannels applied to thermal management of electronic components, *Applied Thermal Engineering* 236 (2024) 121588. <https://doi.org/10.1016/j.applthermaleng.2023.121588>.
- [158] A. Haghighinia, S.M. Tabatabaei, S. Movahedirad, A novel geometrically-hybrid microchannel for performance enhancement in mass transfer: Description of Lyapunov exponent and Poincaré map, *International Journal of Heat and Mass Transfer* 165 (2021) 120700. <https://doi.org/10.1016/j.ijheatmasstransfer.2020.120700>.
- [159] S.K. Oudah, R. Fang, A. Tikadar, A.S. Salman, J.A. Khan, An experimental investigation of the effect of multiple inlet restrictors on the heat transfer and pressure drop in a flow boiling microchannel heat sink, *International Journal of Heat and Mass Transfer* 153 (2020) 119582. <https://doi.org/10.1016/j.ijheatmasstransfer.2020.119582>.
- [160] P. Kumar, Numerical investigation of fluid flow and heat transfer in trapezoidal microchannel with groove structure, *International Journal of Thermal Sciences* 136 (2019) 33–43. <https://doi.org/10.1016/j.ijthermalsci.2018.10.006>.
- [161] D.D. Ma, G.D. Xia, L.X. Zong, Y.T. Jia, Y.X. Tang, R.P. Zhi, Experimental investigation of flow boiling heat transfer performance in zigzag microchannel heat sink for electronic cooling devices, *International Journal of Thermal Sciences* 145 (2019) 106003. <https://doi.org/10.1016/j.ijthermalsci.2019.106003>.
- [162] M. Pan, H. Wang, Y. Zhong, M. Hu, X. Zhou, G. Dong, P. Huang, Experimental investigation of the heat transfer performance of microchannel heat exchangers with fan-shaped cavities, *International Journal of Heat and Mass Transfer* 134 (2019) 1199–1208. <https://doi.org/10.1016/j.ijheatmasstransfer.2019.01.140>.
- [163] G. Wang, N. Qian, G. Ding, Heat transfer enhancement in microchannel heat sink with bidirectional rib, *International Journal of Heat and Mass Transfer* 136 (2019) 597–609. <https://doi.org/10.1016/j.ijheatmasstransfer.2019.02.018>.
- [164] S.A. Memon, S. Akhtar, T.A. Cheema, C.W. Park, Investigation of the hydrothermal phenomena in a wavy microchannel with secondary flow passages through mid-wall inflection points, *Applied Thermal Engineering* 223 (2023) 120010. <https://doi.org/10.1016/j.applthermaleng.2023.120010>.
- [165] M.W. Sulaiman, C.-C. Wang, Effect of contraction on the convective boiling heat transfer of microchannel heat sinks, *Applied Thermal Engineering* 223 (2023) 120026. <https://doi.org/10.1016/j.applthermaleng.2023.120026>.
- [166] W.-R. Liao, L.-H. Chien, M. Ghalambaz, W.-M. Yan, Experimental study of boiling heat transfer in a microchannel with nucleated-shape columnar micro-pin-fins, *International Communications in Heat and Mass Transfer* 108 (2019) 104277. <https://doi.org/10.1016/j.icheatmasstransfer.2019.104277>.

- [167] R. Tiwari, R.S. Andhare, A. Shooshtari, M. Ohadi, Development of an additive manufacturing-enabled compact manifold microchannel heat exchanger, *Applied Thermal Engineering* 147 (2019) 781–788. <https://doi.org/10.1016/j.applthermaleng.2018.10.122>.
- [168] Y. Wang, J.-H. Shin, C. Woodcock, X. Yu, Y. Peles, Experimental and numerical study about local heat transfer in a microchannel with a pin fin, *International Journal of Heat and Mass Transfer* 121 (2018) 534–546. <https://doi.org/10.1016/j.ijheatmasstransfer.2018.01.034>.
- [169] R. Vinoth, B. Sachuthanathan, A. Vadivel, S. Balakrishnan, A.G.S. Raj, Heat transfer enhancement in oblique finned curved microchannel using hybrid nanofluid, *International Journal of Thermal Sciences* 183 (2023) 107848. <https://doi.org/10.1016/j.ijthermalsci.2022.107848>.
- [170] F. Zhang, B. Wu, B. Du, Heat transfer optimization based on finned microchannel heat sink, *International Journal of Thermal Sciences* 172 (2022) 107357. <https://doi.org/10.1016/j.ijthermalsci.2021.107357>.
- [171] K. Fu, W. Gao, X. Xu, X. Liang, Flow boiling heat transfer and pressure drop characteristics of water in a copper foam fin microchannel heat sink, *Applied Thermal Engineering* 218 (2023) 119295. <https://doi.org/10.1016/j.applthermaleng.2022.119295>.
- [172] Y. Lin, Y. Luo, J. Li, W. Li, Heat transfer, pressure drop and flow patterns of flow boiling on heterogeneous wetting surface in a vertical narrow microchannel, *International Journal of Heat and Mass Transfer* 172 (2021) 121158. <https://doi.org/10.1016/j.ijheatmasstransfer.2021.121158>.
- [173] X. Li, Y. Huang, Z. Wu, H. Gu, X. Chen, High conversion hydrogen peroxide microchannel reactors: Design and two-phase flow instability investigation, *Chemical Engineering Journal* 422 (2021) 130080. <https://doi.org/10.1016/j.cej.2021.130080>.
- [174] M. Bhattacharjee, M. Soni, P. Escobedo, R. Dahiya, PEDOT:PSS Microchannel-Based Highly Sensitive Stretchable Strain Sensor, *Adv. Electron. Mater.* 6 (2020) 2000445. <https://doi.org/10.1002/aelm.202000445>.
- [175] S.S. Kumar, G. Kumaraguruparan, Experimental investigation and development of miniature microchannel condenser-based personal cooling system for firefighters, *J Braz. Soc. Mech. Sci. Eng.* 45 (2023) 422. <https://doi.org/10.1007/s40430-023-04324-5>.
- [176] Z. Huang, Y. Hwang, R. Radermacher, Review of nature-inspired heat exchanger technology, *International Journal of Refrigeration* 78 (2017) 1–17. <https://doi.org/10.1016/j.ijrefrig.2017.03.006>.
- [177] Y. Yan, H. Yan, S. Yin, L. Zhang, L. Li, Single/multi-objective optimizations on hydraulic and thermal management in micro-channel heat sink with bionic Y-shaped fractal network by genetic algorithm coupled with numerical simulation, *International Journal of Heat and Mass Transfer* 129 (2019) 468–479. <https://doi.org/10.1016/j.ijheatmasstransfer.2018.09.120>.
- [178] S. Ford, M. Despeisse, Additive manufacturing and sustainability: an exploratory study of the advantages and challenges, *Journal of Cleaner Production* 137 (2016) 1573–1587. <https://doi.org/10.1016/j.jclepro.2016.04.150>.
- [179] R. Saidur, K.Y. Leong, H.A. Mohammed, A review on applications and challenges of nanofluids, *Renewable and Sustainable Energy Reviews* 15 (2011) 1646–1668.

- <https://doi.org/10.1016/j.rser.2010.11.035>.
- [180] Z. Qi, Y. Zheng, J. Wei, X. Yu, X. Jia, J. Liu, L. Chen, J. Miao, C. Li, Surface treatment of an applied novel all-diamond microchannel heat sink for heat transfer performance enhancement, *Applied Thermal Engineering* 177 (2020) 115489. <https://doi.org/10.1016/j.applthermaleng.2020.115489>.
 - [181] B. Shen, M. Yamada, S. Hidaka, J. Liu, J. Shiomi, G. Amberg, M. Do-Quang, M. Kohno, K. Takahashi, Y. Takata, Early Onset of Nucleate Boiling on Gas-covered Biphilic Surfaces, *Sci Rep* 7 (2017) 2036. <https://doi.org/10.1038/s41598-017-02163-8>.
 - [182] S.H. Kim, G.C. Lee, J.Y. Kang, K. Moriyama, H.S. Park, M.H. Kim, The role of surface energy in heterogeneous bubble growth on ideal surface, *International Journal of Heat and Mass Transfer* 108 (2017) 1901–1909. <https://doi.org/10.1016/j.ijheatmasstransfer.2016.10.005>.
 - [183] A.H. Al-Zaidi, M.M. Mahmoud, T.G. Karayiannis, Effect of aspect ratio on flow boiling characteristics in microchannels, *International Journal of Heat and Mass Transfer* 164 (2021) 120587. <https://doi.org/10.1016/j.ijheatmasstransfer.2020.120587>.
 - [184] E. Martin, A. Valeije, F. Sastre, A. Velazquez, Impact of Channels Aspect Ratio on the Heat Transfer in Finned Heat Sinks with Tip Clearance, *Micromachines* 13 (2022) 599. <https://doi.org/10.3390/mi13040599>.
 - [185] X. Ma, X. Ji, J. Wang, X. Yang, Y. Zhang, J. Wei, Flow boiling instability and pressure drop characteristics based on micro-pin-finned surfaces in a microchannel heat sink, *International Journal of Heat and Mass Transfer* 195 (2022) 123168. <https://doi.org/10.1016/j.ijheatmasstransfer.2022.123168>.
 - [186] B. Markal, B. Kul, M. Avci, R. Varol, Effect of gradually expanding flow passages on flow boiling of micro pin fin heat sinks, *International Journal of Heat and Mass Transfer* 197 (2022) 123355. <https://doi.org/10.1016/j.ijheatmasstransfer.2022.123355>.
 - [187] D. Kesavan, R. Senthil Kumar, P. Marimuthu, Heat transfer performance of air-cooled pin–fin heatsinks: a review, *J Therm Anal Calorim* 148 (2023) 623–649. <https://doi.org/10.1007/s10973-022-11691-z>.
 - [188] D. Panda, S. Dilip Saraf, K.M. Gangawane, Expanded graphite nanoparticles-based eutectic phase change materials for enhancement of thermal efficiency of pin–fin heat sink arrangement, *Thermal Science and Engineering Progress* 48 (2024) 102417. <https://doi.org/10.1016/j.tsep.2024.102417>.
 - [189] F. Hadi, H.M. Ali, Z. Khattak, M.M. Janjua, An evaluation of heat transfer and pressure drop performance of superhydrophobic surfaced integral mini-channel heat sinks with nanofluids, *J Therm Anal Calorim* 149 (2024) 1515–1533. <https://doi.org/10.1007/s10973-023-12735-8>.
 - [190] V. Safari, B. Kamkari, N. Hewitt, K. Hooman, Experimental comparative study on thermal performance of latent heat storage tanks with pin, perforated, and rectangular fins at different orientations, *Thermal Science and Engineering Progress* 48 (2024) 102401. <https://doi.org/10.1016/j.tsep.2024.102401>.
 - [191] A. Ateş, V. Yağcı, M.Ç. Malyemez, M. Parlak, A. Sadaghiani, A. Koşar, Flow dynamics characteristics of flow boiling in minichannels with distributed pin fin structures, *International Journal of Thermal Sciences* 199 (2024) 108912. <https://doi.org/10.1016/j.ijthermalsci.2024.108912>.

- [192] A. Shahsavari, H. Ghazizade-Ahsaei, I.B. Askari, M.M. Rashidi, The numerical analysis in heat transfer, fluid flow, and irreversibility of a pin-fin heatsink under the ultrasonic vibration with different transducer power assignment scenarios, *Thermal Science and Engineering Progress* 49 (2024) 102480. <https://doi.org/10.1016/j.tsep.2024.102480>.
- [193] A. Alkhazaleh, F. Alnaimat, B. Mathew, Characterization of MEMS heat sinks having straight microchannels integrating square pin-fins for liquid cooling of microelectronic chips, *Thermal Science and Engineering Progress* 45 (2023) 102154. <https://doi.org/10.1016/j.tsep.2023.102154>.
- [194] T. İzci, M. Koz, A. Koşar, The Effect of Micro Pin-Fin Shape on Thermal and Hydraulic Performance of Micro Pin-Fin Heat Sinks, *Heat Transfer Engineering* 36 (2015) 1447–1457. <https://doi.org/10.1080/01457632.2015.1010921>.
- [195] S.E. Razavi, B. Osanloo, R. Sajedi, Application of splitter plate on the modification of hydro-thermal behavior of PPFHS, *Applied Thermal Engineering* 80 (2015) 97–108. <https://doi.org/10.1016/j.applthermaleng.2015.01.046>.
- [196] R. Sajedi, B. Osanloo, F. Talati, M. Taghilou, Splitter plate application on the circular and square pin fin heat sinks, *Microelectronics Reliability* 62 (2016) 91–101. <https://doi.org/10.1016/j.microrel.2016.03.026>.
- [197] V. Yadav, K. Baghel, R. Kumar, S.T. Kadam, Numerical investigation of heat transfer in extended surface microchannels, *International Journal of Heat and Mass Transfer* 93 (2016) 612–622. <https://doi.org/10.1016/j.ijheatmasstransfer.2015.10.023>.
- [198] J. Xie, H. Yan, B. Sundén, G. Xie, The influences of sidewall proximity on flow and thermal performance of a microchannel with large-row pin-fins, *International Journal of Thermal Sciences* 140 (2019) 8–19. <https://doi.org/10.1016/j.ijthermalsci.2019.02.031>.
- [199] Y. Wang, K. Zhu, Z. Cui, J. Wei, Effects of the location of the inlet and outlet on heat transfer performance in pin fin CPU heat sink, *Applied Thermal Engineering* 151 (2019) 506–513. <https://doi.org/10.1016/j.applthermaleng.2019.02.030>.
- [200] V. Saravanan, D. Hithaish, C.K. Umesh, K. Seetharamu, Numerical investigation of thermo-hydrodynamic performance of triangular pin fin heat sink using nano-fluids, *Thermal Science and Engineering Progress* 21 (2021) 100768. <https://doi.org/10.1016/j.tsep.2020.100768>.
- [201] D. Hithaish, V. Saravanan, C.K. Umesh, K.N. Seetharamu, Thermal management of Electronics: Numerical investigation of triangular finned heat sink, *Thermal Science and Engineering Progress* 30 (2022) 101246. <https://doi.org/10.1016/j.tsep.2022.101246>.
- [202] J. Zhao, S. Huang, L. Gong, Z. Huang, Numerical study and optimizing on micro square pin-fin heat sink for electronic cooling, *Applied Thermal Engineering* 93 (2016) 1347–1359. <https://doi.org/10.1016/j.applthermaleng.2015.08.105>.
- [203] A. Khalili Sadaghiani, A. Koşar, Numerical investigations on the effect of fin shape and surface roughness on hydrothermal characteristics of slip flows in microchannels with pin fins, *International Journal of Thermal Sciences* 124 (2018) 375–386. <https://doi.org/10.1016/j.ijthermalsci.2017.10.037>.
- [204] Y. Jia, G. Xia, Y. Li, D. Ma, B. Cai, Heat transfer and fluid flow characteristics of combined microchannel with cone-shaped micro pin fins, *International Communications in Heat and Mass Transfer* 92 (2018) 78–89. <https://doi.org/10.1016/j.icheatmasstransfer.2017.11.004>.

- [205] S. Souida, D. Sahel, H. Ameer, A. Yousfi, Numerical Simulation of Heat Transfer Behaviors in Conical Pin Fins Heat Sinks, *Acta Mechanica Slovaca* 26 (2022) 32–41.
- [206] D. Sahel, L. Bellahcene, A. Yousfi, A. Subasi, Numerical investigation and optimization of a heat sink having hemispherical pin fins, *International Communications in Heat and Mass Transfer* 122 (2021) 105133. <https://doi.org/10.1016/j.icheatmasstransfer.2021.105133>.
- [207] P. Li, Y. Luo, D. Zhang, Y. Xie, Flow and heat transfer characteristics and optimization study on the water-cooled microchannel heat sinks with dimple and pin-fin, *International Journal of Heat and Mass Transfer* 119 (2018) 152–162. <https://doi.org/10.1016/j.ijheatmasstransfer.2017.11.112>.
- [208] A.O. Elsayed, Numerical investigation of heat transfer from multi-bulges pins, *Case Studies in Thermal Engineering* 12 (2018) 636–643. <https://doi.org/10.1016/j.csite.2018.08.005>.
- [209] L. Zhao, K. Yu, W. Wu, Y. He, H. Dong, J. Wang, Effects of elastic micropillar array on the hydrothermal characteristics of a microchannel heat sink, *Thermal Science and Engineering Progress* 46 (2023) 102223. <https://doi.org/10.1016/j.tsep.2023.102223>.
- [210] Saravanakumar. T, S.Kumar. D, Heat transfer study on different surface textured pin fin heat sink, *International Communications in Heat and Mass Transfer* 119 (2020) 104902. <https://doi.org/10.1016/j.icheatmasstransfer.2020.104902>.
- [211] H. Yan, L. Luo, J. Zhang, W. Du, S. Wang, D. Huang, Flow structure and heat transfer characteristics of a pin-finned channel with upright/curved/inclined pin fins under stationary and rotating conditions, *International Communications in Heat and Mass Transfer* 127 (2021) 105483. <https://doi.org/10.1016/j.icheatmasstransfer.2021.105483>.
- [212] B. Bencherif, D. Sahel, R. Benzeguir, H. Ameer, Performance Analysis of Central Processing Unit Heat Sinks Fitted With Perforation Technique and Splitter Inserts, *ASME Journal of Heat and Mass Transfer* 145 (2022). <https://doi.org/10.1115/1.4055815>.
- [213] M.K.U. Al-Karagoly, M. Ayani, M. Mamourian, S. Razavi Bazaz, Experimental parametric study of a deep groove within a pin fin arrays regarding fin thermal resistance, *International Communications in Heat and Mass Transfer* 115 (2020) 104615. <https://doi.org/10.1016/j.icheatmasstransfer.2020.104615>.
- [214] Q. Zhu, R. Su, L. Hu, J. Chen, J. Zeng, H. Zhang, H. Sun, S. Zhang, D. Fu, Heat transfer enhancement for microchannel heat sink by strengthening fluids mixing with backward right-angled trapezoidal grooves in channel sidewalls, *International Communications in Heat and Mass Transfer* 135 (2022) 106106. <https://doi.org/10.1016/j.icheatmasstransfer.2022.106106>.
- [215] B. Bencherif, D. Sahel, H. Ameer, R. Benzeguir, Investigation of the hydrothermal enhancement of grooved pin fins heat sinks, *International Journal of Ambient Energy* 43 (2022) 8505–8515. <https://doi.org/10.1080/01430750.2022.2101521>.
- [216] H.-C. Chiu, R.-H. Hsieh, K. Wang, J.-H. Jang, C.-R. Yu, The heat transfer characteristics of liquid cooling heat sink with micro pin fins, *International Communications in Heat and Mass Transfer* 86 (2017) 174–180. <https://doi.org/10.1016/j.icheatmasstransfer.2017.05.027>.
- [217] M. Tabatabaei Malazi, K. Kaya, A.S. Dalkılıç, A computational case study on the thermal performance of a rectangular microchannel having circular pin-fins, *Case Studies*

- in Thermal Engineering 49 (2023) 103111. <https://doi.org/10.1016/j.csite.2023.103111>.
- [218] Y.J. Lee, S.J. Kim, Experimental investigation on thermal-hydraulic performance of manifold microchannel with pin-fins for ultra-high heat flux cooling, International Journal of Heat and Mass Transfer 224 (2024) 125336. <https://doi.org/10.1016/j.ijheatmasstransfer.2024.125336>.
- [219] H.A.M. Hussein, R. Zulkifli, W.M.F.B.W. Mahmood, R.K. Ajeel, Effects of design parameters on flow fields and heat transfer characteristics in semicircle oblique-finned corrugated, International Communications in Heat and Mass Transfer 135 (2022) 106143. <https://doi.org/10.1016/j.icheatmasstransfer.2022.106143>.
- [220] M. Abuşka, V. Çorumlu, A comparative experimental thermal performance analysis of conical pin fin heat sink with staggered and modified staggered layout under forced convection, Thermal Science and Engineering Progress 37 (2023) 101560. <https://doi.org/10.1016/j.tsep.2022.101560>.
- [221] E. Rasouli, C. Naderi, V. Narayanan, Pitch and aspect ratio effects on single-phase heat transfer through microscale pin fin heat sinks, International Journal of Heat and Mass Transfer 118 (2018) 416–428. <https://doi.org/10.1016/j.ijheatmasstransfer.2017.10.105>.
- [222] D. Yang, Y. Wang, G. Ding, Z. Jin, J. Zhao, G. Wang, Numerical and experimental analysis of cooling performance of single-phase array microchannel heat sinks with different pin-fin configurations, Applied Thermal Engineering 112 (2017) 1547–1556. <https://doi.org/10.1016/j.applthermaleng.2016.08.211>.
- [223] Y.-T. Shen, Y.-H. Pan, H. Chen, W.-L. Cheng, Experimental study of embedded manifold staggered pin-fin microchannel heat sink, International Journal of Heat and Mass Transfer 226 (2024) 125488. <https://doi.org/10.1016/j.ijheatmasstransfer.2024.125488>.
- [224] Z. Shi, X. Lan, J. Cao, N. Zhao, Y. Cheng, Numerical study of variable density and height flow guided pin fin in an open microchannel heat sink, International Journal of Heat and Mass Transfer 225 (2024) 125405. <https://doi.org/10.1016/j.ijheatmasstransfer.2024.125405>.
- [225] G.-F. Xie, L. Zhao, Y.-Y. Dong, Y.-G. Li, S.-L. Zhang, C. Yang, Hydraulic and Thermal Performance of Microchannel Heat Sink Inserted with Pin Fins, Micromachines 12 (2021) 245. <https://doi.org/10.3390/mi12030245>.
- [226] A. Koşar, Y. Peles, Thermal-Hydraulic Performance of MEMS-based Pin Fin Heat Sink, Journal of Heat Transfer 128 (2005) 121–131. <https://doi.org/10.1115/1.2137760>.
- [227] H. Shafeie, O. Abouali, K. Jafarpur, G. Ahmadi, Numerical study of heat transfer performance of single-phase heat sinks with micro pin-fin structures, Applied Thermal Engineering 58 (2013) 68–76. <https://doi.org/10.1016/j.applthermaleng.2013.04.008>.
- [228] S. Acharya, Thermo-fluidic analysis of microchannel heat sink with inline/staggered square/elliptical fins, International Communications in Heat and Mass Transfer 147 (2023) 106961. <https://doi.org/10.1016/j.icheatmasstransfer.2023.106961>.
- [229] H. Babar, H. Wu, H.M. Ali, W. Zhang, Hydrothermal performance of inline and staggered arrangements of airfoil shaped pin-fin heat sinks: A comparative study, Thermal Science and Engineering Progress 37 (2023) 101616. <https://doi.org/10.1016/j.tsep.2022.101616>.
- [230] H. Kishore, C.K. Nirala, A. Agrawal, Thermal performance index based

- characterization and experimental validation for heat dissipation by unconventional arrayed micro pin-fins, *Thermal Science and Engineering Progress* 43 (2023) 102015. <https://doi.org/10.1016/j.tsep.2023.102015>.
- [231] Experimental investigation of enhanced performance of pin fin heat sink with wings, *Applied Thermal Engineering* 155 (2019) 546–562. <https://doi.org/10.1016/j.applthermaleng.2019.03.139>.
- [232] F. Ismayilov, A. Akturk, Y. Peles, Systematic micro heat sink optimization based on hydrofoil shape pin fins, *Case Studies in Thermal Engineering* 26 (2021) 101028. <https://doi.org/10.1016/j.csite.2021.101028>.
- [233] S. Singh, R.K. Singla, Experimental and numerical analysis of a nonlinear pin fin with temperature dependent properties and disparate boundary conditions, *International Communications in Heat and Mass Transfer* 108 (2019) 104313. <https://doi.org/10.1016/j.icheatmasstransfer.2019.104313>.
- [234] X. Cui, J. Guo, X. Huai, K. Cheng, H. Zhang, M. Xiang, Numerical study on novel airfoil fins for printed circuit heat exchanger using supercritical CO₂, *International Journal of Heat and Mass Transfer* 121 (2018) 354–366. <https://doi.org/10.1016/j.ijheatmasstransfer.2018.01.015>.
- [235] L. Tang, L. Cui, B. Sundén, Optimization of fin configurations and layouts in a printed circuit heat exchanger for supercritical liquefied natural gas near the pseudo-critical temperature, *Applied Thermal Engineering* 172 (2020) 115131. <https://doi.org/10.1016/j.applthermaleng.2020.115131>.
- [236] M.R. Haque, R.R. Redu, Md.A.-A.A. Rafi, M.M. Haque, M.Z. Rahman, Numerical investigation of heat transfer performance for rectangular, elliptical, and airfoil shaped pin fin heatsinks through the novel combination of perforation and bulge inserts, *International Communications in Heat and Mass Transfer* 138 (2022) 106352. <https://doi.org/10.1016/j.icheatmasstransfer.2022.106352>.
- [237] Q. Shi, Q. Liu, X. Yao, C. Sun, X. Ju, M.M. Abd El-Samie, C. Xu, Optimal design on irregular polygon topology for the manifold micro-pin-fin heat sink, *International Communications in Heat and Mass Transfer* 141 (2023) 106574. <https://doi.org/10.1016/j.icheatmasstransfer.2022.106574>.
- [238] R. Ray, A. Mohanty, P. Patro, K.C. Tripathy, Performance enhancement of heat sink with branched and interrupted fins, *International Communications in Heat and Mass Transfer* 133 (2022) 105945. <https://doi.org/10.1016/j.icheatmasstransfer.2022.105945>.
- [239] H. Ma, L. Su, B. He, D. He, Y. Kang, New design of U-turn type minichannel cold plate with hybrid fins for high temperature uniformity, *International Communications in Heat and Mass Transfer* 135 (2022) 106078. <https://doi.org/10.1016/j.icheatmasstransfer.2022.106078>.
- [240] E.M.S. El-Said, G.B. Abdelaziz, S.W. Sharshir, A.H. Elsheikh, A.M. Elsaid, Experimental investigation of the twist angle effects on thermo-hydraulic performance of a square and hexagonal pin fin array in forced convection, *International Communications in Heat and Mass Transfer* 126 (2021) 105374. <https://doi.org/10.1016/j.icheatmasstransfer.2021.105374>.
- [241] J.R. McDonough, A perspective on the current and future roles of additive manufacturing in process engineering, with an emphasis on heat transfer, *Thermal Science*

- and Engineering Progress 19 (2020) 100594. <https://doi.org/10.1016/j.tsep.2020.100594>.
- [242] K. Timbs, M. Khatamifar, E. Antunes, W. Lin, Experimental study on the heat dissipation performance of straight and oblique fin heat sinks made of thermal conductive composite polymers, *Thermal Science and Engineering Progress* 22 (2021) 100848. <https://doi.org/10.1016/j.tsep.2021.100848>.
- [243] C. Woodcock, C. Ng'oma, M. Sweet, Y. Wang, Y. Peles, J. Plawsky, Ultra-high heat flux dissipation with Piranha Pin Fins, *International Journal of Heat and Mass Transfer* 128 (2019) 504–515. <https://doi.org/10.1016/j.ijheatmasstransfer.2018.09.030>.
- [244] M. Harris, H. Wu, Numerical Simulation of Heat Transfer Performance in Novel Biomorphic Pin-Fin Heat Sinks, in: *The 8th World Congress on Momentum, Heat and Mass Transfer*, Avestia, Lisbon, Portugal, 2023. <https://doi.org/10.11159/enfht23.166>.
- [245] S. Wu, K. Zhang, G. Song, J. Zhu, B. Yao, Experimental study on the performance of a tree-shaped mini-channel liquid cooling heat sink, *Case Studies in Thermal Engineering* 30 (2022) 101780. <https://doi.org/10.1016/j.csite.2022.101780>.
- [246] Y. Xu, L. Li, J. Wang, Experimental and numerical investigations of the thermal–hydraulic characteristics of novel micropin-fin heat sinks, *International Journal of Heat and Mass Transfer* 209 (2023) 124079. <https://doi.org/10.1016/j.ijheatmasstransfer.2023.124079>.
- [247] Y. Peles, A. Koşar, C. Mishra, C.-J. Kuo, B. Schneider, Forced convective heat transfer across a pin fin micro heat sink, *International Journal of Heat and Mass Transfer* 48 (2005) 3615–3627. <https://doi.org/10.1016/j.ijheatmasstransfer.2005.03.017>.
- [248] A. Siu-Ho, W. Qu, F. Pfefferkorn, Experimental Study of Pressure Drop and Heat Transfer in a Single-Phase Micropin-Fin Heat Sink, *Journal of Electronic Packaging* 129 (2007) 479–487. <https://doi.org/10.1115/1.2804099>.
- [249] A. Shemelash, B. Tamrat, M. Temesgen, R. Gopal, B. Desalegn, H. Mulugeta, H.G. Solomon, Multi-objective optimization of a Fibonacci phyllotaxis micro pin-fin heat sink, *Heat Transfer n/a* (n.d.). <https://doi.org/10.1002/htj.23083>.
- [250] A.R. Roozbehi, M. Zabetian Targhi, M.M. Heyhat, A. Khatibi, Modified hexagonal pin fins for enhanced thermal-hydraulic performance of micro-pin fin heat sinks, *International Journal of Numerical Methods for Heat & Fluid Flow* 33 (2023) 2902–2926. <https://doi.org/10.1108/HFF-02-2023-0053>.
- [251] M.O. Qidwai, I.A. Badruddin, S. Kamangar, N.Z. Khan, M.A. Khan, M.N. Khan, Heat transfer enhancement in multijet micropin fin heat sink, *Numerical Heat Transfer, Part A: Applications* 0 (n.d.) 1–20. <https://doi.org/10.1080/10407782.2023.2294349>.
- [252] D. Gupta, P. Saha, S. Roy, Multi-Objective Optimization of the Perforated Micro Pin-Fin Heat Sink Using Non-Dominated Sorting Genetic Algorithm-II Coupled With Computational Fluid Dynamics Simulation, *Journal of Heat Transfer* 144 (2022). <https://doi.org/10.1115/1.4054761>.
- [253] M. Harris, H. Wu, J. Sun, Investigating Heat Transfer and Flow Characteristics under Different Wall Heating Conditions in Novel Micro Pin-Fin Heat Sinks, in: *9th World Congress on Momentum, Heat and Mass Transfer (MHMT 2024)*, Avestia, London, 2024. <https://doi.org/10.11159/enfht24.328>.
- [254] H. Xie, B. Yang, S. Zhang, M. Song, Research on the mechanism of heat transfer enhancement in microchannel heat sinks with micropin fins, *International Journal of*

- Energy Research 44 (2020) 3049–3065. <https://doi.org/10.1002/er.5135>.
- [255] Y. Xu, L. Li, Z. Yan, Experimental investigations of the flow boiling characteristics of green refrigerants in a novel petaloid micropin-fin heat sink, *International Journal of Heat and Mass Transfer* 212 (2023) 124243. <https://doi.org/10.1016/j.ijheatmasstransfer.2023.124243>.
- [256] T. David, D. Mendler, A. Mosyak, A. Bar-Cohen, G. Hetsroni, Thermal Management of Time-Varying High Heat Flux Electronic Devices, *Journal of Electronic Packaging* 136 (2014). <https://doi.org/10.1115/1.4027325>.
- [257] T. Ambreen, A. Saleem, C.W. Park, Pin-fin shape-dependent heat transfer and fluid flow characteristics of water- and nanofluid-cooled micropin-fin heat sinks: Square, circular and triangular fin cross-sections, *Applied Thermal Engineering* 158 (2019) 113781. <https://doi.org/10.1016/j.applthermaleng.2019.113781>.
- [258] T. Ambreen, A. Saleem, C.W. Park, Numerical analysis of the heat transfer and fluid flow characteristics of a nanofluid-cooled micropin-fin heat sink using the Eulerian-Lagrangian approach, *Powder Technology* 345 (2019) 509–520. <https://doi.org/10.1016/j.powtec.2019.01.042>.
- [259] F. Keshavarz, A. Mirabdollah Lavasani, H. Bayat, Numerical analysis of effect of nanofluid and fin distribution density on thermal and hydraulic performance of a heat sink with drop-shaped micropin fins, *J Therm Anal Calorim* 135 (2019) 1211–1228. <https://doi.org/10.1007/s10973-018-7711-z>.
- [260] S.K. Rajan, A. Kaul, T.E. Sarvey, G.S. May, M.S. Bakir, Monolithic Microfluidic Cooling of a Heterogeneous 2.5-D FPGA With Low-Profile 3-D Printed Manifolds, *IEEE Transactions on Components, Packaging and Manufacturing Technology* 11 (2021) 974–982. <https://doi.org/10.1109/TCPMT.2021.3082013>.
- [261] T.E. Sarvey, Y. Zhang, C. Cheung, R. Gutala, A. Rahman, A. Dasu, M.S. Bakir, Monolithic Integration of a Micropin-Fin Heat Sink in a 28-nm FPGA, *IEEE Transactions on Components, Packaging and Manufacturing Technology* 7 (2017) 1617–1624. <https://doi.org/10.1109/TCPMT.2017.2740721>.
- [262] X. Zhang, X. Han, T.E. Sarvey, C.E. Green, P.A. Kottke, A.G. Fedorov, Y. Joshi, M.S. Bakir, Three-Dimensional Integrated Circuit With Embedded Microfluidic Cooling: Technology, Thermal Performance, and Electrical Implications, *Journal of Electronic Packaging* 138 (2016). <https://doi.org/10.1115/1.4032496>.
- [263] A. Renfer, M.K. Tiwari, R. Tiwari, F. Alfieri, T. Brunschweiler, B. Michel, D. Poulikakos, Microvortex-enhanced heat transfer in 3D-integrated liquid cooling of electronic chip stacks, *International Journal of Heat and Mass Transfer* 65 (2013) 33–43. <https://doi.org/10.1016/j.ijheatmasstransfer.2013.05.066>.
- [264] X. Han, A. Fedorov, Y. Joshi, Flow Boiling in Microgaps for Thermal Management of High Heat Flux Microsystems, *Journal of Electronic Packaging* 138 (2016). <https://doi.org/10.1115/1.4034317>.
- [265] Y. Zhang, A. Dembla, M.S. Bakir, Silicon Micropin-Fin Heat Sink With Integrated TSVs for 3-D ICs: Tradeoff Analysis and Experimental Testing, *IEEE Transactions on Components, Packaging and Manufacturing Technology* 3 (2013) 1842–1850. <https://doi.org/10.1109/TCPMT.2013.2267492>.
- [266] T.E. Sarvey, Y. Hu, C.E. Green, P.A. Kottke, D.C. Woodrum, Y.K. Joshi, A.G. Fedorov,

- S.K. Sitaraman, M.S. Bakir, Integrated Circuit Cooling Using Heterogeneous Micropin-Fin Arrays for Nonuniform Power Maps, *IEEE Transactions on Components, Packaging and Manufacturing Technology* 7 (2017) 1465–1475. <https://doi.org/10.1109/TCPMT.2017.2704525>.
- [267] Y. Oh, Z. Guo, PREDICTION OF NUSSELT NUMBER IN MICROSCALE PIN FIN HEAT SINKS USING ARTIFICIAL NEURAL NETWORKS, *HTR* 54 (2023). <https://doi.org/10.1615/HeatTransRes.2022044987>.
- [268] V. Çorumlu, V. Altıntaş, M. Abuşka, Evaluation of prediction and modeling performance using machine learning methods for thermal parameters of heat sinks under forced convection: The case of external validation, *International Communications in Heat and Mass Transfer* 151 (2024) 107228. <https://doi.org/10.1016/j.icheatmasstransfer.2023.107228>.
- [269] N. Fallahtafi, S. Rangarajan, Y. Hadad, C. Arvin, K. Sikka, C.H. Hoang, G. Mohsenian, V. Radmard, S. Schiffres, B. Sammakia, Shape optimization of hotspot targeted micro pin fins for heterogeneous integration applications, *International Journal of Heat and Mass Transfer* 192 (2022) 122897. <https://doi.org/10.1016/j.ijheatmasstransfer.2022.122897>.
- [270] N.P. Nguyen, E. Maghsoudi, S.N. Roberts, B. Kwon, Shape optimization of pin fin array in a cooling channel using genetic algorithm and machine learning, *International Journal of Heat and Mass Transfer* 202 (2023) 123769. <https://doi.org/10.1016/j.ijheatmasstransfer.2022.123769>.
- [271] M. Tabatabaei Malazi, K. Kaya, A.B. Çolak, A.S. Dalkılıç, CFD and ANN analyses for the evaluation of the heat transfer characteristics of a rectangular microchannel heat sink with various cylindrical pin-fins, *Heat Mass Transfer* (2024). <https://doi.org/10.1007/s00231-024-03496-7>.
- [272] K. Nilpueng, P. Kaseethong, M. Mesgarpour, M.S. Shadloo, S. Wongwises, A novel temperature prediction method without using energy equation based on physics-informed neural network (PINN): A case study on plate- circular/square pin-fin heat sinks, *Engineering Analysis with Boundary Elements* 145 (2022) 404–417. <https://doi.org/10.1016/j.enganabound.2022.09.032>.
- [273] S. Ghosh, S. Mondal, J.S. Kapat, A. Ray, Parametric shape optimization of pin fin arrays using a multi-fidelity surrogate model based Bayesian method, *Applied Thermal Engineering* 247 (2024) 122876. <https://doi.org/10.1016/j.applthermaleng.2024.122876>.
- [274] B. Heidarshenas, A. Abidi, S.M. Sajadi, Y. Yuan, A.S. El-Shafay, H.Ş. Aybar, Numerical study and optimization of thermal efficiency for a pin fin heatsink with nanofluid flow by modifying heatsink geometry, *Case Studies in Thermal Engineering* 55 (2024) 104125. <https://doi.org/10.1016/j.csite.2024.104125>.
- [275] S.S. Pai, J.A. Weibel, Machine-learning-aided design optimization of internal flow channel cross-sections, *International Journal of Heat and Mass Transfer* 195 (2022) 123118. <https://doi.org/10.1016/j.ijheatmasstransfer.2022.123118>.
- [276] A. Tikadar, S. Kumar, Machine learning approach to predict heat transfer and fluid flow characteristics of integrated pin fin-metal foam heat sink, *Numerical Heat Transfer, Part B: Fundamentals* 0 (n.d.) 1–26. <https://doi.org/10.1080/10407790.2023.2266772>.
- [277] B. Markal, Y.E. Karabacak, A. Evcimen, Machine-learning-based modeling of saturated flow boiling in pin-fin micro heat sinks with expanding flow passages,

- International Communications in Heat and Mass Transfer 158 (2024) 107870. <https://doi.org/10.1016/j.icheatmasstransfer.2024.107870>.
- [278] H. Lee, G. Lee, K. Kim, D. Kong, H. Lee, Multimodal machine learning for predicting heat transfer characteristics in micro-pin fin heat sinks, *Case Studies in Thermal Engineering* 57 (2024) 104331. <https://doi.org/10.1016/j.csite.2024.104331>.
- [279] G. Zhu, S. Liu, D. Zhang, W. Chen, J. Li, T. Wen, Transfer learning model to predict flow boiling heat transfer coefficient in mini channels with micro pin fins, *International Journal of Heat and Mass Transfer* 220 (2024) 125020. <https://doi.org/10.1016/j.ijheatmasstransfer.2023.125020>.
- [280] K. Kim, H. Lee, M. Kang, G. Lee, K. Jung, C.R. Kharangate, M. Asheghi, K.E. Goodson, H. Lee, A machine learning approach for predicting heat transfer characteristics in micro-pin fin heat sinks, *International Journal of Heat and Mass Transfer* 194 (2022) 123087. <https://doi.org/10.1016/j.ijheatmasstransfer.2022.123087>.
- [281] M. Harris, H. Wu, Numerical Simulation of Heat Transfer Performance in Novel Biomorphic Pin-Fin Heat Sinks, in: Avestia, Lisbon, 2023. <https://doi.org/10.11159/enfht23.166>.
- [282] S.A. Abdollahi, A. Alenezi, A. Alizadeh, D.J. Jasim, M. Ahmed, L.H.A. Fezaa, W. Aich, L.B. Said, L. Kolsi, H. Maleki, A novel insight into the design of perforated-finned heat sinks based on a hybrid procedure: Computational fluid dynamics, machine learning, multi-objective optimization, and multi-criteria decision-making, *International Communications in Heat and Mass Transfer* 155 (2024) 107535. <https://doi.org/10.1016/j.icheatmasstransfer.2024.107535>.
- [283] F.-T. Zohora, F. Akter, Md.A. Haque, N.M. Chowdhury, M.R. Haque, A novel pin finned structure-embedded microchannel heat sink: CFD-data driven MLP, MLR, and XGBR machine learning models for thermal and fluid flow prediction, *Energy* 307 (2024) 132646. <https://doi.org/10.1016/j.energy.2024.132646>.
- [284] L. Yang, Q. Wang, Y. Rao, Searching for irregular pin-fin shapes for high temperature applications using deep learning methods, *International Journal of Thermal Sciences* 161 (2021) 106746. <https://doi.org/10.1016/j.ijthermalsci.2020.106746>.
- [285] M.R. Shaeri, S. Sarabi, A.M. Randriambololona, A. Shadlo, Machine learning-based optimization of air-cooled heat sinks, *Thermal Science and Engineering Progress* 34 (2022) 101398. <https://doi.org/10.1016/j.tsep.2022.101398>.
- [286] A. Suzuki, H. Nakatani, M. Kobashi, Machine learning surrogate modeling toward the design of lattice-structured heat sinks fabricated by additive manufacturing, *Materials & Design* 230 (2023) 111969. <https://doi.org/10.1016/j.matdes.2023.111969>.
- [287] A. Aldaghi, A. Banejad, H. Kalani, M. Sardarabadi, M. Passandideh-Fard, An experimental study integrated with prediction using deep learning method for active/passive cooling of a modified heat sink, *Applied Thermal Engineering* 221 (2023) 119522. <https://doi.org/10.1016/j.applthermaleng.2022.119522>.
- [288] A. Salari, R. Ahmadi, M.S. Vafadaran, H. Shakibi, M. Sardarabadi, Predicting the performance of a heat sink utilized with an energy storage unit using machine learning approach, *Journal of Energy Storage* 83 (2024) 110470. <https://doi.org/10.1016/j.est.2024.110470>.
- [289] S.D. Farahani, A.J. Mamoei, A. Alizadeh, Thermal performance of microchannel heat

- sink integrated with porous medium, slip coefficient and phase change material and machine learning approach, *Journal of Energy Storage* 74 (2023) 109357. <https://doi.org/10.1016/j.est.2023.109357>.
- [290] B. Aksoy, O.K.M. Salman, K. Özsoy, The estimation of the thermal performance of heat sinks manufactured by direct metal laser sintering based on machine learning, *Measurement* 225 (2024) 113625. <https://doi.org/10.1016/j.measurement.2023.113625>.
- [291] A. Bard, Y. Qiu, C.R. Kharangate, R. French, Consolidated modeling and prediction of heat transfer coefficients for saturated flow boiling in mini/micro-channels using machine learning methods, *Applied Thermal Engineering* 210 (2022) 118305. <https://doi.org/10.1016/j.applthermaleng.2022.118305>.
- [292] J. Herring, P. Smith, J. Lamotte-Dawaghreh, P. Bansode, S. Saini, R. Bhandari, D. Agonafer, Machine Learning-Based Heat Sink Optimization Model for Single-Phase Immersion Cooling, in: American Society of Mechanical Engineers Digital Collection, 2022. <https://doi.org/10.1115/IPACK2022-97481>.
- [293] M. Shanmugam, L.S. Maganti, Machine learning-based thermal performance study of microchannel heat sink under non-uniform heat load conditions, *Applied Thermal Engineering* 253 (2024) 123769. <https://doi.org/10.1016/j.applthermaleng.2024.123769>.
- [294] B.N. Mengesha, M.R. Shaeri, S. Sarabi, Application of Machine Learning to Predict Thermal Performances of Heat Sinks, in: 2022. <https://doi.org/10.11159/htff22.138>.
- [295] S. Ghosh, S. Mondal, E. Fernandez, J.S. Kapat, A. Roy, Parametric Shape Optimization of Pin-Fin Arrays Using a Surrogate Model-Based Bayesian Method, *Journal of Thermophysics and Heat Transfer* 35 (2021) 245–255. <https://doi.org/10.2514/1.T6094>.
- [296] S. Barathula, S. Chaitanya, K. Srinivasan, Evaluation of machine learning models in the classification of pool boiling regimes up to critical heat flux based on boiling acoustics, *International Journal of Heat and Mass Transfer* 201 (2023) 123623. <https://doi.org/10.1016/j.ijheatmasstransfer.2022.123623>.
- [297] G.M. Hobold, A.K. da Silva, Machine learning classification of boiling regimes with low speed, direct and indirect visualization, *International Journal of Heat and Mass Transfer* 125 (2018) 1296–1309. <https://doi.org/10.1016/j.ijheatmasstransfer.2018.04.156>.
- [298] J. Loyola-Fuentes, L. Pietrasanta, M. Marengo, F. Coletti, Machine Learning Algorithms for Flow Pattern Classification in Pulsating Heat Pipes, *Energies* 15 (2022) 1970. <https://doi.org/10.3390/en15061970>.
- [299] Z.J. Ooi, L. Zhu, J.L. Bottini, C.S. Brooks, Identification of flow regimes in boiling flows in a vertical annulus channel with machine learning techniques, *International Journal of Heat and Mass Transfer* 185 (2022) 122439. <https://doi.org/10.1016/j.ijheatmasstransfer.2021.122439>.
- [300] K. Manikonda, A.R. Hasan, C.E. Obi, R. Islam, A.K. Sleiti, M.W. Abdelrazeq, M.A. Rahman, Application of Machine Learning Classification Algorithms for Two-Phase Gas-Liquid Flow Regime Identification, in: OnePetro, 2021. <https://doi.org/10.2118/208214-MS>.
- [301] M.K. Seal, S.M.A. Noori Rahim Abadi, M. Mehrabi, J.P. Meyer, Machine learning classification of in-tube condensation flow patterns using visualization, *International Journal of Multiphase Flow* 143 (2021) 103755.

- <https://doi.org/10.1016/j.ijmultiphaseflow.2021.103755>.
- [302] L. Zhu, Z. Jhia Ooi, T. Zhang, C.S. Brooks, L. Pan, Identification of flow regimes in boiling flow with clustering algorithms: An interpretable machine-learning perspective, *Applied Thermal Engineering* 228 (2023) 120493. <https://doi.org/10.1016/j.applthermaleng.2023.120493>.
- [303] M. Schepperle, S. Junaid, P. Woias, Computer-Vision- and Deep-Learning-Based Determination of Flow Regimes, Void Fraction, and Resistance Sensor Data in Microchannel Flow Boiling, *Sensors* 24 (2024) 3363. <https://doi.org/10.3390/s24113363>.
- [304] Y. He, C. Hu, H. Li, X. Hu, D. Tang, Reliable predictions of bubble departure frequency in subcooled flow boiling: A machine learning-based approach, *International Journal of Heat and Mass Transfer* 195 (2022) 123217. <https://doi.org/10.1016/j.ijheatmasstransfer.2022.123217>.
- [305] G.M. Hobold, A.K. da Silva, Visualization-based nucleate boiling heat flux quantification using machine learning, *International Journal of Heat and Mass Transfer* 134 (2019) 511–520. <https://doi.org/10.1016/j.ijheatmasstransfer.2018.12.170>.
- [306] J.H. Seong, M. Ravichandran, G. Su, B. Phillips, M. Bucci, Automated bubble analysis of high-speed subcooled flow boiling images using U-net transfer learning and global optical flow, *International Journal of Multiphase Flow* 159 (2023) 104336. <https://doi.org/10.1016/j.ijmultiphaseflow.2022.104336>.
- [307] Y. Suh, R. Bostanabad, Y. Won, Deep learning predicts boiling heat transfer, *Sci Rep* 11 (2021) 5622. <https://doi.org/10.1038/s41598-021-85150-4>.
- [308] S.G. Kandlikar, W.J. Grande, Evolution of Microchannel Flow Passages—Thermohydraulic Performance and Fabrication Technology, *Heat Transfer Engineering* 24 (2003) 3–17. <https://doi.org/10.1080/01457630304040>.
- [309] S. Prakash, S. Kumar, Fabrication of microchannels: A review, *Proceedings of the Institution of Mechanical Engineers, Part B: Journal of Engineering Manufacture* 229 (2015) 1273–1288. <https://doi.org/10.1177/0954405414535581>.
- [310] N. Kumar, S. Shahzeb Hasan, K. Srivastava, R. Akhtar, R. Kumar Yadav, V.K. Choubey, Lean manufacturing techniques and its implementation: A review, *Materials Today: Proceedings* 64 (2022) 1188–1192. <https://doi.org/10.1016/j.matpr.2022.03.481>.
- [311] R.G. Schroeder, K. Linderman, C. Liedtke, A.S. Choo, Six Sigma: Definition and underlying theory, *Journal of Operations Management* 26 (2008) 536–554. <https://doi.org/10.1016/j.jom.2007.06.007>.
- [312] A. Gunasekaran, Y.Y. Yusuf, E.O. Adeleye, T. Papadopoulos, D. Kovvuri, D.G. Geyi, Agile manufacturing: an evolutionary review of practices, *International Journal of Production Research* 57 (2019) 5154–5174. <https://doi.org/10.1080/00207543.2018.1530478>.
- [313] A.M. Deif, A system model for green manufacturing, *Journal of Cleaner Production* 19 (2011) 1553–1559. <https://doi.org/10.1016/j.jclepro.2011.05.022>.
- [314] O. Molloy, E.A. Warman, S. Tilley, *Design for Manufacturing and Assembly: Concepts, architectures and implementation*, Springer Science & Business Media, 2012.
- [315] J.R. Hackman, R. Wageman, Total Quality Management: Empirical, Conceptual, and Practical Issues, *Administrative Science Quarterly* 40 (1995) 309–342. <https://doi.org/10.2307/2393640>.

- [316] G. Singh, I.S. Ahuja, Just-in-time manufacturing: literature review and directions, *International Journal of Business Continuity and Risk Management* 3 (2012) 57–98. <https://doi.org/10.1504/IJBCRM.2012.045519>.
- [317] M. Garetti, M. Taisch, Sustainable manufacturing: trends and research challenges, *Production Planning & Control* 23 (2012) 83–104. <https://doi.org/10.1080/09537287.2011.591619>.
- [318] K. Dorst, The core of ‘design thinking’ and its application, *Design Studies* 32 (2011) 521–532. <https://doi.org/10.1016/j.destud.2011.07.006>.
- [319] M. Saunders, P. Lewis, A. Thornhill, *Research Methods for Business Students*, Pearson Education, 2009.
- [320] J.W. Creswell, J.D. Creswell, *Research Design: Qualitative, Quantitative, and Mixed Methods Approaches*, SAGE Publications, 2017.
- [321] C. Legg, C. Hookway, Pragmatism, (2008). <https://plato.sydney.edu.au/entries/pragmatism/> (accessed October 16, 2024).
- [322] J.E. Osang, A.B. Udoimuk, E.B. Etta, et al., Methods of Gathering Data for Research Purpose and Applications Using IJSER Acceptance Rate of Monthly Paper Publication (March 2012 Edition-May 2013 Edition), *IOSR-JCE* 15 (2013) 59–65. <https://doi.org/10.9790/0661-1525965>.
- [323] S.J. Tracy, Qualitative Quality: Eight “Big-Tent” Criteria for Excellent Qualitative Research, *Qualitative Inquiry* 16 (2010) 837–851.
- [324] K.D. Pimple, Six domains of research ethics, *SCI ENG ETHICS* 8 (2002) 191–205. <https://doi.org/10.1007/s11948-002-0018-1>.
- [325] R.K. Yin, *Case Study Research: Design and Methods*, SAGE, 2009.
- [326] J. Gustafsson, Single case studies vs. multiple case studies: A comparative study, in: 2017. <https://www.semanticscholar.org/paper/Single-case-studies-vs.-multiple-case-studies%3A-A-Gustafsson/ae1f06652379a8cd56654096815dae801a59cba3> (accessed October 16, 2024).
- [327] R. Ben Ruben, S. Vinodh, P. Asokan, Implementation of Lean Six Sigma framework with environmental considerations in an Indian automotive component manufacturing firm: a case study, *Production Planning & Control* 28 (2017) 1193–1211. <https://doi.org/10.1080/09537287.2017.1357215>.
- [328] P. Chiabert, G. D’Antonio, J. Inoyatkhodjaev, F. Lombardi, S. Ruffa, Improvement of Powertrain Mechatronic Systems for Lean Automotive Manufacturing, *Procedia CIRP* 33 (2015) 53–58. <https://doi.org/10.1016/j.procir.2015.06.011>.
- [329] J. Singh, H. Singh, Application of lean manufacturing in automotive manufacturing unit, *International Journal of Lean Six Sigma* 11 (2020) 171–210. <https://doi.org/10.1108/IJLSS-06-2018-0060>.
- [330] Q. Dai, R. Zhong, G.Q. Huang, T. Qu, T. Zhang, T.Y. Luo, Radio frequency identification-enabled real-time manufacturing execution system: a case study in an automotive part manufacturer, *International Journal of Computer Integrated Manufacturing* 25 (2012) 51–65. <https://doi.org/10.1080/0951192X.2011.562546>.
- [331] P. Zhang, T. Cui, Q. Li, Effect of surface roughness on thermal contact resistance of aluminium alloy, *Applied Thermal Engineering* 121 (2017) 992–998. <https://doi.org/10.1016/j.applthermaleng.2017.04.142>.

- [332] M. Palanivel, R. Uthayakumar, A production-inventory model with promotional effort, variable production cost and probabilistic deterioration, *Int J Syst Assur Eng Manag* 8 (2017) 290–300. <https://doi.org/10.1007/s13198-015-0345-7>.
- [333] R.K. Shah, Thermal entry length solutions for the circular tube and parallel plates., in: *In Proceedings of 3rd National Heat and Mass Transfer Conference*, Delhi: Indian Institute of Technology Bombay, 1975: pp. 11–75.
- [334] S.K. Oudah, A. Tikadar, R. Fang, K. Egab, J.A. Khan, THERMOHYDRAULIC CHARACTERISTICS OF A KNURLED MICROCHANNEL HEAT SINK IN SINGLE PHASE REGIME, in: *Proceeding of 3rd Thermal and Fluids Engineering Conference (TFEC)*, Begellhouse, Fort Lauderdale, USA, 2018: pp. 1425–1436. <https://doi.org/10.1615/TFEC2018.hte.021674>.
- [335] R. Ajith Krishnan, K.R. Balasubramanian, S. Suresh, Experimental investigation of the effect of heat sink orientation on subcooled flow boiling performance in a rectangular microgap channel, *International Journal of Heat and Mass Transfer* 120 (2018) 1341–1357. <https://doi.org/10.1016/j.ijheatmasstransfer.2017.12.133>.
- [336] M. Liu, D. Liu, S. Xu, Y. Chen, Experimental study on liquid flow and heat transfer in micro square pin fin heat sink, *International Journal of Heat and Mass Transfer* 54 (2011) 5602–5611. <https://doi.org/10.1016/j.ijheatmasstransfer.2011.07.013>.
- [337] P.J. Roache, Perspective: A Method for Uniform Reporting of Grid Refinement Studies, *Journal of Fluids Engineering* 116 (1994) 405–413. <https://doi.org/10.1115/1.2910291>.
- [338] W. Yuan, J. Zhao, C.P. Tso, T. Wu, W. Liu, T. Ming, Numerical simulation of the thermal hydraulic performance of a plate pin fin heat sink, *Applied Thermal Engineering* 48 (2012) 81–88. <https://doi.org/10.1016/j.applthermaleng.2012.04.029>.
- [339] M.Z.U. Khan, E. Uddin, B. Akbar, N. Akram, A.A. Naqvi, M. Sajid, Z. Ali, Md.Y. Younis, F.P. García Márquez, Investigation of Heat Transfer and Pressure Drop in Microchannel Heat Sink Using Al₂O₃ and ZrO₂ Nanofluids, *Nanomaterials (Basel)* 10 (2020) 1796. <https://doi.org/10.3390/nano10091796>.
- [340] M. Liu, D. Liu, S. Xu, Y. Chen, Experimental study on liquid flow and heat transfer in micro square pin fin heat sink, *International Journal of Heat and Mass Transfer* 54 (2011) 5602–5611. <https://doi.org/10.1016/j.ijheatmasstransfer.2011.07.013>.
- [341] A. Mohammadi, A. Koşar, Review on Heat and Fluid Flow in Micro Pin Fin Heat Sinks under Single-phase and Two-phase Flow Conditions, *Nanoscale and Microscale Thermophysical Engineering* 22 (2018) 153–197. <https://doi.org/10.1080/15567265.2018.1475525>.
- [342] K. Sefiane, A. Koşar, Prospects of heat transfer approaches to dissipate high heat fluxes: Opportunities and challenges, *Applied Thermal Engineering* 215 (2022) 118990. <https://doi.org/10.1016/j.applthermaleng.2022.118990>.
- [343] B. Yousefi-Lafouraki, M. Rajabi Zargarabadi, B. Sunden, Aerothermal analysis of pulsed jet impinging on a flat surface with different pin configurations, *International Communications in Heat and Mass Transfer* 137 (2022) 106263. <https://doi.org/10.1016/j.icheatmasstransfer.2022.106263>.
- [344] P. Gómez-Gálvez, P. Vicente-Munuera, A. Tagua, C. Forja, A.M. Castro, M. Letrán, A. Valencia-Expósito, C. Grima, M. Bermúdez-Gallardo, Ó. Serrano-Pérez-Higueras, F. Cavodeassi, S. Sotillos, M.D. Martín-Bermudo, A. Márquez, J. Buceta, L.M. Escudero,

- Scutoids are a geometrical solution to three-dimensional packing of epithelia, *Nat Commun* 9 (2018) 2960. <https://doi.org/10.1038/s41467-018-05376-1>.
- [345] E.S. Menon, *Transmission Pipeline Calculations and Simulations Manual*, Gulf Professional Publishing, 2014.
- [346] D. Li, *Encyclopedia of Microfluidics and Nanofluidics*, Springer Science & Business Media, 2008.
- [347] S. Akhtar, J.C. Kurnia, T. Shamim, A three-dimensional computational model of H₂–air premixed combustion in non-circular micro-channels for a thermo-photovoltaic (TPV) application, *Applied Energy* 152 (2015) 47–57. <https://doi.org/10.1016/j.apenergy.2015.04.068>.
- [348] M. Shim, M.Y. Ha, J.K. Min, A numerical study of the mixed convection around slanted-pin fins on a hot plate in vertical and inclined channels, *International Communications in Heat and Mass Transfer* 118 (2020) 104878. <https://doi.org/10.1016/j.icheatmasstransfer.2020.104878>.
- [349] A.A.A.A. Al-Rashed, A. Shahsavari, O. Rasooli, M.A. Moghimi, A. Karimipour, M.D. Tran, Numerical assessment into the hydrothermal and entropy generation characteristics of biological water-silver nano-fluid in a wavy walled microchannel heat sink, *International Communications in Heat and Mass Transfer* 104 (2019) 118–126. <https://doi.org/10.1016/j.icheatmasstransfer.2019.03.007>.
- [350] A. Al-Damook, J.L. Summers, N. Kapur, H. Thompson, Effect of Different Perforations Shapes on the Thermal-hydraulic Performance of Perforated Pinned Heat Sinks, 3 (2016).
- [351] D.N. Cosenza, L. Korhonen, M. Maltamo, P. Packalen, J.L. Strunk, E. Næsset, T. Gobakken, P. Soares, M. Tomé, Comparison of linear regression, k-nearest neighbour and random forest methods in airborne laser-scanning-based prediction of growing stock, *Forestry: An International Journal of Forest Research* 94 (2021) 311–323. <https://doi.org/10.1093/forestry/cpaa034>.
- [352] J. Cai, K. Xu, Y. Zhu, F. Hu, L. Li, Prediction and analysis of net ecosystem carbon exchange based on gradient boosting regression and random forest, *Applied Energy* 262 (2020) 114566. <https://doi.org/10.1016/j.apenergy.2020.114566>.
- [353] J. Brownlee, *Ensemble Learning Algorithms With Python: Make Better Predictions with Bagging, Boosting, and Stacking*, Machine Learning Mastery, 2021.
- [354] Z. Wu, X. Chen, Y. Mao, E. Li, X. Zeng, J.-X. Wang, A deep learning algorithm with smart-sized training data for transient thermal performance prediction, *Case Studies in Thermal Engineering* 39 (2022) 102420. <https://doi.org/10.1016/j.csite.2022.102420>.
- [355] P. Kosky, R. Balmer, W. Keat, G. Wise, Chapter 14 - Mechanical Engineering, in: P. Kosky, R. Balmer, W. Keat, G. Wise (Eds.), *Exploring Engineering* (Fifth Edition), Academic Press, 2021: pp. 317–340. <https://doi.org/10.1016/B978-0-12-815073-3.00014-4>.
- [356] G. Wang, F. Yang, K. Wu, Y. Ma, C. Peng, T. Liu, L.-P. Wang, Estimation of the dissipation rate of turbulent kinetic energy: A review, *Chemical Engineering Science* 229 (2021) 116133. <https://doi.org/10.1016/j.ces.2020.116133>.
- [357] M. Awais, A.A. Bhuiyan, Heat transfer enhancement using different types of vortex generators (VGs): A review on experimental and numerical activities, *Thermal Science and Engineering Progress* 5 (2018) 524–545. <https://doi.org/10.1016/j.tsep.2018.02.007>.

- [358] R. Bekkerman, M. Bilenko, J. Langford, *Scaling up Machine Learning: Parallel and Distributed Approaches*, Cambridge University Press, 2011.
- [359] Z. Duan, G. Xie, B. Yu, P. Jin, Multi-objective topology optimization and thermal performance of liquid-cooled microchannel heat sinks with pin fins, *Case Studies in Thermal Engineering* 49 (2023) 103178. <https://doi.org/10.1016/j.csite.2023.103178>.
- [360] M.R. Attar, M. Mohammadi, A. Taheri, S. Hosseinpour, M. Passandideh-Fard, M. Haddad Sabzevar, A. Davoodi, Heat transfer enhancement of conventional aluminum heat sinks with an innovative, cost-effective, and simple chemical roughening method, *Thermal Science and Engineering Progress* 20 (2020) 100742. <https://doi.org/10.1016/j.tsep.2020.100742>.
- [361] R.J. MGlen, An introduction to additive manufactured heat pipe technology and advanced thermal management products, *Thermal Science and Engineering Progress* 25 (2021) 100941. <https://doi.org/10.1016/j.tsep.2021.100941>.
- [362] H.M. Ali, W. Arshad, Thermal performance investigation of staggered and inline pin fin heat sinks using water based rutile and anatase TiO₂ nanofluids, *Energy Conversion and Management* 106 (2015) 793–803. <https://doi.org/10.1016/j.enconman.2015.10.015>.
- [363] M. Harris, H. Babar, H. Wu, Assessing thermohydraulic performance in novel micro pin-fin heat sinks: A synergistic experimental, agile manufacturing, and machine learning approach, *International Journal of Heat and Mass Transfer* 239 (2025) 126581. <https://doi.org/10.1016/j.ijheatmasstransfer.2024.126581>.
- [364] T. Ambreen, M.-H. Kim, Effect of fin shape on the thermal performance of nanofluid-cooled micro pin-fin heat sinks, *International Journal of Heat and Mass Transfer* 126 (2018) 245–256. <https://doi.org/10.1016/j.ijheatmasstransfer.2018.05.164>.
- [365] L. Chai, G. Xia, M. Zhou, J. Li, J. Qi, Optimum thermal design of interrupted microchannel heat sink with rectangular ribs in the transverse microchambers, *Applied Thermal Engineering* 51 (2013) 880–889. <https://doi.org/10.1016/j.applthermaleng.2012.10.037>.
- [366] M.W. Uddin, N.S. Sifat, Comparative study on hydraulic and thermal characteristics of minichannel heat sink with different secondary channels in parallel and counter flow directions, *International Journal of Thermofluids* 17 (2023) 100296. <https://doi.org/10.1016/j.ijft.2023.100296>.
- [367] A. Kosar, C.-J. Kuo, Y. Peles, Hydrooil-Based Micro Pin Fin Heat Sink, in: *American Society of Mechanical Engineers Digital Collection*, 2007: pp. 563–570. <https://doi.org/10.1115/IMECE2006-13257>.
- [368] J. Mohammadpour, S. Husain, F. Salehi, A. Lee, Machine learning regression-CFD models for the nanofluid heat transfer of a microchannel heat sink with double synthetic jets, *International Communications in Heat and Mass Transfer* 130 (2022) 105808. <https://doi.org/10.1016/j.icheatmasstransfer.2021.105808>.
- [369] M. Harris, An Investigation on Engine Mass Airflow Sensor Production via TQM, TPM, and Six Sigma Practices, *Oper. Res. Forum* 2 (2021) 61. <https://doi.org/10.1007/s43069-021-00102-y>.
- [370] A.W. Chu, B.Y. Liu, C.L. Pan, D.H. Zhu, E.X. Yang, Identification of boiling flow pattern in narrow rectangular channel based on TFA-CNN combined method, *Flow Measurement and Instrumentation* 83 (2022) 102086.

- <https://doi.org/10.1016/j.flowmeasinst.2021.102086>.
- [371] B. Zhao, X. Wen, K. Han, Learning Semi-supervised Gaussian Mixture Models for Generalized Category Discovery, in: 2023 IEEE/CVF International Conference on Computer Vision (ICCV), IEEE, Paris, France, 2023: pp. 16577–16587. <https://doi.org/10.1109/ICCV51070.2023.01524>.
 - [372] S. M.AqilBurney, H. Tariq, K-Means Cluster Analysis for Image Segmentation, IJCA 96 (2014) 1–8. <https://doi.org/10.5120/16779-6360>.
 - [373] X. Ran, Y. Xi, Y. Lu, X. Wang, Z. Lu, Comprehensive survey on hierarchical clustering algorithms and the recent developments, Artif Intell Rev 56 (2023) 8219–8264. <https://doi.org/10.1007/s10462-022-10366-3>.
 - [374] R. Al-batat, A. Angelopoulou, S. Premkumar, J. Hemanth, E. Kapetanios, An End-to-End Automated License Plate Recognition System Using YOLO Based Vehicle and License Plate Detection with Vehicle Classification, Sensors 22 (2022) 9477. <https://doi.org/10.3390/s22239477>.
 - [375] I. Muraina, Ideal Dataset Splitting Ratios in Machine Learning Algorithms: General Concerns for Data Scientists and Data Analysts, in: Mardin, Turkiye, 2022: pp. 496–504.
 - [376] Z. Zhang, M. Sabuncu, Generalized Cross Entropy Loss for Training Deep Neural Networks with Noisy Labels, in: Advances in Neural Information Processing Systems, Curran Associates, Inc., 2018. https://proceedings.neurips.cc/paper_files/paper/2018/hash/f2925f97bc13ad2852a7a551802feca0-Abstract.html (accessed March 20, 2024).
 - [377] M.A. Mahdi, K.M. Hosny, I. Elhenawy, Scalable Clustering Algorithms for Big Data: A Review, IEEE Access 9 (2021) 80015–80027. <https://doi.org/10.1109/ACCESS.2021.3084057>.

Appendices

Appendix A: Overview of Recent Trends Table

Author	Shape	DH	AR	PR	MT	WF	Analysis	Country	Contribution	FRIN
Chiriac et al.	Y-shape	0.05	1	LI	PDMS	W, Oil	CFD	Romania	μPIV result verification	M
Hoang, et al.	Rectangle	0.19	30	OF M	CU	Novec	NM	USA	New correlation model	M
Liang, et al.	Rectangle	*	0.22	CM	OMT	W	UA	China	DHCE MC system	M
Martinez et al.	Rectangle	0.42	2.83	CM	OMT	ZnO	SIMUL	Chile	Zn nanofluid arrangement	M
Yin et al.	T-shape	0.4	1	OF M	PMMA	Ethanolamine	NM	China	Chemical absorption	M
Ahmadi et al.	Square	0.97	30.6	LI	AL	W	NM	Turkey	Biphilic surface high HF cooling	M
Dalkılıç et al.	Rectangle	0.42	0.81	MM	CU	R134a	UA	Turkey	R134a in two-phase flows	M
Venegas et al.	Rectangle	0.29	20	CM	Steel	WM	NM	Spain	Membrane-based micro-desorber design	M
Ding et al.	Spiral	0.9	1	CM	OMT	DW, TiO2	NM	China	TiO2-H2O nanofluid	M
Jayaramu et al.	Rectangle	0.32	2.08	MM	CU	DW	NM	India	Different Wettability surfaces	M
Roumpea et al.	Rectangle	0.19	1.03	OF M	OMT	HY	MATLAB	UK	MC with surfactants	M
Yameen et al.	Rectangle	0.65	0.48	3D	Steel	Air-W	NM	USA	3D-printed MC manifold	M
Abdulbari et al.	Rectangle	0.17	5	LI	PDMS	WM	NM	Malaysia	Drag-reducing agent assessment	M
		0.16	4							
		0.15	3							
		0.13	2							
Guo et al.	Rectangle	0.08	4.26	LI	PDMS	HY	NM	China	EGaIn usage in MC	M
Sarafraz & Arjomandi	Square	0.4	1	MM	CU	W, Ga	NM	Australia	Application of gallium nano-suspensions	M
Sarafraz & Arjomandi	Rectangle	0.31	0.63	MM	CU	W, CuO2(I)	NM	Australia	CuO/liquid indium nanofluid	M
Sarafraz et al.	Rectangle	0.31	0.63	MM	CU	DW, Ag	NM	Iran	biological silver-water nanofluid	M
Simsek et al.	Rectangle	0.08	4	OF M	Glass	HY	NM	Turkey	silver nanowire suspension	M
		0.07	2							

		0.06	1.4							
Zhang et al.	Rectangle	0.69	1.33	3D	CU	DW	NM	China	3D heterogeneous wetting MC surfaces	M
Zhang et al.	Rectangle	0.3	1.56	3D	Inconel	N2	NM	USA	3D-printed Inconel 718 MC manifold	M
Bae et al.	Rectangle	0.02	0.2	ETC	SiC	R245fa	NM	USA	Embedded cooling system	M
Li et al.	Rectangle	0.2	1	MM	Si	DW	NM	China	MC with hydrophobic surfaces	M
Sarafaraz et al.	Rectangle	0.31	0.63	MM	PDMS	HY	NM	Iran	carbon nanotube nanofluid	M
Wang et al	Square	0.38	4.86	ETC	Si	DW	NM	China	Non-wetting fraction/pitch distance effects	M
Jiang et al	Rectangle	0.8	0.25	MM	CU	DW	NM	China	Counter flow diverging microchannels	M
Jiang et al	Rectangle	0.8	0.25	MM	CU	DW	NM	China	Surface modification of microscale cavities	M
Mohammad et al	T-shape	1	1	3D	Steel	h2/Ar	CFD	USA	3D-printed microreactors for (F-T) synthesis	M
Chiriac et al.	Y-shape	0.09	0.125	LI	PDMS	W, Oil	CFD	Romania	Trifurcation microchannel	M
Lei, et al.	T-shape	0.4	1	MM	PMMA	Glycerol, Si	MATLAB	China	Prediction scaling laws	E
Lin, et al.	Rectangle	0.2	1	OFM	OMT	W, Si	CFD	China	Novel CFD solver	E
Matin & Moghaddam	Rectangle	0.12	4	OFM	PDMS	OWF	NM	USA	Critical shear stress at liquid-vapour interface	E
	Rectangle	0.2	2							
	Square	0.3	1							
Oudebrouckx et al.	Rectangle	0.02	4	OFM	CU, AU	WM	NM	Belgium	Transient Thermal Offset method	E
Zhang et al.	Rectangle	1	5	OFM	AL	W	CFD	China	Corrugated MCHS	E
Al Siyabi et al.	Rectangle	0.67	0.5	OFM	AL	W	NM	UK	MLM heat sinks	E
Garg & Agrawal	Rectangle	0.13	0.49	LI	PDMS	N2	NM	India	High Knudsen number experiments	E
Garg & Agrawal	Rectangle	0.13	0.49	LI	PDMS	N2	NM	India	Mach/Re number relationship	E
Ji et al..	Rectangle	0.4	2	OFM	PMMA	W, Oil	NM	France	High flowrate emulsification	E
		0.6	1							

Panda et al.	Circular	0.86	1	OF M	OMT	OWF	CFD	Japan	Two-phase refrigerant maldistribution	E
Wang et al.	Rectangle	0.3	0.41	ETC	OMT	R134a	NM	China	New empirical method	E
Al-Siyabi et al.	Rectangle	0.67	0.5	MM	AL	W	CFD	UK	MLM arrangements	E
Qian et al.	Square	0.6	1	OF M	GLAS S	WM	CFD	China	Dynamic dispersed phase injection	E
Ronshin & Chinnov	Rectangle	0.1	200	OF M	Steel	DW	NM	Russia	Method to determine regime boundaries	E
Xia et al.	Rectangle	0.1	1.88	ETC	Si	W	NM	China	Triangular corrugated MC	E
		0.12	1							
Kovalev et al.	T-shape	0.12	1	CM	SU8	WM	SIMUL	Russia	New hydrodynamic features of plug flows	E
		0.16	0.5							
Kravtsova et al.	T-shape	0.12	1	CM	SU8	WM	SIMUL	Russia	Flow regime distribution features	E
		0.16	0.5							
Wang et al.	Rectangle	0.12	7.14	OF M	PDMS	DW	CFD	USA	Surface acoustic wave pumping	E
Zhai et al.	Rectangle	0.11	3.57	MM	Si	DW	NM	China	Flow prediction theoretical model	
Zhang et al.	Rectangle	0.13	2	ETC	Si	WM	NM	China	Two phase flow condensation	E
Abdo et al.	Rectangle	0.15	3	3D	OMT	W	UA	Egypt	Hybrid CPV-TEG-MCHS	E
Li et al	Rectangle	0.4	2	MM	CU	DW	NM	China	Bidirectional counter-flow microchannels	E
Jin et al	Rectangle	0.5	1	OF M	Cu	W	MATLAB	China	Feedforward and feedback control	E
Kumar et al.	Rectangle	0.55	0.62	MM	CU	W	NM	India	Asymmetric fluid flow distribution	E
Fu et al	Rectangle	0.66 8	0.45 9	MM	CU	DW	NM	China	Flow boiling in copper foam MCHS	E
		0.66 1	0.49							
Pontes et al	Rectangle	0.66 7	0.5	3D	PDMS	HFE-7100	NM	Portugal	Fluid flow and heat transfer	E
Sulaiman and Wang	Rectangle	0.37 5	15	MM	CU	R-134a	NM	Taiwan	Effect of contraction on the convective boiling	E
Wang et al	Rectangle	1	1	MM	AL	DW	NM	China	Gas-liquid Taylor flow in a square microchannel	E

Wang et al	Heirarchical	0.4	1	OF M	OMT	HY	CFD	China	Secondary vortices drag reduction	E
Tian et al.	Rectangle	1.6	4	OF M	CU	W	NM	China	Experimental correlation assessments	E
		3	3							
Saffar et al.	Curved	0.45	1	3D	PMMA	W	NM	Canada	Deformation of droplets in curved microchannel	E
Haghighinia et al.	Circular	0.8	1	LI	PDMS	W, Rhodamine	CFD	Iran	Split and recombine mixing	D
		0.16	1							
Özdemir et al.	Rectangle	0.56	2	CM	CU	DW	NM	Turkey	Small AR comparison	D
		0.56	0.39							
Ringkai et al.	T-shape	0.57	0.2	OF M	PMMA	Oil, Polystyrene	MATLAB	Malaysia	Time-resolved image sequencing	D
		0.4	1							
		0.5	1							
		0.75	1							
Vinoth & Sachuthanathan	Rectangle	1	1	MM	CU	AL2O3/CU O	NM	India	AL/CU based nanofluids	
Hou & Chen	Square	*	*	MM	Steel	W	CFD	China	Re-entrant cavity shapes	D
Luo et al.	Rectangle	1	1	OF M	OMT	W	CFD	China	Annular flow boiling hydrodynamics	D
Oudah et al.	Rectangle	0.83	0.2	MM	CU	W	NM	USA	Optimum IR dimensions	D
Ye et al.	Rectangle	0.71	13.1 2	LI	PDMS	DW, N2	CFD	China	Microchannel with gas cavities	D
Kumar	Triangular	0.46	3.33	OF M	Si	DW	CFD	India	Trapezoidal MC with grooves	D
	Rectangle	0.35	0.32							D
Liao et al.	Circular	0.51	1.04	MM	TA	FC-72	NM	Taiwan	Inlet alignments	D
Ma et al.	Rectangle	0.05	1	ETC	Si	Acetone	NM	China	Zigzag MC flow boiling	D
Nadaraja et al.	Rectangle	0.15	10	MM	CU	W	NM	Malaysia	MLM arrangements	D
Pan et al.	Circular	0.89	0.8	OF M	CU	DW	NM	China	FSC design	D
Tiwari et al.	Elliptical	1	1	3D	CU	W	UA	USA	Novel 3D-printed MCHE	D

Wang et al.	Rectangle	0.5	0.7	MM	Si	DW	CFD	China	MC with bi-directional ribs	D
Jia et al.	Rectangle	0.47	0.9	ETC	Si	OWF	NM	China	Porous wall MCHS	D
Wang et al.	Rectangle	0.35	7.5	ETC	Si	Novec	CFD	USA	Single-phase flow	D
Duryodhan et al.	Spiral	0.09	3.33	Li	PDMS	W	CFD	India	Spiral MC mixing	D
		0.13	2							
		0.2	1							
Li et al.	Rectangle	0.38	20.5	ETC	Si	Acetone	OAM	China	MC with triangular cavities	D
Vinoth & Senthil	Square	0.85	1.13	MM	CU	HY	UA	India	Oblique-finned MCHS	D
	Circular	0.85	1.13							
	Trapezoid	0.85	1.13							
Walunj & Satyabhama	Square	0.5	1	ETC	SI	DW	NM	India	Open microchannels	D
	Parabolic	0.57	1.3							
	Parabolic	0.43	0.75							
	Stepped	0.57	1.3							
	Stepped	0.43	0.75							
Li et al	Rectangle	0.4	2	MM	CU	DW	NM	China	Counter-flow stepped microchannels	D
Kumar and Singh	Rectangle	1	3.33	MM	AL	W	NM	India	Microchannel with microinserts	D
Zhang et al	Rectangle	0.75	1.67	OF M	AL	W	CFD	China	Analysis of optimised internal fins	D
Tang et al	Rectangle	0.29	2.5	ETC	Si	DW	NM	China	Expansion areas	D
Cheng et al	Rectangle	0.08	4	MM	Si	DW	NM	China	Groove-wall microchannel	D
		0.01 1	2.4							
		0.2	1							
Ge et al	Rectangle	1	1	MM	PMMA	W, NaOH	NM	China	Converging-diverging geometries	D
Cui and Lui	Rectangle	0.38	1	MM	CU	DW	NM	China	Ultra AR MCHS flow boiling	D
		0.38	5							
		0.39	15							
		0.38	25							
Han et al.	Rectangle	0.40 5	0.68	OF M	CU	DW	NM	China	Heat transfer in Saw Tooth MCHS	D

	Saw-tooth	0.31 5	0.46							
Liu et al.	T-shape	0.46 2	1.33	OF M	CU	DW	NM	China	Open diverging MCHS	D
Marseglia et al	Rectangle	0.4	1	3D	Steel	HFE-7100	NM	Italy	Effect of channel geometry on HFE-7100 boiling	D
		0.66 7	2							
		0.85 7	3							
		0.4	4							
Memon et al	Wavy	0.15	1	OF M	OMT	Water	CFD	Korea	Wavy microchannel with secondary flow passages	D
Vinoth et al	Rectangle	0.9	1	MM	CU	DW	NM	India	Oblique finned curved microchannel	D
	Curved	0.9	1			HY				
Wang et al	Hierarchical	1.2	1	OF M	OMT	HY	CFD	China	Hierarchical microchannels and nanofluids	D
		0.9	1							
		0.6	1							
Yin et al.	Rectangle	0.57	20	CM	CU	DW	NM	China	Large AR	D
Li, et al.	Rectangle	0.38	0.04	ETC	SI	H2O2	MATLAB	China	H2O2 decomposition method	S
Lin, et al.	Rectangle	0.91	10	OF M	SI	DW	NM	China	Heterogeneous wetting surface	S
Wang et al.	Triangular	*	*	CM	OMT	W	NM	China	DCHE-based dehumidification	S
Bhattacharjee et al.	Circular	0.18	1	OF M	PDMS	Polymer	NM	UK	Strain sensor feedback control	S
Kumar and Kumaraguruparan	Rectangle	0.77 6	1.12 5	CM	CU	R134a	NM	India	Miniature personal cooling system	S
		1	1.11 1							
Ali et al	Rectangle	0.85	0.89	MM	AL	HY	NM	Korea	Dehydrogenation of perhydro-dibenzyltoluene	S

Appendix B: CNC Machine Specification

Jingdiao Machine Tools: CTA series CNC Machining Center

From: <https://us.jingdiao.com>

Processing Quenching Material and Difficult-to-cut Material High rigidity because of the application of three rails heightened structure, cooling technology used on spindles, optimization of machining accuracy and motion accuracy by control system, CTA series is the one for hard material processing.

CTA400: Meet the composite processing requirements of precision die mold parts, and stably achieve processing accuracy of 10~20 μ m.

X/Y/Z Travel:	15.7/15.7/11.8 in.
Worktable Size:	20.9×17.0 in.
Max. Load:	661.4 lb.
Tool Magazine	Umbrella Type (16 Tools)
Spindle Type	High-Speed Precision Spindle JD150S-20-HA50/C (Standard)
Spindle Specification	20000rpm/HSK-A50



Information and Images provided by Dr. Jianfei Sun

Appendix C: Python Codes and Raw Data

C1: Python Script for Sustainability and Cost Analysis

The script generates a detailed comparison of production cost predictions using Linear Regression and Random Forest models for two production strategies: Full UK Production and Hybrid Production. First, synthetic data for 500 production instances is generated, incorporating features such as units produced, production type, material costs, machining times, labour costs, energy consumption, and shipping costs. The production type (0 for Full UK, 1 for Hybrid) determines the material costs and other parameters specific to each region (e.g., higher labour costs in the UK and lower energy consumption in China). The script then calculates the total production cost for each scenario, building a comprehensive dataset. This data is split into training and testing sets to train both models. The Linear Regression and Random Forest models are trained separately and used to predict production costs for the testing data. The script then evaluates both models using Root Mean Squared Error (RMSE) and R^2 (Coefficient of Determination), displaying the results visually through a scatter plot comparing Actual vs. Predicted Costs. Linear Regression predictions are shown using square markers, while Random Forest predictions use circular markers. A red dashed line indicates the perfect prediction line, and the scatter plot is colour-coded based on production type, with a colour bar for clarity. The plot is saved as a high-resolution 300 DPI PNG image, making it suitable for reporting and presentations. Finally, the script outputs the RMSE and R^2 values to highlight the Random Forest model's superior accuracy compared to Linear Regression.

✓ Calculation for Cost and Sustainability Benefits

```
# Define number of units for both mini-channels and pin-fin structures
units_mini_channel = 1000 # Number of mini-channel units
units_pin_fins = 1000 # Number of micro pin-fin units

# --- Full UK Production Calculation ---
# Full UK: Producing both mini-channels and pin-fins in the UK

# Cost Parameters for Full UK Production
uk_material_cost_per_kg = 2.56 # USD per kg for aluminium
uk_machining_rate_per_hour = 70 # USD per hour
uk_machining_time_per_unit_mini_channel = 1 # Machining time for mini-channel
uk_machining_time_per_unit_pin_fins = 2 # Machining time for pin-fins (higher complexity)
uk_assembly_cost_per_unit = 5 # Assembly cost in USD per unit
uk_energy_per_unit_mini_channel = 1.8 # kWh per unit for mini-channel
uk_energy_per_unit_pin_fins = 2.0 # kWh per unit for pin-fin structures
uk_emission_factor = 0.21 # kg CO2 per kWh for UK

# Material Costs for 1,000 mini-channels and 1,000 pin-fins
uk_total_material_cost = (units_mini_channel + units_pin_fins) * uk_material_cost_per_kg

# Machining Costs for Mini-Channels and Pin-Fins
uk_machining_cost_mini_channels = units_mini_channel * (uk_machining_rate_per_hour * uk_machining_time_per_unit_mini_channel)
uk_machining_cost_pin_fins = units_pin_fins * (uk_machining_rate_per_hour * uk_machining_time_per_unit_pin_fins)

# Assembly Costs for both components
uk_total_assembly_cost = (units_mini_channel + units_pin_fins) * uk_assembly_cost_per_unit

# Total Production Cost in the UK
total_uk_production_cost = uk_total_material_cost + uk_machining_cost_mini_channels + uk_machining_cost_pin_fins + uk_total_assembly_cost

# Energy Consumption and Carbon Emissions for Full UK Production
total_uk_energy_consumption = (units_mini_channel * uk_energy_per_unit_mini_channel) + (units_pin_fins * uk_energy_per_unit_pin_fins)
total_uk_emissions = total_uk_energy_consumption * uk_emission_factor # Total carbon emissions in kg CO2

# --- Hybrid Production Calculation (UK + China) ---
# Mini-Channels in UK and Pin-Fins in China

# Cost Parameters for Hybrid Production
china_material_cost_per_kg = 2.30 # USD per kg for aluminium
china_machining_rate_per_hour = 20 # USD per hour
china_machining_time_per_unit_pin_fins = 2 # Machining time for pin-fins in China
china_shipping_cost_per_unit = 4 # Shipping and customs cost in USD per unit
china_energy_per_unit_pin_fins = 0.9 # kWh per unit for China production
china_emission_factor = 0.30 # kg CO2 per kWh for China

# Material Costs: UK for mini-channels, China for pin-fins
hybrid_material_cost_uk = units_mini_channel * uk_material_cost_per_kg # UK material cost for mini-channels
hybrid_material_cost_china = units_pin_fins * china_material_cost_per_kg # China material cost for pin-fins

# Machining Costs: UK for mini-channels, China for pin-fins
hybrid_machining_cost_mini_channels = units_mini_channel * (uk_machining_rate_per_hour * uk_machining_time_per_unit_mini_channel)
hybrid_machining_cost_china = units_pin_fins * (china_machining_rate_per_hour * china_machining_time_per_unit_pin_fins)

# Shipping and Customs Costs for Pin-Fins (China to UK)
hybrid_shipping_cost = units_pin_fins * china_shipping_cost_per_unit

# Assembly Costs in the UK
hybrid_assembly_cost = (units_mini_channel + units_pin_fins) * uk_assembly_cost_per_unit

# Total Hybrid Production Cost
total_hybrid_production_cost = hybrid_material_cost_uk + hybrid_material_cost_china + hybrid_machining_cost_mini_channels + hybrid_machining_cost_china + hybrid_shipping_cost + hybrid_assembly_cost

# Energy Consumption and Carbon Emissions for Hybrid Production
total_hybrid_energy_consumption = (units_mini_channel * uk_energy_per_unit_mini_channel) + (units_pin_fins * china_energy_per_unit_pin_fins)
total_hybrid_emissions = (units_mini_channel * uk_emission_factor) + (units_pin_fins * china_emission_factor)

# --- Savings Calculations ---

# Cost Savings
cost_savings = total_uk_production_cost - total_hybrid_production_cost
percentage_cost_savings = (cost_savings / total_uk_production_cost) * 100

# Energy Savings
energy_savings = total_uk_energy_consumption - total_hybrid_energy_consumption
percentage_energy_savings = (energy_savings / total_uk_energy_consumption) * 100

# Carbon Emissions Savings
```

```

emission_savings = total_uk_emissions - total_hybrid_emissions
percentage_emission_savings = (emission_savings / total_uk_emissions) * 100

# --- Output Results ---
print("---- Full UK Production ----")
print(f"Total UK Production Cost: {total_uk_production_cost:.2f} USD")
print(f"Total Energy Consumption (UK): {total_uk_energy_consumption:.2f} kWh")
print(f"Total Carbon Emissions (UK): {total_uk_emissions:.2f} kg CO2")

print("\n---- Hybrid Production (UK + China) ----")
print(f"Total Hybrid Production Cost: {total_hybrid_production_cost:.2f} USD")
print(f"Total Energy Consumption (Hybrid): {total_hybrid_energy_consumption:.2f} kWh")
print(f"Total Carbon Emissions (Hybrid): {total_hybrid_emissions:.2f} kg CO2")

print("\n---- Savings Analysis ----")
print(f"Cost Savings: {cost_savings:.2f} USD ({percentage_cost_savings:.2f}%)")
print(f"Energy Savings: {energy_savings:.2f} kWh ({percentage_energy_savings:.2f}%)")
print(f"Carbon Emissions Savings: {emission_savings:.2f} kg CO2 ({percentage_emission_savings:.2f}%)")

```

```

---- Full UK Production ----
Total UK Production Cost: 225120.00 USD
Total Energy Consumption (UK): 3800.00 kWh
Total Carbon Emissions (UK): 798.00 kg CO2

---- Hybrid Production (UK + China) ----
Total Hybrid Production Cost: 128860.00 USD
Total Energy Consumption (Hybrid): 2700.00 kWh
Total Carbon Emissions (Hybrid): 648.00 kg CO2

---- Savings Analysis ----
Cost Savings: 96260.00 USD (42.76%)
Energy Savings: 1100.00 kWh (28.95%)
Carbon Emissions Savings: 150.00 kg CO2 (18.80%)

```

✓ Comparison for Predicted and Actual Cost Variations

```

# Import necessary libraries
import numpy as np
import pandas as pd
import matplotlib.pyplot as plt
from sklearn.model_selection import train_test_split
from sklearn.linear_model import LinearRegression
from sklearn.ensemble import RandomForestRegressor
from sklearn.metrics import mean_squared_error, r2_score

# Step 1: Generate Synthetic Data for Both Production Strategies
np.random.seed(42)
data_size = 500

# Generate data for various production features
units = np.random.randint(500, 2000, size=data_size) # Number of units
production_type = np.random.choice([0, 1], size=data_size) # 0 for Full UK, 1 for Hybrid

# Material costs based on production type (UK vs. China)
material_cost_uk = np.random.uniform(2.5, 3.0, size=data_size)
material_cost_china = np.random.uniform(2.0, 2.5, size=data_size)
material_cost = np.where(production_type == 0, material_cost_uk, material_cost_china)

# Machining times for mini-channels and pin-fin structures
mini_channel_time = np.random.uniform(1.0, 1.5, size=data_size)
pin_fin_time = np.random.uniform(2.0, 3.0, size=data_size)
machining_time = np.where(production_type == 0, mini_channel_time, pin_fin_time)

# Labour costs: Higher for UK, Lower for China
labour_cost_uk = np.random.uniform(20, 50, size=data_size)
labour_cost_china = np.random.uniform(5, 15, size=data_size)
labour_cost = np.where(production_type == 0, labour_cost_uk, labour_cost_china)

# Energy consumption per unit (UK vs. China)
energy_uk = np.random.uniform(1.8, 2.2, size=data_size)
energy_china = np.random.uniform(0.8, 1.2, size=data_size)
energy_consumption = np.where(production_type == 0, energy_uk, energy_china)

# Shipping costs only for Hybrid Production (Production Type = 1)
shipping_cost = np.where(production_type == 1, np.random.uniform(0.5, 2.0, size=data_size), 0)

# Calculate total cost for each scenario
total_cost = np.where(
    production_type == 0,
    units * (material_cost + (machining_time * labour_cost) + (energy_consumption * 0.1)),
    units * (material_cost + (machining_time * labour_cost) + (energy_consumption * 0.1) + shipping_cost)
)

```

```

    units * (material_cost + (mini_channel_time * labour_cost) + (energy_consumption * 0.1) + shipping_cost)
)

# Create a DataFrame for modeling
df = pd.DataFrame({
    'Units': units,
    'ProductionType': production_type,
    'MaterialCost': material_cost,
    'MachiningTime': machining_time,
    'LabourCost': labour_cost,
    'EnergyConsumption': energy_consumption,
    'ShippingCost': shipping_cost,
    'TotalCost': total_cost
})

# Step 2: Split data into training and testing sets
X = df[['Units', 'ProductionType', 'MaterialCost', 'MachiningTime', 'LabourCost', 'EnergyConsumption', 'ShippingCost']]
y = df['TotalCost']
X_train, X_test, y_train, y_test = train_test_split(X, y, test_size=0.2, random_state=42)

# Step 3: Train a Linear Regression Model
linear_regressor = LinearRegression()
linear_regressor.fit(X_train, y_train)
y_pred_linear = linear_regressor.predict(X_test)

# Step 4: Train a Random Forest Regressor Model
rf_regressor = RandomForestRegressor(random_state=42)
rf_regressor.fit(X_train, y_train)
y_pred_rf = rf_regressor.predict(X_test)

# Step 5: Evaluate both models
linear_rmse = mean_squared_error(y_test, y_pred_linear, squared=False)
rf_rmse = mean_squared_error(y_test, y_pred_rf, squared=False)
linear_r2 = r2_score(y_test, y_pred_linear)
rf_r2 = r2_score(y_test, y_pred_rf)

# Step 6: Visualise Predictions vs Actual Costs for Both Models
plt.figure(figsize=(14, 7))

# Linear Regression with square markers ('s')
plt.scatter(y_test, y_pred_linear, c=X_test['ProductionType'], cmap='coolwarm', alpha=0.7, marker='s', s=70, label='Linear Regression Pre

# Random Forest with default circular markers ('o')
plt.scatter(y_test, y_pred_rf, c=X_test['ProductionType'], cmap='viridis', alpha=0.5, s=70, label='Random Forest Predictions')

# Perfect prediction line
plt.plot([y_test.min(), y_test.max()], [y_test.min(), y_test.max()], 'r--', lw=2, label='Perfect Prediction Line')

# Colorbar for Production Type
cbar = plt.colorbar()
cbar.set_label('Production Type (0 = Full UK, 1 = Hybrid)')

# Set larger font sizes for axes and labels
plt.xlabel('Actual Production Cost (USD × 105)', fontsize=16)
plt.ylabel('Predicted Production Cost (USD × 105)', fontsize=16)

# Apply scientific notation for better space management
plt.ticklabel_format(style='sci', axis='both', scilimits=(5, 5))

# Title and legend
plt.title(f'Actual vs Predicted Production Costs: Linear Regression vs Random Forest\n'
        f'LR RMSE: {linear_rmse:.2f} USD, R²: {linear_r2:.3f} | '
        f'RF RMSE: {rf_rmse:.2f} USD, R²: {rf_r2:.3f}', fontsize=18)
plt.legend(fontsize=14)
plt.grid(False)

# Save the plot as a high-resolution PNG image
plt.savefig('production_cost_comparison.png', dpi=300, format='png')

# Display plot
plt.show()

# Output RMSE and R-squared values for clarity
print(f"Linear Regression RMSE: {linear_rmse:.2f} USD, R²: {linear_r2:.3f}")
print(f"Random Forest RMSE: {rf_rmse:.2f} USD, R²: {rf_r2:.3f}")

```

C2: Python Script for Sample Bagging and Stacking Regression

```
import pandas as pd
from sklearn.ensemble import BaggingRegressor
from sklearn.ensemble import StackingRegressor
from sklearn.linear_model import LinearRegression
from sklearn.model_selection import train_test_split
from sklearn.metrics import mean_squared_error
from sklearn.preprocessing import StandardScaler
from sklearn.metrics import mean_absolute_percentage_error

# Load the data from the CSV file
data = pd.read_csv('CFD.csv')

# Extract the independent variables (X) and the dependent variable (y)
X = data[['Re', 'V_in', 'Volume', 'SA']]
y = data['HTC']

# Data normalization
scaler = StandardScaler()
X_scaled = scaler.fit_transform(X)

# Split the data into training and test sets
X_train, X_test, y_train, y_test = train_test_split(X_scaled, y, test_size=0.2, random_state=42)

# Train a BaggingRegressor
bagging = BaggingRegressor(base_estimator=LinearRegression(), n_estimators=4, random_state=42)
bagging.fit(X_train, y_train)

# Train a StackingRegressor
estimators = [('linear', LinearRegression())]
stacking = StackingRegressor(estimators=estimators, final_estimator=LinearRegression())
stacking.fit(X_train, y_train)

# Make predictions on the test set
y_pred_bagging = bagging.predict(X_test)
y_pred_stacking = stacking.predict(X_test)

# Calculate MSE, RMSE, and MAPE
mse_bagging = mean_squared_error(y_test, y_pred_bagging)
mse_stacking = mean_squared_error(y_test, y_pred_stacking)

rmse_bagging = mean_squared_error(y_test, y_pred_bagging, squared=False)
rmse_stacking = mean_squared_error(y_test, y_pred_stacking, squared=False)

mape_bagging = mean_absolute_percentage_error(y_test, y_pred_bagging)
mape_stacking = mean_absolute_percentage_error(y_test, y_pred_stacking)

print("Bagging - Mean Squared Error:", mse_bagging)
print("Bagging - Root Mean Squared Error:", rmse_bagging)

print("Stacking - Mean Squared Error:", mse_stacking)
print("Stacking - Root Mean Squared Error:", rmse_stacking)

print("Mean Absolute Percentage Error (MAPE):", mape_bagging)
print("Mean Absolute Percentage Error (MAPE):", mape_stacking)

🔍 Bagging - Mean Squared Error: 42.85328977313548
Bagging - Root Mean Squared Error: 6.546242416313001
Stacking - Mean Squared Error: 39.413936985705796
Stacking - Root Mean Squared Error: 6.2780520056547635
Mean Absolute Percentage Error (MAPE): 0.04901521730783303
Mean Absolute Percentage Error (MAPE): 0.04480820462100264
/usr/local/lib/python3.10/dist-packages/sklearn/ensemble/_base.py:166: FutureWarning: `base_estima
warnings.warn(
```


C3: Python Script for Sample Principal Data Analysis (PCA)

```
import numpy as np
from sklearn.preprocessing import StandardScaler
from sklearn.decomposition import PCA
import matplotlib.pyplot as plt

# Data for Curve 150W
data_curve_150w = {
    'PD': [189.44544, 733.36216, 1378.6012, 2337.3212, 3550.52],
    'Re': [101.3018555, 202.6037109, 303.9055664, 405.2074219, 506.5092774],
    'Pr': [4.266283386, 4.585017136, 4.715834383, 4.79854389, 4.838288859],
    'Nu': [8.873100478, 10.49248387, 11.0815278, 11.9815343, 12.87198073],
    'Rth': [0.053123657, 0.044924686, 0.042536693, 0.039341501, 0.03661997],
    'Pu': [0.000569473, 0.004408973, 0.012432226, 0.02810395, 0.053364316]
}

# Data for Curve 250W
data_curve_250w = {
    'PD': [160.02466, 657.74064, 1348.5276, 2319.5538, 3462.5004],
    'Re': [101.3018555, 202.6037109, 303.9055664, 405.2074219, 506.5092774],
    'Pr': [4.131557383, 4.468266392, 4.540595274, 4.515855497, 4.470644532],
    'Nu': [8.3935458, 9.981789947, 11.14842415, 11.90606567, 12.37673459],
    'Rth': [0.05615881, 0.047223148, 0.04228145, 0.039590874, 0.038085291],
    'Pu': [0.000481034, 0.003954337, 0.012161022, 0.027890315, 0.052041381]
}

# Data for Edge 150W
data_edge_150w = {
    'PD': [288.93188, 1023.6796, 1896.1254, 3035.0502, 4185.3924],
    'Re': [101.3018555, 202.6037109, 303.9055664, 405.2074219, 506.5092774],
    'Pr': [5.519578109, 5.630542568, 5.64621401, 5.547700161, 5.454401292],
    'Nu': [7.88516603, 9.245673647, 9.438316156, 9.689444172, 10.17197741],
    'Rth': [0.058045885, 0.049504391, 0.048493972, 0.04723712, 0.044996309],
    'Pu': [0.000868529, 0.006154362, 0.017099259, 0.036493444, 0.062906448]
}

# Data for Edge 250W
data_edge_250w = {
    'PD': [366.59436, 1130.19008, 1957.1378, 3000.312, 4001.5376],
    'Re': [101.3018555, 202.6037109, 303.9055664, 405.2074219, 506.5092774],
    'Pr': [4.455515725, 4.834315156, 4.88081157, 4.818447487, 4.70413957],
    'Nu': [7.55912361, 8.611117866, 8.946245163, 9.133611244, 9.562407547],
    'Rth': [0.060549538, 0.053152384, 0.05116129, 0.050111772, 0.047864666],
    'Pu': [0.001101983, 0.006794703, 0.017649469, 0.036075751, 0.06014311]
}

# Data for Bypass 150W
data_bypass_150w = {
    'PD': [204.32434, 802.04088, 1437.6594, 2409.6592, 3335.2416],
    'Re': [101.3018555, 202.6037109, 303.9055664, 405.2074219, 506.5092774],
    'Pr': [4.775854719, 5.089778974, 5.171048524, 5.180101353, 5.182386531],
    'Nu': [5.24614079, 6.65648142, 7.255281636, 7.738669892, 7.899825132],
    'Rth': [0.082115305, 0.064717142, 0.059375841, 0.055666989, 0.054531391],
    'Pu': [0.000614199, 0.00482187, 0.012964812, 0.028973742, 0.050128681]
}

# Data for Bypass 250W
data_bypass_250w = {
    'PD': [219.74, 781, 1460, 2425, 3339],
    'Re': [101.3018555, 202.6037109, 303.9055664, 405.2074219, 506.5092774],
    'Pr': [4.358563202, 4.732192727, 4.799679872, 4.762424475, 4.710846059],
    'Nu': [5.285172252, 6.966535503, 7.676341974, 8.568132295, 9.153032529],
    'Rth': [0.081508876, 0.061836827, 0.056118976, 0.050277988, 0.047065106],
    'Pu': [0.000660538, 0.004695372, 0.01316628, 0.0291582, 0.05018517]
}

# Data for Splitter 150W
data_splitter_150w = {
    'PD': [239.42248, 858.51744, 1782.7552, 2858.6586, 4154.9584],
    'Re': [101.3018555, 202.6037109, 303.9055664, 405.2074219, 506.5092774],
    'Pr': [6.676965436, 6.65836494, 6.534000421, 6.306617978, 6.118346994],
    'Nu': [9.780166095, 10.87548809, 11.34254081, 11.55980892, 12.47404991],
    'Rth': [0.042487811, 0.038208662, 0.036635341, 0.035946775, 0.033312184],
    'Pu': [0.000719704, 0.005161407, 0.016076886, 0.034372511, 0.062449025]
}

# Data for Splitter 250W
data_splitter_250w = {
    'PD': [215.6134, 902.75696, 1870.9072, 3011.0878, 4224.0156],
    'Re': [101.3018555, 202.6037109, 303.9055664, 405.2074219, 506.5092774],
    'Pr': [4.783529053, 5.219599311, 5.249602417, 5.208254863, 5.109026863],
```

```

# Create DataFrames
df_curve_150w = pd.DataFrame(data_curve_150w)
df_curve_250w = pd.DataFrame(data_curve_250w)
df_edge_150w = pd.DataFrame(data_edge_150w)
df_edge_250w = pd.DataFrame(data_edge_250w)
df_bypass_150w = pd.DataFrame(data_bypass_150w)
df_bypass_250w = pd.DataFrame(data_bypass_250w)
df_splitter_150w = pd.DataFrame(data_splitter_150w)
df_splitter_250w = pd.DataFrame(data_splitter_250w)

# Combine DataFrames
df_combined = pd.concat([
    df_curve_150w,
    df_curve_250w,
    df_edge_150w,
    df_edge_250w,
    df_bypass_150w,
    df_bypass_250w,
    df_splitter_150w,
    df_splitter_250w
], ignore_index=True)

# Drop any rows with missing values (if necessary)
df_combined = df_combined.dropna()

# Separate features
X = df_combined[['PD', 'Re', 'Pr', 'Nu', 'Rth', 'Pu']]

# Standardize the features
scaler = StandardScaler()
X_scaled = scaler.fit_transform(X)

# Apply PCA
pca = PCA()
X_pca = pca.fit_transform(X_scaled)

# Plot explained variance
plt.figure(figsize=(10, 6))
plt.plot(np.cumsum(pca.explained_variance_ratio_), marker='o')
plt.xlabel('Number of Components')
plt.ylabel('Cumulative Explained Variance')
plt.title('Explained Variance by Principal Components')
plt.grid()
plt.show()

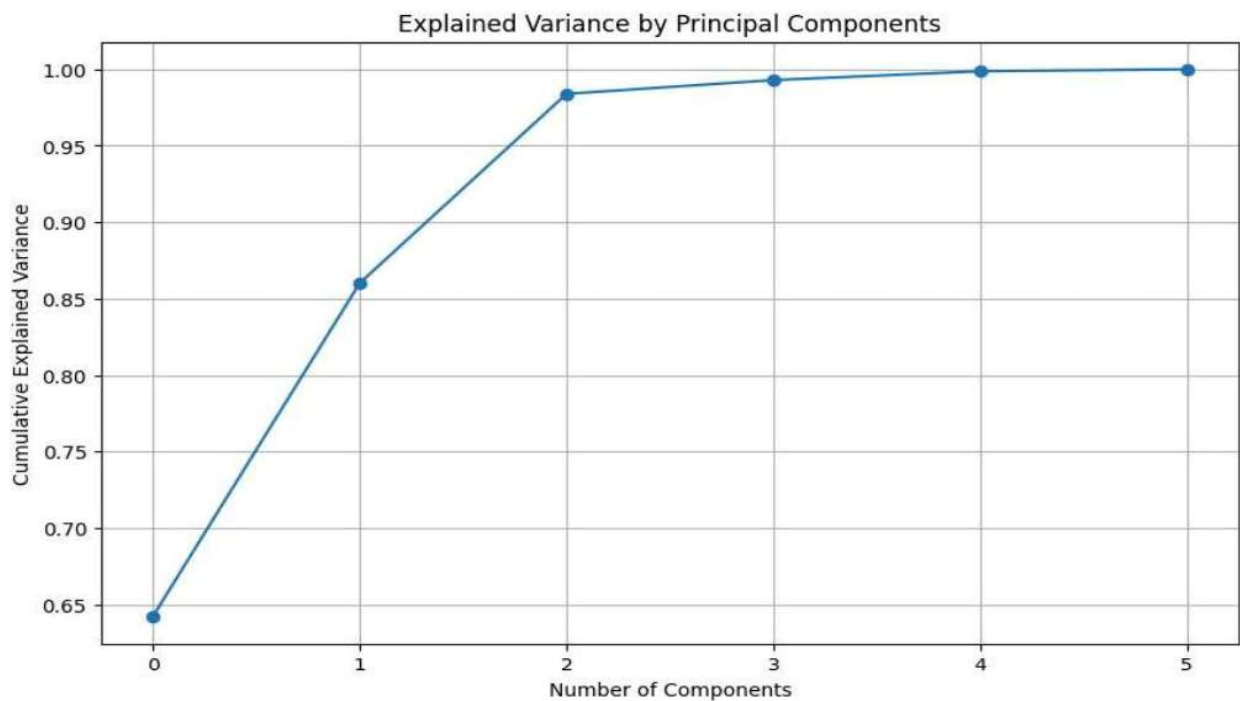
# Print explained variance ratio
print("Explained variance ratio by component:")
print(pca.explained_variance_ratio_)

# Get the PCA components
components = pd.DataFrame(pca.components_, columns=X.columns)
print("\nPCA Components (loadings):")
print(components)

# Identify the most important variables for the first two principal components
importance = np.abs(components.iloc[:2]).sum()
importance_sorted = importance.sort_values(ascending=False)

print("\nVariables contributing most to the first two principal components:")
print(importance_sorted)

```



Explained variance ratio by component:

```
[0.64232733 0.21789716 0.12369737 0.00898408 0.00577462 0.00131944]
```

PCA Components (loadings):

	PD	Re	Pr	Nu	Rth	Pu
0	-0.473212	-0.468182	-0.145831	-0.403303	0.401800	-0.459906
1	-0.288261	-0.300600	0.594181	0.392541	-0.458426	-0.330533
2	-0.174866	-0.098544	-0.783929	0.454078	-0.335517	-0.162501
3	0.067260	-0.677935	0.018113	0.335797	0.295728	0.579083
4	0.087000	-0.354704	-0.098223	-0.602316	-0.652960	0.260438
5	-0.806415	0.308744	0.034083	-0.039093	-0.044935	0.499663

Variables contributing most to the first two principal components:

Rth	0.860226
Nu	0.795843
Pu	0.790438
Re	0.768783
PD	0.761472
Pr	0.740011

import seaborn as sns

Create a DataFrame for the PCA scores

```
pca_df = pd.DataFrame(X_pca, columns=[f'PC{i+1}' for i in range(X_pca.shape[1])])
```

Plot the scores of the first two principal components

```
plt.figure(figsize=(10, 6))
sns.scatterplot(x='PC1', y='PC2', data=pca_df)
plt.title('PCA: Scatter Plot of the First Two Principal Components')
plt.xlabel('Principal Component 1')
plt.ylabel('Principal Component 2')
plt.grid()
plt.show()
```

Biplot to visualize the principal components and feature contributions

```
def biplot(scores, coefficients, features):
    plt.figure(figsize=(12, 8))
    plt.scatter(scores[:, 0], scores[:, 1], alpha=0.5)

    for i, feature in enumerate(features):
        plt.arrow(0, 0, coefficients[i, 0], coefficients[i, 1],
                  head_width=0.05, head_length=0.1, fc='r', ec='r')
        plt.text(coefficients[i, 0]*1.15, coefficients[i, 1]*1.15, feature, color='r')

    plt.title('PCA Biplot')
    plt.xlabel('Principal Component 1')
    plt.ylabel('Principal Component 2')
    plt.grid()
    plt.show()
```

Plot biplot

```
biplot(X_pca, components.iloc[:2].T.values, X.columns)
```

C4: Python Script for Base CNN Architecture

```
In [1]: import tensorflow as tf
import numpy as np
```

```
In [2]: base_dir=r"C:\Test4"
```

```
In [ ]: IMAGE_SIZE=224
        BATCH_SIZE=64

        #pre=processing
        train_datagen=tf.keras.preprocessing.image.ImageDataGenerator(
            rescale=1./255,
            shear_range=0.2,
            zoom_range=0.2,
            horizontal_flip=True,
            validation_split=0.1
        )

        test_datagen=tf.keras.preprocessing.image.ImageDataGenerator(
            rescale=1./255,
            validation_split=0.1
        )

        train_datagen=train_datagen.flow_from_directory(
            base_dir,
            target_size=(IMAGE_SIZE,IMAGE_SIZE),
            batch_size=BATCH_SIZE,
            subset='training'
        )

        test_datagen=test_datagen.flow_from_directory(
            base_dir,
            target_size=(IMAGE_SIZE,IMAGE_SIZE),
            batch_size=BATCH_SIZE,
            subset='validation'
        )
```

```
In [20]: cnn=tf.keras.Sequential()
cnn.add(tf.keras.layers.Conv2D(filters=64,padding='same',strides=2,kernel_size=3))
cnn.add(tf.keras.layers.MaxPool2D(pool_size=2,strides=2))

cnn.add(tf.keras.layers.Conv2D(filters=32,padding='same',strides=2,kernel_size=3))
cnn.add(tf.keras.layers.MaxPool2D(pool_size=2,strides=2))

cnn.add(tf.keras.layers.Conv2D(filters=32,padding='same',strides=2,kernel_size=3))
cnn.add(tf.keras.layers.MaxPool2D(pool_size=2))


cnn.add(tf.keras.layers.Flatten())
cnn.add(tf.keras.layers.Dense(4,activation='softmax'))
```


```
In [21]: cnn.compile(optimizer=tf.keras.optimizers.Adam(),loss='categorical_crossentropy')
```


```
In [ ]: cnn.fit(train_datagen,epochs=20,validation_data=test_datagen)
```


```
In [ ]: cnn.fit(train_datagen,epochs=20,validation_data=test_datagen)
```


Sample Raw Data Gaussian Model (Train 20 Epochs)


Epoch 1/20
23/23  17s 551ms/step - accuracy: 0.8916 - loss: 0.3416 - val
_accuracy: 0.8805 - val_loss: 0.4522


Epoch 2/20
23/23  17s 526ms/step - accuracy: 0.8668 - loss: 0.3579 - val
_accuracy: 0.9686 - val_loss: 0.2282


Epoch 3/20
23/23  17s 508ms/step - accuracy: 0.8872 - loss: 0.3711 - val
_accuracy: 0.8679 - val_loss: 0.4555


Epoch 4/20
23/23  17s 544ms/step - accuracy: 0.8896 - loss: 0.3293 - val
_accuracy: 0.8365 - val_loss: 0.6796


Epoch 5/20
23/23  17s 528ms/step - accuracy: 0.8962 - loss: 0.3125 - val
_accuracy: 0.9057 - val_loss: 0.3830


Epoch 6/20
23/23  17s 524ms/step - accuracy: 0.9165 - loss: 0.2734 - val
_accuracy: 0.9686 - val_loss: 0.2104

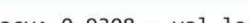
Epoch 7/20
23/23  17s 522ms/step - accuracy: 0.8614 - loss: 0.3687 - val
_accuracy: 0.7547 - val_loss: 1.2125


Epoch 8/20
23/23  17s 532ms/step - accuracy: 0.8413 - loss: 0.4343 - val
_accuracy: 0.8491 - val_loss: 0.6346

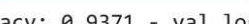
Epoch 9/20
23/23  17s 508ms/step - accuracy: 0.9007 - loss: 0.3000 - val
_accuracy: 0.9057 - val_loss: 0.4290

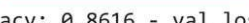
Epoch 10/20
23/23  17s 522ms/step - accuracy: 0.9172 - loss: 0.2621 - val
_accuracy: 0.8994 - val_loss: 0.3721


Epoch 11/20
23/23  17s 543ms/step - accuracy: 0.9218 - loss: 0.2446 - val
_accuracy: 0.9057 - val_loss: 0.3515


Epoch 12/20
23/23  17s 527ms/step - accuracy: 0.9325 - loss: 0.2278 - val
_accuracy: 0.9308 - val_loss: 0.3460


Epoch 13/20
23/23  17s 529ms/step - accuracy: 0.9478 - loss: 0.2005 - val
_accuracy: 0.9119 - val_loss: 0.3533


Epoch 14/20
23/23  17s 535ms/step - accuracy: 0.9461 - loss: 0.1836 - val
_accuracy: 0.9371 - val_loss: 0.2641


Epoch 15/20
23/23  17s 525ms/step - accuracy: 0.9514 - loss: 0.1849 - val
_accuracy: 0.8616 - val_loss: 0.5076

Epoch 16/20
23/23  17s 522ms/step - accuracy: 0.9433 - loss: 0.1971 - val
_accuracy: 0.8616 - val_loss: 0.5463

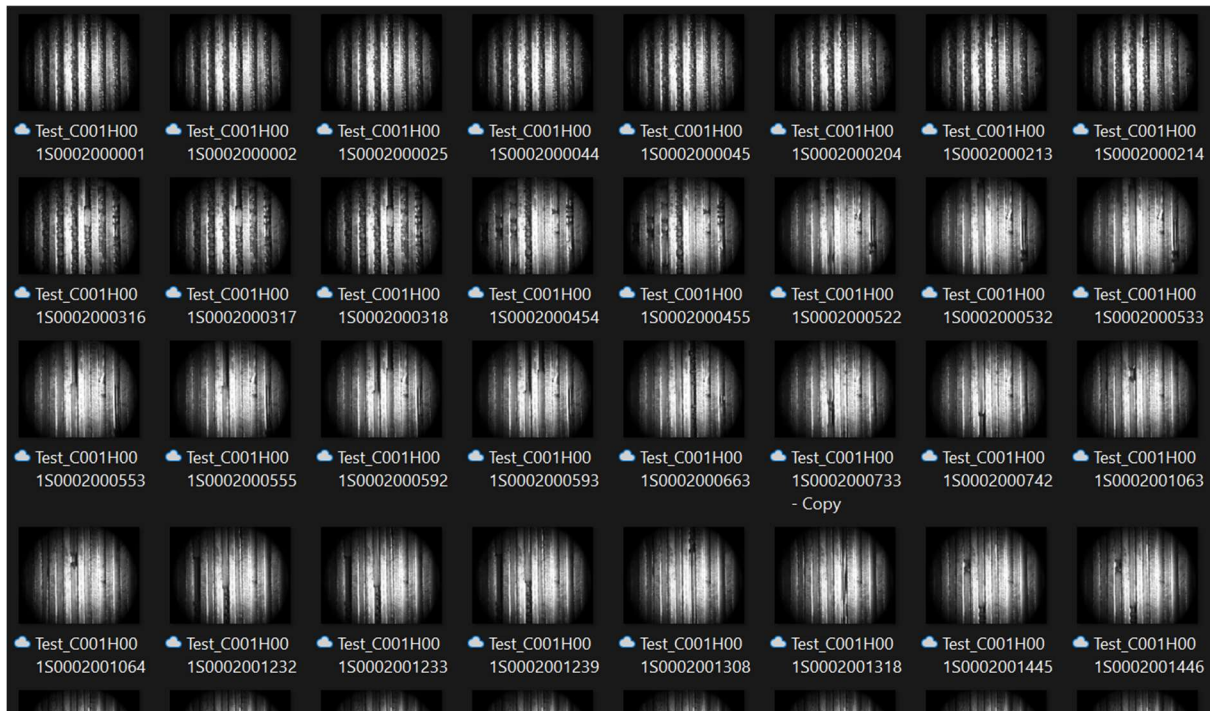
Epoch 17/20
23/23  17s 524ms/step - accuracy: 0.9511 - loss: 0.1824 - val
_accuracy: 0.8994 - val_loss: 0.3356

Epoch 18/20
23/23  17s 542ms/step - accuracy: 0.9382 - loss: 0.1701 - val
_accuracy: 0.8616 - val_loss: 0.5736

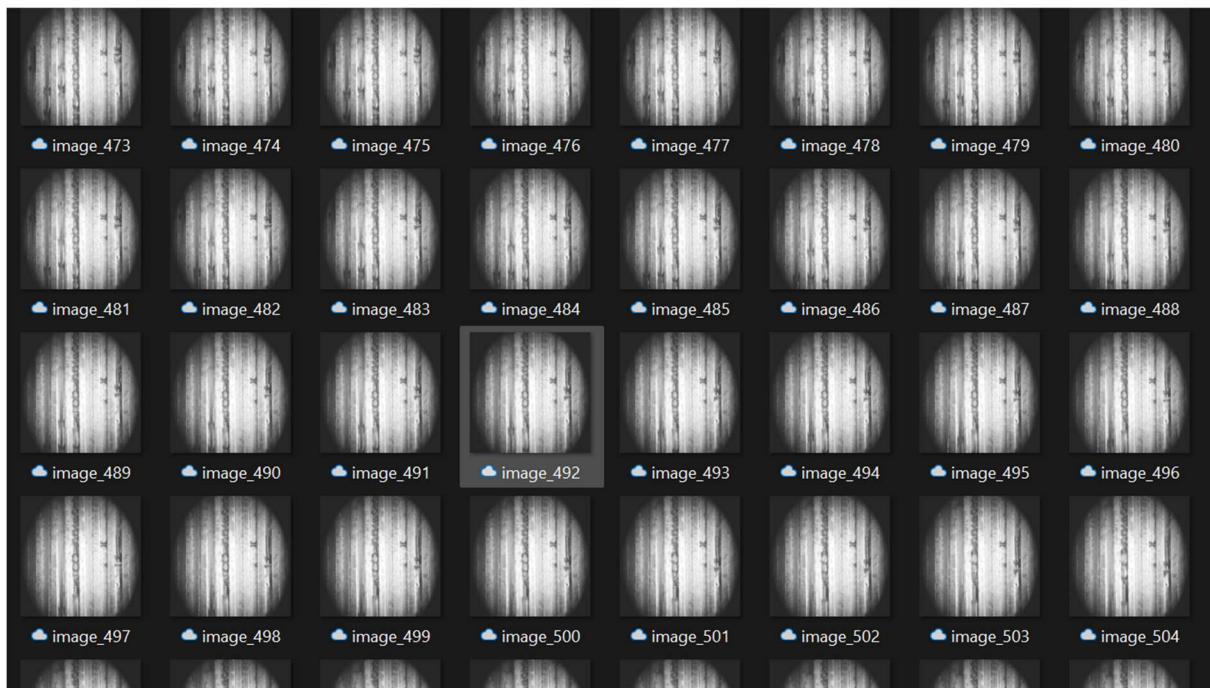
Epoch 19/20
23/23  17s 523ms/step - accuracy: 0.9444 - loss: 0.1888 - val
_accuracy: 0.7673 - val_loss: 0.4961

Epoch 20/20
23/23  17s 533ms/step - accuracy: 0.9384 - loss: 0.1823 - val
_accuracy: 0.8994 - val_loss: 0.3308

Sample Raw Data Flow Boiling Images (Validation Set)



Sample Raw Data (Augmented Flow Boiling Images)



Appendix D: Published Research

International Journal of Heat and Mass Transfer 239 (2025) 126581



Contents lists available at ScienceDirect

International Journal of Heat and Mass Transfer

journal homepage: www.elsevier.com/locate/ijhmt



Assessing thermohydraulic performance in novel micro pin-fin heat sinks: A synergistic experimental, agile manufacturing, and machine learning approach

Mohammad Harris^{*}, Hamza Babar, Hongwei Wu^{*}

School of Physics, Engineering and Computer Science, University of Hertfordshire, College Lane Campus, Hatfield, AL10 9AB, UK

ARTICLE INFO

Keywords:

Heat transfer
Micro pin-fins
Mini and microchannels
Machine learning
Thermal management

ABSTRACT

As advancements in technology and rapid product development redefine engineering paradigms, this study examines the influence of innovative and bio-inspired designs on heat transfer efficiency. The research evaluates the thermohydraulic performance of new biomorphic pin fins employing various strategic approaches and agile manufacturing techniques to optimise the design process. Experimental assessments were conducted on four hybrid pin fin configurations within Reynolds Numbers ranging from 101 to 507 and power outputs of 150 W and 250W. The investigation focused on how different geometrical features impact critical performance metrics, including the Nusselt Number, thermal resistance, and pressure drop. Results indicate a significant enhancement in heat transfer performance, ranging from 25 % to 45 %, compared to traditional designs, even at lower Reynolds Numbers and energy consumption levels. Additionally, new empirical correlations were developed specifically for these hybrid designs. Machine learning models demonstrated high accuracy in predicting the Nusselt Number, using Reynolds and Prandtl Numbers as key variables, achieving a mean absolute percentage error (MAPE) of less than 3.5 % and an R^2 value exceeding 0.95. Among the models evaluated, XGBoost, Random Forest, and Polynomial Regression exhibited superior performance with both real and synthetic data. This study underscores the potential of unconventional biomorphic geometries, highlighting the benefits of agile manufacturing and cutting-edge technologies in optimising resource use and improving predictive accuracy. The findings advocate for a reassessment of traditional heat sink designs and propose promising directions for future research in advanced sustainable thermal management.

1. Introduction

Currently, thermal management is beyond just a technical necessity and is a critical factor for success and sustainability. For instance, in electronic devices, cooling is fundamental to preventing overheating and safeguarding the reliability and lifespan of smartphones, micro-processors, and high-performance computing systems [1]. Similarly, the aerospace sector relies heavily on precise thermal control to ensure optimal performance and aircraft safety. Also, the automotive industry sees significant benefits from advanced thermal management, which enhances engine efficiency and extends the battery life of electric vehicles [2]. Effective heat transfer and management can boost machinery efficiency and reduce energy consumption in industrial settings.

Various cooling technologies and thermal management strategies have been introduced to address these sustainable needs. These range

from traditional methods like heat sinks [3], film and flow boiling [4,5], and nanomaterials [6] to more sophisticated approaches such as microchannel heat exchangers, heat pumps, and synthetic jet cooling combined with the current state-of-the-art in machine learning and artificial intelligence [7]. Among these, micro pin-fins (MPF) stand out due to their capacity to expand the surface area and generate turbulence, making them a crucial technology in thermal management [8]. However, as electronic devices continue to shrink and power densities climb, relying solely on traditional pin-fin geometries is unsuitable [9].

Recent works have highlighted a significant amount of research on pin-fin-based heat sinks, with a reliance on traditional geometries [1,10,11]. However, the prevalence of MPFs and non-conventional or combined and hybrid pin-fins is an area that requires much more attention to gain a comprehensive understanding of their effectiveness for optimal performance [8]. Peles et al. [12] were among the first to examine micro-pin fins; they investigated heat transfer and pressure drop

^{*} Corresponding authors.

E-mail addresses: m.harris8@herts.ac.uk (M. Harris), h.wu6@herts.ac.uk (H. Wu).

<https://doi.org/10.1016/j.ijheatmasstransfer.2024.126581>

Received 2 September 2024; Received in revised form 4 December 2024; Accepted 12 December 2024

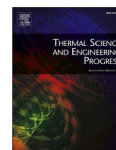
Available online 16 December 2024

0017-9310/© 2024 The Authors. Published by Elsevier Ltd. This is an open access article under the CC BY license (<http://creativecommons.org/licenses/by/4.0/>).



Contents lists available at ScienceDirect

Thermal Science and Engineering Progress

journal homepage: www.sciencedirect.com/journal/thermal-science-and-engineering-progress

Heat transfer optimisation using novel biomorphic pin-fin heat sinks: An integrated approach via design for manufacturing, numerical simulation, and machine learning

Mohammad Harris^{a,*}, Hongwei Wu^{a,*}, Anastasia Angelopoulou^b, Wenbin Zhang^c, Zhuohuan Hu^d, Yongqi Xie^e

^a School of Physics, Engineering and Computer Science, University of Hertfordshire, College Lane Campus, Hatfield AL10 9AB, UK

^b School of Computer Science and Engineering, University of Westminster, 115 New Cavendish Street, London W1W 6UW, UK

^c School of Science & Technology, Nottingham Trent University, Clifton Lane, Clifton, Nottingham NG11 8NS, UK

^d School of Energy and Power Engineering, University of Shanghai for Science and Technology, Shanghai 200093, China

^e School of Aeronautic Science and Engineering, Beihang University, Beijing 100191, China

ARTICLE INFO

Keywords:

Heat transfer enhancement
Biomorphic pin fins
Mini and microchannels
Machine learning
Numerical simulation

ABSTRACT

With the availability of advanced manufacturing techniques, non-conventional shapes and bio-inspired/biomorphic designs have shown to provide more efficient heat transfer. Consequently, this research investigates the heat transfer performance and fluid flow characteristics of novel biomorphic scutoid pin fins with varying volumes and top geometries. Numerical simulations were conducted using four hybrid designs for Reynolds Number 5500–13500. The impact of pin fin 'top' geometrical features on the heat transfer coefficient (HTC) was evaluated by combining computational fluid dynamics (CFD), experimental data, and machine learning. The results highlighted that the new pin fins saved 6.3 % to 14.3 % volume/material usage but produced around 1.5 to 1.7 times more heat transfer than conventional square/rectangular fins. Also, manipulating pin fins via the top geometrical properties can lead to more uniform velocity and temperature distributions while demonstrating the potential for increased thermal efficiency with reduced thermal resistance. Furthermore, six machine learning models accurately predict HTC using volume and surface area as key variables, achieving less than 5 % mean absolute percentage error (MAPE). Overall, this research introduces innovative biomorphic designs with unconventional geometries, emphasising resource optimisation and efficient HTC prediction using machine learning. It simplifies design processes, supports agile product development, calls for re-evaluation of conventional heat sink geometries, and provides promising directions for future research.

Nomenclature

Latin Symbols

A	Area, m ²
C _p	Specific heat capacity, J/kg·K
D	Diameter, m
D _h	Hydraulic diameter, m
h	Heat transfer coefficient, W/m ² ·K
H	Height, m
K	Thermal conductivity, W/m·K
L	Length, m
ṁ	Mass flow rate, kg/s
Nu	Nusselt number, no unit

(continued on next column)

Nomenclature (continued)

Q	Heat energy rate, W/m ²
R	Thermal resistance, K/W
Re	Reynolds number, no unit
SA	Surface area, m ²
T	Temperature, °C
U, V, W	Dimensionless parameter
u, v, w	Directional velocity, m/s
V	Volume, m ³
W	Width, m
x, y, z	Directional vectors
X, Y, Z	Dimensionless parameter

Greek Symbols

η	Efficiency, dimensionless
---	---------------------------

(continued on next page)

* Corresponding authors.

E-mail addresses: m.harris@herts.ac.uk (M. Harris), h.wu6@herts.ac.uk (H. Wu).<https://doi.org/10.1016/j.tsep.2024.102606>

Received 10 February 2024; Received in revised form 8 April 2024; Accepted 29 April 2024

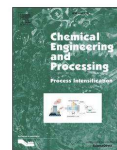
Available online 1 May 2024

2451-9049/© 2024 The Author(s). Published by Elsevier Ltd. This is an open access article under the CC BY license (<http://creativecommons.org/licenses/by/4.0/>).



Contents lists available at ScienceDirect

Chemical Engineering and Processing - Process Intensification

journal homepage: www.elsevier.com/locate/cep

Overview of recent trends in microchannels for heat transfer and thermal management applications

Mohammad Harris^a, Hongwei Wu^{a,*}, Wenbin Zhang^b, Anastasia Angelopoulou^c

^a School of Physics, Engineering and Computer Science, University of Hertfordshire, Hatfield AL10 9AB, UK

^b Nottingham Trent University, Clifton Lane, Clifton, Nottingham NG11 8NS, UK

^c University of Westminster, 115 New Cavendish Street, London W1W 6UW, UK

ARTICLE INFO

Keywords:

Microchannels
Heat transfer
Thermal management
Fluid
Sustainability

ABSTRACT

Distinctive recent research and experimental trends in microchannels for heat transfer and thermal management applications are investigated via a novel framework. The qualitative literature analysis was performed from four perspectives: materials, enhanced flow control, design, and sustainability (MEDS). The findings revealed that enhanced microchannel (MC) heat transfer performance (HTP) could be achieved by adding asymmetrical barriers, pin-fins, non-conventional geometries, mixed-wettability/biphilic surfaces, hybrid/silver nanofluids, and adopting innovative experimental and analysis methods. Additionally, researchers urged to focus on new microchannel designs and flow boiling/phase change-based experiments to understand the physics and different effects caused by various parameters. Furthermore, the qualitative analyses were transformed into quantitative results from the evaluated described methods and datasets, followed by a critical discussion of the findings. Finally, this article points out a set of promising future investigations and draws conclusions about current state-of-the-art. It is observed that, despite the decent progress made so far, microchannel-based applications still rely on traditional rectangular shapes, water-based working fluids, and numerical methods. Therefore, the role and focus on Industry 4.0 technologies to drive further innovations and sustainability in microchannel technologies are still in the early stages of adoption; this arguably acts as a barrier that prevents meeting current thermal and heat transfer needs.

1. Introduction

Consumer, industrial and digital electronic devices are now ever-present. With the emergence of Industry 4.0 and increased computational power, electronic devices are incorporated into almost all major or minor applications. Recent reports value consumer electronic markets

alone at around \$1 trillion; despite the COVID-19 pandemic, it is forecast to grow another 6% in 2022 [1]. Also, there has been a notable shift towards compact electronic devices; albeit, at the cost of more intense operating power and heat dissipation [2]. Thus, it can be claimed that whilst devices are increasingly and rapidly becoming portable and powerful, thermal management techniques are not efficiently catching

Abbreviations: additive manufacturing, AM/3D; aluminium, Al; aspect ratios, AR; bare copper surface, BCS; Biphilic surface, BS; carbon nanotube, CNT; centimetres, cm; coefficient of performance, COP; commercially/pre-made, CM; complementary metal oxide semiconductor, CMOS; computational fluid dynamics, CFD; concentrated photovoltaic, CPV; copper, Cu; critical heat flux, CHF; deionised water, DW; desiccant-coated heat exchanger, (DCHE); etching, ETC; eutectic gallium-indium, EGaIn; fan-shaped cavity microchannel, FSC; film evaporation and enhanced fluid delivery system, FEEDS; further research is needed, FRIN; gallium, Ga; heat flux, HF; heat transfer coefficient, HTC; heat transfer fluid, HTF; heat transfer performance, HTP; high concentrated photovoltaic, HCPV; hybrid nanofluid/microfluids, HY; hydraulic diameter, DH; hydrogen, H/H₂; indium, In; kilowatts, kW; Knudsen number, Kn; liquid organic hydrogen carriers, LOHC; lithography, Li; manifold microchannel, MMC; mass flux, MF; materials, experimental, design, sustainability, MEDS; Metres, m; Micro, μ ; microchannel heat exchanger, MCHE; microchannel heat sink, MCHS; microchannel with gas cavities, MGC; microchannels, MC; micromachining, MM; micrometres, μ m; moisture transfer coefficient, MTC; multi-layered microchannel, MLM; nitrogen, N₂; numerical method, NM; other analysis methods, OAM; other fabrication method, OFM; other materials, OMT; other working fluids, OWF; oxide, O/O₂/O₃; phase change materials, PCM; polydimethylsiloxane, PDMS; polymethyl methacrylate, PMMA; porous wall, PW; research question, RQ; Reynolds number, Re; silicon, Si; silver, Ag; tantalum, TA; test surfaces, TS; thermal conductivity, K; thermo-electric power generator, TEG; three dimensional, 3D; titanium, Ti; uncertainty analysis, UA; water-mixture, WM; watts, W; working fluid, WF; zinc, Zn; Z-score, z.

* Corresponding author.

E-mail address: h.wu6@herts.ac.uk (H. Wu).

<https://doi.org/10.1016/j.cep.2022.109155>

Received 31 May 2022; Received in revised form 2 September 2022; Accepted 24 September 2022

Available online 29 September 2022

0255-2701/© 2022 The Author(s). Published by Elsevier B.V. This is an open access article under the CC BY license (<http://creativecommons.org/licenses/by/4.0/>).

Comparative Analysis of Micro/Minichannel Flow Boiling Pattern Recognition and Classification using a Combined CNN-Clustering Algorithms Approach

Mohammad Harris

*School of Physics, Engineering and Computer Science
University of Hertfordshire
College Lane Campus, Hatfield, UK
m.harris8@herts.ac.uk*

Hongwei Wu

*School of Physics, Engineering and Computer Science
University of Hertfordshire
College Lane Campus, Hatfield, UK
h.wu6@herts.ac.uk*

Anastasia Angelopoulou

*School of Computer Science and Engineering
University of Westminster
115 New Cavendish Street, London, UK
a.angelopoulou@westminster.ac.uk*

Wenbin Zhang

*School of Science & Technology
Nottingham Trent University
Clifton Lane, Clifton, Nottingham, UK
wenbin.zhang@ntu.ac.uk*

Abstract—Microchannel heat sinks have attracted considerable attention in thermal management applications owing to their high heat transfer capabilities and compact size. Amongst the cooling techniques, flow boiling in microchannels has emerged as a promising method for efficient heat dissipation. However, the intricate flow patterns in microchannels present challenges for accurate classification, pattern recognition, and inefficient data handling practices. This paper presented a comparative analysis of flow boiling classification techniques for pattern recognition in microchannel heat sinks. Three different clustering algorithm-driven convolutional neural networks (CNNs) were analysed and compared alongside a base CNN to establish a data pipeline capable of agile flow boiling pattern recognition. The Gaussian Mixture Model Clustering-based CNN exhibited the best performance, achieving an overall mean accuracy of 88% for the test set validation. Thus, this study lays the groundwork for improving the performance of flow boiling pattern recognition in microchannel heat sinks.

Index Terms—pattern recognition, image analysis, clustering algorithm, flow boiling, thermal management, case study

I. INTRODUCTION

Micro-technologies have become integral components of electronic devices in today's world. Microchannels fall among these technologies, employing narrow passages/lanes and exploiting high surface area-to-volume ratios to boost convective heat transfer. Thus, this makes them exceptionally effective for cooling applications in electronic gadgets, energy systems, and automotive and aerospace industries. Despite the array of cooling methods used in microchannel heat sinks, flow boiling remains one of the most promising techniques for achieving high heat transfer and optimal thermal performance [1].

The flow boiling mechanism involves intricate interactions between liquid and vapour phases, resulting in varied flow patterns and heat transfer dynamics within microchannel heat sinks. However, due to the complex interchange and physical

phenomena involved, flow boiling classification contains many challenges related to subjectivity, interpretability, generalisability, and accuracy, amongst other issues [2]. Therefore, understanding and accurately categorising these flow patterns is crucial for enhancing heat transfer efficiency and ensuring dependable thermal management. Furthermore, classifying flow boiling regimes helps engineers to tailor microchannel designs to specific operational conditions, thereby maximising heat dissipation while minimising thermal resistance, pressure drops, or energy consumption.

Consequently, this study conducts a comparative assessment of flow boiling classification in micro/mini channel heat sinks, employing neural network-based classification and pattern recognition via clustering algorithms under varying mass flow rate conditions (ranging from 180 mL/min to 600 mL/min using 1600 images). The research aims to offer a new perspective and evaluate different algorithms via a custom dataset gained from experimental findings; thus, the focus lies in assessing machine learning-based approaches, specifically clustering methods, for accurately recognising and labelling boiling patterns in microchannel heat sinks. Thus, the research provides the following major contributions:

- 1) A streamlined, generalisable flow boiling image segmentation pipeline;
- 2) A semi-automated system to generate data and classify images for flow boiling analysis;
- 3) A baseline boiling regime classifier using a combined CNN-clustering that can be expanded/built upon;
- 4) A methodological comparative analysis of clustering algorithms not reported in similar preceding works;
- 5) Furthermore, the system considers a mixture of different bubble formations and regimes with data augmentations,



An Investigation on Engine Mass Airflow Sensor Production via TQM, TPM, and Six Sigma Practices

Mohammad Harris^{1,2}

Received: 17 January 2021 / Accepted: 3 October 2021
© The Author(s), under exclusive licence to Springer Nature Switzerland AG 2021

Abstract

In the Industry 4.0 era, companies need to be highly efficient in utilising their resources to remain competitive. This paper aims to investigate, appraise, and suggest possible improvements for engine mass airflow sensors (MAFS) production at a UK automotive parts manufacturer via combining total quality management (TQM), Six Sigma practices, and total productive maintenance (TPM)—with a focus on overall equipment effectiveness (OEE). The aim is achieved through a systems approach, root cause analyses, and investigating three variables: [availability](#), [performance](#), and [quality](#). Data are extracted both autonomously and manually to determine diverse root causes. The key findings showed that the majority of availability losses stem from maintenance waiting times (16%), performance losses from packaging cycles (31%), and improper housing selection leading to quality rejects (1–3%). Critical appraisal suggested introducing universality amongst staff, continuous improvement via technology, TPM activities, and employing a newly developed optimisation matrix. Also, changes in data infrastructure, reliance on data-driven decision-making instead of traditional methods, and adopting pay-per-use Cloud solutions are advised. These recommendations can effectively monitor processes; reduce underlying losses; boost OEE, total quality, and profits; and support future manufacturing processes. This investigation contributes towards enhancing automotive engine parts production research, presents a novel case study highlighting the effectiveness of combining management techniques to resolve problems in a UK enterprise, and indicates scope for future developments.

Keywords Operations management · Automotive · Quality management · Six Sigma · Manufacturing case study

✉ Mohammad Harris
itsharris@yahoo.com; m.harris8@herts.ac.uk

¹ University of Bolton, Bolton, Greater Manchester, UK

² University of Hertfordshire, Hatfield, Hertfordshire, UK

Investigating Heat Transfer and Flow Characteristics under Different Wall Heating Conditions in Novel Micro Pin-Fin Heat Sinks

Mohammad Harris^a, Hongwei Wu^a, Jianfei Sun^{b c d}

^aUniversity of Hertfordshire; College Lane Campus, Hatfield, United Kingdom

^bSchool of Mechanical Engineering and Automation; Beihang University, Beijing 100191, China

^cJingdezhen Research Institute of Beihang University; Jingdezhen 333000, China

^dBeijing Engineering Technological Research Centre of High-efficient and Green CNC Machining and Equipment, China

m.harris8@herts.ac.uk; h.wu6@herts.ac.uk; sjf@buaa.edu.cn

Abstract – The escalating power density in electronic devices demands effective and sustainable heat dissipation solutions. Micro pin-fin designs offer potential enhancements to thermal management in electronic cooling. Consequently, this short paper numerically investigates heat transfer and flow characteristics in micro pin-fin heating under distinct wall heating conditions. The results indicate that the new scutoid design exhibits a commendable heat transfer coefficient of 3298 W/m²K, with the lowest pressure drop and operating base temperatures. Thus, the findings provide a foundation for future designs and efficient heat transfer strategies.

Keywords: heat sinks; heat transfer; thermal management; CFD; micro pin-fins; microchannels

1. Introduction

The surge in miniaturised electronic devices in the Industry 4.0 era is reshaping various sectors. Modern components including computer chips, high-power LEDs, power amplifiers, and lasers, designed with microscale components, generate substantial heat during continuous use. This heat adversely impacts system performance and risks damaging critical components. Efficient thermal management is now a paramount design requirement for handling high heat fluxes in miniature systems. In a global push for sustainability, ineffective thermal management leads to energy wastage, contributing to unsustainable impacts. Therefore, addressing the thermal challenges of electronic devices is crucial for optimal performance, prolonged component lifespan, and alignment with global sustainability goals.

Currently, tackling cooling challenges in electronic devices is a pivotal engineering obstacle. With the availability of advanced manufacturing techniques for microfabrication and metal-based 3D printing, heat sinks based on micro pin-fin configurations have emerged as promising solutions for effective electronics cooling and generated considerable interest across various applications [1]. However, there is still a lack of consensus on optimal microscale heat transfer strategies and the underlying physics required to meet future heat transfer requirements [2]. Consequently, further studies are essential to provide novel insights into new designs that integrate micro pin-fin and heat transfer.

Thus, this short paper aims to numerically examine heat transfer and flow under different wall heating conditions in a novel micro pin-fin heat sink. Building on extant literature findings, the investigation analyses how changes in wall heating conditions impact heat transfer and flow performance. The objective of this research is to bridge gaps in microscale heat transfer, offering insights for efficient cooling systems. The paper is structured around the research aim, with the initial sections covering model design, methods, simulation, results, and evaluation. Subsequent sections include discussions, conclusions, and recommendations for further research.

2. Numerical Methods and Materials

In this research, two designs were compared. The first base design featured inline rectangular pin fins (RF) and was used for numerical validation from the works of [3]; The second design, containing pentagonal-hexa-prism fins (SF), drew inspiration from a skin cell shape called scutoid. The SF combined the effects of two different shapes and offered new insights. Then, a CFD study analysed heat transfer and flow characteristics to understand the underlying physics. The microfin geometries, heat sink design, along with the different wall heating setup, are depicted in Fig. 1; the heat sinks had identical dimensions and number of pin fins (17 × 34).

Numerical Simulation of Heat Transfer Performance in Novel Biomorphic Pin-Fin Heat Sinks

Mohammad Harris¹, Hongwei Wu¹

¹University of Hertfordshire
College Lane Campus, Hatfield, United Kingdom
m.harris8@herts.ac.uk; h.wu6@herts.ac.uk

Abstract – Pin-fins are effective strategies to enhance heat sink performance; moreover, bio-inspired designs present endless geometrical potential. In this work, a comparative investigation of two biomorphic pin-fin-based heat sinks was carried out via ANSYS CFD simulations. The results showed that the heat transfer performance of the pentagonal and sharp-edged design reported approximately 14% higher Nusselt number compared to a circular and smoother-edged design. Furthermore, the pressure drops or variations within both heat sinks were minimal. The findings from this research provide a baseline for future bio-inspired heat sink designs and heat transfer improvement strategies.

Keywords: heat sinks; heat transfer; thermal management; CFD; mini-channels; pin-fins; bio-inspired design

1. Introduction

Miniaturised electronic gadgets have sparked a revolution in the electronics industry. These electronic devices heat up immensely from constant operation in the microscales — lowering their performance, efficiency, and potentially damaging the overall components/system. The design of miniature heat transfer systems with high heat flux has become crucial as ineffective thermal management can reduce device lifespan, waste energy, and produce unsustainable impacts. Thus, the cooling mechanism of electronic gadgets is one of the key engineering challenges with current-generation technology. As a result, various investigations have been carried out to offer an integrated efficient cooling system. Hence, due to their outstanding potential to efficiently cool electronics, pin-fin-based heat sinks have gained interest in many applications [1].

Despite that, recent research has highlighted a lack of consensus regarding optimum strategies, mechanisms to cope with future heat transfer requirements, and underlying physics within microscale heat transfer [2]. Whilst CFD simulations to determine flow and heat transfer characteristics have been explored, further design analysis and studies are required to provide novel insights, knowledge on optimal heat transfer, and thermal management solutions. Additionally, authors have explored bio-inspired designs to provide unique shapes and understandings into heat transfer improvement; however, further exploration and experiments are warranted in this area as well [3]. Therefore, this paper aims to investigate heat transfer characteristics in novel mini heat sinks with biomorphic pin-fins, emphasising design, heat transfer, flow characteristics, and CFD analysis. Acknowledging extant literature and adopting a biomimetic/biomorphic technology approach, this paper appraises bio-inspired shapes to improve understanding of flow dynamics and provide enhanced heat transfer. The term biomimetic relates to solving complex problems whilst adopting systems that occur in nature; on the other hand, biomorphic designs are inspired by naturally occurring shapes or living organisms.

This short paper is divided into sections and organised around the research aim. The design process that helped to shape this work is described in Section 2. The model simulation, results and an evaluation of the findings are covered in Section 3. The closing parts of this paper include discussions, conclusions, and recommendations for further research.

2. Numerical Methods and Materials

In this paper, two designs have been created inspired by parasol fungus/mushrooms. The first design had smoother circular stems/pin-fins and flat tops (CSFT), but the second design maintained sharp edges, pentagonal stems, and diamond-shaped tops (PSDT). Next, a numerical study was performed to analyse the heat transfer and flow characteristics and compare the designs using CFD. The geometry of the parasol-inspired pin-fin heat sinks can be seen in Fig. 1. A sample of 30 pin-fins was selected to reduce simulation time and cost. Both designs had identical sizes, pin-fin spacing, and dimensions.

Afterwords

As I wrap up this adventure of a thesis on enhancing heat transfer in micro heat sinks, I can't help but reflect on the whirlwind journey that has shaped both my research and personal growth. Starting my PhD during the chaos of the COVID-19 pandemic felt like diving into the deep end of a pool that I was not even sure existed. The challenges were plentiful—think navigating a maze with occasional pitfalls—but each turn taught me something invaluable.

Navigating Mental Health Challenges: Let's be honest: my mental health took a nosedive. juggling procurement, searching for elusive equipment, the university's bureaucracy, and dealing with limited facilities was like solving a Rubik's Cube while blindfolded! The stress of it all was real, and some days, the weight of uncertainty felt heavy. Yet, these trials fuelled my determination to persevere and find creative solutions.

Embracing the Unknown: Venturing into a field that was new to me was exhilarating. Equipped with curiosity and grit, I embraced every complex concept and methodology as a puzzle piece waiting to fit into a larger picture. With each breakthrough—be it a successful simulation or a promising design—I became more fascinated with micro-thermal management.

A Testament to Resilience: This thesis isn't just a collection of findings; it's a testament to the resilience built through testing times. From developing innovative biomorphic pin-fin designs to harnessing machine learning, this work highlights the magic that happens when diverse disciplines collide. True innovation thrives on collaboration, weaving together threads from engineering, materials science, and sustainability.

Looking Ahead: The implications of this research reach far beyond these pages. I hope to spark a conversation about improving energy efficiency and sustainability in thermal management solutions. Future researchers, I encourage you to embrace the challenges ahead. Innovation isn't just about overcoming obstacles; it's about weaving a tapestry of effective engineering solutions.

Final Thoughts: As I close this academic chapter, I carry invaluable lessons and the joy of discovery. I urge future scholars to embrace their journeys, enthusiastically tackle their challenges, and pursue their passions with fervour and perseverance. The path may be bumpy, but the thrill of exploration makes it all worthwhile! And remember this final quote:

"The end of one journey is the beginning of another." – Unknown

(And... If you have made it this far, thank you for reading! – Harris)